VIBRATION ASSISTED FILLING OF THIN SECTION CASTINGS

By

WALEED ABDUL KAREM

A thesis submitted to The School of Engineering
The University of Birmingham
For the degree of

DOCTOR OF PHILOSOPHY

School of Engineering
The University of Birmingham
Birmingham B15 2TT
United Kingdom
August 2009

Abstract

Understanding of the mechanism of the vibration needed to fill thin section or one with sharp edges in profile shapes and clarifying the dominant control parameters of the vibration in thin wall investment casting is key to producing sound casting (one free of misrun defects). It's also a central issue for study in this thesis. The filling capability in thin wall investment casting method was assessed in relation to metal head. It was found that the effect of the vibration on the metal head is markedly dependent on acceleration. Generally, it was observed that the metal head required to force the metal in thin sections in the casting vibrated at (1g) acceleration is approximately half that used in castings made without vibration. Two potential mechanisms were observed from the experimental result during the filling process in thin wall casting i] discontinuous propagation flow in vibration conditions; and ii] continuous propagation flow without vibration. These mechanisms may be acting to modify the contact angles between liquid metal and a wall of the mould.

Experiments also showed that two features of the transition can be observed from the front of the morphology; i] a coherent liquid metal front - this occurs in thin wall investment casting when the acceleration due to vibration is less than (1g); and ii] jetting at the free surface - this occurs in thin wall investment casting when the acceleration due to vibration exceeds 1g. This is present in terms of a unifying concept, using a frequency and amplitude ($f - a$) map. The time of the vibration operation has a moderate effect on the relative filling area when the acceleration is less than 1g. However, it is more effective when the acceleration of the vibration is greater than 1g.

The mathematical models comprised one-dimensional heat transfer with phase change and had an established flow field for molten A356 alloys flow in the thin section ceramic channel mould. The work was concerned with the fluidity of A356 alloys in thin wall investment casting with and without vibration in two type of filling (flowability and fillability filling types), combining heat and metal flow in addition to the simultaneous solidification stage. The results of the mathematical model, produced agreement with the experimental test carried out in the foundry and also agreed with other published data. The results on fluidity indicated that the fluidity of the molten metal was affected by mould temperature, pouring temperature, the velocity of the molten metal flow relative to the surface tension and the channel thickness. The data used in the mathematical model of the fluidity in thin section under vibration condition were deduced

experimentally; namely, velocity of the molten metal and the heat transfer coefficient between the liquid metal and the chilled surface of the mould. This model was used to estimate the fluidity characteristics in thin wall investment casting with and without vibration.

Real-time X-ray observation and computer modelling of the metal head-driven mould filling sequences reveal that no surface turbulence occurred when the liquid metal flowed into the thin section and the advance metal front continued to flow under surface tension control. X-ray was also used to measure the flow time and the velocity of the metal inside the thin channel and confirm the modification on Bernoullis Equation (kinetic energy+ potential energy = constant) to estimate the velocity relative to surface tension in the fluidity mathematical model. Flow-3D software was used to calculate the velocity of the liquid metal in the flowability filling type and the fluidity characteristics.

Weibull analysis identifies the acceleration vibration as practical criterion to judge the reliability of casting.

A vibration mould with vertical direction in the thin wall investment casting after filling can make the liquid metal flow into the thin section under surface tension control. This technique is used to achieve mould filling free from misrun defects and surface turbulence and this makes vibration casting a promising technique for producing high quality castings. On the basis of these findings, an operation window for the production of reliable castings has for the first time been developed in this research.

I would like to dedicate this Thesis to my wife Najla, my two daughters Aya and Dalia, and my son Ali.

The best gifts that god ever gave me.

Also my Mother, Brothers and Sisters.

ACKNOWLEDGMENTS

I would sincerely like to thank my supervisor, Professor Nick Green, for his excellent supervision, advice, inspiration and guidance. This work would not be possible without his invaluable help and it was an honour to be able to work under his supervision.

I would like to thank Professor John Campbell, Dr. W.D.Griffiths and Dr J. Gebelin for their help and useful discussions.

My sincere thanks also due to Mr. Adrian Caden, for his technical support. I would not have been able to carry out the experimental work without his help. I also want to express my appreciation of the help and assistance of Mr. Mick Wickins, and other technical staff at the school of Metallugry and Materials.

Finally, I would like to thank my wife, Najla, for her wonderful support, devotion and patience throughout the course of this research.

List of content

Chapter 1

Introduction

Chapter 2

Literature survey

Chapter 3

Apparatus and Experimental procedure

Chapter 4

Experimental Results

List of Tables

Table 4.6 Results of the experiment to determine the velocity in fillability filling type casting, pouring temperature750C, mould temperature 660ºC to 700ºC, using X-ray machine

Table 4.7 Results of experiments to determine metal velocity in flowability filling type casting, pouring temperature750˚C, mould temperature 400˚C.

Table 4.8 Experimental results of the effect of acceleration due to vibration on the metal head with strips of thicknesses $0.55^{\pm 0.05}\,mm$ **and** $0.75^{\pm 0.05}\,mm$ **. Pouring temperature750˚C** ± 5 **ºC. Mould temperature 620˚C to 660˚C, vibration time 10s.**

Table 4.9 Experimental results of the effect of vibration time on the metal head and filling relative area with a strip ($0.55^{\pm 0.05}\,mm$**) thick, Pouring temperature.** $750C \pm 5$ **ºC, Mould temperature ºC** ≈ 620 **to** 660 **ºC, acceleration of vibration varying between 0.8g to 1.3g**

Table 4.10. Dependence of the relative filling area as a function of vibration time and acceleration in strip thickness 0.55mm, pouring temperature 750ºC, and mould temperature 660 to 750 ºC

Table 4.11 Experimental results to determine the effect of the vibration parameter (frequency and amplitude) on the flow of liquid metals in strip with thickness of ($0.55^{\pm 0.05}\,mm$**) and using A356 alloys, Pouring temperature** $750C \pm 5$ **ºC, Mould Temperature** ≈ 620 **ºC to** 660 **ºC.**

Table4.12 Experimental results from experiments to determine the effect of the metal head on the length of jetting at a constant acceleration of vibration (1g), with a strip thickness of $0.55^{\pm 0.05}\,mm$**, Pouring temperature** $750C \pm 5$ **ºC, Mould temperature** ≈ 620 **ºC to** 660 **ºC.**

Table 4.13 Experimental results to determine the effect of the acceleration of vibration on the length of jetting at constant metal head (45mm), with a strip thickness of ($0.55^{\pm 0.05}\,mm$**) and using aluminum alloys, Pouring Temperature** $750C \pm 5$ **ºC, Mould Temperature** ≈ 620 **ºC to** 660 **ºC.**

Table 4.14 Summary result of the experiment to determine the velocity of mercury in each frequency cycle, using high speed camera.

Table 4.15 Number of defect in each interval of 1000 μm^2**, 10000** μm^2 **increase in defect size**

Table 4.l6 Hardness measurement for each method of casting

Table 4.17 UTS and elongation of the specimens for each method of casting: without vibration, with vibration 0.8g and 1.2g acceleration after filling and vibration 0.8g acceleration during filling. Pouring temperature 750ºC, mould temperature 660ºC to 700ºC.

Table 5.2 Radius of the peak in a surface roughness profile of the ceramic mould, distance between two peak around (50 to 60 μm).

Table 5**.5 UTS and elongation measured in 0.75 mm thick strip cast with and without vibration of 0.8g acceleration during filling. Pouring temperature 750ºC, mould temperature 420ºC**

Table 5.8 Results of the fluidity experiment

Appendix
List

X-ray Frames, Flow-3D Simulations, SEM and EDX

List of Symbols

Q	Initial volume flow rate, $m^3 s^{-1}$
U	Velocity of molten metal, ms^{-1}
h	Metal head, m
A	area, m^2
r	Radius, m
W	Casting weight, kg
t	Fill time, Sec
L	Length of fluidity in superheat, m
T_p	Pouring temperature, ^0C
K	Thermal of conductivity $Wm^{-1}k^{-1}$
C_p	Specific heat, $Jkg^{-1}k^{-1}$
Acc.	Acceleration (g)
γ	surface tension, Nm^{-1}
ρ	density, kgm^{-3}

Chapter 1

Introduction

Casting is one of the most important mass production methods in a manufacturing process. It can be simply defined as follows: pouring a liquid metal into a cavity of the desired size and shape until it is full and solidifying the metal to take the shape of the cavity (see Figure 1.1).

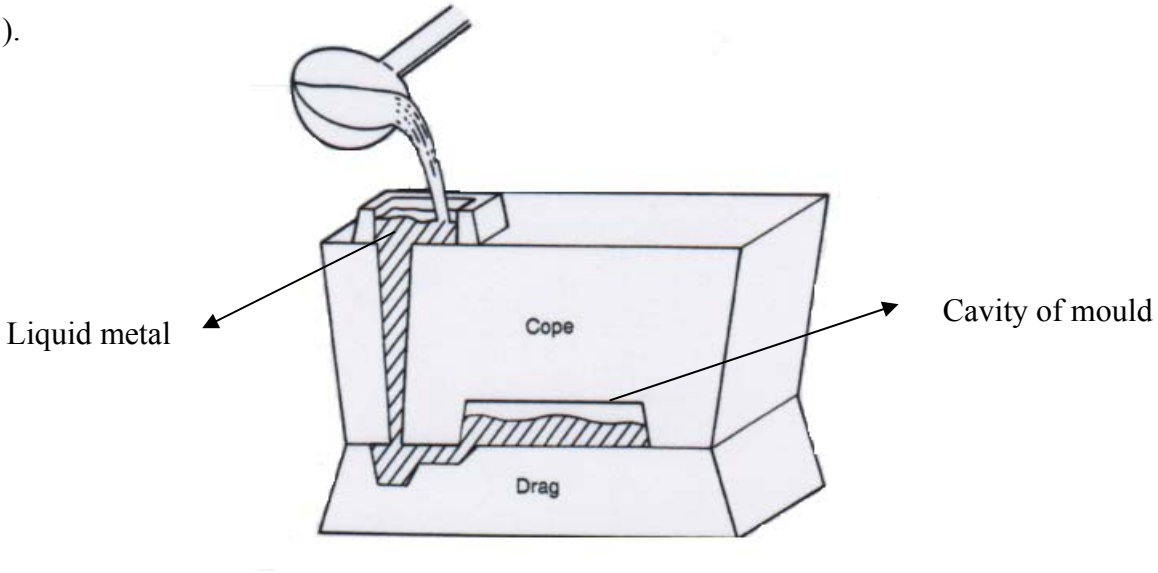

Figure 1.1 gravity top pouring of metal into a mould: the mould is partially sectioned to show the liquid metal flow [1]

Many defects can appear during the casting process [2]. Generally, defects can be defined as observable and unplanned variations of a specification. The identification or diagnosis of a particular casting defect is based upon the specific shape, appearance, location and dimension or profile of the anomaly. Correcting and controlling the quality of castings cannot be done without properly identifying the specific cause of each one, for example: misrun, shrinkage cavity, porosity and cracking or tearing in the casting. These are described in the following sections. Most defects influence the mechanical properties of a metal and this influence reflects on the quality of the casting. Green and Campbell were

among the first to have evaluated the quality of the casting in different conditions with respect to mechanical properties, by using statistical methods [3,4].

Recently, the aim of many researchers [5,6] in the field of casting has been to reduce or eliminate the defects in the casting by using different techniques, for example, centrifugal casting, additional pressure and vacuum assisted casting, These techniques are used in thin wall casting, to improve the quality and produce sound casting (casting free of misrun defects). A mechanical vibration technique was used in this study to explore what effects vibration has on the efficiency of production with respect to misrun defects and the 'quality' of the casting, such as porosity, in a thin wall investment casting.

Most investigations in the available literature [7, 8 9 and 10] have assumed that vibration applied during casting of components with normal dimensions was done for the purpose of refining the grain structure, in order to improve the mechanical properties. However, in this project vibration was applied in thin wall castings to investigate its effect on the capability of the liquid metal to fill thin section and produce castings without misrun defects and reduce other defects. The following section discusses briefly some of the most common defects in casting

1.1 Casting defects

(i). Misrun

Misrun is a term used to describe the incomplete filling of the mould cavity (see Figure 1.2). It is a major defect in the investment casting process when used to produce turbine blades, impellers and impulse blades for turbo pumps which have complex profiles, thin walls and sharp edges. Such components are often cast in alloys with high melting points. In the best practice of gravity pouring of investment castings, when a wall section is around 0.2mm to 0.55mm, scrap may reach 40%-50%. Most of the discards are due to misrun defects [11].


Figure 1.2 Misrun defects in thin section turbine blade castings

Misruns may be caused by too low a pouring temperature or pouring rate, or poor fluidity of the alloy. In addition, some of the following factors may result in mould back pressure high enough to cause a misrun: low mould permeability, poor venting, and atmosphere [12].

In general, misruns are commonly eliminated by controlling the mould and metal temperature during casting. In the case of thin wall castings further steps include increasing the pouring rate and increasing the metal pressure in the gating system. The pressure may be increased by the application of a vacuum, vibration or by using centrifugal force. Modification of the gating system may also be helpful in preventing misruns by providing vents to allow for the escape of gas and ensure a smooth rapid flow of metal into the thinner sections of the casting [6, 13, 14 and 15].

(ii). Hot Tears and Porosity

Hot tears are crack-like defects forming during the latter stage of solidification. A crack occurs when the partially solidified metal is placed in tension by the constrained cooling and contraction of the surrounding casting. Hot tears are characterized by a heavily

oxidized surface, as compared with the relatively clean surface of a crack made at room temperature [2 and 12].

Campbell was the first researcher to have commented on and emphasized the role of entrained oxide films as the main cause of defects in most castings. The new concept proposed by Campbell is a defect structure [6 and13] constituted by fragments of the entrained oxidized liquid surface. Since the liquid surface is commonly covered with an oxide film, it is entrained into the melt by a simple folding action. This doubled-over film can remain unbonded (essentially folded dry side to dry side) containing a film of air between surfaces which do not touch each other (see Figure 1.3). This defect has been called a “bifilm” and behaves like a crack in the liquid.

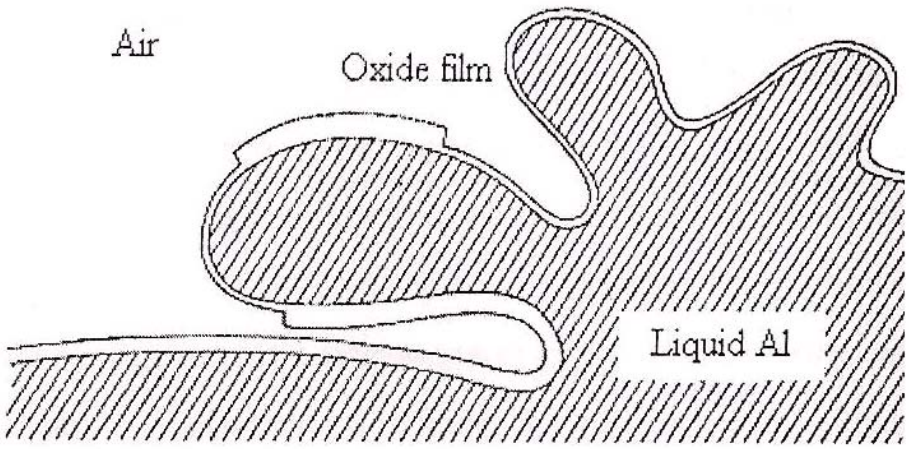

Figure 1.3 Formation of a double oxide film defect in Al alloys [6]

With regard to porosity, researchers assume that it is caused by precipitation of gases dissolved in the molten metal or by volumetric contraction occurring during solidification [12].

All the common casting defects (misruns, cracks, hot tears, shrinkage cavities and porosity) which occur in thin wall investment castings are generally the same as those found in

castings produced by other processes and can be limited but not eliminated if the foundry uses filling and other foundry factors (pouring temperature, mould temperature, and suitable casting condition) controlled by a properly designed gating system.

1.2 Fluidity

Fluidity is one of the important casting characteristics. The term fluidity can be defined as that quality of a liquid metal which enables it to flow through the mould, providing a sharp outline and faithful reproduction of all design details. It follows that inadequate fluidity may be a factor in misrun or in poorly defined surface features. Fluidity is not a simple physical property, as density and viscosity are, but is a unique property related to casting practice [16-18].

1.3 Surface Films

When the hot metal interacts with the environment, the most common reaction is the formation of a surface film. There are two common film-forming reactions: 1) oxidation films formed by the decomposition of moisture, and 2) graphitic films formed from the decomposition of hydrocarbon mould gases at the liquid metal surface. In the case of aluminum alloys both result in increased hydrogen concentration in the melt [6]. On molten aluminium and aluminium alloys the oxide film usually starts as a simple amorphous layer but quickly converts to one of the crystalline varieties as the film ages and thickens. Some films remain thin because they have formed only during the surface turbulent associated with pouring and in this case they are entrained before they have time to thicken. If the surface film is solid, it would always rupture during filling, but continuously reforms anew [21-23].

1.4 Grain and grain boundaries

Randomly oriented and variously located crystals are formed in the liquid metal when the mass of the molten metal starts to solidify. These crystals are called grains and the surface which separates any two grains is called the grain boundary. The size of the grains is controlled by their number and rate of growth. Generally, rapid cooling produces smaller grains and slow cooling produces larger grains.

The size of the grains and the consequent number of grain boundaries has a powerful effect on the properties of castings. A slow cooling rate and large grain size are generally associated with low strength and hardness. When sufficiently the grain boundaries impede dislocation motion and enhance the strength of the metal [24].

In the present work, the microstructure and mechanical properties of thin wall investment cast A356 alloys: were studied with and without applied vibration, and the effect of vibration in refining the microstructure was evident.

1.5 Aim of the Work

The aims of this research project are:

1. To investigate the effective of mechanical vibration as a way of filling sharp edges in profile shapes and to characterize the dominant control parameters.

2. To investigate the effect of vibration on misrun defects and the mechanical properties of materials produced in a range of casting conditions.

3- To analyze and quantify the reliability of castings and define an operational window for the production of reliable castings.

Aluminum alloys and ceramic moulds were used in the practical work to establish principles and clarify the key parameters in the aims of the work.

1.6 Thesis structure

This thesis consists of eight chapters. Chapter 1 has briefly introduced the purpose of this study and objectives of the research. A comprehensive literature review is presented in Chapter 2. The experimental procedures and results are presented in Chapters 3 and 4 respectively. Chapter 5 covers the theoretical considerations of fluidity in thin wall investment casting and development of a predictive model for filling. A discussion of the results is presented in Chapter 6. The conclusions are highlighted in Chapter 7 and future work is suggested in Chapter 8.

Chapter 2

Literature review

2.1 Casting

Casting has been defined in Chapter 1. It is the oldest method for shaping metals, and was first used in about 4000 BC to make such objects as copper arrowheads. Many metals are difficult to fabricate by welding or a cold forming method, but easy to cast. When compared with forging and welding, generally, casting is the cheapest method among the mass production processes for structure components.

The classification of a casting process depends on the combination of the moulding method and the material from which the casting is made or some particular aspect of the processes employed in production [12].

The casting processes most often used are set out in Table 2.1.

Table 2. 1 Summary of the main moulding and filling processes used for casting.

			Filling Method					
			Gravity	Low pressure	Vacuum	Centrifugal	Tilt	High pressure
Moulding Method	Investment casting	Ceramic	yes	No	yes	yes	yes	No
		Cored ceramic	yes	No	yes	yes	yes	No
		Plaster block	yes	No	yes	yes	yes	No
	Sand casting	Green sand	yes	No	No		No	No
		Resin bounded	Yes	Yes	No	yes	Yes	No
		Loose	Yes	No	Yes	no	No	No
	Die casting	Metal cored	Yes	Yes	No	yes	Yes	Yes
		Sand cored	yes	No	No	No	No	No

By considering the advantages and taking into account the limitations of each casting method it is normally possible to identity the best manufacturing process. It is necessary to take into account the casting size and shape, dimensional accuracy and tolerance. Specification, surface finish, metallurgical properties, alloy type, production quantity and target cost. Moulds used in the casting process are usually made at least in two parts, apart from investment casting which uses a one-piece monolithic mould. Die casting or semi permanent-mould casting may use moulds or dies made up of more than two parts for the casting of complex shapes.

2.2 Investment casting

The investment casting process is also known as the lost wax, lost pattern or precision casting method. In investment casting, a pattern material is used which will melt at the baking temperature of a normal ceramic or plaster mould and for this reason it is known as the lost-wax process. Such a method was used for making statues many centuries ago in China and Japan and is still used for this purpose in Europe [25].

The industrial adaptation of the ceramic shell mould investment casting process took place during the Second World War, when many small intricate parts had to be made from materials which cannot be machined or fabricated by any other manufacturing method [25 and 26] .

In this method the pattern is made of wax, plastic or even frozen mercury. Suitable gates and risers are attached to it and the assembly is then dipped into a slurry of refractory material, such as very fine zircon and alumino silicates. The bonding agents which tend to be used in the slurry are colloidal silica, hydrolyzed ethylsilica and sodium silicate. After this initial coating has dried, the pattern is then coated several times with molachite to increase its thickness (see Figure (2.1)).

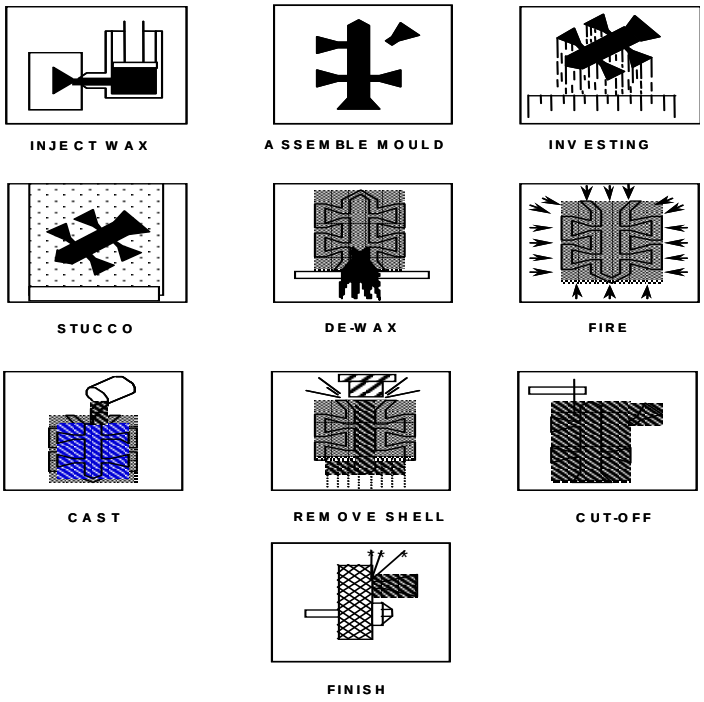

Figure 2.1 Basic principles of the investment casting process [80]

The one-piece mould is dried in air and heated for about 2 hours to a temperature of 90ºC-175ºC, depending on the metals involved, until the last traces of wax are melted. After the mould has been cast and the metal has solidified, the mould is broken and the casting is recovered [17, 27 and 28].

Two distinct processes, differing in the method of mould preparation, are used in the production of investment casting, namely, the shell process and solid investment or block mould casting. However, the patterns for the shell process are always precoated; whereas no precoating of the pattern for the block mould process is generally required unless the properties of the back-up refractory are inadequate for some special application. The precoating method for both processes is similar [12 and 29].

A major advantage of the investment casting method is that it can be used to produce parts with intricate and complex shapes, which may be very difficult or impossible to produce by any other means of manufacture. Although the labour and material involved make the lost-

wax process costly, it has been found suitable for casting high-melting point alloy with high dimension accuracy, excellent detail and good surface finish.

Snowden reported that an emerging trend in the aerospace turbine industry is to replace forged blades with near-net shape investment cast blades. This substitution reduces the number of parts and reduces the cost of material and subsequent labour. The cost advantages of near-net-shape parts are evident from the "buy: fly" ratio, which is the amount of material that must be purchased to make a unit weight of a finished part. The ratio in the early 1970s has lately been reduced from 7:1 to 5:1 [30].

During the casting of thin section turbine blades for aerospace applications, filling the aerofoil section, which often tapers to a thickness of 0.5 mm is resisted by the back pressure arising due to surface tension. This is one of the chief problems in the casting of polycrystalline equiaxed blades. Misrun and cavity defects are common causes of scrap in thin sections. Even with best practice, substantial scrap is still generated [6 and 11].

In the last fifty years, much research [e.g. 31, 32, 33] has confirmed that investment casting is a suitable method to produce turbine blades of thin section and intricate shapes. The likelihood of misrun defects in equiaxed investment castings is further influenced by the fluidity, the metal often being cast into the mould at temperatures hundreds of degrees below the solidus temperature. Improvement fluidity and mould filling without misrun defects in thin sections is only possible by the operation of additional pressure (centrifugal, vacuum and pressure after filling)[6, 12, 13, 33].

2.3 Thin wall investment casting

The fluidity, liquid flow, surface tension and the design of the runner system constitute the main factors to consider in the design of production processes for thin walled castings [5 and 13]. The filling capacity of the aerofoil shape (the turbine blade) in thin wall investment casting is limited by surface tension even if the temperature of the mould exceeds that of the liquidus temperature, regardless of the pouring temperature.

Campbell and Olliff [34] described the filling process in thin wall investment castings by analyzing the results for vacuum-casting Ni-base alloy (turbine blade), which are reproduced in Figure (2.2). They found that at sufficiently high casting temperatures the degree of filling in the thin section depended on the balance between the filling pressure, due to the metal head, and the effective back pressure due to surface tension, regardless of the melt temperature. These authors distinguished between two aspects of filling: flowability and fillability. Flowability occurs at low metal temperature and is a function of superheat and is limited by heat transfer, whereas fillability occurs at higher metal temperatures and is controlled by a mechanical balance between the surface tension and the hydrostatic pressure in the liquid due to gravity, or other effects.

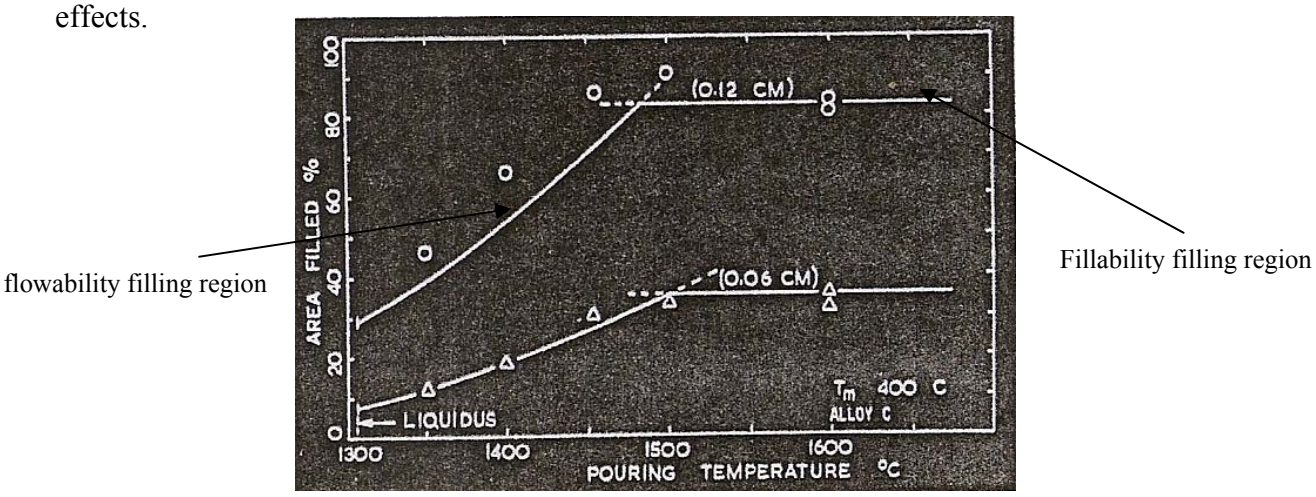

Figure 2.2 show the fillability and flowability filling type regions in thin section [34]

Another aspect of thin wall investment casting is the runner system design. Flemings [35] found that a critical metal head is necessary to force a molten metal into small diameter. This critical head is whatever is required to overcome surface tension, regardless of the melt temperature, and is illustrated in Figure 2.3.

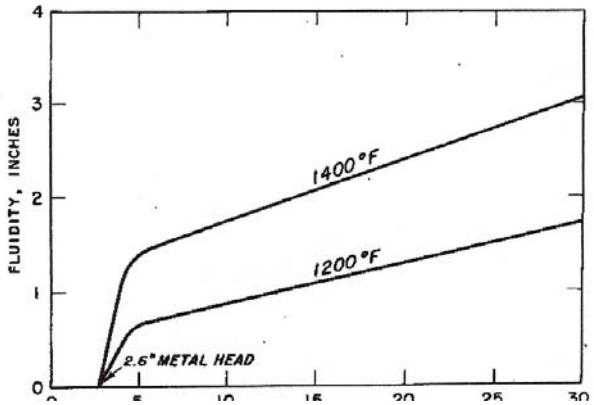

Figure 2.3 Fluidity vs. metal head for tubes 0.07 in. diameter. [15]

The main factors involved in the thin wall investment casting process will be discussed in turn below.

2.4 Fluidity

2.4.1 Measurement of fluidity

Fluidity is one of the most important factors in the casting process**.** Fluidity is defined by Campbell [18] and Fleming [17] as the distance covered by quality liquid metal in a channel of fixed geometry before solidifying. This does not involve its physical properties, and it can be measured by using a standardized system of enclosed channels (Beeley [16]).

Kondic [36] states that it is very difficult to find a definition for the fluidity which can be accepted by metallurgists and foundrymen, the reason being that the fluidity from the point of view of many metallurgists is understood as a matter of flow behaviour only, whereas for foundrymen, it is a question of the flow and mould

filling. Hence, he defines the fluidity as the ability of the melt to flow and fill the mould. In his definition, Kondic covers all the terminology related to fluidity.

Disagreement between metallurgists and foundrymen on the proper terminology for fluidity has prompted many researchers to develop different experiments to test and quantify fluidity. Tests have been conducted under two scenarios involving 1) flow; and 2) flow and solidification. The spiral type of test is generally used when the investigation deals with the effect of the flow of liquid metal effect on the fluidity. However, the straight channel is used when the investigation relates to the ability of the metal to fill the mould related to the effect of the flow and solidification variables on the fluidity [36]. The fluidity test mould design for the spiral and straight channels are illustrated in Figure 2.4

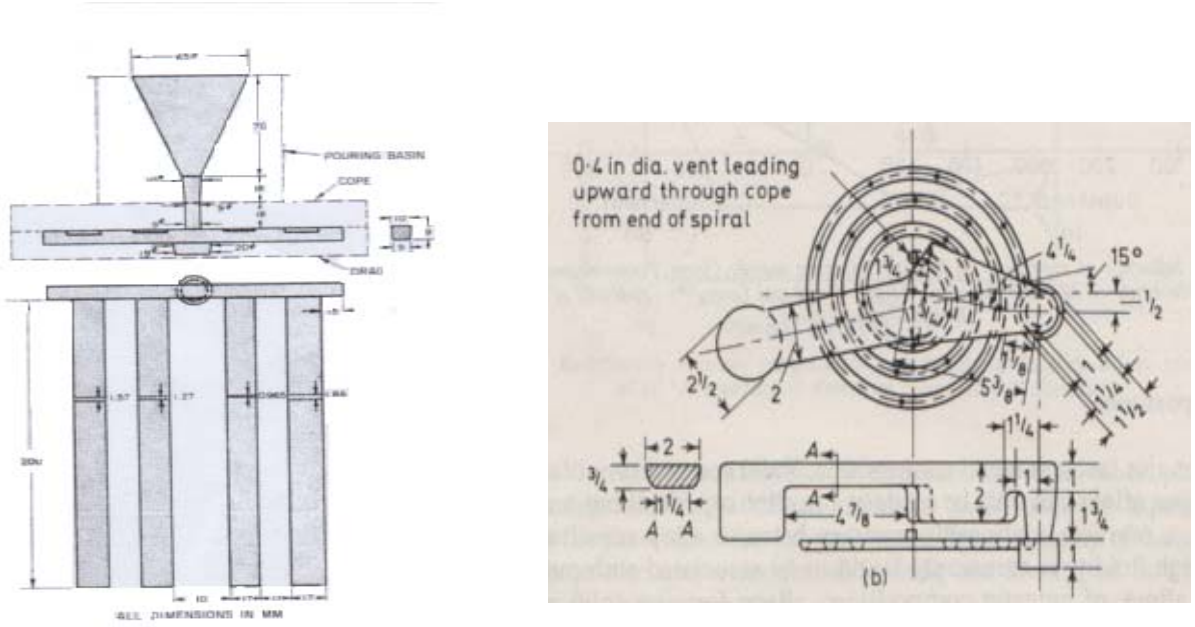

(a) (b)

Figure 2.4 design of the fluidity test mould. (a) Straight channel test [36]. (b) Spiral channel test [16]

Krynisky (cited by Beeley and Kondic) [25 and 36] reviewed much of the work on fluidity testing using a straight channel. These tests suffered from excessive length but, as a result, they yielded fluidity measurements which were sensitive even to small

changes in the thermal properties and surface characteristics of the mould. Taylor solved the problem of excessive length by using the spiral fluidity test and Kondic minimized the variation of the thermal properties and surface characteristics of the mould problem by using a graphite mould [16]. Murthy [37] assessed the fluidity of cast irons using both spiral and straight channel tests and found that the average length of spiral fluidity was more than double the average flow length measured using the straight channel test. In order to measure fluidity as a property of the metal alone, Ragone [38] and Fleming [15] used the vacuum fluidity test system, illustrated in Figure 2.5. In this system, the metal flows through a smooth glass tube under suction induced by a partial vacuum. By this procedure of testing, they eliminated the effect of the human factor on fluidity during the pouring process and fixed the value of the pressure head.

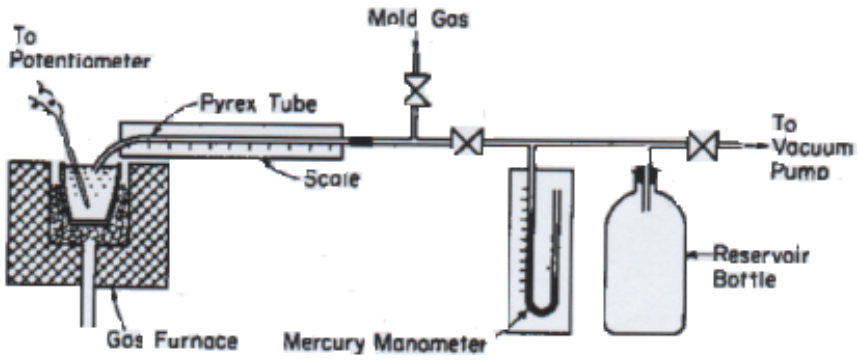

Figure 2.5 Vacuum fluidity test [15]

Horacek, developed a new method to evaluate the fluidity of alloy steel, casting into ceramic shell moulds with variable cross sections [39]. This new type of test incorporated ceramic foam filters to investigate the effect of the temperature of pouring and of the mould on the fluidity characteristics. The interesting finding of this work was that the fluidity of alloy steel was hardly affected at all by the filtration. Neff [40] measured the fluidity of aluminum foundry alloys with and without ceramic filtering. He found that filtering the

molten metal improved the fluidity, often by as much as 25%. Campbell and Green confirmed these results [41].

2.4.2 Solidification characteristic

Fleming [17] found that two types of solidification mode and flow arrest arise in pure metals and alloys, namely 1) the skin type; and 2) the pasty type. Their effect on the fluidity of A356 alloys is shown in Figure 2.6.

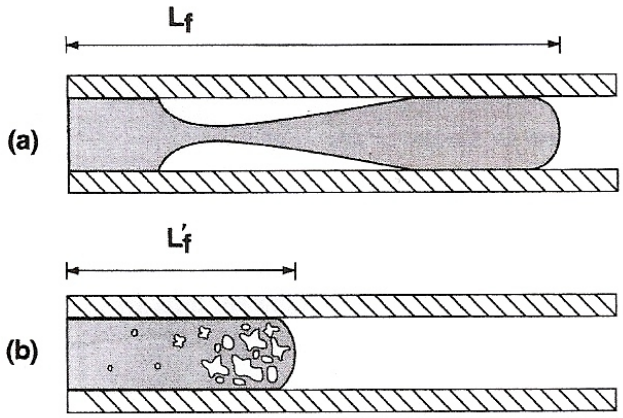

Figure 2.6 Arrest of flow by (a) complete solidification of a pure metal or eutectic and (b) partial solidification by long freezing range alloys [18]

The difference between these two flow arrest types is easily shown. In skin type solidification, columnar grains or a planar eutectic front grow from the mould wall in an approximately perpendicular direction aligned slightly against the stream of the liquid metal flow. The grains /fronts meet in the middle of the section, arresting the flow. Plane front solidification occurs in pure metals and eutectics, which have a short freezing range. Pasty type freezing and flow arrest occurs as a result of equiaxed grains that accumulate at the tip of advancing liquid. Flow is arrested as a result of friction between the impinging grains. This occurs in alloys which have a wide freezing range. Flemings [42] states that the amount of solid material required to arrest the flow depends on the metal head height. Campbell [6] has observed that, in

most practical situations, the critical fraction solid $f_{S_{Crit.}}$ required to arrest flow in the long freezing range alloys is between approximately 0.2 and 0.5. Therefore, it can be concluded that alloys with a long freezing range may have between only a fifth to a half the fluidity of pure metals.

2.4.3 Solidification time t_f

The solidification time is another parameter affecting the fluidity of metals, a point on which much research has been done. The purpose for most of this research is the attainment of good fluidity [1, 6].

Fleming estimated that the length of flow L_f can be related to the time of flow t_f, using a simple equation $L_f = V \times t_f$, assuming that the liquid had an approximately constant velocity, V. This equation demonstrates that the fluidity value is modified by the solidification time and implies that the longer the solidification time the further the metal will run before freezing, often giving a long period of fluidity. Even with an accurate estimate of t_f this equation will not apply, since the restriction of the channel does to some extent lower the velocity and give a reduced fluidity length [6, 18].

Chvorinov, cited by [6 and 42], has accounted for the effect of channel geometry on the freezing time, using the volume/cooling area ratio of the casting. This ratio is called the modulus of solidification (m). It is the equivalent to the ratio of the cross section channel area / channel perimeter. Thus, in Fleming's equation,

the solidification time $t_s = \frac{\pi}{16 k_m \rho_m C_m} \left(\frac{a \rho H}{T_m - T_O}\right)^2$ ----------2.1 equation becomes;

$$t_f = K_M m^2 \text{ ----------2.2}$$

Where k_m = thermal conductivity of mould $(Wm^{-1}K^{-1})$; ρ_m = density of the mould (kgm^{-3}); C_m = specific heat of mould (J/k_g); ρ = density of metal (kgm^{-3}); H = latent heat of solidification $(kJkg^{-1})$; a = section thickness of casting (m); T_o = ambient temperatire (ºC); T_m = melting point of metal (ºC); t_f = solidification time (s).

In general, Equation 2.2 is applicable where the heat flow from the casting can be controlled by the thermal conductivity of the mould. The value of K_M can be estimated by experiment.

The concept of the modulus is that the solidification time of the metals can be controlled by the modulus and any shape of channel can be understood and compared with any other [6].

2.4.4 Effect of the latent heat on fluidity

In practice it is important to realize that the improved fluidity of short versus long freezing range alloys forms the basis of much foundry technology, for instance, the relative importance of cast irons in the Fe-C system, and the eutectic Al-Si alloys contrasted with Al-Cu alloys [6].

Enthalpy also has an significant effect on the fluidity, because the solidification time is related directly to the quantity of heat ($Q = \rho_S V H_f$) which is released from the metal during solidification [43]. Campbell [18] used Fleming's Equation (2.1) to compare the fluidity of pure Si and Al and found that pure Si would have over 21 times the fluidity of pure Al, as a result of its higher latent heat. Campbell points out that the equation of Fleming which is used for comparison particularly is not quite correct; however, when it is used to compare the freezing time for two different metals, it gives consistent results.

2.4.5 Effect of the Velocity of the molten metal on fluidity

As regards the thin wall investment casting, many have stated that any increase in the velocity of the liquid metal leads to increased fluidity, thereby making it easier to fill completely a thin section. This is self evident from the simple formula assumed by Flemings $L_f = V \times t_f$. However, Campbell has since [6, 1] pointed out that, to produce a good casting, the melt velocity should not exceed a critical velocity V_{crit} above which the advancing metal stream may become free surface turbulent. The critical velocity is a function of the ratio of internal pressure and surface tension γ forces, $V=2(\gamma g/\rho)^{\frac{1}{4}}$ [6]. The critical velocities of liquid metals and alloys are in the range of 0.3 to 0.5 m/s.

Filling at a velocity that exceeds V_{crit} therefore results in folding and splashing from the flow and entrainment of air and oxide films with a consequent deleterious effect on the mechanical properties of the casting. The strength and ductility drop with increased velocity [6] (See Figure 2.7).

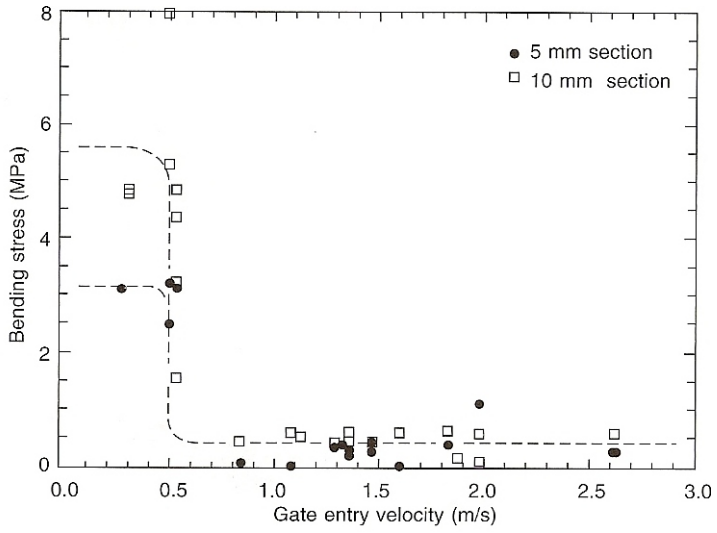

Figure 2.7 bending strength in Al alloys cast at different ingate velocities [6]

In a filling system which is not subject to the friction effect, the head height (h) of the casting rises. This is predictable given that $V= (2gh)^{0.5}$, because this makes fluidity

increase proportionally to $h^{0.5}$. But at the same time there is greater resistance to flow generated by $1/2\ \rho v^2$ due to turbulence in the bulk of the liquid [1]. Thus the velocity loses its tendency to increase. Tiryakioglu [45] has confirmed this finding

2.4.6 Fluid flow parameters in fluidity.

For several decades, numerical analysis of things such as fluid flow and heat transfer has been applied to mould filling system. A review of state-of–art was published by Cross et al. [46]. An aim of most casting process design activities is to find an optimum design of the runner system to achieve the objectives of quiescent flow and a suitable filling time [47].

Hwang [48] concluded that computation techniques for modelling the flow during filling can be divided into two categories:

1 -Energy balance techniques, based on the Bernoulli equation

2-Momentum balance techniques solving the Navier-Stokes equation, as embodied in the Marker-And-Cell group of programs (MAC).

The energy balance techniques are commonly used for the modelling of flow through the sprue, runner and ingates when the flow is controlled by the geometry of the system. Momentum equation balancing techniques are needed to calculate the flow inside the mould cavity where the direction and location of the fluid must be calculated.

Weng Sing [34] simulated the flow pattern of the molten metal during the filling of the runner system, using the MAC technique. This technique allows the evolution of flow domain as well as velocity and pressure distribution within the fluid to be computed. The calculated flow patterns were also compared with experimental

observations obtained using high speed filming of a plexiglass-water mould and showed good agreement.

In general, modelling is a numerical solution of the governing differential equation for a physical phenomenon under limited conditions. Thus it is necessary to understand the numerical method under boundary conditions which are selected to solve the particular problem and mathematical properties of the model.

Many commercial software packages are available for simulating the mould filling process. The background knowledge summarized in the following section relates particularly to the Flow Science Inc Flow-3D [49] software, which was applied in this research to model liquid metal flow.

1-Governing equations

Continuity, momentum and energy equations are the governing equations to describe the flow pattern of the liquid metal flowing into a thin channel [35]. The equations are described below.

2-Continuity equation

The continuity equation expresses the conservation of any quantity represented by the density which moves by flowing from one point to the next. The general form for a continuity equation is [50]:

$$\frac{\partial u}{\partial x}+\frac{\partial v}{\partial y}+\frac{\partial w}{\partial z}=0 \text{ ----------2.3}$$

where u, v and w are the velocity components in the x- y- z directions.

3-Momentum equation

The Navier-Stokes equation combines the fluid kinetics and constitution related to the momentum equation to express the motion of the incompressible, turbulence-free Newtonian fluid, where the fluid parameters exist with respect to the time. The general form in the x-direction is:

$$\frac{\partial u}{\partial t} + u\frac{\partial u}{\partial x} + v\frac{\partial u}{\partial y} = -\frac{\partial p}{\partial x}\mu(\frac{\partial^2 u}{\partial x^2} + \frac{\partial^2 u}{\partial y^2}) + g_x \text{ ----------2.4}$$

and in the y-direction is:

$$\frac{\partial u}{\partial t} + u\frac{\partial v}{\partial x} + v\frac{\partial v}{\partial y} = -\frac{\partial p}{\partial y} + \mu(\frac{\partial^2 v}{\partial x^2} + \frac{\partial^2 v}{\partial y^2}) + g_y \text{ ----------2.5}$$

where t is time, p is the pressure/density, μ is the viscosity/density and g is the acceleration of gravity. In the case of turbulent flow, v is replaced by the effective viscosity. Therefore, the Navier-Stokes equation in the x-direction and y-direction, together with the continuity equation, are the means for calculating the velocity pressure fields for the interior region. Generally, in the surface region the momentum balance principle still applies and hence the Navier-Stokes equation applies.

4-Energy equation

The energy equation for a Newtonian fluid is [51]:

$$\rho\frac{dh}{dt} = \frac{dp}{dt} + div(k\nabla T) + \tau'_{IJ}\frac{\partial u_i}{\partial x_j} \quad \text{----------2.6}$$

where h = fluid enthalpy, k = thermal conductivity, T = temperature, p = pressure.

This equation is determined under the first law of thermodynamics to simplify the general energy equation.

2.4.7 Heat loss during the filling of the mould

Recently, the fluid flow and heat transfer principles have become acceptable methods for use as a tool to improve the fluidity and the quality of the yield (free of misrun) in the casting process Campbell [1, 6].

Pioneering work has been done on the loss of heat from the flowing molten metal into the mould. The research carried out by Hlinka et al. [52] obtained plots of temperature drop versus time, using the ratio of runner total surface area (sq. in) to flow rate (lb/min) as a parameter (See Figure 2.8).

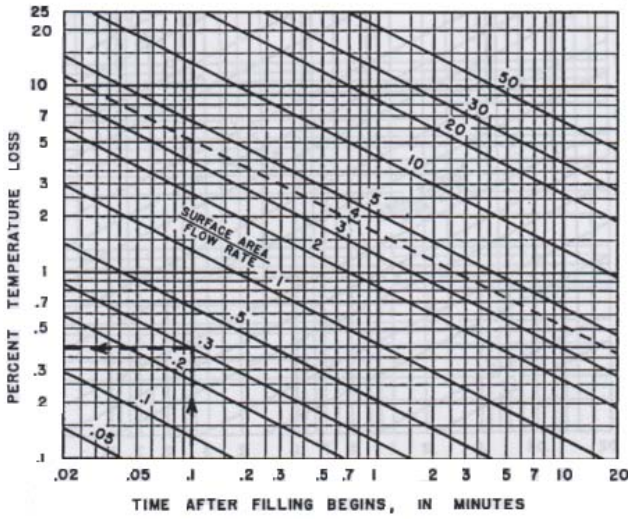

Figure 2.8. Per cent temperature loss vs. time for fixed value of the critical ratio of surface area to flow rate [52].

This method was implemented under two assumptions: 1) that there was no contact resistance between the sand mould and the flowing metal; and 2) that the flow advanced with constant velocity in the runner. This method showed that as metal flow velocity increases the heat lost decreases and the analysis permitted calculation of the progressive drop in heat loss throughout casting. Kim [53] developed a finite-element solution, for the mould-metal interface temperature for a very short time after pouring, based on the mathematical models of the transient filling process (See Figure 2.9).

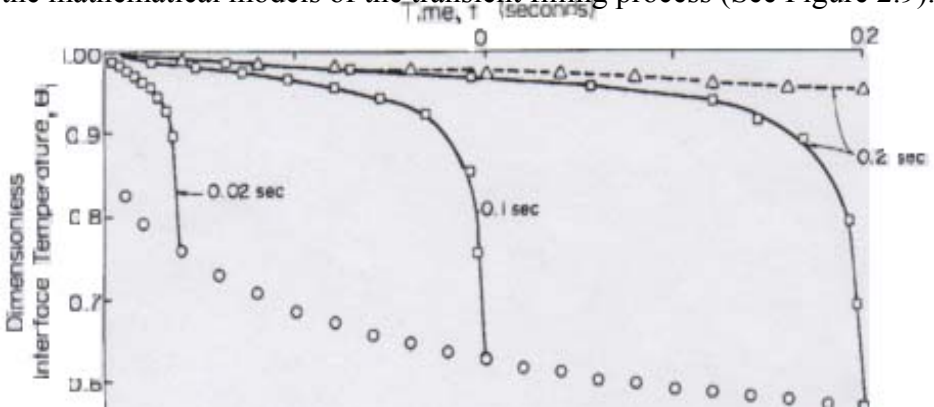

Figure 2.9 interface temperature distribution at the certain time [53]

The temperature profiles across the channel at various times were calculated by Sturm [39], who stated that a "successful filling of an investment casting is a decisive problem and determines the boundary conditions of the entire process. This is due to the heat loss of the melt in the thin walled section of the casting," and that " Estimation of the heat loss during filling the mould is a very complex problem as simulation of the flow pattern of the melt and the combined, heat transfer need much more physical effort than a poor heat flow." Sturm mentions that the first successful analytical modelling techniques were proposed by Wang [40].

A analytical method of evaluating fluidity was introduced by Flemings. He obtained fluidity values for cast metals from thermal properties alone. Using fluid flow and heat transfer, Flemings [9, 41] derived an equation for the fluidity length L of skin forming alloys, as follows:

$$L = \frac{\rho_s dU}{2h(T_{mould} - T_{Oo})}(H_f + C_p \Delta T) \text{ ---------- (2.7)}$$

Where $\rho =$ density of metal (kgm^{-3}); $d =$ radius of channel (m); $U =$ velocity of liquid stream tip (ms^{-1}); $C_p =$ specific heat of liquid metal (J/k_g); $H_f =$ latent heat of fusion (Jkg^{-1}); $h =$ average heat transfer coefficient $Wm^{-2}K^{-1}$; $\Delta T =$ superheat (ºC); $T_{mould} =$ mould temperature (ºC); $T_o =$ ambient temperatire (ºC).

Whilst the equation cannot give the temperature distribution along the channel, the main advantage of the equation is that it suffices to obtain the approximate fluidity of metals from their thermal properties alone, making minimal assumptions about their mode of freezing.

2.4.8 Effect of Process Variable on Fluidity

There are several variables as regards the metals, as well as the mould side, which have been found to affect fluidity; however, the combined effect of two or more variables on fluidity is sometimes disproportionately high [54]. Such effects are described in the following sections.

1- Pouring temperature

Most investigators have found that fluidity has a linear function with the pouring temperature [35, 18, 55-57]. Beeley [8] points out that the superheat is the quantity of heat which is released from the liquid metal before the solidification process begins; it directly affects the fluidity characteristics. . In discussing the relationship between fluidity and composition in the Al-Zn system cast at constant temperature in the experiments carried out by Lang [58], Campbell [18] found total fluidity to be a function of composition, equal to the sum of fluidity at zero superheat and an additional fluidity due to superheat at a certain temperature (See Figure2.10).

Campbell [3,10] has concluded that superheat has two effects on the fluidity of pure metals and eutectics: 1) the depression of the freezing temperature of the eutectic increases the relative superheat when studying fluidity of binary alloys cast at constant temperature, and 2) a diminished effect or benefit of intermetallic compounds on fluidity due to their normally high melting temperature that reduce the effective superheat casting at constant temperature. These effects are summarized in Figure 2.11. (Figure suggested from Campbell)

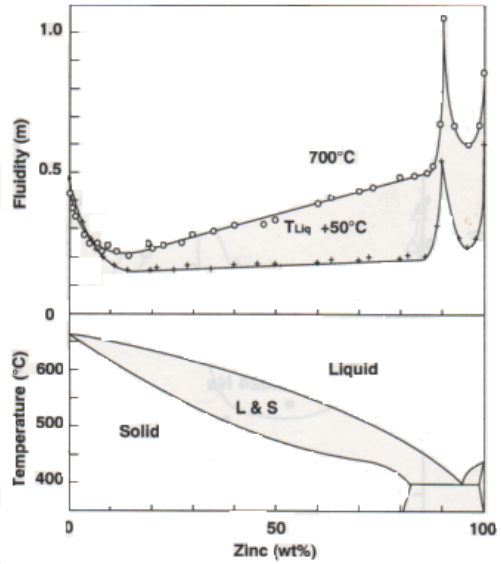

Figure 2.10 showing the fluidity at constant temperature, and the of enhanced fluidity of the eutectic when cast at constant temperature [18]

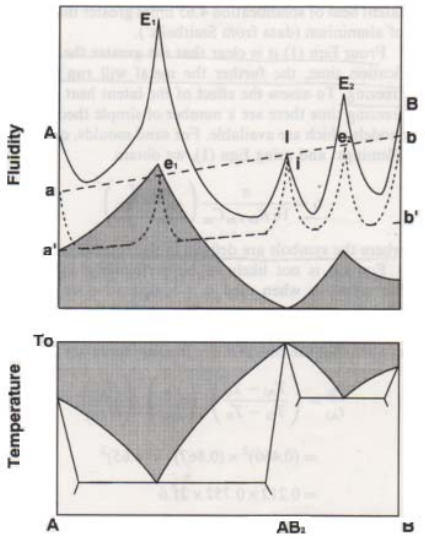

Figure 2.11 show the different behaviors of eutectic and intermetallic compound [18]

2-Casting Mould

The reduction in the rate of heat transfer between the mould and the environment benefits fluidity. For this reason, insulating ceramic coatings are normally applied to thin wall gravity castings in metal moulds.

Rivas [59], has investigated the effect of mould coating on fluidity. Flemings [60] reported that by using acetylene black coating on the sand mould, one can increase the fluidity by a factor of 2 or 3. He proposed that the action of carbon was an insulation effect, thus reducing interfacial heat transfer.

Campbell [6] suggested that if a mould or die coating is applied to prevent reaction, this will affect the filling. The action of wetting the mould prompts the familiar process of capillary attraction, which then draws the metal into the section. But capillary repulsion is induced by the curving meniscus, which discourages wetting.

In the field of investment casting, Brezina and Kondic [61] investigated the influence of the investment shell thickness. A thicker shell reduced the permeability of the mould

wall, thus causing back pressure from the residual air trapped in the mould, reducing the fluidity.

3-Chemical composition

Changes in the composition of alloys affect fluidity in different ways. In the case of phosphorus being added to grey iron, the fluidity is quantified in Figure (2.12). The powerful effect of phosphorus immediately reduces the liquidus temperature of the grey iron. Evans [62] has proved that fluidity is not affected by changes in the composition of the alloy, provided that the change of melting point is allowed for.

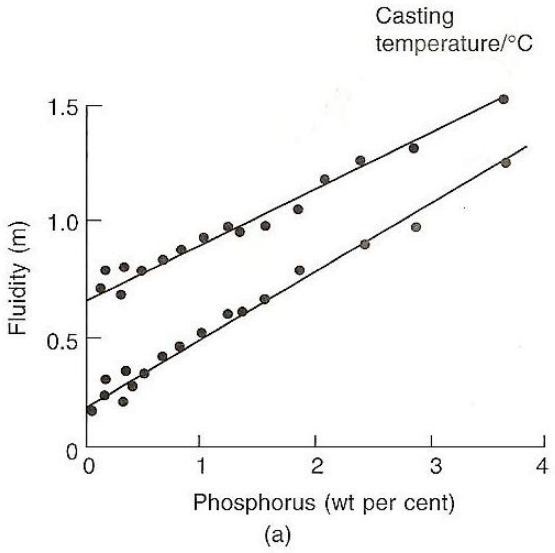

Figure 2.12 Effect of phosphorus on the fluidity of grey iron plotted [62]

Flemings [17] omits alloy composition effects from his account of fluidity. From his point of view, good fluidity is the only function of superheat. Campbell [6], however, discerned that any increase in fluidity is the result of three things: an increase in superheat, of composition change and of mode of solidification. Beeley [16] noted that the constitution, the mode of solidification, heat content, thermal properties of the metal and the time for cooling to reach freezing are the major factors which should be considered in comparing the fluidity of different alloys.

From his experimental data, Adefuye [63] has calculated the relationship of the fluidity composition between fluidity and Si level in an Al-Si alloy containing various levels of Si. The fluidity composition relationship shows an increase in fluidity as Si is increased, as a result of the high latent heat of the Si. Results are illustrated in Figure 2.13.

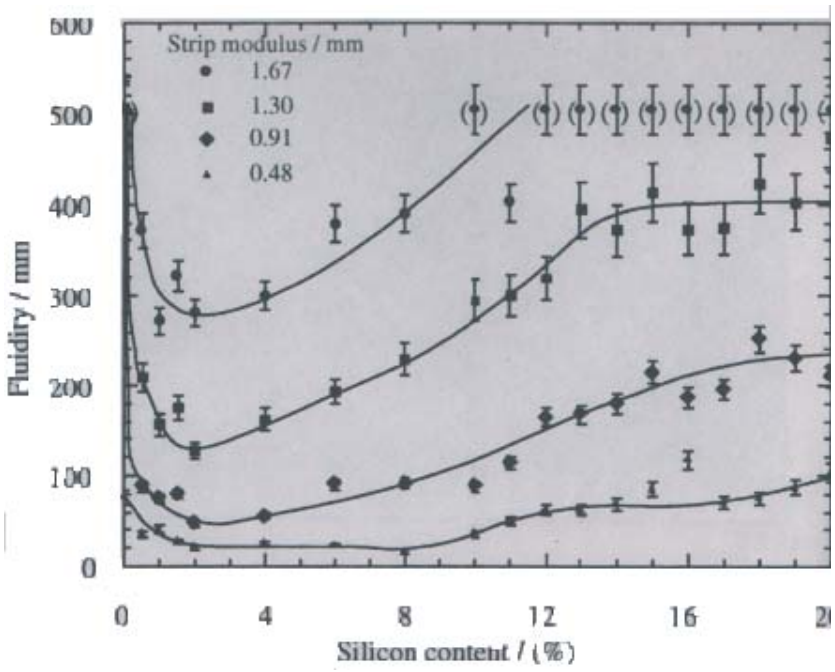

Figure 2.13 fluidity of super pure Al-Si alloys as a function of silicon content.[63]

Campbell [6,18] has stated that the fluidity of the eutectic appears to be higher than the straightforward method of mixing the alloy components. This increase in fluidity may result from one of two factors: 1) the effect of superheat on fluidity relative to the low freezing point eutectic; and 2) the effect of the shape of the crystals on fluidity relative to the intermetallic and eutectic with respect to their pure constituent elements.

Portevin [64] discusses the fluidity in the (Sb-Cd) system results. He suggests that the shape of the precipitating solid crystal affects the flow of molten metal, keeping it

liquid. This is because the dendritic crystal coherence point occur at low fraction solid creates more friction than the smooth crystals formed when the intermetallic compound solidifies.

2.4.9 Effects on fluidity of the thickness of the wall

Hoar and Atteron [65] have found that the surface tension is a significant factor in the flow into thin passages, and there is a relationship between surface tension and the metal head required to push the metal into the voids in a sand mould during casting. This is illustrated in Figure 2.14.

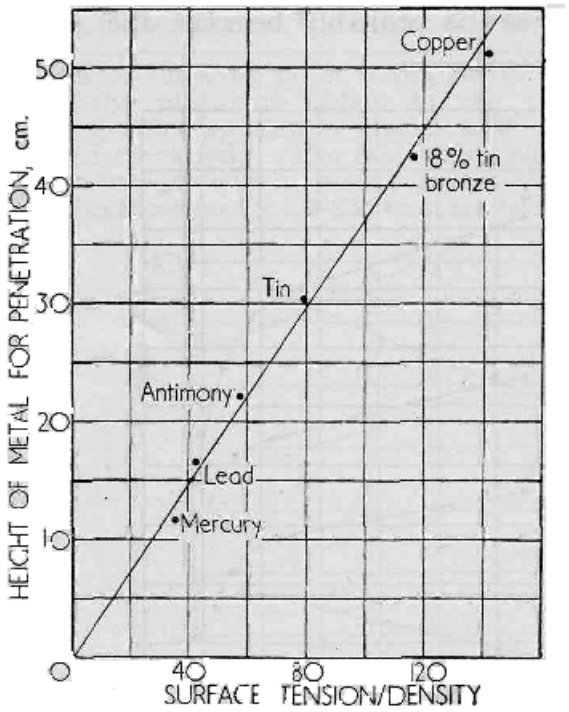

Figure 2.14 Relation between metal head and the ratio surface-tension / density for the molten metal [65].

Previously Sahoo and Whiting [66], in investigating the effect of the pouring temperature on the fluidity characteristics, plotted the relationship between the length of fluidity and various strip thicknesses, using the VK fluidity test, to assess the fluidity in a spiral. They found that the length of fluidity in certain pouring temperatures was proportional to the thickness of the strip. This is illustrated in Figure 2.15

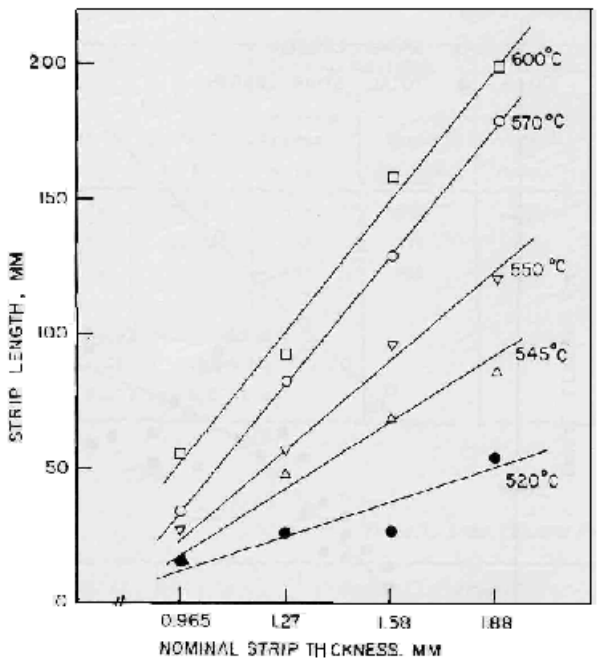

Figure2.15 Fluidity of ZA27 alloy as a function of the channel thickness [ ]

In Figure 2.16, Campbell [6] reinterpreted the experimental results of Sahoo and Whiting as fluidity as a function of strip thickness, to estimate the effect of surface tension in filling a thin section; he showed that the effect of surface tension is essential for making a comparison of the various sorts of fluidity. He revealed that the result indicates that the liquid metal can enter a minimum thickness of strip, so long as a suitable pressure head is available. The value of interest was over double that found for the surface tension of pure Al. Campbell justified this value as double the surface tension by saying that a strong oxide film was present on the stationary surface (as the result of the surface tension in a narrow channel) and therefore the thin section required additional tension in the surface to overcome the tensile strength of the film before the metal could advance. However, Anson and Gruzlieski [67] have measured the surface tension for aluminum alloy at 680ºC. From their experimental results it was found that oxygen absorption at the surface decreased the surface tension by more than 10%, confirming the earlier results of Gourmini and Joud [68].

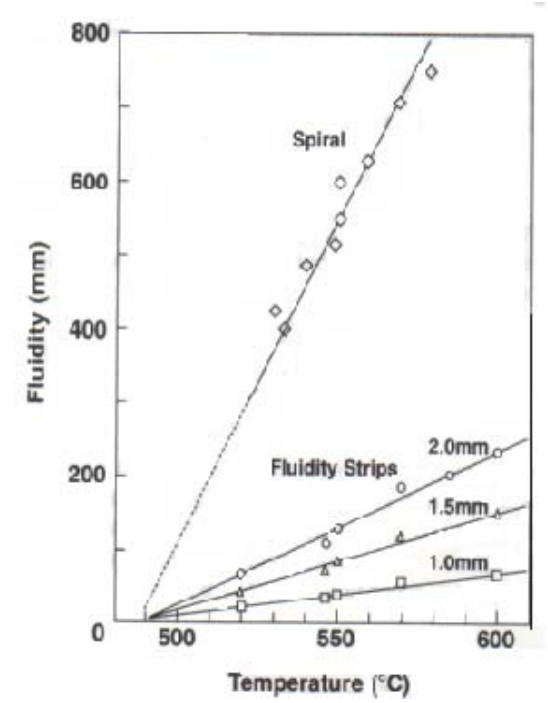

Figure 2.16 showing the effect of superheat explicity, as thought from strips with different thickness, using the data from Sahoo and Whiting

2.5 The effect of surface tension in thin section casting

Surface tension is a physical property. Accurate knowledge of the surface tension is important for improving fillability to produce castings free of misrun defects.

There are two force effects inside all liquids: 1) the coherence force: this force exists between molecules in liquids and is responsible for the surface tension phenomenon. (See Figure 2.17); and 2) the adhesive force, F : this force exists between the molecules of the liquid and the wall of the container and is responsible for the capillary phenomenon. This force can be quantified by the following equation: $F = \gamma 2\pi r$ where the r is shown in Figure 2.17) [69].

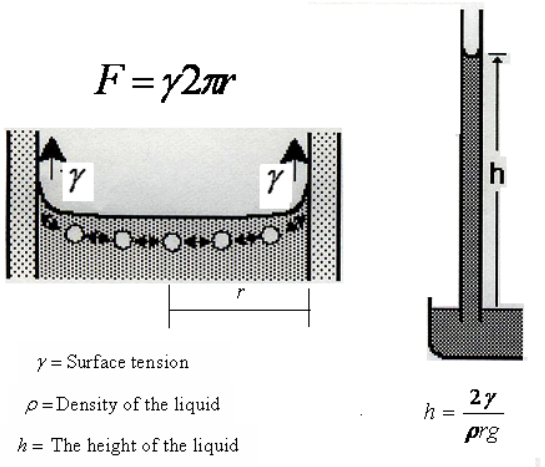

Figure 2.17 Adhesive forces [69]

2.5.1 Measuring surface tension

Surface tension is practically measured in Nm^{-1}. From a dynamic point of view, surface tension equals the force required to break off a length of 1 cm. at a constant temperature (N/m). This unit (N/m) is equivalent to the surface free energy (J/m^2) and the unit is also frequently used [70].

There are four methods of measuring surface tension [70]. These are: 1) the sessile drop method, the change in the profile of a drop observed under the effect of gravity; 2) the capillary height method: utilizing the capillary effect; 3) the bubble pressure method: assessing how much pressure is required to form and expand bubbles in the liquid; and 4) the Wilhelmy plate method: assessing how much force is required to pull an object from the liquid. The sessile drop method is commonly used to measure surface tension because it gives a good result at high temperatures and the mathemetical treatment of the result is simple [67] (see Figure 2.18).

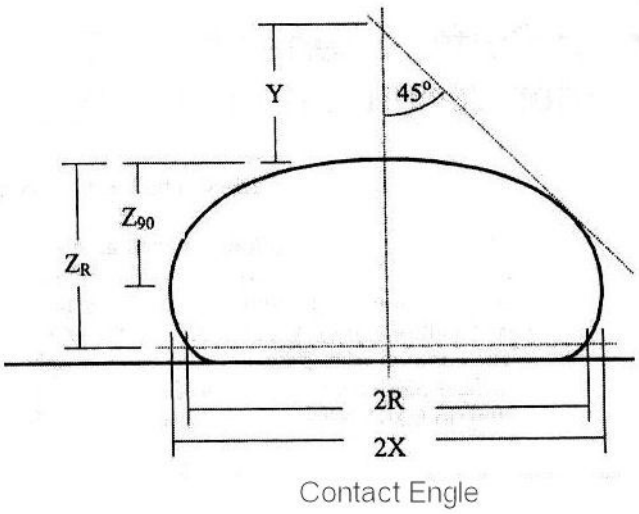

Figure 2.18 the dimension of a droplet for calculation of surface tension in sessile drop method [67]

From the size of the drop as a result of its own weight, surface tension can be calculated by the Dorsey equation. $\gamma = g\rho A^2$ ----------2.8

where $A^2 = X^2(0.05200/f - 0.12263 + 0.048f)$

and $f = Y/X - O.4142$

It is very difficult, however, to obtain accurate values for the surface tension of molten alloys, because the liquid density is not known accurately for most common alloys and the contamination (from bulk, substrate or temperature) is also another source of error in measuring surface tension [67]

2.5.2 Effect of oxidation on surface tension

In practice, the reactive nature of molten metals with oxygen and water vapour present in the atmosphere results in the formation of an oxide film, which affects the measured value of the surface tension for alloys. Keen, reviewing the surface tension of liquids [71], says that many studies have investigated the melt and that it tends to have an oxide layer, lowering surface tension in pure metals, and he concludes that the approximate value of surface tension for pure, unoxidised aluminum is between 1.05 and 1.10 N/m. Goumiri and Joud [68] investigated the effect of the oxygen on the surface tension of liquid aluminum, measured by using the sessile drop method. They

found that the surface tension is proportional to the oxygen and that it is reduced by more than 10% when the oxide layer is approximately one monolayer thick. They have concluded that the value of the surface tension for oxidised aluminum is equal to 0.865 N/m (See Figure 2.19).

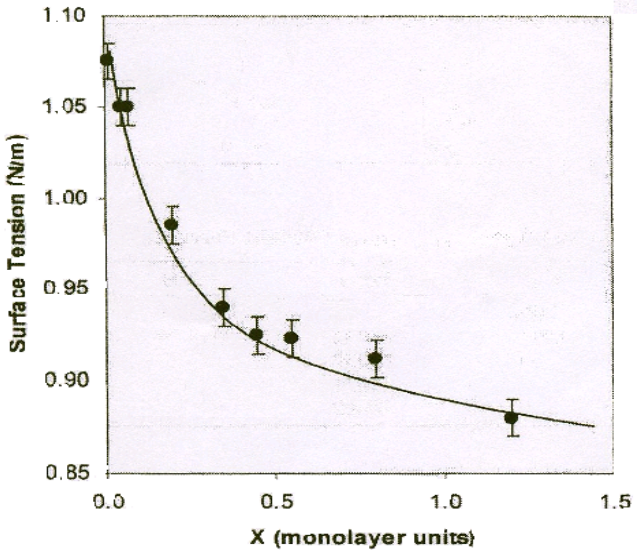

Figure 2.19 Dependence surface tension of aluminum as a function of monolayers of oxygen adsorbed on the liquid surface [68]

Anson and Gruzleski [67] used the sessile drop method to measure the surface tension coefficient of pure aluminum and aluminium-alloys. They observed two types of oxide and oxidation occuring on the liquid surface. The first were small islands of oxides on the sample surface; the second had the appearance of a greyish skin. The presence of islands did not affect the surface tension, but the film reduced γ by about 10%.

Likewise, Jimbo [72] measured the surface tension of liquid Fe-Cr-O alloys with varying oxygen content, using the sessile drop method. The result is plotted as surface tension versus oxygen content (see Figure 2.20). He observed that the surface tension decreased with increasing in the oxygen and chromium content.

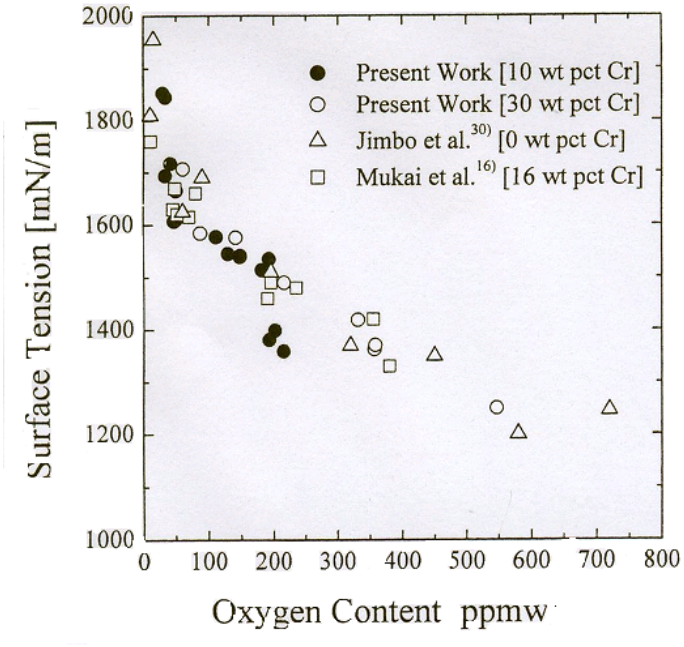

Figure 2.20 Surface tension of liquid Fe-Cr-O alloys as function of oxygen [72]

2.5.3 Temperature effect on the surface tension

Steven and Hani [73] used a new method to calculate the surface tension of molten aluminum as a function of temperature. In this method, a new formulation is developed to include potential, kinetic and surfaces force to describe the fluid dynamic of a liquid draining through an orifice under gravity. Bernoulli's equation was modified to include an additional term, namely, the quantity of pressure arising from surface tension. The formula is as follows:

$$\gamma = \rho g r \left[h_{\exp} - \frac{1}{2g} \left(\frac{Q_{\exp}}{C_d \pi r} \right)^2 \right] \text{----------2.9}$$

Where $Q_{\exp}$ = volumetric flow rate (m^3/s); C_d = discharge coefficient; $h_{\exp}$ = liquid heat (m).

Steven and Hani measured the surface tension of aluminium as a function of the temperature between 1973K to 1173K. The results are shown in Figure 2.21. Goicoechea [74] also measured the surface tension of Al-7Si% as a function of temperature. The results are illustrated in Figure 2.22

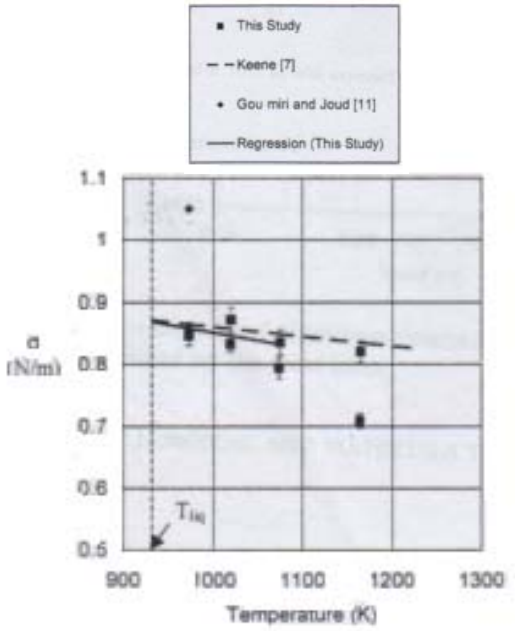

Figure 2.21 Surface tension as a function temperature for aluminum [73]

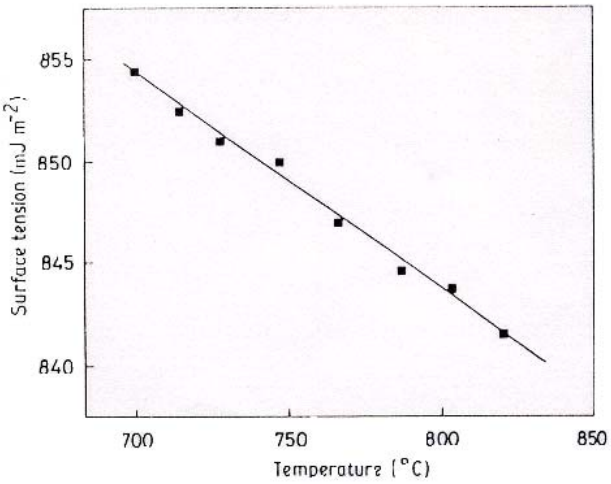

Figure 2.22 Surface tension as A function temperature for Al-Si alloys [74]

Steven and Hani explained the reduction in surface tension as being caused by increasing oxygen content, as a result of the increase in temperature.

Keen [71], in his review, proposed that the correlation of the surface tension of aluminum is a function of the temperature. The function is as follows:

$$(\gamma_T = \gamma_{liq} - \frac{d\gamma}{dT}(T - T_{liq})).\text{----------2.10}$$

Where $\gamma_T = $surface tension at constant temperature T (ºC) and $T = $constant temperature (ºC).

This correlation was done by examining the average results of most studies. The value given in the literature for surface tension showed agreement with Keen's formula; surface tension decreased with each increase in temperature.

Zushu and Kusuhiro [75] established that the surface tension of Nickel-base alloys decreased with increasing temperature (See Figure 2.23). They stated that the level of soluble oxygen has a significant effect on the surface tension value; Nickel-base alloys always tend to form an oxide film. Air is dissolved in the metal at high temperatures; this would cause an increase in the soluble oxygen content and the result is a sharp decrease in surface tension.

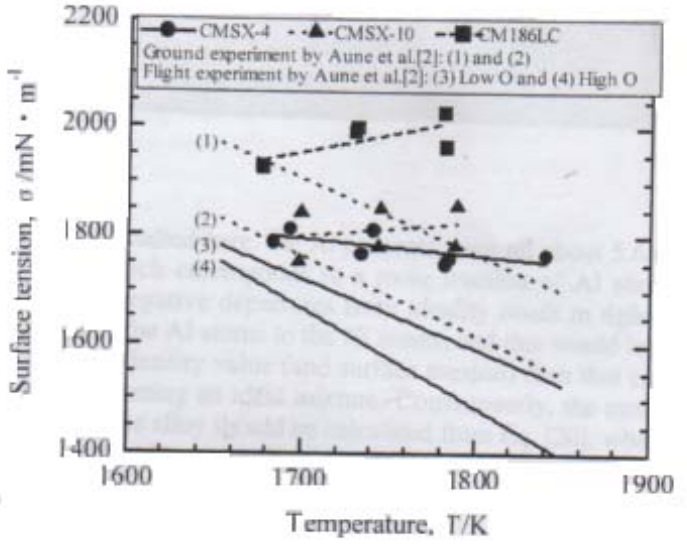

Figure 2.33 Surface tension of liquid superalloys as a function of temperature [75]

2.5.4 Dependence of surface tension on alloy composition

Goicoechea [74] stated that the surface tension decreases with increasing levels of silicon, magnesium and strontium in aluminum alloys. The results of Goicoechea are shown in Figure 2.24 and 2.25. The steep decline observed in surface tension with increasing solute content was considered to increase the oxidation of the elements (Mg, Si) in aluminum -alloys.

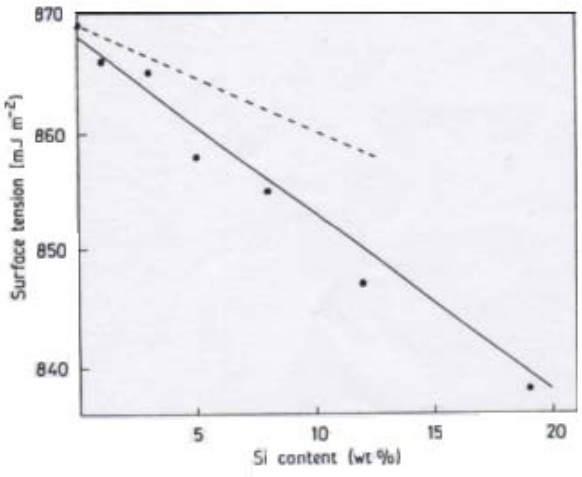

Figure 2.24 experimental data for Al-Si alloys as a function of Si content at 973K [74]

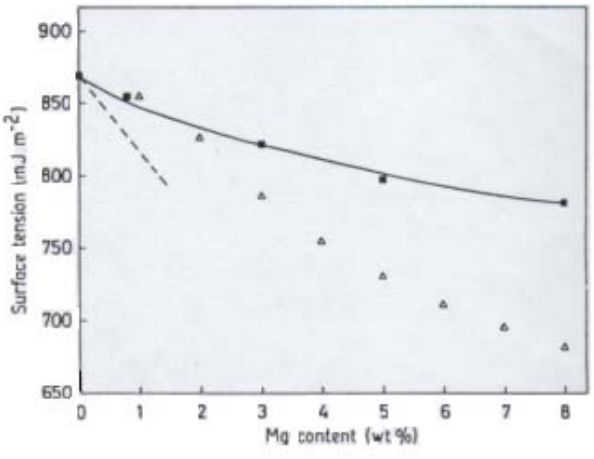

Figure 2.25 experimental data for Al-Mg alloys as a function of Mg content at 973K [74]

Jooho et. al. [65] used the sessile drop method to measure surface tension in liquid Fe-4%C-S alloys at 1623ºC. The surface tension of the liquid alloys was also calculated using thermodynamic models that were derivatives based on Butler's equation [77];

$$(\gamma = \gamma_i + \frac{RT}{S_i} \ln \frac{a_i^{\ s}}{a_i^{\ b}}) \text{ ----------2.11}$$

Where γ_i = surface tension of element i; R = gas constant; T = absolute temperature S_i = molar surface area; $a_i^{\ s}$ = activity of element i at the surface; $a_i^{\ b}$ = activity of element i in the bulk phase.

The calculations were found to be in good agreement with experimental data. It was found that surface tension was reduced in the samples with high Sulfur concentration at the surface, confirming that the surface tension in liquid Fe-4%C-S alloys decreases with increased Sulfur activity, as suggest by other researchers [78 and 79].

Summary

From the above, it is clear that fluidity has a major effect on the process of filling the mould and can be improved by controlling the factors relating to flow and heat transfer, including superheat, alloy composition and mode of solidification. However, providing the solidification effects are limited by a high enough temperature of the metal and the mould, fluidity plays no part in filling thin wall castings. This limitation with respect to filling in a gravity pouring condition is another matter, referring to the mechanical balance of the surface tension and hydrostatic pressure in the liquid. Possible techniques to increase the hydrostatic pressure, thus countering the repulsion of surface tension to improve the fluidity and produce sound casts (free of misrun defects) in thin wall investment casting are the subject of this thesis.

2.6 Heat transfer coefficient calculation in the casting

Numerical process simulation techniques applied to manufacturing processes is a commonplace activity in the design and development of efficient production. However, the results obtained from models still depends on the accuracy of the data describing the thermophysical properties of the material involved in the modelling processes and the boundary condition [80].

The physical meaning of the heat transfer coefficient is the amount of heat that can be passed through the unit area of the medium when the temperature in one boundary of the system is different from the temperature in the other and it is often used to evaluate the convection heat transfer rate between a moving fluid and a solid in thermodynamics [81].

The combination of the thermal boundary layer (caused by the heat transfer from the surface) and the velocity boundary layer (caused by friction between the solid surface and the liquid) governs the heat transfer from the surface. In relation to these two parameters, the heat transfer coefficient can be calculated by knowing the friction coefficient and the velocity gradient on the wall [82]. An important relationship can be derived from the conservation law related to the heat transfer coefficient and to the friction coefficient C_f:

$$C_f \frac{\mathrm{Re}_l}{2} = Nu$$

Where Nu the Nusselt number and Re is the Reynolds number.

For a fully developed laminar flow in a circular tube, the analytical Nusselt number is:

$$Nu = \frac{hD}{K} = 4.36$$

Molecular conduction refers to the way in which liquid metals transfer the heat in the bulk of the liquid. Sleicher and Rouse cited by [83], developed a correlation for liquid

metals for constant wall temperatures and constant heat flow. This correlation is reproduced in Equation (2.12); the result of this correlation is used primarily to gain understanding of the heat transfer mechanisms.

$$N_{Nu} = 4.8 + 0.0156(N_{\mathrm{Re}})^{0.85}(N_{\mathrm{Pr}})^{0.93} \text{----------(2.12)}$$

N_{Nu} = Nusselt number; N_{Pr} = Prandt number; N_{Re} = Reynold number

The thermal contact properties relative to the surface microtopology of the solid and the surface tension of the liquid influences the value of the heat transfer coefficient at the liquid-solid boundary during the casting of metals.

Timsit [84] has investigated the deformation of the surface of liquids with high surface tension by a rough solid substrate using an idealized geometry (See Figure 2.26), when the liquid does not fully wet the solid. He found that the true area of contact between a liquid and a rough solid depended on the surface microtopology of the solid and that the menisci of a liquid with relatively large lateral dimensions can be sustained around the idealized asperities, this is illustrated in Figure 2.27. Equation (2.13) (2.14) was derived by Timsit to calculate the true contact area between the liquid and solid boundaries under the effects of surface tension and hydrostatic pressure at the surface.

$$\alpha = \left(\frac{\gamma}{\rho g}\right)^{\frac{1}{2}} \text{ ---------- 2.13}$$

$$f = 1 - \frac{2\alpha^2}{d}\left(\frac{2h_s}{h(\alpha^2 + \beta h)}\right)^{\frac{1}{2}} \text{----------2.14}$$

where f = The ratio of the true area to the nominal area of contact; h_s = longitudinal asperity (μm); β = the radius of the curvature (μm) ; d = distance between two asperities (μm); h = liquid metal head (m)

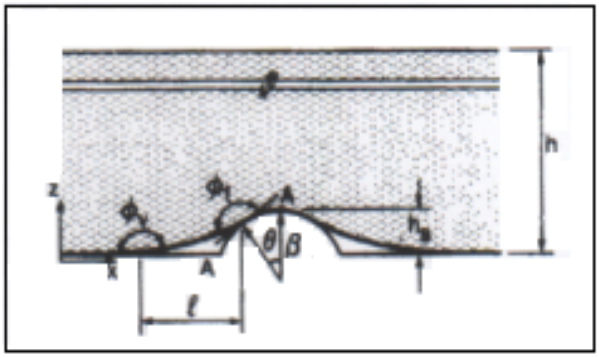

Figure 2.26 Geometry of the contact meniscus formed with the an asperity [84]

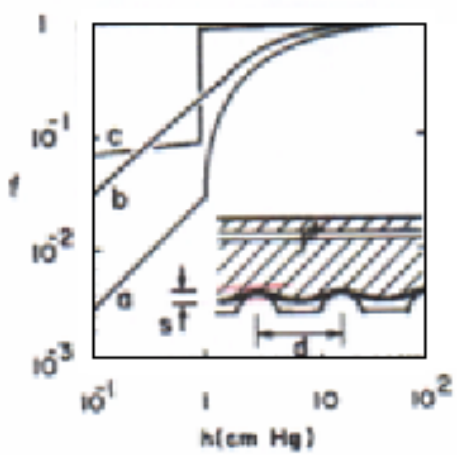

Figure 2.27 the ratio of the true of contact to the nominal area of contact as a function of metal head [84]

There are three ways in which heat is transferred to and from surfaces; conduction, convection and radiation. In the investment casting processes, most of the heat of the molten metal is transferred to the mould surface by conduction (through the gas arrest in the void between the rough casting and the wall of the mould). Griffiths [85], and Stemmler [86] ignored the heat loss in the radiation and convection phases during heat transfer coefficient calculations in aluminum casting processes.

The thermal resistance, R which is inversely proportional to the heat transfer coefficient, between the surface of the casting and the surface of the mould in the casting process can be estimated by the sum of the thermal resistances (R1) from the heat transfer properties of the mould and the thermal resistance (R2) from the heat transfer properties of the casting-mould interface.

From the literature available [86-90], two scenarios have been suggested to calculate the value of (R2) in the investment casting technique. In the first scenario, mould and casting are in contact when the metal is in the liquid state. The second scenario is the formation of an air gap between the mould and the casting.

Stemmler [86] assumed that when a gap is formed between the casting and the mould wall in the investment casting process, the value of (R2) can be calculated by two

components: one from radiation if the gap is very small, using Equation 2.15 and the other from the heat conduction of the gases, using Equation 2.16. However, in the case of contact between the casting and the mould the heat transfer coefficient can be calculated by using Equation 2.17.

$$h_{rsd} = \frac{\sigma(T_c^{\,4} - T_m^{\,4})}{(T_c - T_m)\left(\frac{1}{\varepsilon_c} + \frac{1}{\varepsilon_m}\right)} \quad \text{---------- 2.15}$$

Where $\sigma =$ Stefan-Boltzmann constant; $T_C =$ liquid metal temperature; $T_m =$ mould temperature; ε_c and ε_m are the radiation emissivities of the casting and the mould, respectively.

$$h_{gas} = \frac{\lambda_g}{g_n + l_o} \text{---------- 2.16}$$

Where $\lambda_g =$ thermal conductivity of the gap filling gas; $g_n =$ gap width; $l_o =$ gas molecules

$$h_{con} = h^* \left(\frac{P}{P_O}\right)^{\gamma} \text{---------- 2.17}$$

Where $P =$ contact pressure; $\gamma =$ constant value between 0.6 and 1. h^* and p_o have to be determined experimentally in order to gat a smooth transition for h_{con} between contact and gap situation

Ho and Pehlke [88] investigated the mechanisms under which the heat is transferred through the interface between the casting and the cooling surface, this mechanism is illustrated in Figure 2.28. They suggested that, initially, a thin skin of solid metal formed when the molten metal contacted the chilled surface and that heat is transferred from the casting to the chilled mould by conduction, through the peaks of the rough surface of the casting and the wall mould. During solidification an air gap is

formed as a result of the expansion of the mould and contraction the casting. This situation may lead to complete separation between the casting and the chilled surface. In this case a sharp drop will occur in the value of the heat transfer coefficient, because the heat extracted from the casting is insulated by the air gap. Griffiths [85] pointed out that it is convenient to assume that the atmosphere in the air gap between the casting and wall mould consists of air. It may also contain other gases with different thermal conductivity. Heat transfer by convection and radiation is negligible during the heat transfer coefficient calculation (in Al), because the air gap between the casting and the chilled surface is very small [84].

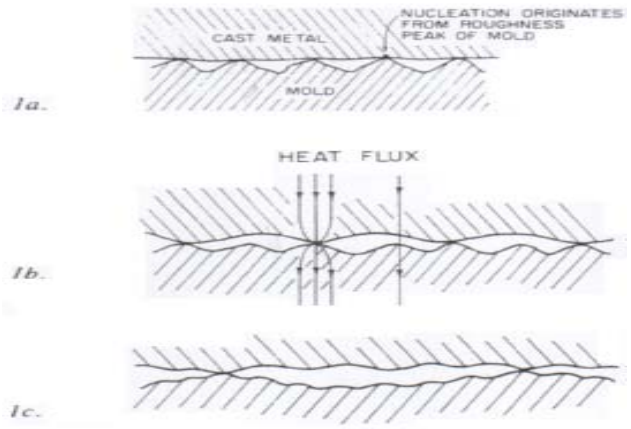

Figure 2.28 Mechanism of heat transfer at a metal-mould interface [88]

During the calculation of the true area of contact between liquid and solid, Timsit [84] observed that the length of the meniscus depends on the pressure which is applied. This observation is illustrated in Figure 2.29. With regard to this figure, it is clear that the length of the meniscus decreases when the pressure increases. This indicates that the true contact area between liquid and solid also increased: it increasing the value of the heat transfer coefficient between solid and liquid in the casting process. This assumption was confirmed by Mishida and Matsubara [91], cited in Pehlke [88]; they studied the effect of pressure on the metal-mould interfacial

heat transfer in die-casting. The results of this study are illustrated in Figure 2.30. It is clear from this figure that the heat transfer coefficient increase with each increased in the pressure applied.

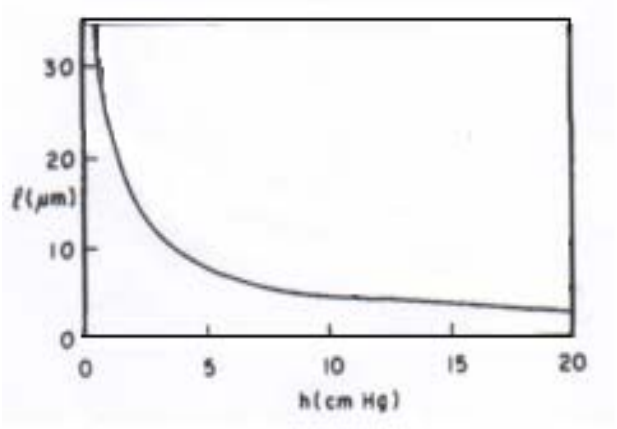

Figure 2.29 Meniscus length l depended on liquid height h [84]

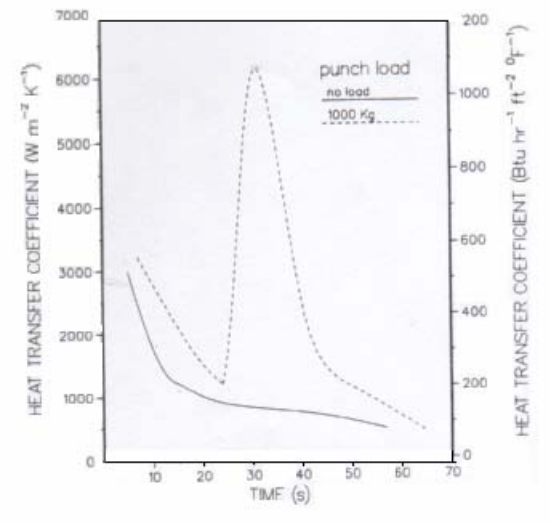

Figure 2.30 Transient metal mould interfacial heat transfer coefficient [91]

2.7 Vibration Method in Casting

Chernov made the first study of the use of vibration during the solidification of steel castings in 1868 (as cited by Deshpande [92]). He managed to produce some refinement of the grain structure by the rocking action of the mould. Campbell provided a critical review of more than two hundred studies concerning the influence of vibration during solidification [93].

Levinson [94] observed that a small pinhole in the welded seams of a mold leaked liquid only while vibration was applied. This has been interpreted to mean that vibration can inject liquid metal into a constricted channel, thereby augmenting the fluidity. Levinson tried to demonstrate quantitatively the effect of vibration on fluidity in a permanent mould fluidity test but was unsuccessful and he explained this by the fact that the chilling action of the mould inhibited fluidity. He inferred that vibration

might have an influence on apparent fluidity when this property is limited by the action of surface tension or surface oxide film.

Using vibration in the vacuum fluidity test. Flemings found that vibration does not increase the ability of metal to enter the small diameter test channel, because the vibration could not be applied so as to alter the effective metal head. However, he explained the effect of vibration in improving the ability of metal to enter holes of small diameter, on the basis that vibration increases the effective metal head. In addition, vibration increased the distance which the metal runs (its fluidity) into small holes in a casting. These effects were found to be greatest with small metal heads and are again attributable to an increased effective metal head. Vibration effect on metal head was illustrated in Figure 2.31.

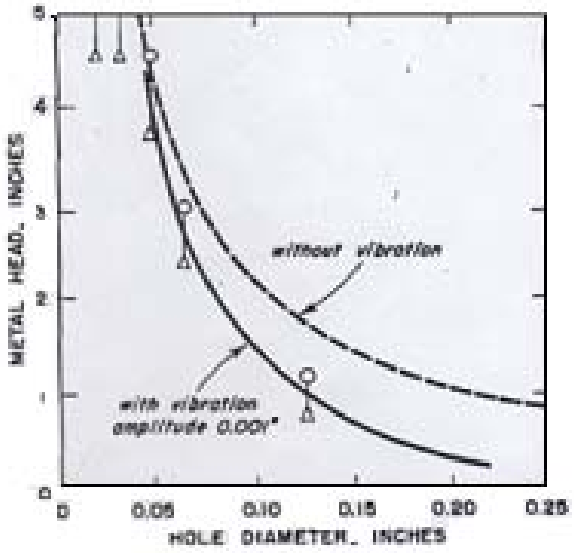

Figure 2.31 vibration effects on metal head in thin wall casting [15]

Wachter [95], in 1952, during a research programme into the effect of vibration on molten metal found that the low frequency vibration of most metals during solidification resulted in grain refinement, degassing and the separation of impurities. Work done with various liquid slurries in an attempt to find the physical phenomena

which caused the separation of impurities resulted in finding no change during conditions of vibration to the apparent fluidity or any other physical property of the liquid. Wachter explained the various phenomena due to vibration as resulting from fluctuating pressure generated due to the vibration acceleration forces on the liquid and the particles suspended in it. Upon analyzing the vibration of the forces acting on the metal in the mould, it was found that there was a pumping force generated at the entrance to the vertical passages used to evaluate the fluidity of the molten metal.

2.7.1 Vibration effect on filling process

From all the above studies, three main concepts emerge which explain why vibration improves the capability to fill thin section.

First is the ability of liquid metal to enter a small channel and the ability of liquid metal to flow through a constricting channel and both fill and feed a larger connecting channel. Both of these effects can be controlled either by surface tension or by the presence of surface oxide film. Vibration is employed to improve the apparent fluidity in any instance where the rate of freezing is not the controlling factor [94].

Second, vibration is a pumping force generated at the entrance to the vertical passages used to evaluate the fluidity of molten metals [95].

$$P_d = (\frac{a_d + g}{g})P_s \text{ ----------2.18}$$

where P_d (dynamic pressure), P_s (hydrostatic pressure), a_d (acceleration due vibration) and g (acceleration of gravity).

Third, vibration increases the distance run (fluidity) in a small channel; this effect is attributable to the increased effective metal head [35].

$$h = (\frac{g + a}{g} h) \text{ ----------2.19}$$

Where $h =$ metal head; $a =$ acceleration due to vibration; $g =$ acceleration of gravity

In fact, all these concepts assume that vibration generates acceleration to improve the apparent fluidity in the positive phase of the vibration frequency cycle. However, during the negative half of the cycle, it might be expected that any positive effect would be reversed, resulting in no net effect. However, the reverse action seems not to occur, for reasons which are not obvious at this stage, and will be a central issue for study in this thesis.

2.7.2 Vibration of the mould effect on the flow pattern of the liquid metal

Even without vibration, the hydrodynamic system in the fluid can generate periodical motion and has eigen-frequencies (capillary-gravitation waves). These eigen-frequencies are damped due to viscous dissipation (Dmitri [96]). Vibration influences equilibrium and flows in the hydrodynamic system with fluid interfaces, because the energy due to the vibration transfer to the system can lead to resonance excitation oscillation. The formation of harmonic waves on a free surface has been known since Faraday's first report of them in 1831 [97] (cited in [98-99]). Such imposed motion is known as 'Faraday excitation'. It causes parametric growth in one of the waves, when the forcing frequency becomes double that of the linear frequency of the wave and viscous dissipation is small [84].

Royna [100] and Lyubimov [101 and 102] modified the Faraday equation of the vibrational excitation of resonance oscillation of the fluid, and identified the regime of the parametric wave's excitation. A theoretical investigation of instability of parametric waves was carried out by Fauve, cited in [96]. Calculation showed that viscosity is the strongest factor affecting the threshold of excitation of parametric resonance.

Forster [103] derived an equation to describe the situation of the capillary-gravitation wave in a liquid generating second or sub-harmonic resonance at precise frequencies, when the container was vibrated in a vertical direction. By evaluating the equation in

two types of forcing frequency (external resonance and internal resonance), he found that with Faraday forcing of the waves at low frequency, the equation can be transformed into an unforced resonance equation, and the solution can never grow without bound, because the resonant interaction of the two waves always prevents a continuous gain of energy from the container oscillations. However, if the wave is forced to greater frequency, the equation cannot be solved. Then sub-harmonic resonances are absent and the excited wave frequency coincides with the frequency of the container vibration, although the resonance is also parametric. Vertical high frequency vibration experiments were made by Bezdenezhnykh, cited in [96]. The results showed a stabilization of the fluid interface at a frequency higher than the critical value, which depended on viscosity. A horizontal high frequency vibration experiment by Wolf [104] and Lyubimov [101] showed that the instability threshold of the free surface of the liquid can be controlled by a vibration velocity parameter $(a\omega)$, but not by the vibration amplitude a and frequency ω applied separately.

Campbell [93] stated that when the thickness of the casting is greater than the wavelength of the high frequency vibration, the standing-wave pattern appears, as shown in Figure 2.32; the resonance condition arises under condition where there is intense vibration in the antinodes.

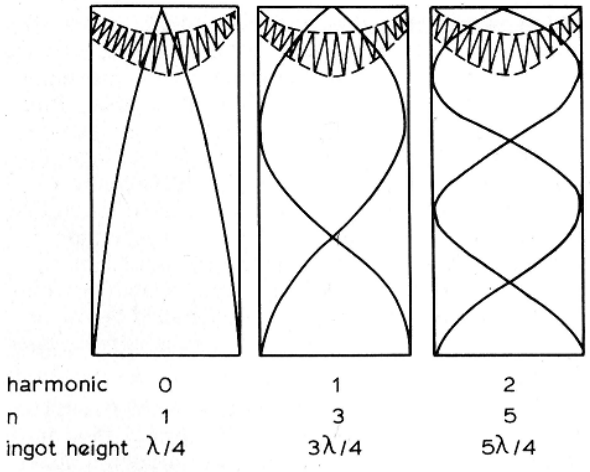

Figure 2.32 standing wave patterns with ingot height vibrated from the base [93]

The amplitude-frequency $(f-a)$ map of the occurrence of standing-waves on the free liquid surface under vibration casting conditions, see Figure 2.33, shows that the harmonic number of the resonance provides sufficient energy for the liquid to be ejected from the melt.

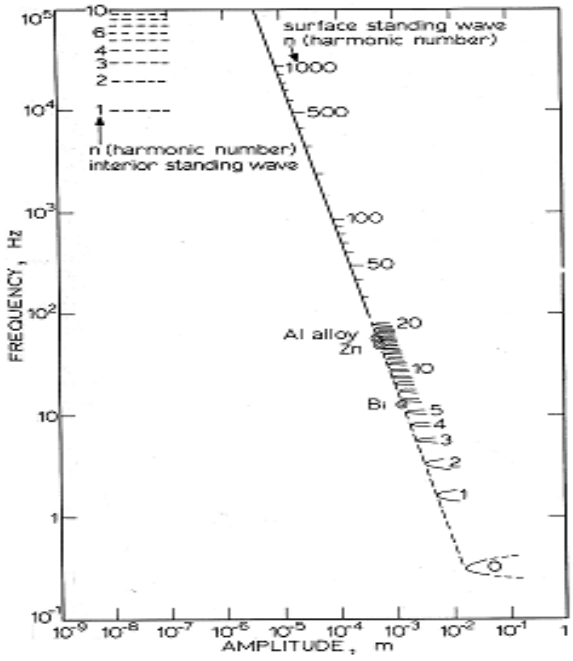

Figure 2.33 $(f-a)$ map, show the harmonic number of resonances required to eject the liquid metal from the free surface at top of casting [93]

Campbell [93] used a formulation for the velocity of the surface wave $(u = 2\pi\gamma / \lambda\rho^{1/2})$ [105] to calculate which frequency of resonance is required to eject

the liquid from the melt on the surface on top of the casting under vibration conditions: and obtained the relationship

$$f^2 = \frac{\pi\gamma}{4\rho}\left(\frac{2n}{D}\right)^2 \text{---------- 2.20}$$

Where $n =$ harmonic number; f = frequency (Hz); D = diameter of ingot (m).

It is evident that resonance can occur at a frequency above 10 kHz and below 3 kHz in two aluminum castings, both in the same section with different heights (100mm and 300mm respectively) [93].

Recent work by Boris [106], in a study of the effect of vibration on the structure and flow of the liquid during a phase change, revealed that vibration applied orthogonally to the flow direction decreased the shear viscosity in the fluid flow, but only when it was in the semisolid state. However, the liquid state rheological properties showed structural behavior remains insensitive to the application of vibration.

2.7.3 Advantages and disadvantage of vibration

It seems clear that vibration improves in some way the mould filling capacity. This improvement has a linear relationship with the applied acceleration at low frequencies and low frequency vibration is more easily applied than high frequency vibration. Actually, higher vibration intensities are not desirable for use in casting, because they create many problems, such as hot tear defects and actual ejection of the metal from the mould, cavitations in the liquid leading to porosity and damage to the mould [94, 95]. Campbell [93] concluded in his review of the effect of vibration during solidification that shrinkage porosity can be reduced by vibration operating below the cavitations threshold, but there seems a small risk of increased porosity if the threshold is exceeded (see Fig. (2.34)).

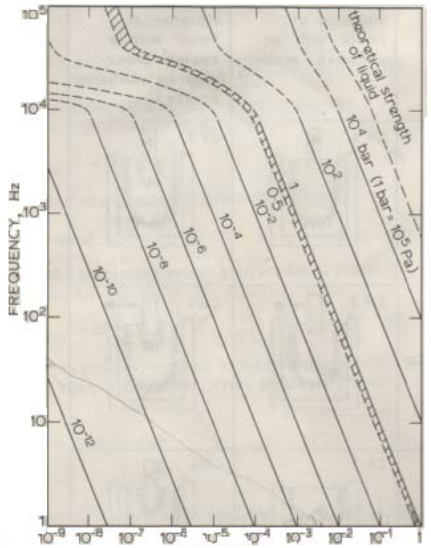

Figure 2.34 ($f - a$) Map showing peak pressure generated by vibration, shaded region indicates threshold for cavitations [93]

Recent research by Deshpande and Makhlouf [92] found that vibration of the mould during the solidification process of Al-Cu alloys caused a reduction in the average grain diameter in the casting and shifts the dendrite coherency point towards a lower temperature and higher fraction solid. Both these factors acted in such a way as to reduce the hot tearing tendency of the alloys. They assessed these defects by modifying the Crack Susceptibility Criterion. In addition, they found that vibration reduced the solidification time of the casting studied.

Recent research done by Campbell [6, 107] showed that hot tear is often a result of opened bifilms, previously straightened by dendrite pushing or other processes. The hot tear results simply from the contraction strain causing the bifilms to open and create a hot crack [107] such defects thus nucleate from poor filling system design that causes surface turbulent flow during the pouring process.

Therefore, these crack and hot tear defects in the casting process, are not exacerbated by and do not result from vibration, as some supposed, but are caused by unsound filling system designs.

Campbell [93] stated that the advantages of the application of vibration to a casting during solidification are: i) homogeneity of structure and properties; ii) reduced microseagregation and improved resistance to corrosion; iii) improvement in apparently all mechanical properties measured (so far), such as hardness, ultimate tensile strength, elongation and reduction of area for all the material checked so far. Pillai [108] confirmed that during investigation of the vibration effect on the mechanical properties of casting he found that mould vibration improved hardness, UTS and elongation in the casting. Abu-Dheir [8] also noted that the vibration applied during solidification of Al-Si alloys is an acceptable technique for improving mechanical properties.

Davey [109] added that the improvement of the surface finish of pressure die castings was achieved by applying vibration to the die.

2.8 Filling System Design

Green and Campbell have studied the effect of surface turbulence on the mechanical reliability of Al-7Si-Mg castings [3,4]. They found that the crack defects in the casting result from the folding action in the surface of the liquid metal when the velocity of the advancing liquid metal front exceeded the critical velocity in the range of 0.5m/s, as defined by Runyoro et. al. [110]. Such defects reduced the strength of the castings. Green was the first one to use the Weibull statistic to quantify the randomness of the properties and the effect of surface turbulence [11]. He has found that where the surface turbulence results from the metal velocity in the range of 40-80 m /s, the Weibull modulus is in the range of 1 to 5; however, in good gravity filling system the range is 50-150.

Campbell formulated the mechanism of formation of casting defects, such as double oxide films in the liquid, bubble damage as a result of air entrainment in the liquid

and bubbles as the result of core outgassing. He concluded that to avoid these defects it is important to provide a good filling system, and he recommended that certain general rules should be taken into account in the filling system design to produce a good casting. These rules cover all the specific features of the casting (basin, sprue, runner and gate) [13].

Much research has been done at Birmingham University to establish the principles of filling systems design to avoid such common defects in the casting process as porosity and inclusions. It has been established that by controlling the velocity of the liquid metals at the ingate, this being targeted to be less than a critical velocity of 0.5 ms^{-1} improved casting integrity can be achieved. Thus features and dimensions of the runner, basin, sprue and ingates are chosen to ensure that the velocity of melt entering the mould cavity does not exceed this critical value. Of course, reducing the velocity excessively encourages mis-runs [11].

Generally, in a casting process there are two types of filling system: top filled and bottom filled. In the case of top filling, the liquid metal is poured directly from above and falls into the cavity of the mould at high speed. It is commonly used because it is simple and wax assemblies for investment casting are inherently more mechanically robust. The disadvantages of this kind of filling system are :1) uncontrolled surface turbulence of the liquid metal, which generates entrainment defects in the casting, such as double oxide films; and 2) the operator affects the quality of casting, not the filling system itself (see Figure (2.35)). In contrast, in the bottom-filled design, the metal enters the mould at its base and fills the mould cavity in substantially counter-gravity mode (see Figure (2.36)). If this mode of filling is carried out correctly, we can eliminate the surface turbulence of the liquid during the filling of the mould

cavity. Therefore this can produce castings of good quality [11]. For this reason the bottom filling system will be used in the present work.

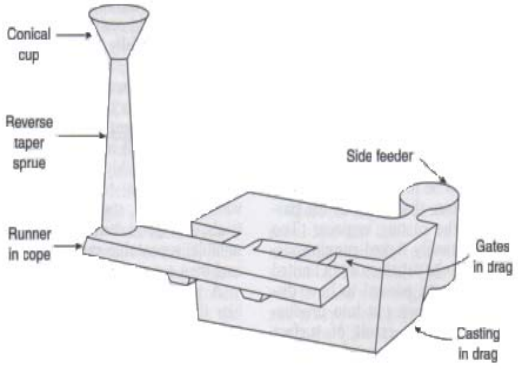

Figure 2.35 Top-filling system

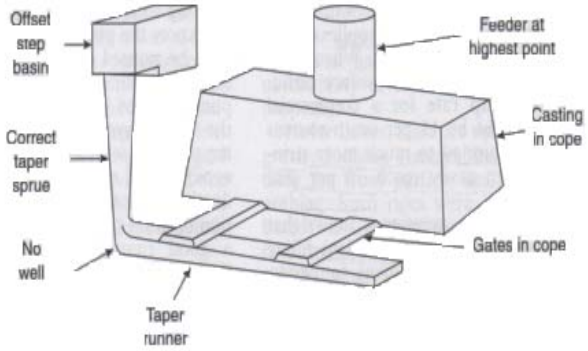

Figure 2.36 Bottom-filling system

2.9 Reliability of castings

During the investigation of filling defects such as porosity and oxide films and their effect on the quality of casting for Al-7Si-Mg alloy, Green and Campbell [95] used the Weibull distribution function to analyze the tensile strength data and used the Weibull modulus as a criterion to assess the reliability so as to identify the optimized casting condition. They found that filling defects were associated with a scatter of tensile properties and Weibull modulus; this reflected on the reliability of the casting. Nyahumwa and Green [98] used the Weibull modulus to indicate the quality of casting during their investigation of the oxide film effect on the fatigue life properties. The Weibull distribution function together with real time X-ray visualisation and computer modelling fluid flow proof is a powerful tool to assess the quality of casting and it allows us to investigate the oxide film and porosity effects on the quality in more quantitative ways.

2.9.1 Assessment of reliability of the casting

When a great many mechanical tests are made on the material, the data which are obtained from experiments such as UTS are commonly scattered about the median value. The reliability of the mechanical properties of the metal can be estimated by the scale of this scatter [111].

There are many statistical techniques used as tools to assess the distribution of the data scatter, such as normal distribution, Log-normal distribution, Gamma and Weibull distribution (Green and Campell [3]).

Green and Campbell [4] used these techniques to determine which of them gives the best estimation of the quality of casting by describing the scale of the data scatter for tensile tests. They concluded that the Weibull distribution was the most suitable model to describe the distribution of tensile strength of Al-Si-Mg castings. This statistical function was introduced by Weibull in 1951 and is applied in many fields to analyze data [112]. Over the years, the Weibull distribution has been a powerful tool to describe the mechanical property data of material which failed because of a single defect and has been established in engineering materials as a tool in the field of fracture, due to its mathematical simplicity and relatively high success in describing most data (Khalili and Kromp [113]).

2.9.2 Weibull parameter

Two independent parameters determine the shape of the Weibull probability function, which is used to describe the scatter of the data from the mean value. Its form is

$$Fw = 1 - \exp\left[-\left(\frac{x}{\sigma}\right)^{\lambda}\right] \qquad \text{----------(2.21)}$$

Where Fw is the probability of failure

x is the measured variable (tensile strength)

σ is the characteristic value (stress) at which 1/e specimens survive

λ is the modulus (the greater value of modulus λ, the narrower the spread of the variable x)

The Weibull distribution can be plotted as a straight line by taking the double natural logarithm of the probability of failure survival $(1 - Fw)$ and plotting this as a function of the natural logarithm of tensile strength. This is often referred to as a Weibull plot and produces a best fit line with slope λ.

The true value of Fw for each specimen can be estimated by ranking the tensile result in order from the highest to the lowest in value, where j represents the rank order. Then the probability of failure-based Fj on rank can be estimated from $Fj = (j - 0.5)/N$, where N is the total number of specimens tested (Khalili [113]). The Weibull distributed function is applied to fit each data set so as to quantify the scatter of the data. Linear regression is used to evaluate the Weibull modulus λ.

Chapter 3

Apparatus and Experimental procedure

A series of experiments were designed to evaluate the effect of vibration conditions on the filling capability of molten metal in thin section thickness of 0.55mm in investment shell moulds and to investigate the mechanisms of liquid advance, determining the dominant control parameter.

The experiment adopted two different filling processes: the fluidity (flowability) filling type and the fillability filling type, and compared results with and without vibration.

3.1 Equipment

3.1.1 Vibrator table

An experimental vibrator table was operated in a manner as similar as possible to that envisaged of an industrial process.

The vibrator table of dimension $0.75m \times 0.75m$ was manufactured by (MOGENSEN) with an output of 500 N force, sufficient to vibrate the weight of investment shell moulds and securely fixture then. The table was vibrated by an eccentric rotor motor. The frequency can be set to between 0 to 25 Hz and was controlled through the current input, whilst the amplitude of vibration of between 0 and 2mm was controlled by adjusting the weight on the rotor main shaft. The table is shown in Figure 3.1.

Figure 3.1 Vibrator table

3.1.2 Vibration meter

An electronic accelerometer VOBSUM3000 (frequency range 5 to 600Hz, amplitude range 0 to 30mm) (see Figure 3.2) was used to measure and set the experimental frequency and amplitude. The unit also reported acceleration in the range 0.2 to 100g. The wave form was sufficiently close to sinusoidal to permit the calculation of peak acceleration from the amplitude and frequency without serious error.

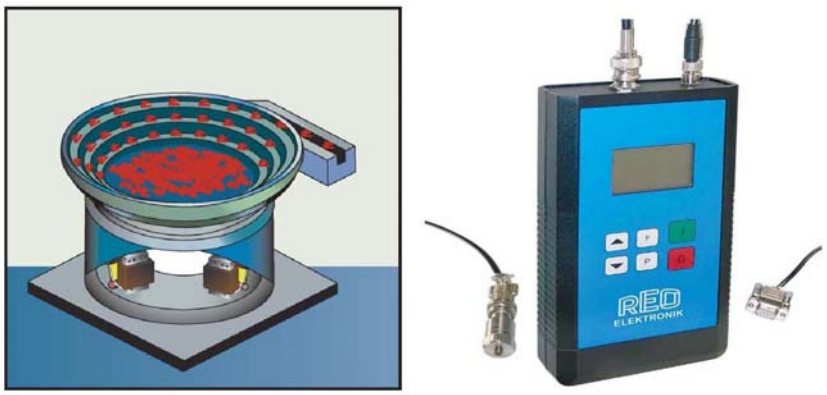

(a) (b)

Figure 3.2 (a) Electronic accelerometer (with 5% accuracy) and (b) VOBSUM3000 device with LCD-Display.

3.1.3 Fixture

A fixture to secure moulds to the table was made of steel sheets. It consisted of two pieces, an upper and a lower plate with dimensions of $300mm \times 200mm \times 5mm$ and $500mm \times 500mm \times 10mm$ respectively. The upper plate had a hole of 120mm diameter and the lower plate had 4 screws bolts (M10). The fixture clamped the ceramic mould upon the vibrator table by the 4 bolts to ensure that all the vibration energy was transferred to the ceramic shell, preventing any secondary motion during operation. The ceramic mould was usually placed in the centre of the fixture. The fixture is shown in Figure3.3. To ensure that mould survived the vibration experiments a minimum shell thickness of 11mm was used.

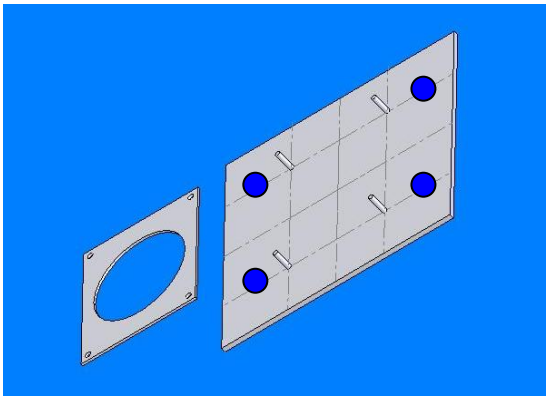

Figure 3.3 view of the fixture used to secure mould to the vibrating table

3.2 Materials

For all experiments the commercial aluminum alloy A356 was used, the chemical composition of which is shown in Table 3.1.

The Al-Si-Mg alloy was selected on grounds of, it's relatively narrow-freezing range, reaction with oxygen in the air to generate an oxide film (Al_2O_3) on the surface of the melt (potentially leading to instances of defects in castings) and reasonable fluidity. Thermodynamic data and material property data are also well established. Solidification with an equiaxed dendritic grain structure is anticipated.

3.3 Runner system design

The mould design is shown in Figure 3.4. The design complies with the requirement of ensuring that a gate entry velocity is less than the critical filling velocity (V_{ingate} <0.5m/s) [121]. The specific features of the casting system (pouring basin, down sprue, runners and ingate (See Table 3.2)) were designed to confirm to the rules for bottom gated filling system design developed and outlined previously by Campbell [13].A vent was added to the top of the mould to eliminate the influence of back pressure due to residual gas in the cavity mould.

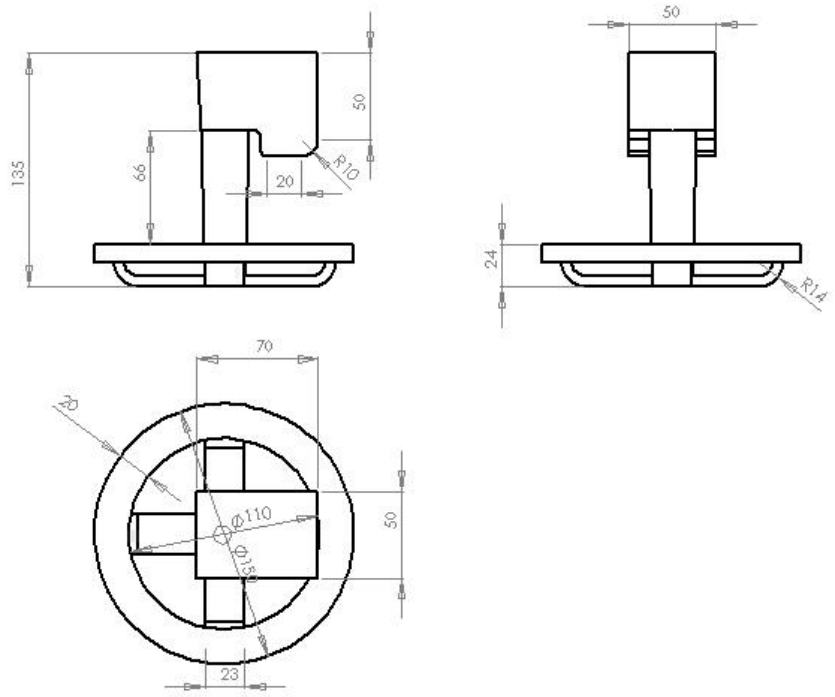

Figure 3.4 Runner system design

The following parameters were investigated before the actual casting process to find the optimum experimental condition.

3.31 Pouring Basin

An off-set basin (with a radius over the top of the sprue inlet) was used to ensure smooth flow of metal out of the basin and into the sprue [122]. The dimensions of the basin were chosen as $50mm \times 50mm$ and height ($50mm$). It was designed to be large enough to allow the melt to be poured in quickly and to then maintain a constant head height. The casting time was between approximately 1.5 to 2 s.

3.3.2 Pouring Rate.

The total weight of the strip and runner system was estimated to be 1.5 kg and the filling time, guided by experience, was selected to be 1.5 sec. These values defined an

average filling rate of $1\,Kgs^{-1}$ giving an initial rate of $0.468\times10^{-3}\,\mathrm{m}^3\,\mathrm{s}^{-1}$ [13] assuming the density of A 356 is 2400 kg /m^3.

3.3.3 Sprue

The velocity of metal in the sprue entrance and exit was estimated from the height of the metal in the pouring basin. The velocity into the sprue entrance during the experiments without and with vibration (V_1) was 1 ms^{-1} when the height of metal above the entrance was 50mm. The exit velocity from the sprue V_2 was 1.98 ms^{-1} and 1.5 ms^{-1} without and with vibration when the total height of the system was 200mm and 110mm respectively. The cross section area for the entrance and exit of the sprue were then calculated from a simple conservation of volume assuming $Q = A_1V_1 = A_2V_2 = A_3V_3$. Where A is the cross section area at position x and V the fluid velocity at that position.

The sprue entrance and exit in the vibration test were calculated to be $A_1 = Q/V_1$ = $0.468\times10^{-3}\ m^2$ and $A_2 = Q/V_2$ = $0.312\times10^{-3}\ m^2$. For a straight-tapered square section, these dimensions gave roughly 21 x 21 mm at the entrance and 17 x 17 mm at the exit.

The sprue entrance and exit without vibration were calculated to be 0.468×10^{-3} $\mathrm{m}^3\,\mathrm{s}^{-1}$ and 0.236×10^{-6} $\mathrm{m}^3\,\mathrm{s}^{-1}$ for the tapered round section, these dimensions gave nearly 24 mm diameter at the entrance and 16 mm diameter at the exit. The runner dimensions were selected to provide A_3 sufficiently large to give velocity V_3 well below the critical value of $0.5\,ms^{-1}$.

A series of further casting where produced using a downsprue in which the diameter of the exit area of the sprue in the runner system of 7 mm, to decrease the filling rate

and momentum; this modification the runner system also gave a smooth flow of the liquid metal out of the sprue.

3.3.4 Test piece design

The test piece was designed specifically to study the filling capability in the thin section of the investment shell mould, with and without vibration conditions. A thin vertical channel was formed which was attached around the upriser. The upriser and channel geometry are shown in Figure 3.5. The thickness of the channel was varied by introducing shim material into the joint line of a wax die used for test piece production. To account for the variability in the die closure and contraction of the waxes, the thickness of the channel was controlled to a repeatability of $0.03mm$. Waxes showing excessive variation in section thickness along their lengths were not used thickness. This corresponded to a variation in capillary back pressure ($\frac{\gamma}{r}$) of $\pm 5\%$ in strip of thickness 0.75mm.

A statistical method can be used to work out the value of the thickness variation acceptable if the variation of the metallostatic pressure percentage is 5% See Tables (3.3, 3.4)

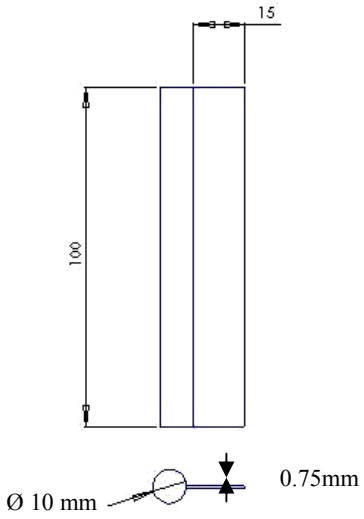

Figure (3.5) test Piece design

3.3.5 Preheating.

To establish the drop in temperature of the ceramic shell mould during the transfer from the mould preheating furnace to the instant of pouring a thermocouple was inserted into the base of the down sprue, and readings taken at intervals of 0.5 seconds using a datalogger. The test indicated that, in five minutes, the temperature dropped from 750ºC to the target minimum temperature of 350ºC. The test was done on a bare ceramic shell without insulation. Result of the cooling study shown in Figure (3.6).

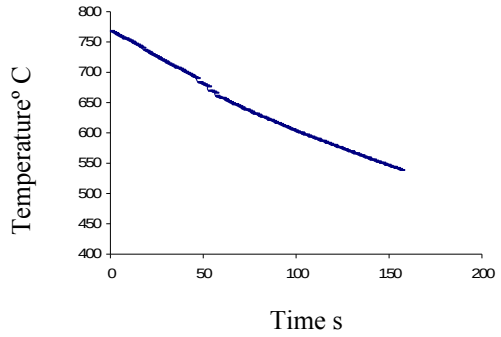

Figure 3.6 Temperature drop of ceramic shell during transfer from furnace to point of casting

3.4 Experimental procedure

The following steps were involved in the making and casting of the mould.

3.4.1 Wax Die

The die was made of aluminum and consisted of a simple channel 200mm long and 10mm in diameter. Spacing strips of accurate thicknesses $0.45mm$, $0.55\ mm$ and $0.75mm$ were used to create an attached strip-like cavity.

3.4.2 Wax Pattern

Wax patterns were made by injecting liquid wax into the die. The wax was injected at temperature of 70ºC and pressure of $40\,Kg/cm^2$, using an MPI wax injection machine.

A typical liquid wax is (RM0091) into which is incorporated a high percentage of resin to reduce shrinkage. It solidifies at 60 – 62 ºC.

After the wax had been allowed to cool and solidify, the wax pattern was carefully removed and lifted out.

3.4.3 Assembly of the Wax Pattern

The runner system and test piece patterns were assembled by softening the wax components with electrically heated knives and then sealing the components together by gentle contact pressure. In wax welding, care was taken to avoid excessive melting of the wax pattern, thereby avoiding any distortion of the patterns. (See Figure 3.7).

Figure 3.7 Typical Wax assembly

3.4.4 Wax Pattern Cleaning

Before coating assembled wax patterns were rinsed in liquid soap to remove grease and dirt and then allowed to dry.

3.4.5 Shell production

Initial experiments suffered from shell failure when subjected to acceleration of vibration higher than 2g. This was overcome by increasing the percentage of the binder agent SiO_2 in the slurry secondary coating to 30% and using a series of eleven

backing coats to give the shell a thickness of 11mm to 12mm (See Figure 3.8). The ceramic system formulation and shelling parameters are given in Tables 3.5 and 3.6.

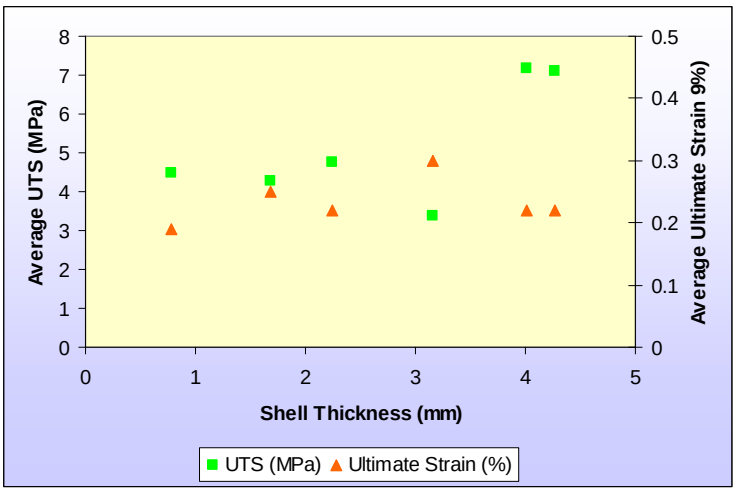

Figure 3.8: Graph of Ultimate Tensile Strength and Ultimate Strain versus shell thickness for the aluminium shell [123]

The building up of the ceramic shell proceeded in several steps. The wax assembly was dipped into aqueous slurry forming the primary coat, which was comprised of binder and fine zircon powder. The wax assembly was then lifted out and rotated to ensure proper and uniform coating, filling inside corners and permitting the drainage of excess slurry. The assembly was then hung up to dry in a humidity and temperature controlled drying cabinet. After two and a half hours the next coating was applied by dipping in the secondary slurry and stucco coating. This was similarly allowed to dry for two hours. The process was then repeated a further ten times to obtain the desired thickness for the ceramic shell mould (11-12mm). When the mould was completed the dewaxing stage was started**.**

3.4.6 Dewaxing process

The ceramic mould was placed inside an autoclave (Leeds and Bradford Boiler Company) in an inverted position and heated to 200ºC by superheated steam at 10 bar pressure. Most of the wax melted and flowed out of the mould.

3.4.7 Mould firing

The residue of the wax was removed and the mould sintered to develop full strength by firing in air in Max Sievert furnace at a temperature of 1000 ºC for one hour. The mould was then ready for preheating and casting.

3.5 Casting processes

The purpose of the experiments was to assess the filling capability in the thin wall investment casting method in two different filling types, Fillability filling type and Flowability filling type relative to two characteristics, metal head and fluidity as defined in Figure 3.9 a and b.

Fillability filling type = Metal head

Flowability filling type = Fluidity

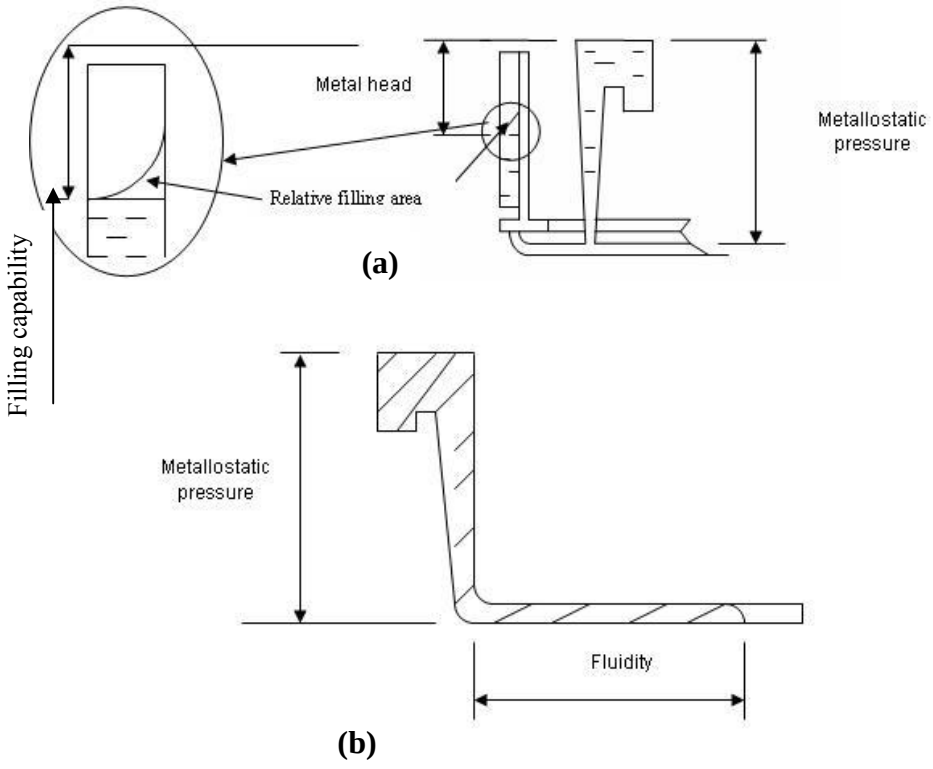

Figure 3.9 (a) and (b) illustrating metal head, metallostatic pressure and fluidity

3.6 Thin wall casting regime

A series of experiments was made to estimate the regions of flowability and fillablity filling type in thin wall investment casting relative to variation in the height of the metal head, using different thicknesses of strip castings of 0.45mm, 0.55mm and 0.75mm. The temperature of the mould, as measure at the base of the sqrue, was varied between 450ºC, 550ºC, 660ºC and 700ºC, and the pouring temperature was 750ºC.

Before casting shells were covered by a insulating ceramic fibre blanket. The shell was then heated to a temperature above the desired casting temperature in a Max Sievert electrical resistance heater and left to soak for a minimum of two hours. The melting process was then performed in a medium frequency induction furnace. 2 Kg charges of A356 alloy were melted and held at approximately 650ºC for a minimum of 20 minutes, to allow the alloy to outgas passively. At the end of the outgassing period, the melt was heated rapidly to raise its temperature to the pouring temperature and then removed from the furnace to cast. The preheated metal was transferred to the casting station and poured immediately into the mould. The casting time was approximately 2 seconds and at the end of filling the uprisers could be determined as the point when the metal filled the vents. After filling was completed, the casting was left to solidify and cool in situ.

3.7 Static fillability tests.

Castings were made by pouring into moulds whose temperatures were greater than the liquidus temperature (610ºC).

3.7.1 Pouring temperature effect on the filling capacity.

In this series of experiments, the mould preparation and casting process was the same as the procedure described in section 3.6.

The mould design is shown in Figure 3.10 (a) and (b) and the test pieces were, 200mm in height, 15mm width and thicknesses of 0.45mm, 0.55mm and 0.75mm, were used to determine the effect of the different thickness of the strip on the metal head. In this series of experiments, the pouring temperature varied between 670ºC to 750ºC and the mould temperature between 660-700˚C.

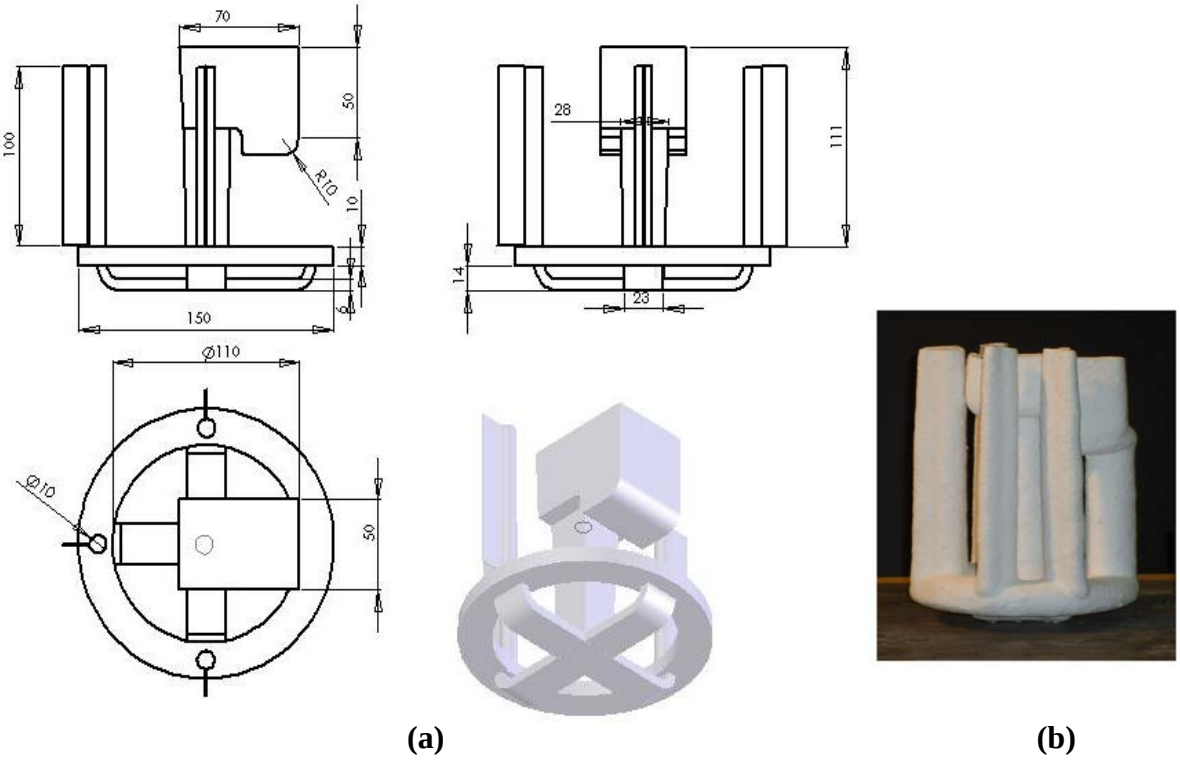

Figure 3.10 (a) Mould design for filling capability test (b) ceramic mould

3.8 Casting without vibration in flowability filling type conditions

Castings were made, when the temperature of the mould was less than liquidus temperature.

3.8.1 To establish the effect of pouring temperature on filling capability

In initial series of experiments the mould design in Figure 3.10 and the test pieces used were the same as those used in fillabality filling type castings.

Prior to casting, the shells were wrapped a ceramic fiber blanket. The shell was then heated to a temperature of 400˚C and left to soak for a minimum of two hours. Three casting were made with metal, pouring temperatures of 680ºC, 700ºC

3.8.2 Fluidity test without vibration

Fluidity test moulds of design shown in Figure 3.11 [36] were cast to study flow in thin channels and establish a fluidity database for verification of mathematical models of thin wall investment casting filling (Chapter 4). The same casting procedures were used as for previous experiments. This series of experiments were made with pouring temperatures 680ºC, 700ºC and 750ºC at a constant mould temperature of 420 ± 5ºC and strips of thicknesses 0.55mm and 0.75mm.

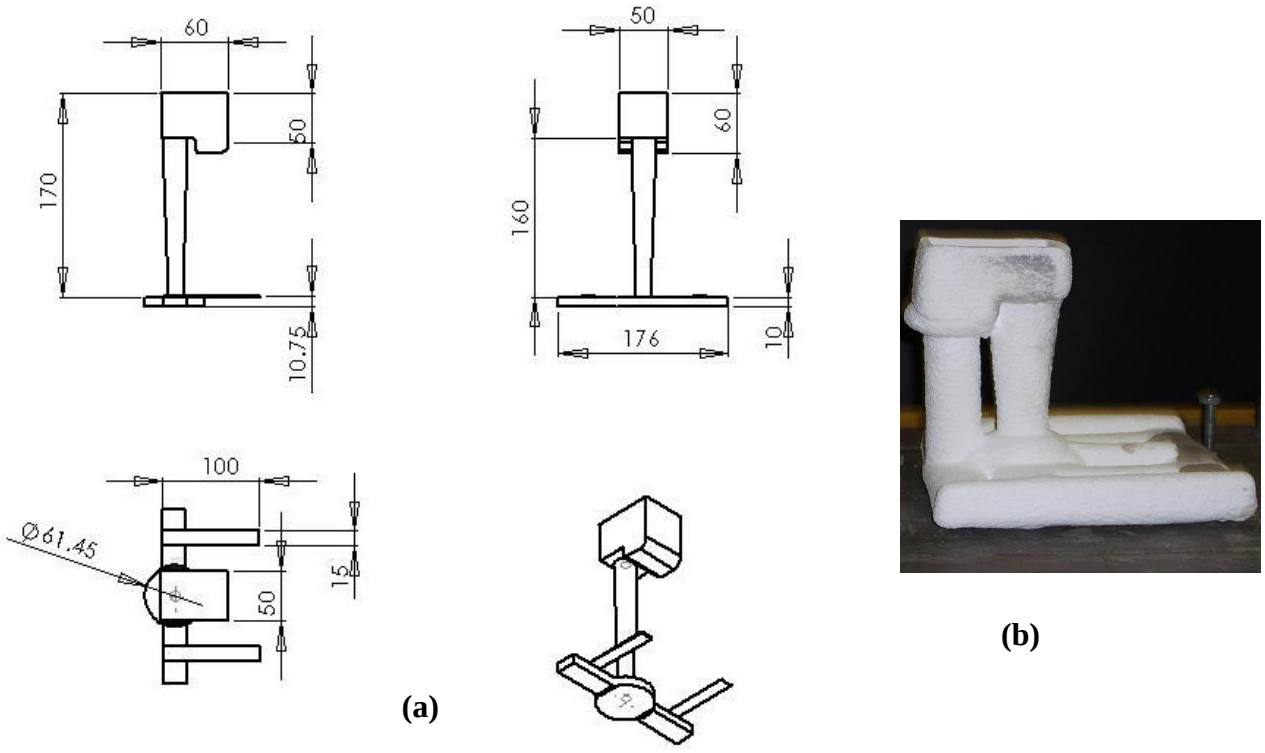

Figure 3.11 (a) Mould design for fluidity test strip thickness 0.75mm metal height 170mm, pouring temperature 450ºC, mould temperature 660ºC-700C (b) ceramic mould

3.9 Radiographic flow imaging.

A real time X-Ray video-recording camera was used to observe and record flow in strip channel at a capture rate of 60 frames per second and resolution 800×600 pixels. The system was used to record the flow phenomena during the filling of sections with thickness 0.75mm in horizontal and vertical strip positions. The velocity of the liquid metal front in flowability and fillability type filling were measured without vibration. Unfortunately the clarity of the images from the X-Ray system was limited by the low metal thickness relative to the shell thickness. When the mould was subject to vibration during filling the image would not be clear enough to resolve the metal flow. It was therefore deemed impractical and was not pursued.

3.9.1 Flow imaging to measure velocity in fillability filling regime.

In the mould design, account was made for the fact that the momentum of flow in the exit area of the sprue in the runner system affects the velocity value at the junction area between the sprue and the test piece. This influence was eliminated by increasing the length of the base of the sprue as shown in Figure 3.12 a and b. The wrapped mould was cast into at temperature of 650ºC, and cast inside the X-Ray machine, using a charge heated to 750ºC.

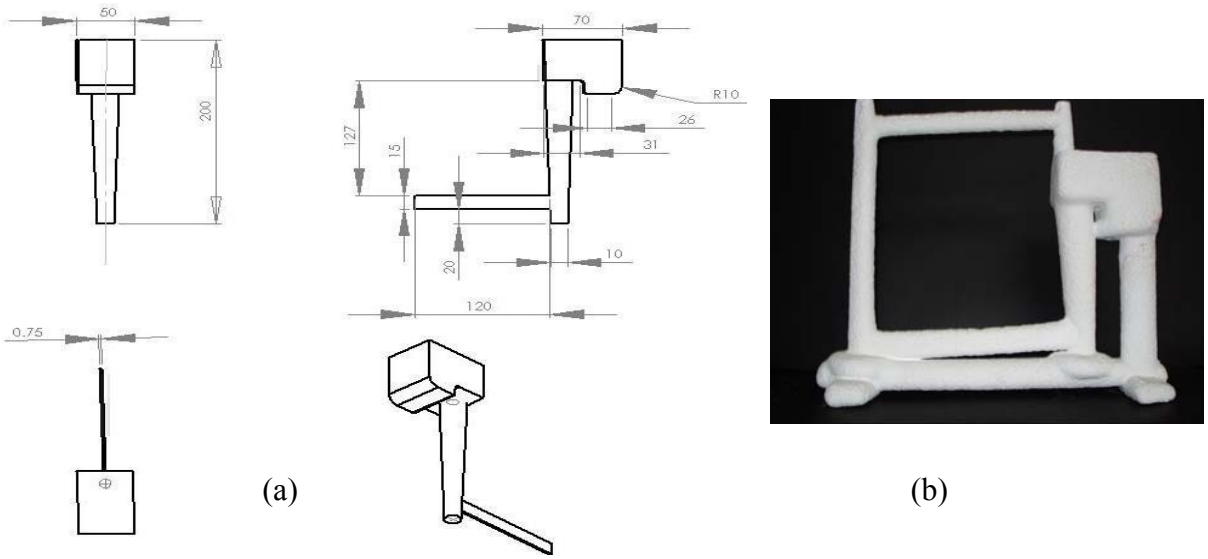

Figure 3.12 (a) Mould design for velocity measurements, horizontal strip thickness 0.75mm metal height 170mm, pouring temperature 750ºC, mould temperature 660ºC-700C (b) ceramic mould

Filling was recorded in horizontal strips with dimension of $150mm \times 15mm \times 0.75mm$ with a metal head of 170mm.

Another experiment was done with castings in fillability filling type condition using the mould design illustrated in Figure 3.13, using a reduced sprue exit diameter of 7mm. The strip with dimensions, $100mm \times 15mm \times 2mm$, was set in a horizontal direction with the runner in the filling system at a height of 120mm, to measure the velocity of the meniscus of the liquid metals front.

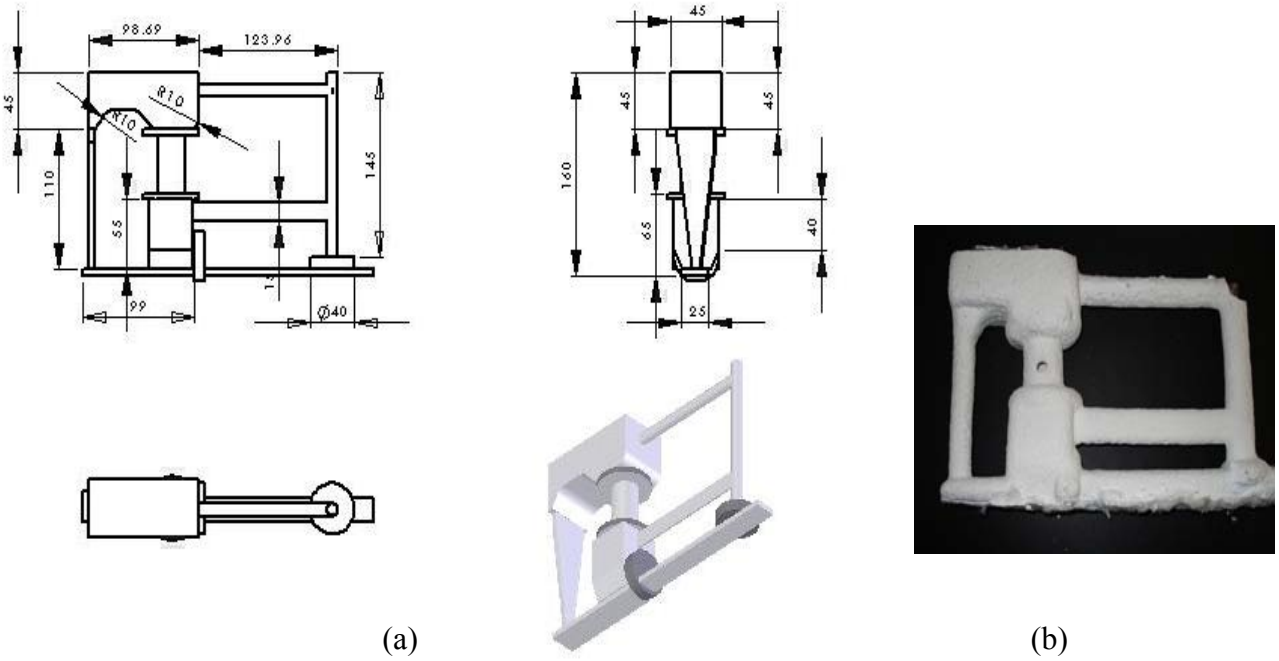

(a) (b)

Figure 3.13 (a) Mould design for velocity measurements, horizontal strip thickness 2mm metal height 120mm, pouring temperature 750ºC, mould temperature 660ºC-700C (b) ceramic mould

3.9.2 Flow imaging to measure velocity in flowability filling regime.

The filling of a 0.75mm thick strip of dimension $200mm \times 15mm$, was recorded. The casting was made with a mould temperature of 450ºC and metal temperature 750ºC using a mould illustrated in Figure 3.12. The flow velocity was measured from the captured images using i-speed software.

3.9.3 Flow pattern study in thin section without vibration condition using real time X-ray digital video machine.

The mould designs shown in Figures 3.14 and 3.15 were used to investigate the flow pattern of the liquid metals of the A356 in thin sections. Experiments were conducted with a strip thickness of 0.75mm of dimension $200mm \times 15mm$ oriented in both the horizontal and vertical positions under fillability filling type conditions. The region to be imaged using a real time digital X-Ray system during casting (the strips) were joined with an upriser

(both horizontal and vertical). The casting was made with a mould temperature of 650ºC and metal temperature 750ºC. The filling system height was 200mm.

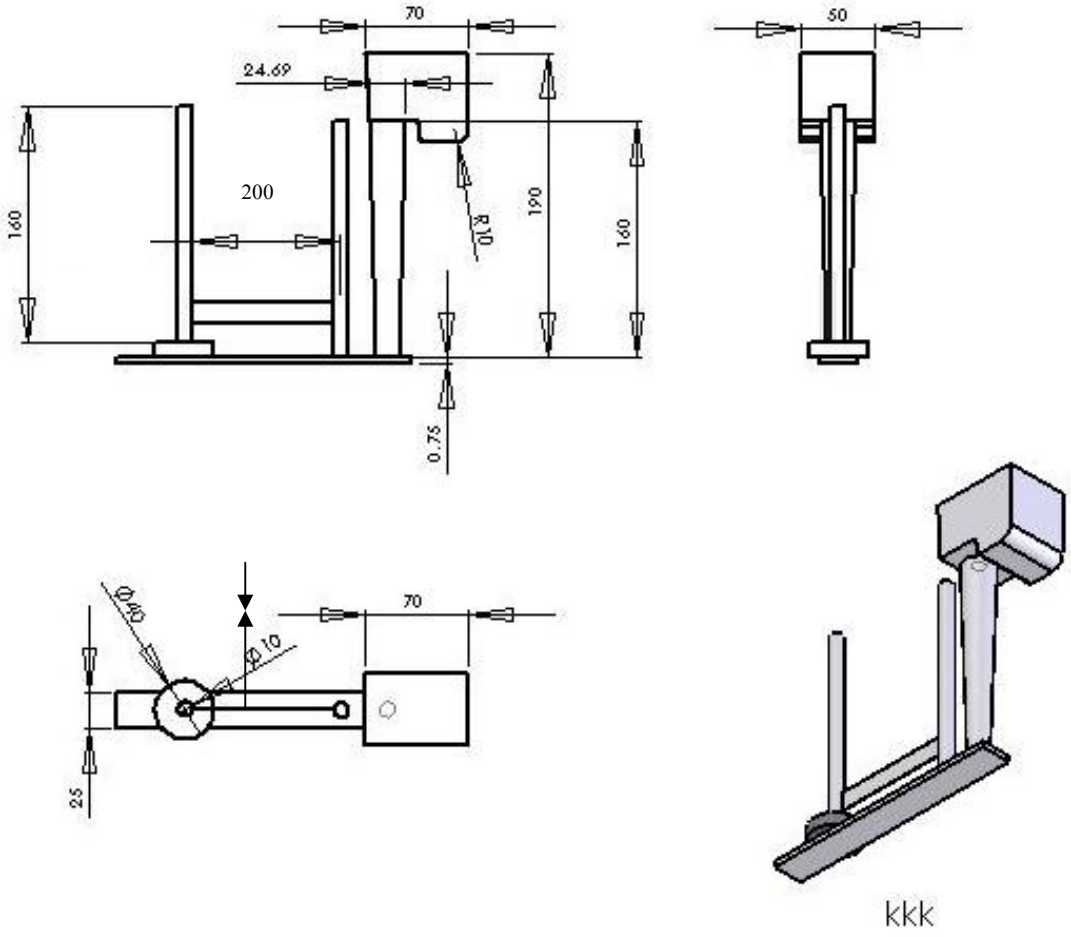

Figure (3.14) Mould design for flow pattern investigation, strip with thickness 0.75mm in horizontal position cast without vibration, filling system height 200mm.

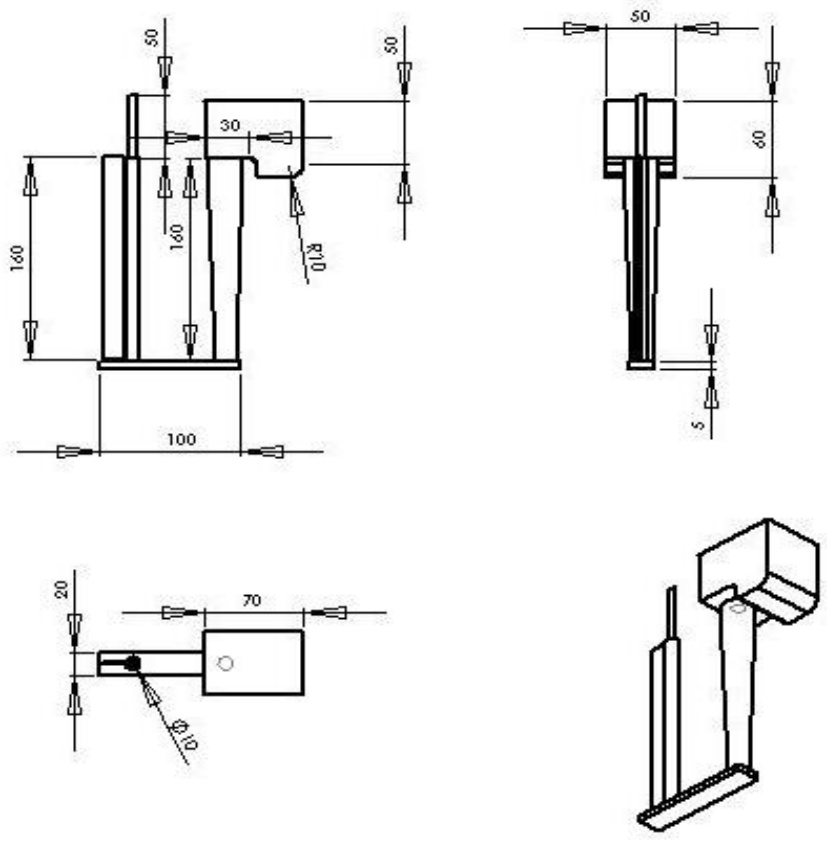

Figure (3.15) Mould design for flow pattern investigation, stripe with thickness 0.75mm in vertical position cast without vibration, filling system height 200mm.

3.10 Modelling of the liquid metals flow in thin section without vibration.

The Flow-3D software package was employed to model and investigate the flow patterns and velocities of the liquid metal for the A356 alloy. Physical properties of the liquid alloy were referenced from the Flow-3D database. Simulations were preformed without vibration in thin channels (thickness 0.7.5mm), with a height of metal present in the pouring basin and sprue of 180mm. The casting parameters applied were gravity top pouring. The moulds geometry of the velocity test in the fillability filling type Figure (3.12) and the filling capability test Figure, (3.14 and 3.15) were imported as STL CAD files into Flow-3D, and meshed, material properties and boundary conditions applied is illustrated in Figure 3.16.

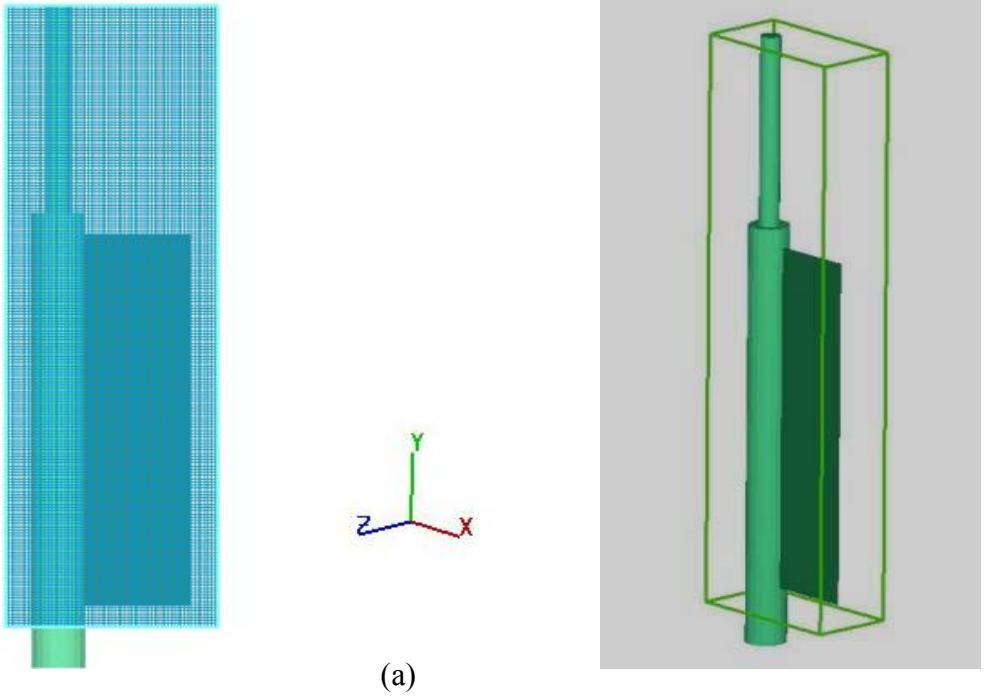

(a)

(b)

Material properties of the A356 Al alloys

Physical properties	Value
Density	$2400\, kgm^{-3}$
Surface tension	$0.92\ Nm^{-1}$
Contact angle	160º
Viscosity	$0.003\ N/m^2 s$

(C)

Figure 3.16 (a) Show the meshed models and (b) number and the size of the mesh in three coordinates X, Z and Y (c) physical properties table

The simulation of the flow pattern was made using a single-phase model in which the cavity pressure remained constant during the calculation. The single- phase model was chosen for two reasons;

- Mould filling is predominantly quiescent so very little air would be entrained (no bubbles seen in X-ray studies). Due to low entrainment, no mixing of air into the liquid metal (flow bulking) occurred.
- Quicker simulation

The wall boundary was set to a free slip condition and the RNG turbulence model chosen as recommended by Flow Science for the robustness of the solver and simulation results achieved in previous studies, eg. Sirrell. [124]. Heat transfer was not modeled during the calculation.

To reduce the calculation time, pouring of liquid metal from the crucible to the basin and from the basin to the runner was not simulated. A boundary condition was applied at the sprue inlet using a constant pressure.

The flow pattern of the liquid metal flowed into the strips with dimensions of $150\text{mm} \times 15\text{mm} \times 0.75\text{mm}$ were set in the vertical direction. Another liquid filling profile was simulated in the Flow-3D programs with the strip set in a horizontal direction.

3.11 Casting with vibration.

The aim of experiments was to determine the capability to fill sections of thickness less than 0.75mm using vibration, to investigate the mechanisms of the liquid advance and determine the dominant filling control parameters.

3.11.1 Casting with vibration under fillability filling type condition.

The mould design shown in Figure 3.10 and strips with 100mm height, 15mm width and thicknesses of 0,4mm, 0.55mm, 0.75mm, and 1mm were used to determine the effect of the vibration on filling capacity.

Prior to casting, the shells were covered by a ceramic fibre blanket. The shell was then heated to a temperature of 670-700˚C and left to soak for a minimum of two hours. The melting process as described in section 3.6 was carried out.

During the heating of the charge, the mould was removed from the preheating furnace and installed on the vibrating table. The mould was clamped to the table by a fixture. The preheated metal was transferred to the casting station and poured immediately into the secured mould. The casting time was approximately 2 seconds and the end of filling the uprisers could be determined as the point when metal filled the vents.

Immediately after filling was completed, the vibrating table was switched on to apply a pre-set acceleration (see Figure (3.17)). After vibration, the castings were left in situ to solidify and cool.

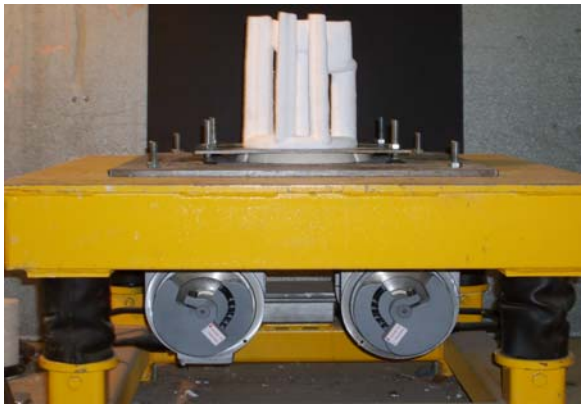

Figure 3.17 Ceramic mould clamped with vibrator table

In this series of experiments, the frequency of vibration varied between 13Hz and 18Hz and the vibration peak to peak amplitude varied between 2.15mm and 2.01mm

corresponding to accelerations between 0.8g, and 1.3g. The experimental parameters of individual test are summarized in Table 3.7.

3.11.2 Effect of the vibration parameters (frequency, amplitude) on the propagation flow

The mould used in the experiments is illustrated in Figure 3.18. The experiments were carried out with the same procedure as described in section 3.11.1

A range of amplitude and frequency of vibration as set out in Table 3.8 were applied with acceleration of between 0.9g and 1.2g imposed. In each instance the vibration was applied for 10 second after the end of filling.

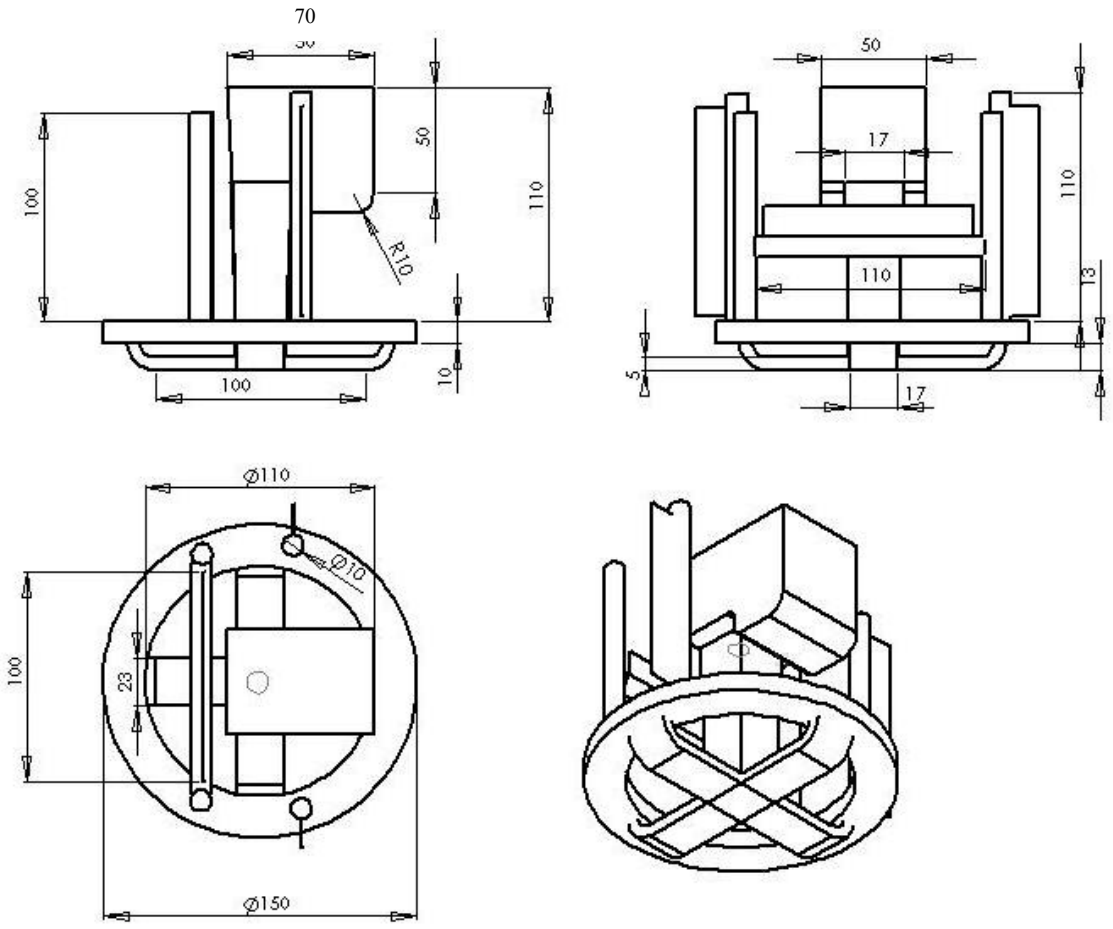

Figure (3.18) Mould design to examine a jetting length and propagation flow features in thin wall investment casting with vibration condition fillability filling type

3.11.3 The effect of the acceleration of vibration on the length of jetting

A series of experiments was done in the fillability filling type under vibration conditions of 1g, 1.1 and 1.2g using a strip 0.55mm thick to investigate the influence of the acceleration of vibration and the metal head on the jetting length (as illustrated and defined in figure 6,12).

Figure (3.18) shows the mould design used to investigate the effect of the acceleration of vibration on the jetting length by varying the magnitude of the frequency of vibration from 15.37Hz to 17.97Hz and amplitude from 2.14mm to 2.03mm respectively at constant metallostatic pressure of 2828 P_a. The times of the vibration operation was 10s. Table 3.9 summaries the experimental conditions.

3.11.4 Effect of vibration time on filling capability.

In the first part, from the series of experiments was done to investigate the operation time of the vibration effect on the metal head, the frequency of vibration was 14.71Hz and the amplitude was 2.14mm, corresponding to peak acceleration of 0.9g. The time of vibration operation was 10, 20, 40 and 60s. The second part of the experiments assessed the frequency of the vibration 17.17Hz and the amplitude 2.04mm corresponding to peak acceleration 1.2g. The vibration continued for was 10s, 20s, 40s and 60s.

Experimental limitations were encountered in applying short vibration cycles. The equipment suffered long start up and shut down phases of approximately 3 seconds before the system ran in a steady state. This precluded repeatable investigation of vibration cycles any shorter than approximately 3 seconds. Table 3.10 summarizes the experimental condition studied.

3.11. 5 Direct imaging of flow propogation under vibration condition.

To investigate mode of the propagation of liquid metal into thin sections a simple experimental apparatus was built in which liquid mercury filled laterally a thin channel under the action of vibration.

Mercury was selected because its surface tension is accurately known [20]. A mould was made of Plexiglas with geometry, shown in Figure 3.19.

Figure 3.19 Plexiglas mould

The Weber number was used to calculate a scaling ratio between the dimensions of the cast channel and that of the Plexiglas mould (see Appendix 4). A high speed video camera of resolution 512×512 pixels, capture rate 500 frames per second, was used to record the liquid advance.

The mercury was poured to fill the upriser to a height of 76mm. The vibrating table, pre-set at a frequency of 19.68Hz and amplitude of 1.3mm, acceleration 0.9g, was run for 10s (See Figure 3.20).

A series of experiments were conducted with and without vibration using the mercury and the Plexglass mould to establish the metallostatic pressure head required to force the metal into the thin channel.

Figure 3.20 mercury experimental to investigate the liquid metal advance and velocity of the metal under vibration condition

3.11.6 Modelling flow in thin channel with vibration condition.

Flow 3D software was employed to model fluid flow sequences in thin wall castings under vibration conditions. A pressure boundary condition was applied to the entry into the thin wall during the simulation, the value of which was equivalent to that arising due to vibration. This approach was adopted because it was not possible to model the vibration of the moulds using Flow-3D (or any other fluid dynamics software package) due to limitation in the computing resources available.

To reduce the calculation time, transfer of liquid metal from the crucible to the basin and from the basin to the runner was not simulated.

The simulation was preformed in two steps using a single phase fluid model, using the geometry shown in Figure 3.21. The strip dimensions were $100mm \times 15mm \times 0.55mm$.

For the first second of calculation the pressure remained constant and was calculated by gravitation alone (ρgh). In the next second the pressure was adjusted to be the sum of the maximum acceleration $a_{\max}$ due to vibration and gravitation ($\rho h(g + a_{\max})$).

A second simulation was performed in which the pressure after the first second was time dependent and defined as ($P = \rho h(g + af^2\pi^2 \sin(\pi f^2 t)$). A turbulence model was chosen to evaluate the viscosity. Heat transfer was not calculated.

3.11.7 Fluidity tests under vibration condition.

In this series of experiments, mould preparation and casting process as the same as procedure was similar to that described in section 3.6

In the first part of the experiment, the mould of the fluidity test shown in Figure 3.11 of height 170mm was used to evaluate the fluidity in a strip of thickness 0.75mm under vibration of 0.8g acceleration applied during the pouring processes with pouring temperatures of 665, 700 and 750ºC and mould temperature 400ºC. Experiments were also preformed with vibration applied after filling process at an acceleration of 0.8g with pouring temperature 700ºC. Details of the casting tests are summarized in Table 3.11.

3.12 Microstructural characterization.

Specimens were selected close to the tip of castings from each series of experiments (flowability and fillability). Using digital vernier calipers to measure the amount of material removed, samples with thicknesses of 0.75mm were mounted in bakelite and ground with a silicon carbide paper (P800) to remove (0.37mm) from the test pieces. A series of diamond polishing steps 9,6,3,1 μm were used until polishing was completed using colloidal silica to produce a mirror-like finish. Specimens were examined using an optical microscope and quantitative image analysis used to

characterize casting defects including oxide films and microporosity resulting from shrinkage and gas precipitation, as well as microstructural variations in grain size and secondary dendrite arm spacing.

An area ($10\text{mm} \times 15\text{mm}$) samples were sectioned from the width of test pieces for each method of casting. Sample preparation was as described previously. Examination of defects was performed using Zeiss 300A image analysis software. Images were taken from each sample at a magnification of (100×10) and the number of defects counted and the area of each defect measured. Measurements were exported to Microsoft Excel for further analysis.

3.13 Effect of vibration on casting reliability

Experiments to establish the effect of vibration on the tensile reliability of thin wall investment castings were conducted. A Weibull modulus for the tensile strength and elongation of strip specimens with thickness 0.75mm, cast with and without vibration, was used as the indicator of reliability of the castings and process.

3.13.1 Experimental procedure

3.13.1.1 Casting parameter

A bottom filled system was designed with test pieces oriented vertically and cast into ceramic moulds. The design is illustrated in Figure 3.21. The running system was designed in accordance with the rules set out by Campbell [13] such that at the ingates the metal velocity would not exceed the critical velocity of 0.5m/s.

A356 alloy was used. The composition is reported in Table 3.1. No returns were used in the melt charges.

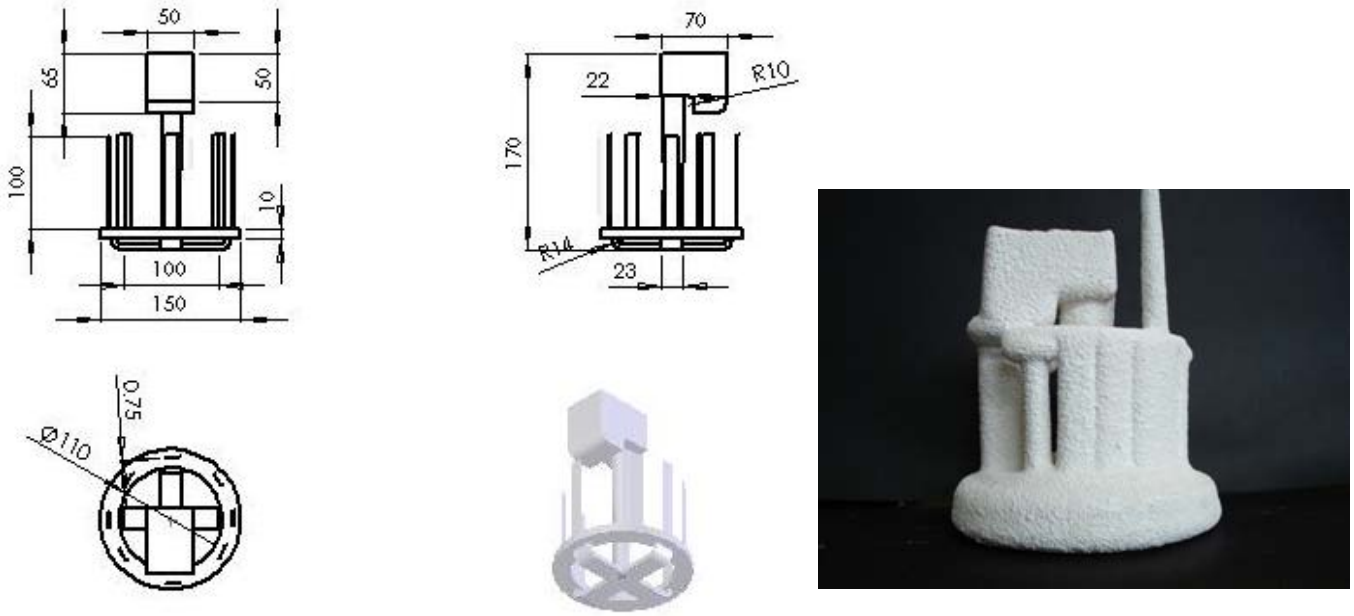

(a) (b)

Figure 3.21 Ceramic moulds design to produce test pieces with thickness 0.75mm for a tensile test

Four groups of castings were made without vibration, with 0.8g and 1.2g acceleration of vibration after filling and casting with 0.8g acceleration of vibration during filling. Three moulds were cast for each condition, each mould consisting of a ten test pieces. All castings were poured at temperature of 750-755ºC. The moulds cast without vibration were poured under fillability filling type conditions (mould temperature 660-700ºC) with a metal head of 120mm above the top of the test strips which was sufficient to "force" the melt into the test pieces. The second group was cast with a 0.8g acceleration of vibration applied immediately after the filling process with a metal head 65mm which was enough to fill the test pieces. The third group was cast with 1.2g acceleration of vibration applied after the filling process in fillability filling type conditions with metal head of 50 mm. The fourth group was cast with 0.8g

acceleration of vibration applied during filling process in the fillability filling type condition with metal head 65mm

3.13.1.2 Machining

A fixture was designed to clamp together for machining each group of the test pieces. This avoided any specimen distortion, damage and dimensional variability that may arise if each specimenwas machined separately. The test pieces were machined using a side cutting mill to produce tensile test specimens confirming to British standard [140]. The geometry of the specimens is shown in Figure 3.22.

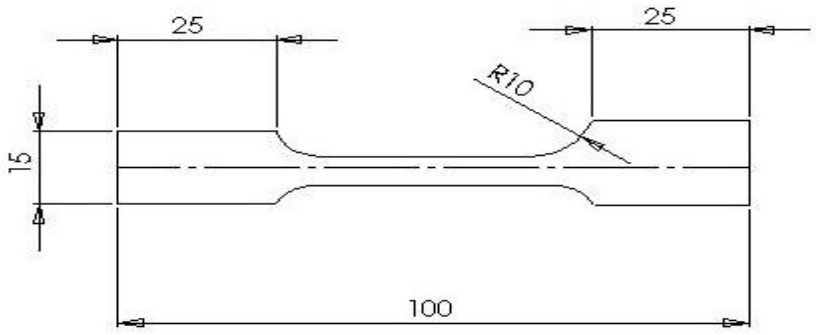

Figure 3.22 Specimen geometry

3.13.1.3 Heat-treatment.

Each group of test pieces were clamped by the fixture before all the test pieces were loaded into an air circulating furnace. Specimens were jigged to prevent deformation. Test pieces were heat-treated to near peak-aged condition: solution- treated for six hours at 540 ± 5ºC, quenched in water at room temperature then artificially aged at 160 ± 5ºC four hours.

3.13.1.4 Mechanical testing.

Tensile testing was carried out using a computer-controlled 200 kN dynamic loads servo-hydraulic testing machine (Zwick). 0.2% and 0.5% proof stress was measured using a clip gauge extensometer of length 25mm, together with the UTS and plastic

strain at fracture. A constant cross head speed of 0.5mm/min was used. A data logger was used to record the load and displacement of each test and data was subsequently exported to Microsoft Excel for analysis.

3.14 Statistical analysis of the fracture strength.

A Weibull distribution function was used to qualify the scatter in ultimate tensile strengths obtained from each casting method. The calculation protocol was as that set out in section 2.9.2. Weibull Modulus, λ, and position parameter, σ, was calculated for each set of specimens.

3.14.1 Fracture surface charactarisation

Microfractographic examination on the surfaces of tensile test pieces from each method of casting was studied using a Joel 6060 scanning electron microscope. Digital images were captured and energy dispersive X-ray analysis conducted to identify initiators.

Chapter 4

Experimental Results

4.1. Thin wall investment casting filling regime

The resulting data from this series of experiments are illustrated in Figure 4.1 and listed in Table 4.1.

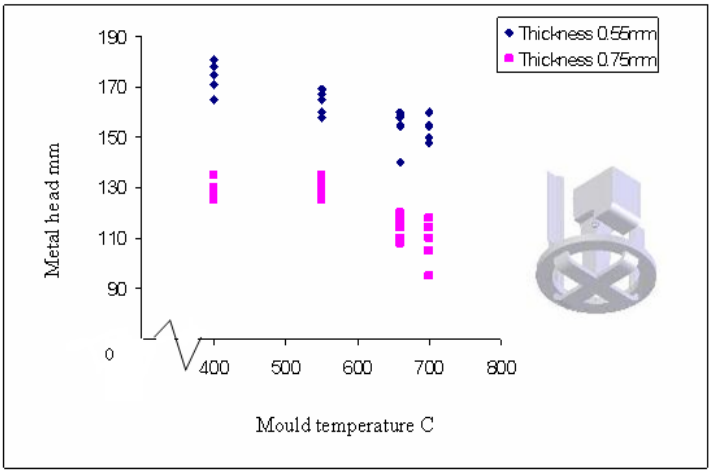

Figure 4.1 Fillability and flowability results obtained in thin wall investment castings, A356. Critical metal head occurs at liquidus temperature, pouring temperature 750ºC, metallostatic pressure head height 200mm

Figure 4.1 shows that the flowability was determined by the temperature of the mould in the temperature range 400ºC to 650ºC, the magnitude of the metal head (using digital vernier caliper as illustrated in Figure 3.9) decreasing with increasing mould temperature. At the alloy's liquidus temperature (610ºC) it can be seen that further increases in mould temperature had no repeatable effect on metal head height. Thus, the metal head value reached when the mould temperature was at or above the liquidus temperature is the critical metal head required to force the liquid metal into the thin section.

The results also indicate that the trend in the height of the metal head in thin wall investment casting will occur only in the flowability filling regime. However, in the fillability filling type, the metal head will, with some range of variation, be constant.

4.2 casting without vibration flowability filling type

4.2.1 Effect of pouring temperature on in flowability

The results of the castings without vibration in the fowability filling type, using moulds illustrated in Figure 3.10, are listed in Table (4.2). The data for these experimental results were plotted in Figure 4.2 by using the filling capacity represented by the metal head as a function of the pouring temperature in different thicknesses, to find the influence of the pouring temperature on the metal head in thin wall investment casting.

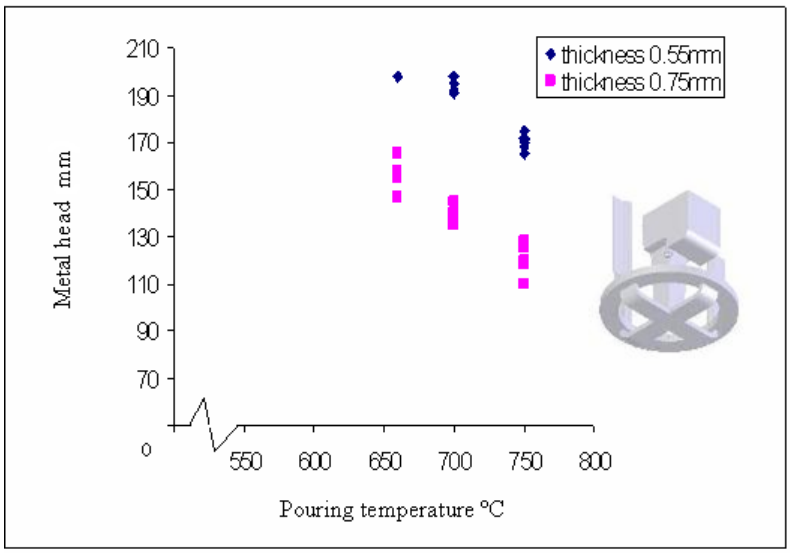

Figure 4.2 The effect of pouring temperature on the critical metal head in the thin wall investment castings, A356, flowability filling, mould temperature 400ºC, pressure head 200mm

It is clear from Figure 4.2, that for a strip with a thickness of 0.75mm, the filling capability increases as the pouring temperature increases in flowability filling type castings (high pouring temperature, low mould temperature). This increase is the commonly observed and reported improvement in fluidity with increasing pouring temperature [18, 27, and 115]. Therefore, in this case it can deal with the filling capability problem as a heat transfer problem. However, the pouring temperature effect had no effect when the casting was 0.45mm thick. In this case, it is believed

that the cooling rate and surface tension for the liquid metal in thin section has an inverse relationship with the thickness of the channel [5]. Thereby, they become the major parameters effective on the filling capability when the thickness is too small so that, the problem in this situation seems to be a combination of a thermal problem and a mechanical problem. Chapter (4) explains these problems in more detail.

4.3. casting without vibration fillability filling type

4.3.1 Effect of pouring temperature on fillability

Experimental results showing the effect of pouring temperature on the metal head required to fill castings poured in the fillability filling type condition are listed in Table 4.3 and plotted in Figure 4.3.

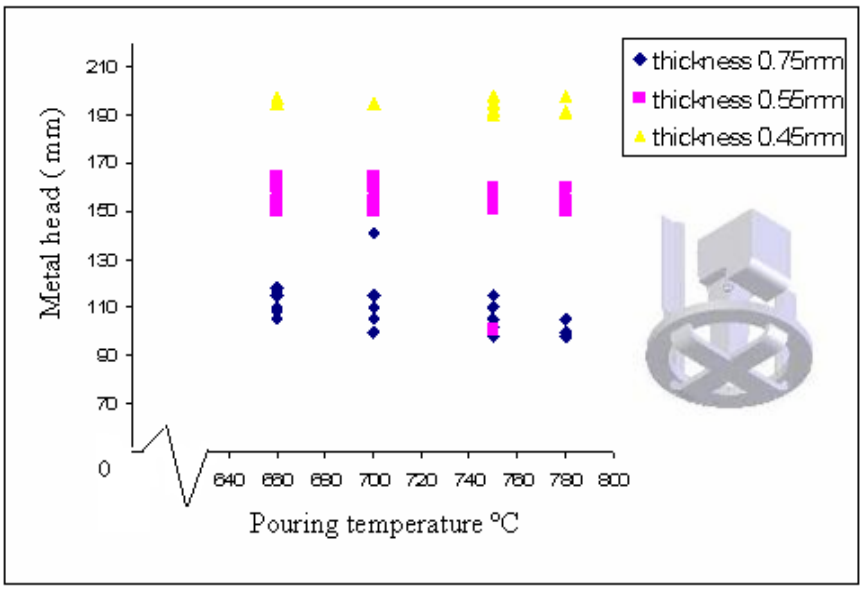

Figure 4.3 Pouring temperature effects on the critical metal head required to fill thin wall vertical strips, fillability filling, mould temperature 660-700ºC, pressure head 200mm

The result show that in strips of 0.75mm thickness the metal head decreased slightly with increasing pouring temperature; however, no such correlation was found for a strips of thickness 0.45mm and 0.55mm. This indicates that foundry parameters such as pouring temperature has no impact on the filling capability in thin wall castings in fillability filling type conditions.

4.3.2 Effect of strip thickness on fillability

The details and result of the castings with fillability filling type experiments are summarized in Tables 4.4, and plotted in Figure 4.4 by using the filling capacity represented by the metal head as a function of the thickness of the strips, to investigate the critical metal head required to fill a thin section in the investment casting method, without solidification interfering with the filling mechanism.

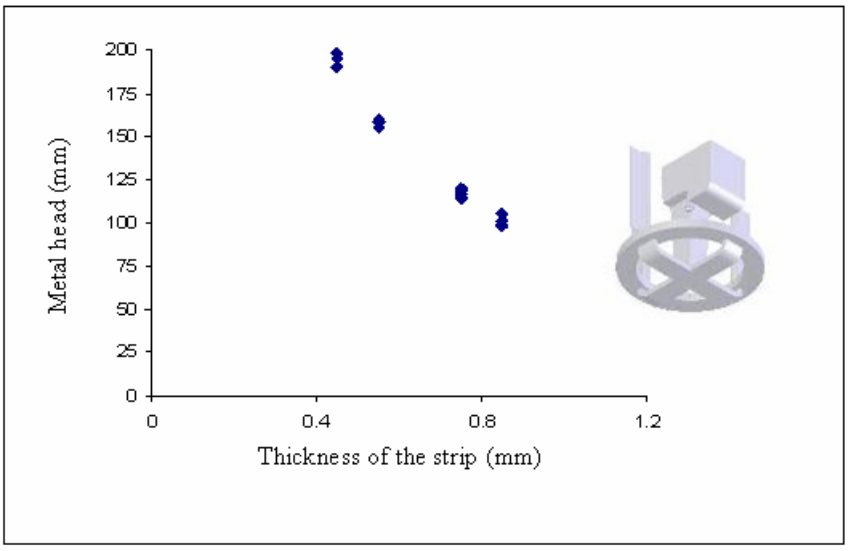

Figure 4.4 Relationship between metal head and different test pieces thickness in fillability filling type, A356, pouring temperature 750ºC, mould temperature 660C-700ºC

From the figure 4.4, it is clear that the strips with a thickness of 0.85mm, 0.75mm, 0.55mm and 0.45mm have an average metal head of 102mm, 116.8mm, 157.5mm and 194.5mm respectively. This result indicates that the metal head increases with every decrease in the thickness of the strip. Therefore it is expected that the reason for the decrease in the metal head in regard to the nature of the relationship between the metal head and the thickness of the channel if we take into account surface tension repulsion [42]. In other words, the problem in this case might instead be determined by the mechanical balance of forces between the surface tension and hydrostatic pressure [6].

It should be noted that a channel of circular cross-section, the back pressure as a result of the surface tension doubles in value because there are two radii of the meniscus at the metal front (see figure(4.5)) [16].

Such that

$$\text{Pressure due to surface tension} = \gamma\left(\frac{1}{r_1} + \frac{1}{r_2}\right) = \frac{2\gamma}{r}$$

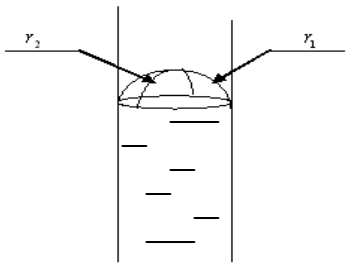

Figure 4.5 Principal radii of a curvature of the meniscus of a liquid metal flowing in a tube of circular cross-section.

4.3.3 The X-ray flow studies of filling of thin sections

4.3.3.1 Flow front imaging

Key frames of the X-ray flow sequence of the mould design illustrated in Figure 3.15 are shown in Figure 4.6 (Appendix). Result reveals that the liquid metal flowed into the upriser until it reached a certain height (the metallostatic pressure required to force the metal into the thin section) and then the liquid metal entered the thin section from the base of the strip until stopped by the mould wall. After this, the flow of the metal proceeded as a layer in a vertical direction to fill the thin section until it reached a certain metal head.

Key images of the strip filling was sited horizontally are shown in Figure 4.7. (Appendix) When poured into the mould, the liquid metals flowed into the sprue and runner until it reached a certain minimum height in the upriser; after this, the melt entered from the lower point of the junction area between the strip and upriser and the meniscus of the liquid advance continued to move in a horizontal direction until it filled the whole strip.

4.3.3.2 Velocity measurement in the thin section without vibration

The i-speed software already installed with X-Ray images analysis programming was used to calculate the velocity of the meniscus of the metal advance in different positions along the strip, starting from the junction area between the strip and the upriser. From Figure 4.7, velocity calculations of the experiment are listed in Table 4.5 and plotted in Figure 4.8.

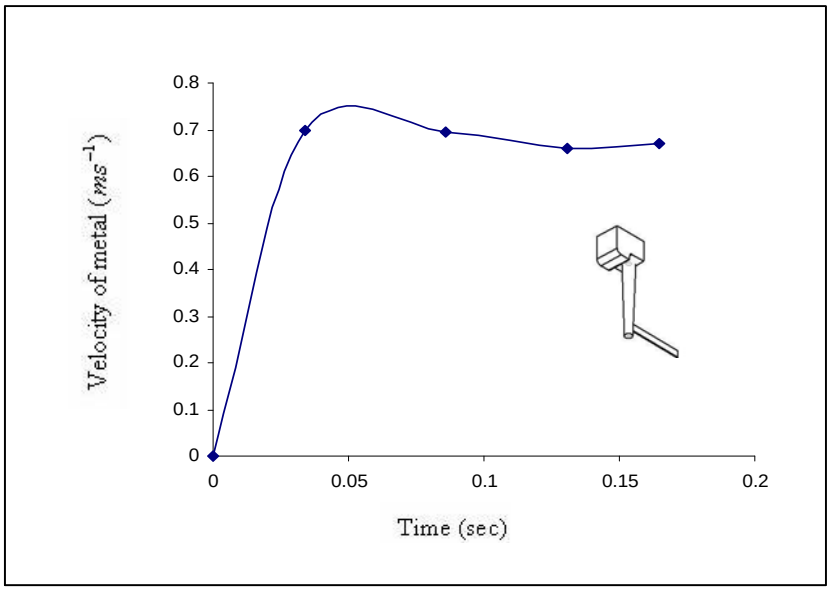

Figure 4. 8 Velocity measurements, fillability filling condition, piece thicknesses 0.75mm, mould Temperature 660-700ºC, pouring Temperature 750ºC, metal head 170mm

The frames of the X-Ray video digital camera shown in Figure 4.9 (Appendix) is another result of experiment using mould design illustrated in Figure 3.13 are listed in Table 4.6 and plotted in Figure 4.10.

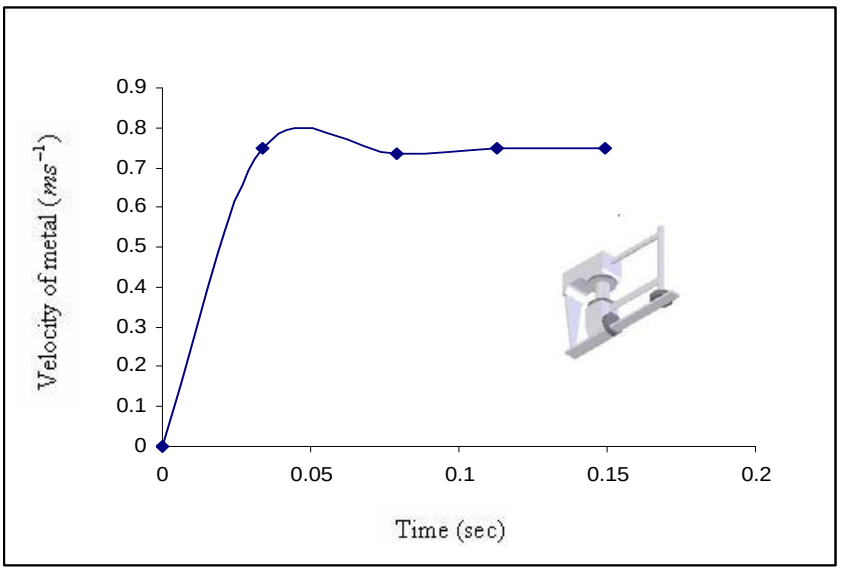

Figure 4.10 Velocity measurements, fillability filling condition, piece thicknesses 2mm, mould Temperature 660-700ºC, pouring Temperature 750ºC, metal head 120mm

The results of the experiments were done in flowability filling type are listed in Table 4.7 and plotted in Figure 4.11. Key frames of the X-ray flow sequence shown in Figure 4.12 (Apendix).

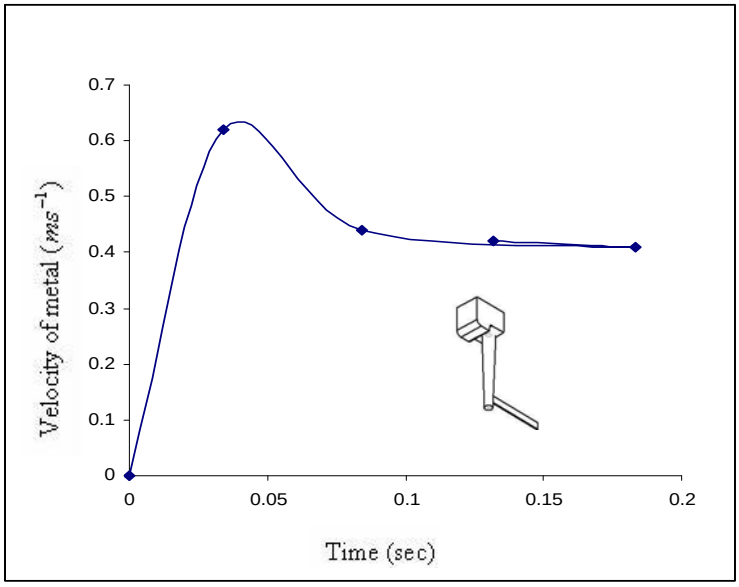

Figure 4.11 Velocity measurements, flowability filling condition, piece thicknesses 0.75mm, mould Temperature 450ºC, pouring Temperature 750ºC, metal head 170mm

According to Figures 4.8 and 4.10, its clear that the average velocity of liquid metals along the thin section is proximately constant about 0.65 ms^{-1} and 0.75 ms^{-1} respectively, when casting in fillability filling type condition. However the velocity in casting cast in flowability was varied from 0.6 ms^{-1} to 0.42 ms^{-1} .

4.3.4 Modelling filling of thin section casting .

The flow pattern of the liquid metal flowed into the strips with thicknesses 0.75mm, modelled by using Flow-3D software packages, as illustrated in Figure 4.13 and 4.14 (Appendix). Generally, the result of the Flow-3D modelling reveals that the flow pattern in the thin section agrees closely with the filling sequences frames observed using real-time X-ray flow imaging.

In the situation when the strip is set in vertically, results show a strong correlation between experiment and model Figure 4.13(12-14) and the Figure 4.6(6-8). When the metal height in the side riser reached 92mm the liquid stopped advancing and instead propagated horizontally into the thin channel under action of the metal head. After

this Figure 4.13(21-26) and Figure (4.6(17-27)) reveal that the melts propagated as overlapping fingers until stopped at a metal head 120mm.

In simulation of the strip horizontally, as illustrated in Figure 4.14, the flow pattern predicted bears little similarity to the image obtained from the real-time X-Ray video experiment. Figure 4.14(8-32) and Figure 4.7(1-18)) show that the liquid metal entered the thin section from the junction area with high velocity when the metal reached a certain height. This was because the melts were pushed under the momentum effects and the mensicuses of the metal front continued to flow with approximately constant velocity, at about ($0.62\,m/s^{-1}$ to $0.68\,m/s^{-1}$) along the strips until they were filled.

4.4 Thin wall investment casting with vibration condition.

The experiments were used to assess the influence of vibration on filling capability in the thin section casting.

4.4.1 Effect of vibration on fillability

In the first part of the experiment, the purpose was to evaluate the influence of vibration on the fillability; the ability of metal to fill a thin section. The experimental results in Figure 4.15 shows the effect of application of vibration of 1.3 g for 10 sec.

(a) casting with vibration (b) casting without vibration

Figure 4.15 (a) Casting with 1.3g acceleration of vibration, metal head 60mm, strip thickness 0.55mm, fillability filling type (b) casting without vibration, metal head 60mm, strip thickness 0.55mm, fillablity filling type

From the figure it can be observed that there is a substantial difference between the non-vibrated and the vibrated specimen, showing the dramatic effect of vibration on the filling of the mould. The vibration resulted in the metals having a significantly greater ability to run into the small channel and increase the filling capability from 0% to 100% at a 0.55 mm thick section at a constant metal head of 60 mm.

Results from further experiments run with the vibration in a vertical strips for ten seconds after the filling process, are reported in Table 4.8 and the data plotted in Figure 4.16 as metal head for the different filled sections (0.55mm, 0.75mm) as a function of the acceleration of vibration (0.8g, 0.9g, 1g, 1.2g) at a constant metallostatic pressure head height of 120 mm. data are replotted in Figure 4.17, using the thickness of the strip as a function of the metal head at constant acceleration. From Figure (4.16 a and b), it is clear that the average metal head of the strip with thicknesses of 0.55mm and 0.75mm under zero vibration is 157mm and 117mm, respectively. However, the averages for each of the two metal heads under 1g vibration acceleration are 76mm and 54mm, respectively. This indicates that the metal head required to force the metal in thin sections in the casting vibrated at (1g) acceleration is approximately half that of castings made without vibration.

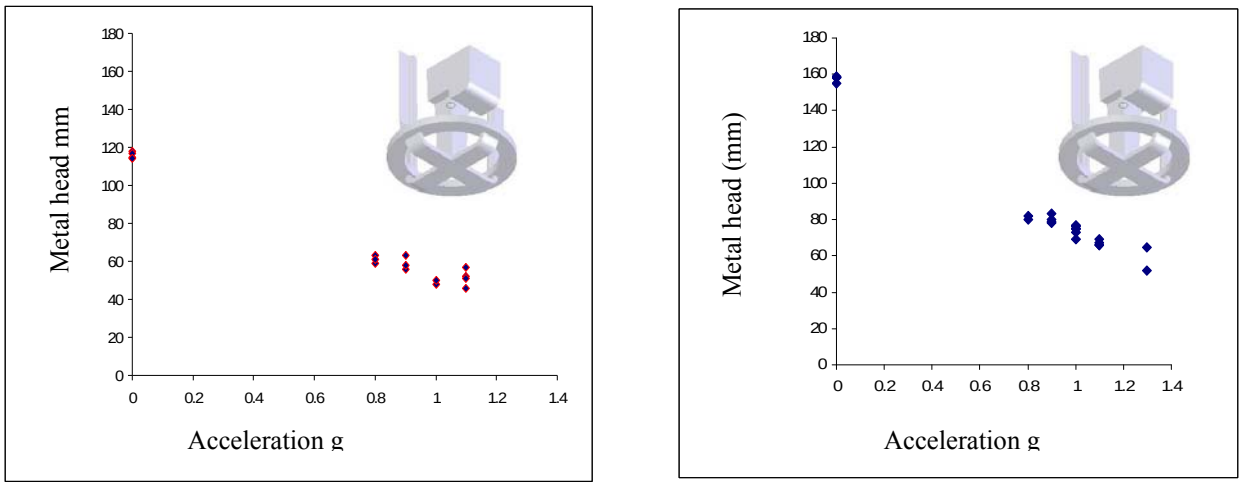

(a) (b)

Figure 4.16 vibration effects on metal head required to fill thin section, fillabillity filling condition (a) strip $0.75^{\pm 0.005}\,mm$ thick. (b) a strip $0.50^{+0.05}\,mm$ thick.

From Figure 4.17 it is seen that the metal head increases with each decrease in the thickness of the strip under any given acceleration.

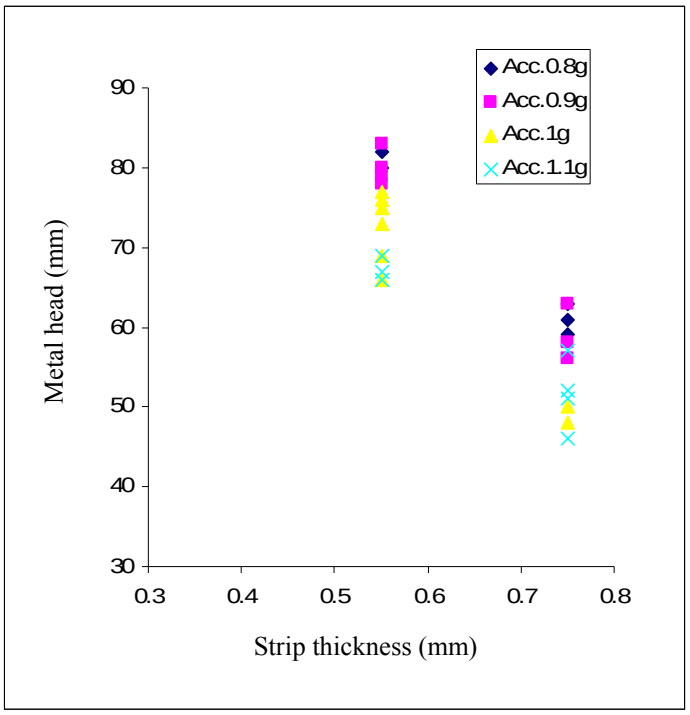

Figure 4.17 acceleration effect on filling capability in different test pieces thickness ($0.55^{\pm 0.05}$ mm, $0.75^{\pm 0.05}$ mm), acceleration varying between (0.8g to 1.3g). Fillability filling condition.

Generally, the results indicate that the effect of the vibration on the metal head is markedly dependent on acceleration and any increase in acceleration leads to a reduction in the size of the metal head needed to fill thin sections (0.55mm and 0.75mm).

4.4.2 Effect of vibration time on the filling capacity

Experiments were run to investigate the time of the vibration operation effect on the filling capability in a thin section and in fillability filling type conditions. The result of the experiment is summarized in Table 4.9, and the data of the results are plotted in Figure 4.18 as metal head as a function of the operation time of vibration at each of the constant accelerations of the vibration and replotted in Figure 4.19, using the relative filling area as a function of the operation time of vibration.

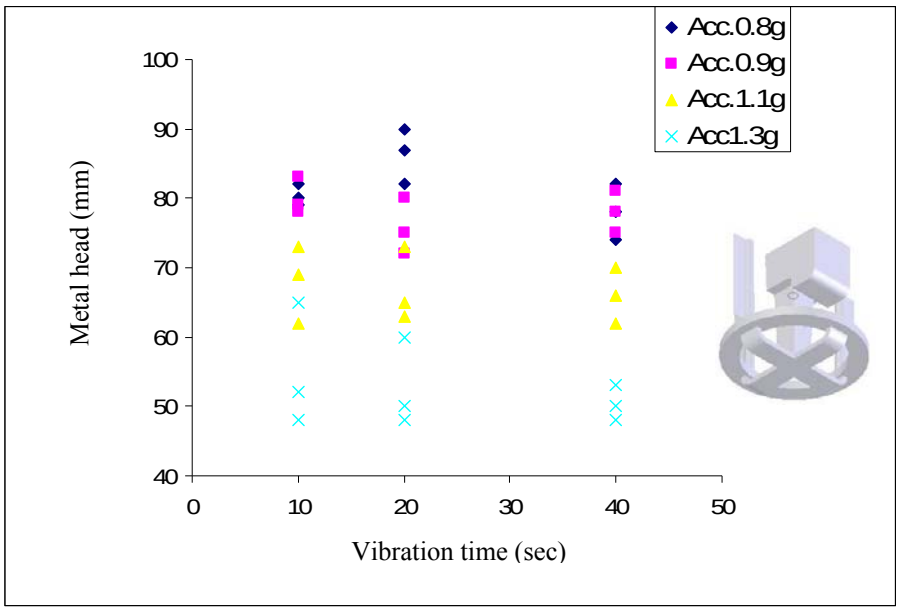

Figure 4.18 shows a vibration time effect on the metal head with a strip ($0.55^{\pm 0.05} mm$) thick and using A356. Pouring temp. 750ºC, Mould temp. $\approx$ 660 ºC to 700 ºC, acceleration of vibration varying between 0.8g to 1.3g

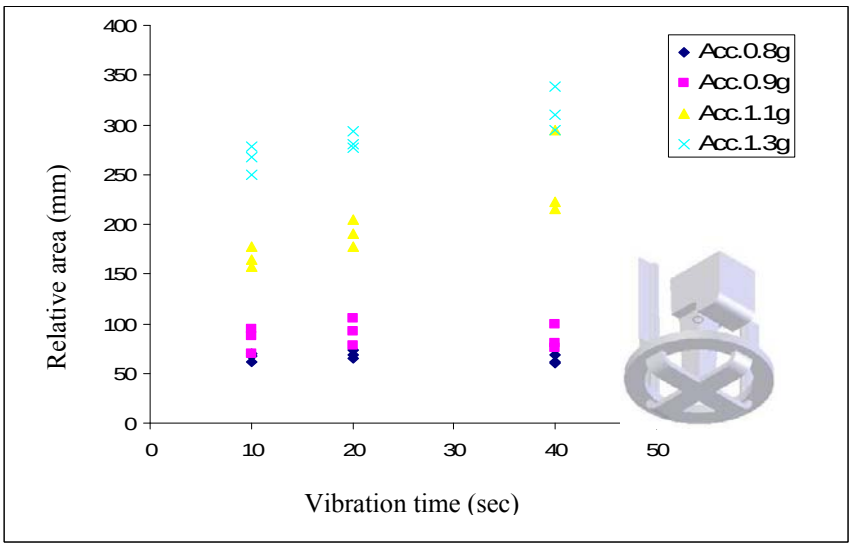

Figure 4.19 shows a vibration time effect on the relative area with a strip ($0.55^{\pm 0.05} mm$) thick and using A356. Pouring Temp. $750C \pm 5$, Mould Temp. $\approx$ 620 ºC to 660 ºC, acceleration of vibration varying between 0.8g to 1.3g

The experiments show that the vibration time had a weak influence on the filling result, and the metal head required to fill a thin section did not change if the vibration time was more than 10 sec.

The vibration time has an influence only on the relative filling area; it increased with every increase in the time of vibration. (See Fig. 4.20). A moderate effect was observed on the relative filling area when the acceleration of the vibration is less than 1g. However, a greater effect was found on the relative filling area when the acceleration of the vibration was greater than 1g.

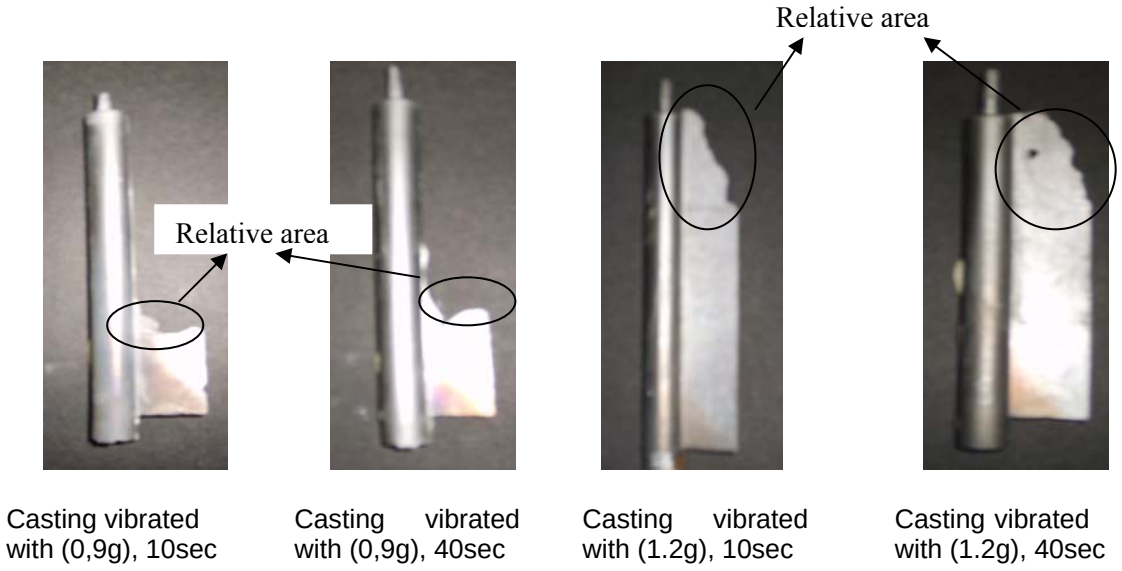

Fig.4.20 Effect of vibration time on the relative filling area, strip thickness 0.75mm, fillability filling type, metallostatic pressure120mm

The statistical of the method can be used to work out the percentage of the relative area and metal head variation with respect to vibration time during constant acceleration; see Tables, 4.10. The data according to these tables were plotted in Figure (4.21 a and b) as a percentage of the relative area and the metal head with respect to vibration time, a function of the acceleration.

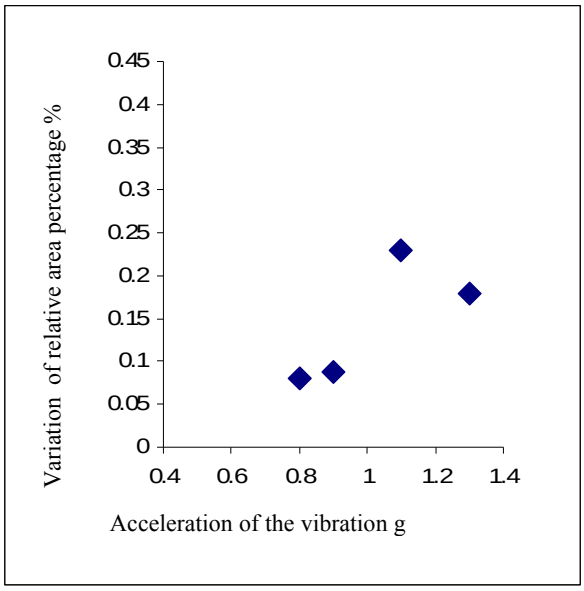

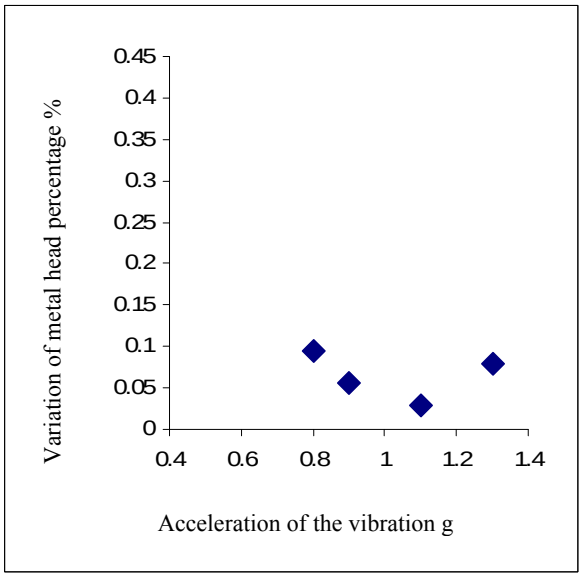

(a) (b)

Figure 4.21 shows;(a) a percentage of the relative area variation with respect to vibration time as a function of the acceleration (b) a percentage of the metal head variation with respect to vibration time as a function of the acceleration with a strip ($0.55^{\pm 0.05} mm$) thick and using A356. Pouring Temp. $750C \pm 5$, Mould Temp. ≈ 620 ºC to 660 ºC, acceleration of vibration varying between 0.8g to 1.3g

Figure (4.21 a and b) shows that the vibration time has influence only on the relative area when the vibration acceleration is greater than 1g

Inspection of castings filled with vibration of more than 1g and with thicknesses of both 0.55mm and 0.75mm, identified lines aligned with the direction of the vibration. These lines are shown in Figure 4.22**.**

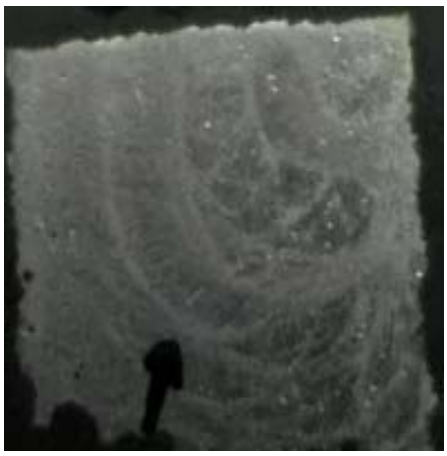

Figure 4.22 Lines on the surface of casting with 1.2g acceleration of vibration, a strip thickness 0.55mm, A356 alloy, pouring temperature 750ºC, mould temperature 660ºC.

4.4.3 The influence of frequency and amplitude on flow pattern

In a series of experiments preformed with the strips put in horizontal and vertical positions, the influence of the vibration parameters (frequency and amplitude) on the propagation flow of the liquid front in thin sections (0.55mm and 0.75mm) at constant acceleration were studied. The detailed results of the experiment are listed in Table 4.11 for each acceleration of vibration.

Two features of the transition can be observed from the front of the morphology: (i) a coherent liquid metal front which occurs in thin wall investment casting when the acceleration due to vibration is less than (1g); and (ii) jetting at the free surface which occurs in thin wall investment casting when the acceleration due to vibration exceeds 1g; this effect is shown in Figures 4.23.

Results are summarized in Figure 4.24. This shows that for the entire combination of frequency and amplitude studied the transition to a jetting of filling mode occurs at an acceleration of 1g.

Casting with 0.9g vibration

Casting with 1g vibration

Casting with 1.1g vibration

(a)

Casting with 0.9g vibration

Casting with 1.1g vibration

(b)

Figure 4.23 Shows a propagation flow of the liquid front in the strip ($0.55^{\pm 0.05} mm$) thick, using A356 alloys. Pouring Temp. $750C \pm 5$, Mould Temp. ≈ 620 ºC to 660 ºC, acceleration of vibration varying between 0.8g to 1.2g, (a) vertical position, (b) horizontal position

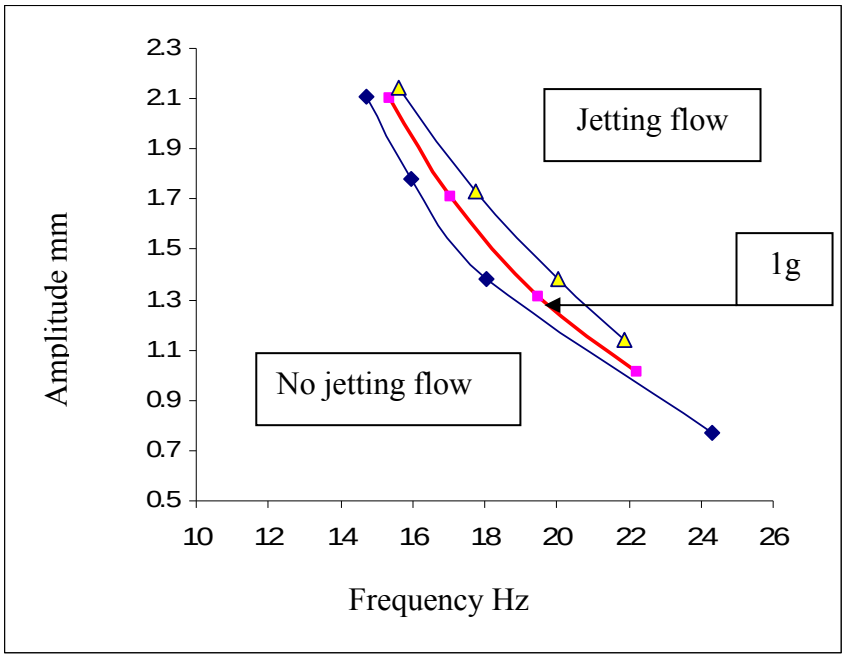

Figure 4.24 Frequency-Amplitude $(f-a)$ map showing peak acceleration which can be generated when the whole casting is vibrated. The red line indicates threshold for the jetting flow

It is clear from Figure 4.24 and table 4.11 that the effect of vibration on the filling capability represented by metal head and the jetting on the free surface liquid can be controlled by a vibration accelerations parameter $(4\pi^2 af^2)$, but not the vibration amplitude a and frequency f separately. 1g is the threshold between the jetting and the non-jetting areas.

4.4.4 Measurment of Jet length

Results obtained from jet length experiments are listed in table (4.12, 4.13) and plotted in Figure 4.25, with the acceleration of the vibration as a function of the jetting length and plotted in Figure 4.26 with metal head as a function of the jetting length.

The experimental result shows that the jetting length in vibration conditions can be controlled and limited, but not wholly eliminated, by reducing the effect of the acceleration due to vibration and the metal head (see Figures 4.27 and 4.28). The length of jetting seems to have a linear relationship with both the metal head and the acceleration generated by vibration.

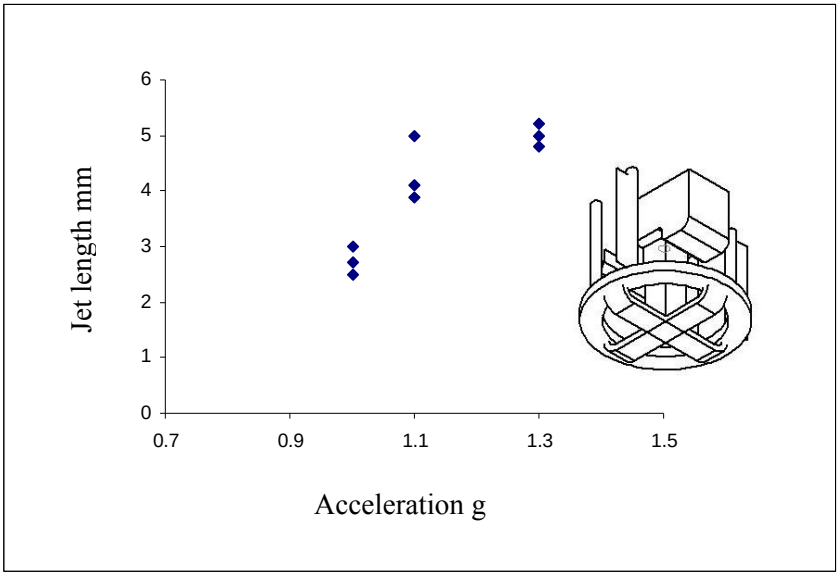

Figure 4.25 length of the jetting affect by acceleration of vibration at a constant metal head 45mm, a thickness of the strip is 0.55mm. Fillability filling type

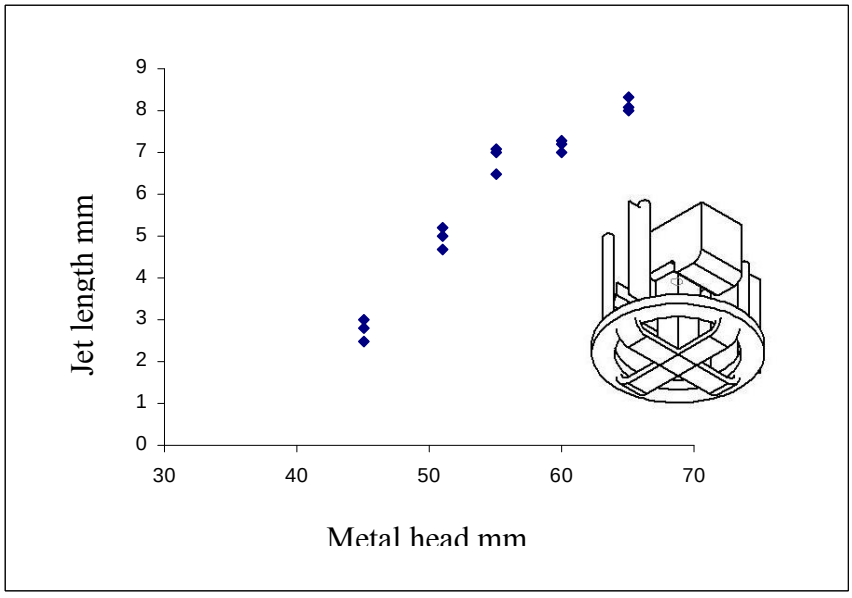

Figure 4.26 length of the jetting affect by metal head at a constant acceleration of vibration 1g. A thickness of the strip is 0.55mm. Fillability filling type

(a) a jetting length at 45mm metal head

(b) a jetting length at 55mm metal head

(c) a jetting length at 60mm metal head

Figure 4.27 (a, b, and c) shows the length of jetting affect by the acceleration of vibration at a constant metal head (45mm), a thickness of the strip is 0.75mm., Fillability filling type.

4.4.

(a) a jetting length at 1g acceleration of vibration

(b) a jetting length at 1.1g acceleration of vibration

(c)a jetting length at 1.2g acceleration of vibration

Figure 4.28 (a, b and c) shows the length of the jetting effect by the metal head at a constant acceleration of vibration (1g) on a strip 0.55mm in thickness. Fillability filling type

4.4.5 The flow pattern imaging- mercury experiments

The frames of the high speed video digital camera for the mercury experiment with acceleration 0.9g are shown in Figure 4.29 (Appendix) and the flow distance for the meniscus of the mercury motion measured for each interval are listed in Table 4.14 and plotted in Figure 4.30 as a function of time.

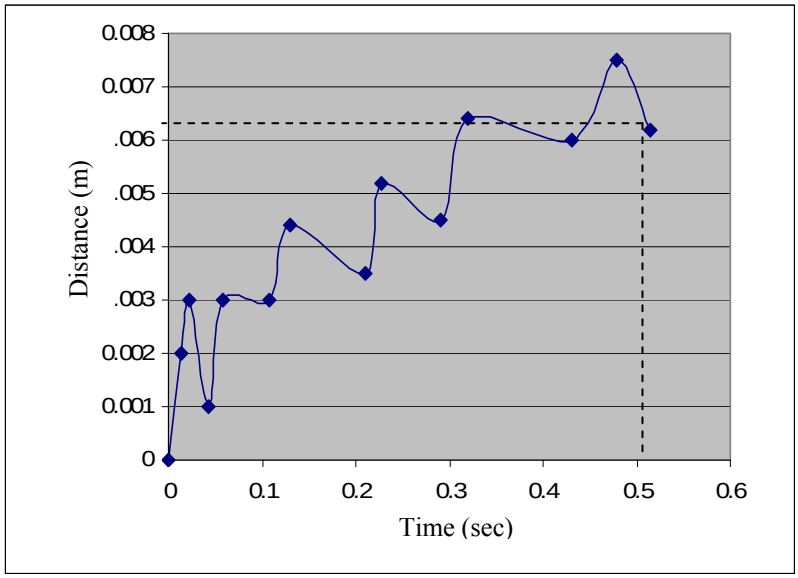

Figure 4.30 Moving distance for the meniscus of the mercury vs time

From Figure 4.30 it is clear that the average velocity of the metal, when Plexiglas mould moves from the peak point in the negative phase to the peak point in the positive phase in a frequency cycle (the opposite direction to gravitation) was found to be ($0.0983\,ms^{-1}$) compare with ($0.16\,ms^{-1}$) obtained from velocity of metal in one frequency cycle at maximum acceleration $U = \sqrt{2(g + a_{\max})\left(h - \frac{\gamma}{\rho r(g + a_{\max})}\right)}$.

However, the velocity of the liquid metal drops to zero when the Plexiglas mould moves from the peak point in the positive phase to the negative phase (the mould moves in the same gravitational direction). If the stopping time of the meniscus front of the liquid is subtracted from the total time of the filling section the average

translational velocity of the mercury in the channel with thickness of 0.060mm in vibration condition was found to be $0.012\,ms^{-1}$.

4.4.6 Simulation of filling under the action of vibration

Result of the calculated liquid flow pattern modelled using a Flow-3D with a constant pressure boundary condition ρhg in the first second of filling and applying a pressure as boundary condition ($\rho h(g + a_{Max})$ in the next second from the start of calculation are shown in Figure 4.31(Appendix), for a vertical strip position with dimensions of ($100\text{mm} \times 15\text{mm} \times 0.55\text{mm}$). According to Figure 4.31 it is clear that in the first second of the calculation the metal flowed into the upriser until it reached a height of (100mm). In the next second of the calculation, the metal started to enter the strip from the junction area between the strip and the upriser at the base of the strip and continued to flow until stopped by the wall. This is because the metal head at this point is at it's maximum value; meanwhile the liquid metal continued to entering from the upriser until it filled the whole strip.

Results show that the flow pattern obtained from the Flow-3D modelling did not confirm with filling sequences observed.

Figure 4.32 (Appendix) shows simulated filling of flow pattern when a time dependent pressure $P = \rho h(g + af^2\pi^2 \sin(\pi f^2 t)$ was applied as boundary condition in the next second from the start of calculation. Generally, results of the simulation revealed that the overall flow patterns obtained from Flow-3D modelling under conditions when the vibration pressure is constant or depends on the time appeared to disagree with the experimental. This is because the Flow-3D modelling and experiments were made under different conditions.

4.5 Defects distributions

Casting defects can be caused by many different foundry parameters, such as high gas content, an unsound filling system design, or insufficient feeding. These defects are presented in casting as a feature of the bubble, oxide film and porosity [4, 107, 125].

In general, defects such as gas porosity were found in the polished casting for all groups of castings as shown in Figures 4.33, 4.34 and 4.35 (Appendix). Examination also identified: surface depression and collapsed bubbles, on the surface. No oxide films were observed in the middle of the castings, but anumber were found at the edge. Generally, the large oval pores accumulated in the middle of the casting, but were small in size, of the gas pores accumulated in the edge, gas pores usually associated with the Al-Si eutectic phase or grain boundaries.

To find the distribution of the defects in each method of casting (casting without vibration, casting with 0.8g and 1.2g vibration after filling and casting with 0.8g vibration during filling), a minimum of 30 fields of view from each method were used to measure the size and the number of defects, as described in section 3.12. The results are reported in Table 4.15. the data is ploted in Figure 4.36.

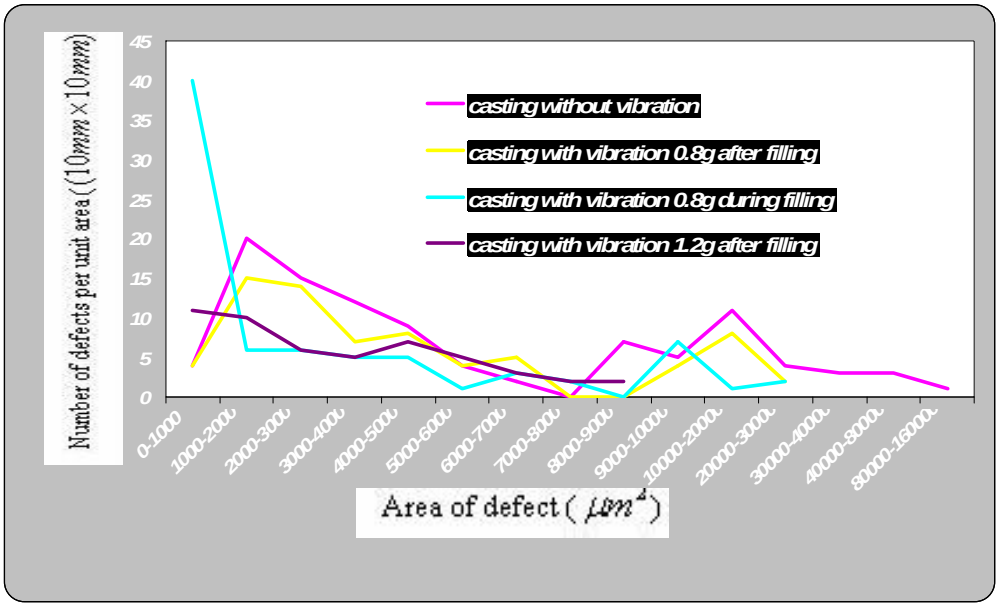

Figure 4.36 the distribution of defects for each method of casting

From the result, it is clear that the lowest number of defects 51 per $100mm^2$ resulted from a casting which used 1.2g acceleration vibration and the largest number 96 per $100mm^2$ resulted from the castings produced without vibration. Moreover, the size of defect decreased, from casting without vibration to casting with vibration. Defects of maximum size were observed in the castings without vibration of 160,000 μm^2; and the peak munbers of defects occurred at intervals of (1000-2000), (1000-2000), (0-1000) and (1000-2000) for casting with vibration 1.2g after filling, casting without vibration, casting with vibration during filling and casting with vibration after filling, respectively.

4.6 Optical microscope and SEM examination

Optical micrographs of defects are shown in Figure 4.37 (Appendix), with a closer SEM views in Figure 4.38 (Appendex), show the polished surface for six test pieces, two pieces with a thickness of 0.75mm for each method of casting (casting without vibration in the fillability and flowability filling types and casting using vibration with acceleration of 0.8g and 1.2g in the fillability and flowability filling types after or during filling process) chosen at random. SEM was used to examine this phase in each method of casting and identify such defects as bubbles, oxide films or any other defects. The image displayed in Figure 4.38a is shown in more detail in Figure 4.38b; it is the SEM examination of the critical area. Generally the microstructures of all the casting alloys were similar and every method of casting shows phase and structure typical of A356 alloys [126]. This indicate that the vibration action in the casting had no effect on the microstructure when casting in the fillability filling type condition.

4.6.1 Microstructure of castings without vibration

Figure 4.33 and 4.39 (Appendex) show the microstructure for a number of fields for speicmens cast without vibration. They reveal that the microstructure in area ($10\text{mm} \times 10\text{mm}$) for specimen has three different phases; aluminum dendrites (α-Al) , Al-Si binary eutectic and a small volume of the ternary Al-Si-Mg_2Si eutectic. They appeared as white, grey and dark respectively. No non-metallic inclusion was found in the whole polished section. By carrying out a search over a wide area of the polishing section, pores of uniform shape and different sizes were distributed randomly, with no crack-like defects detected.

4.6.2 Microstructure castings with acceleration vibration of less than 1g after filling

Figure 4.34 and 4.40 (Appendex) shows that the microstructure for the specimens cast with vibration conditions 0.8g acceleration in a number of fields of an area of $10\text{mm} \times 10\text{mm}$. The casting has the same microstructure as described above (section 4.6.1). However, the bubbles and pores were more compact in shape and of different sizes, with irregularly distributed porosity. Large pores were concentrated in the middle of the specimen and small ones accumulated at the edges of the specimen. No oxide film in the middle area of the specimen. no crack defects were found in the whole of the area examined. gases and shrinkage pores size, was, a little smaller than the gases and shrinkage size in the specimen which was cast without vibration. Dark spots of Mg_2Si were distributed randomly on the grain-boundaries.

4.6.3 Microstructure casting with vibration of more than 1g after filling

the microstructure in an area of about $10\text{mm} \times 10\text{mm}$, showing the three phases Al, Si and Mg_2Si (see Figure 4.41) (Appendix)). Oval and compact bubbles were observed

in this area and were randomly distributed in the whole of the examined area. No significant oxide film was found in the middle of this area. Dark spots (Mg_2Si) were distributed randomly on the grain-boundaries.

4.6.4 Microstructure of casting with acceleration vibration of less than 1g during filling

Figure 4.35 and 4.42(Appendix) shows the microstructure of the casting with acceleration vibration of 0.8g during filling. Three phases were observed: A collapsed and oval bubbles distributed randomly were observed, oxide film were found randomly distributed in the middle of the section that were examined.

4.7 Hardness test

This test was carried out on three groups of specimen (6, 4, and 4 in number) in the casting without vibration and with vibration accelerations of 0.8g and 1.2g respectively. The main aim was to check the effect of the cooling rate during the heat treatment process on the mechanical properties for these groups of castings by the variation value of the hardness for each group. The hardness test was done at the four points of each specimen which covered most of its width . The hardness test results are presented in Table 4.16 for each method of casting. Result indicating that the hardness was more uniform and so was the related mechanical strength. Hence, this confirms that the cooling rate had the same effect on the mechanical properties for each group of specimens.

4.8 Analysis of the tensile and elongation properties

The ultimate tensile strength (UTS) and elongation to failure of test pieces for each method of casting: are listed in Table 4.17. The ultimate tensile strength and elongation

of the test pieces as a function of the number of the specimen for each method of casting were plotted in Figures (4.43 to 4.46

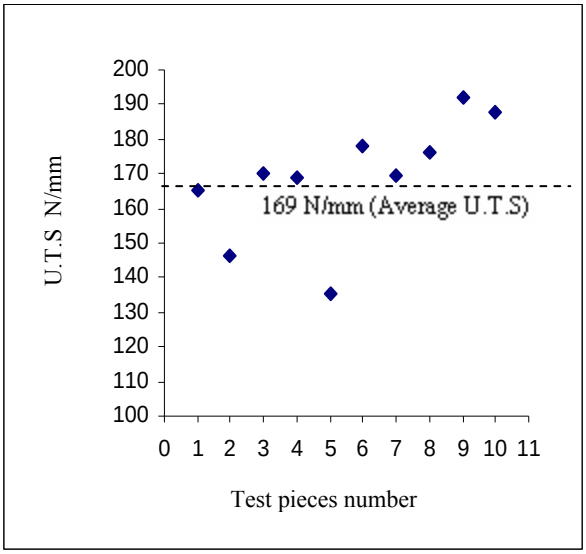

(a)

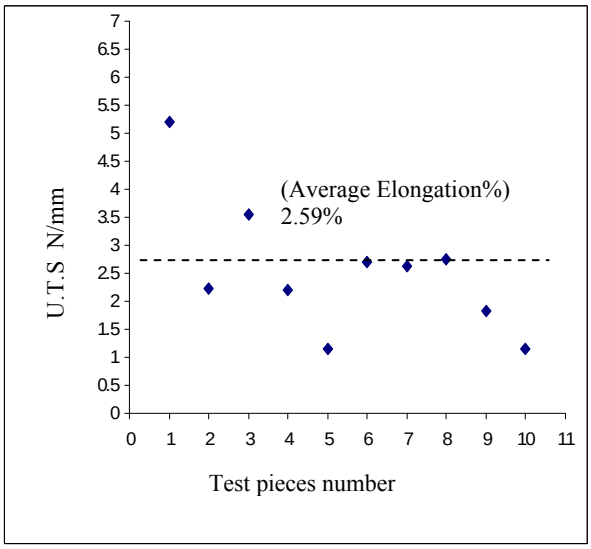

(b)

Figure 4.43 Ultimate tensile strength and elongation to failure of test pieces 0.75mm thick, cast without vibration, fillability filling type condition, pouring temperature 750ºC, metal head 250mm, (a) UTS (b) Elongation to failure

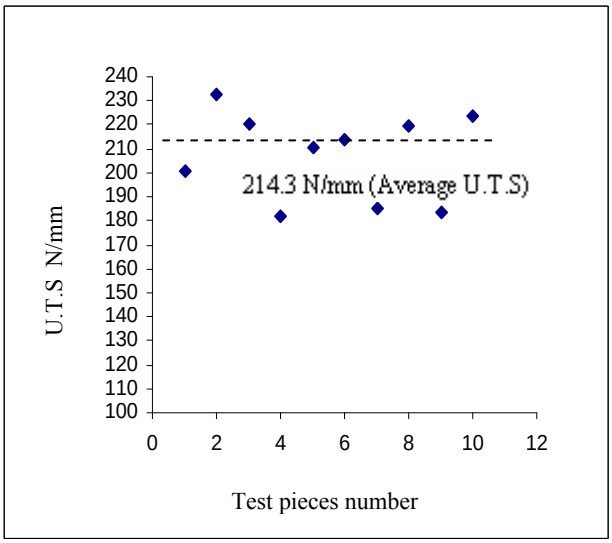

(a)

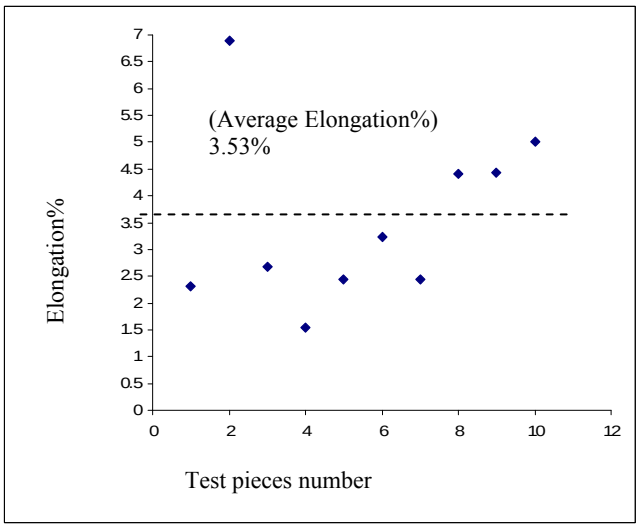

(b)

Figure 4.44 Ultimate tensile strength and elongation to failure of test pieces 0.75mm thick, cast with the acceleration of vibration 0.8g after filling, fillability filling type condition, pouring temperature 750ºC, metal head 250mm, (a) UTS (b) Elongation to failure

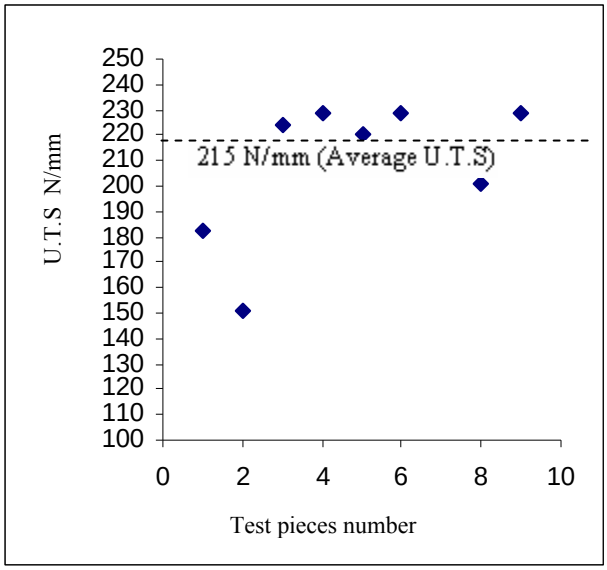

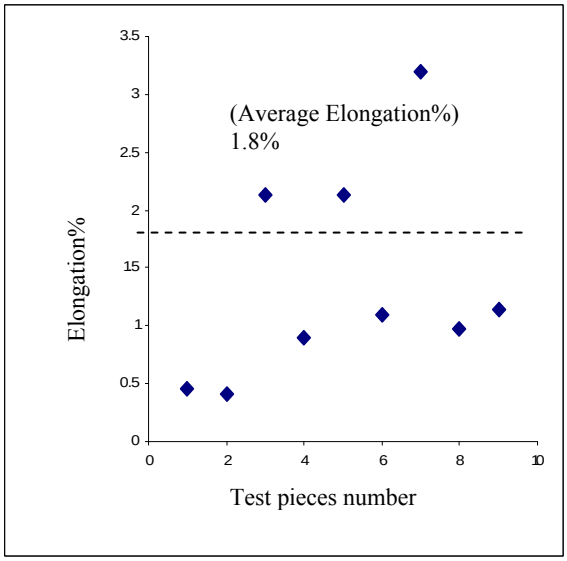

(a) (b)

Figure 4.45 Ultimate tensile strength and elongation to failure of test pieces 0.75mm thick, cast with the acceleration of vibration 0.8g during filling, fillability filling type condition, pouring temperature 750ºC, metal head 250mm, (a) UTS (b) Elongation to failure

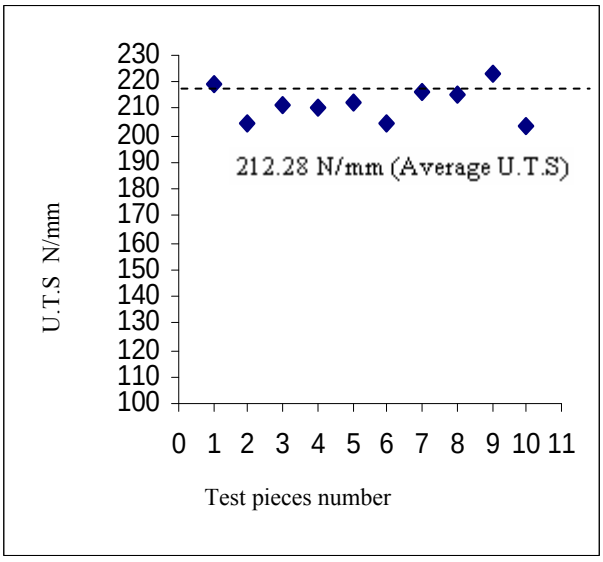

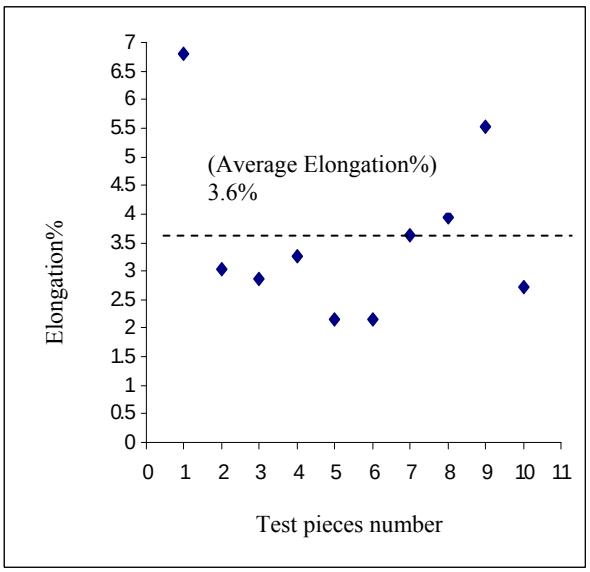

Figure 4.46 Ultimate tensile strength and elongation to failure of test pieces 0.75mm thick, cast with the acceleration of vibration 1.2g after filling, fillability filling type condition, pouring temperature 750ºC, metal head 250mm, (a) UTS (b) Elongation to failure

According to the data in table 4.17and figures(4.43a, to 4.46a) in the part of (UTS), it can be seen that:

1-It evident from these figures that the failure strength are distributed randomly with respect to the mean and there was no discrenible effect of position in the heat treament fixture on final strength

2- The average UTS, increases in the following order: casting without Vibration, then casting with vibration increasing in strength with increases in acceleration.

3- The average UTS of the specimens from casting with vibration was about 212.2MPa greater than that of casting without vibration 168.9MPa.

4- In the case of cast with vibration acceleration of less than 1g most of the failures occurred close to the point of maximum UTS. However, there were a number of castings associated with low strength

5- In a casting with vibration acceleration of more than 1g the failure occurred close to the mean UTS and there were also a number of castings with low strength.

6- In speciemens cast without vibration, most of the failures occurred close to the point of mean tensile strength There is, however, a low strength associated with some castings.

Acorrding to the data in table 4.17 , concering elongation to failure and figures (4.43b, to 4.46b), it can be seen that;

1- Castings made without vibration showed a large scatter of elongation ranging from1.4% to a relatively large elongation of 5.2%, with an average elongation of 2.53%.

2- The elongation data of the casting with an acceleration of vibration of 0.8g after

filling were scattered between 1.55% and 6.9% with an average elongation of 3.53%

3- the average elongation to failure from the specimen cast with vibration conditions of 0.8g and 1.2g acceleration was about 1.07% greater than that of the specimens which were cast without vibration

The ultimate tensile strength and the elongation to failure of the ten test pieces for each method of casting are plotted in Figures 4.47 and Figure 4.48. Generally the figures indicate that the ultimate tensile strength and elongation progressively increases from casting without vibration to casting with vibration.

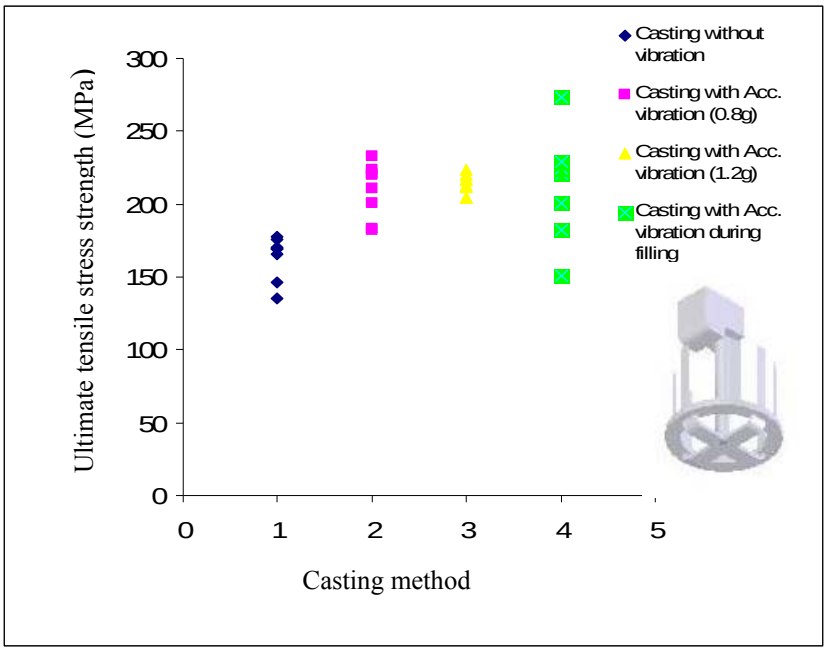

Figure 4.47 scatter plot of the ultimate tensile strength of the test pieces for each group of castings, fillability filling condition.

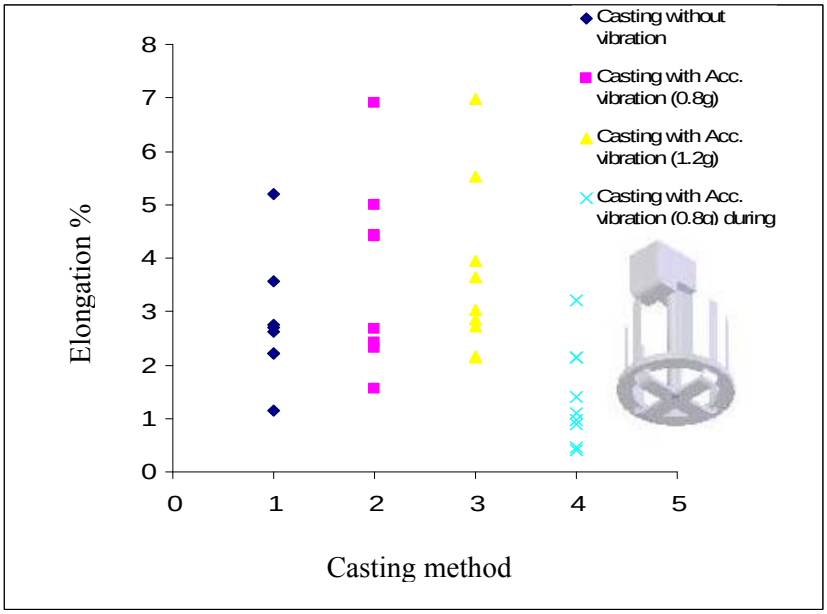

Figure 4.48 scatter plot of the Elongations % to failure of the test pieces for each group of castings.

4.9 Weibull modulus

Weibull plots of the tensile strengths and elongation are plotted in Figures (4.59, to 4.52) for the specimens cast by each method of casting.

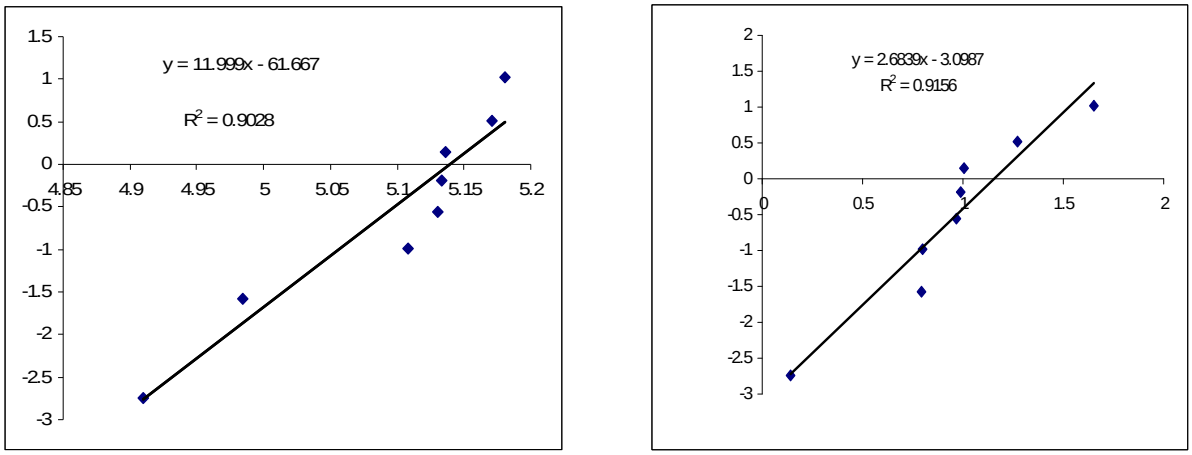

(a) (b)

Figure 4.49 Weibull plots for UTS and elongation to failure, test piece thicknesses (0.75mm) cast without vibration, fillability filling condition, pouring temperature 750ºC; (a) UTS (b) Elongation

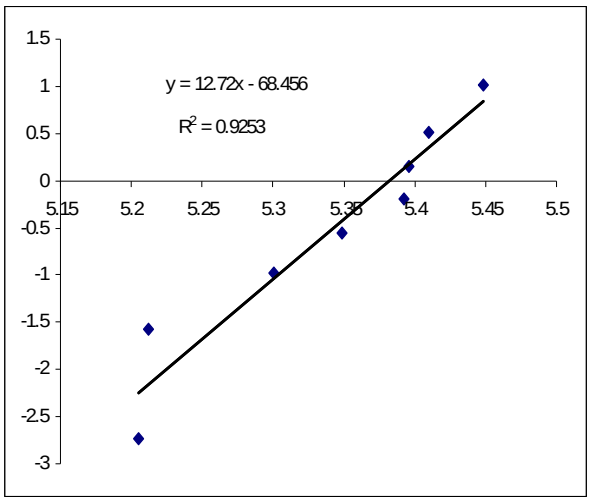

(a)

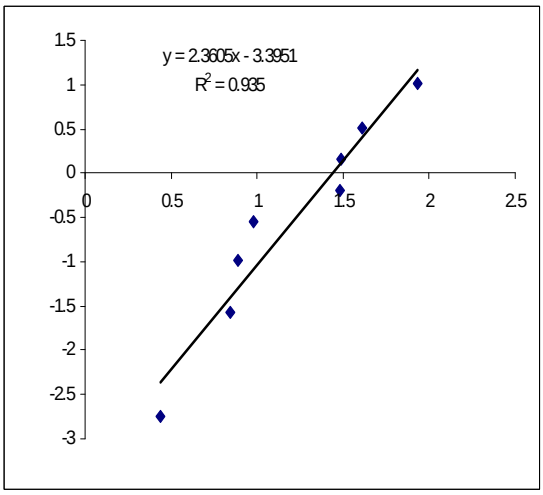

(b)

Figure 4.50 Weibull plots for UTS and elongation to failure, test piece thicknesses (0.75mm) cast with vibration (0.8g) after filling, fillability filling condition, pouring temperature 750C; (a) UTS (b) Elongation

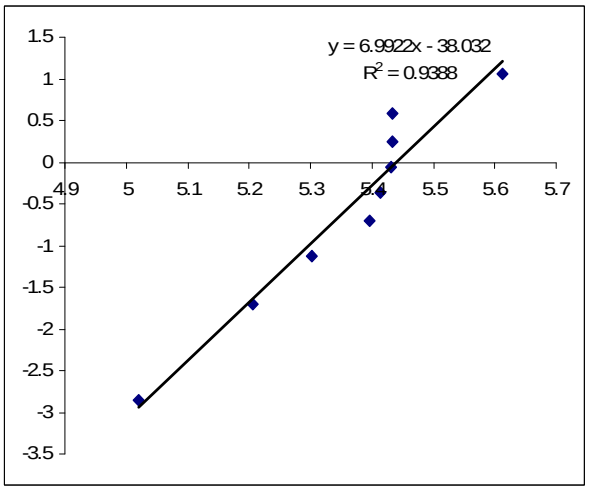

(a)

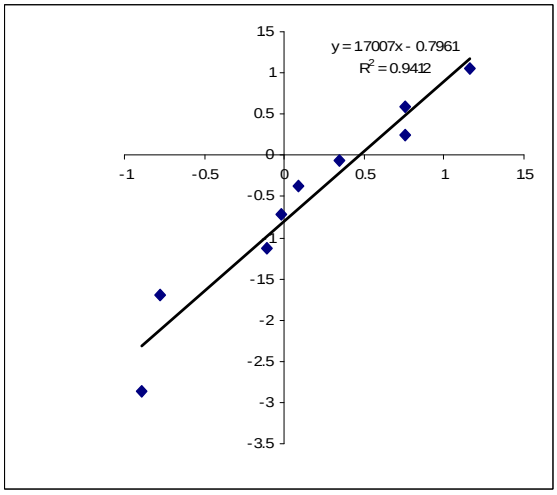

(b)

Figure 4.51 Weibull plots for the (UTS) and elongation to failure, test piece thicknesses (0.75mm) cast with vibration (0.8g) during filling, fillability filling condition, pouring temperature 750C, (a) UTS (b) Elongation

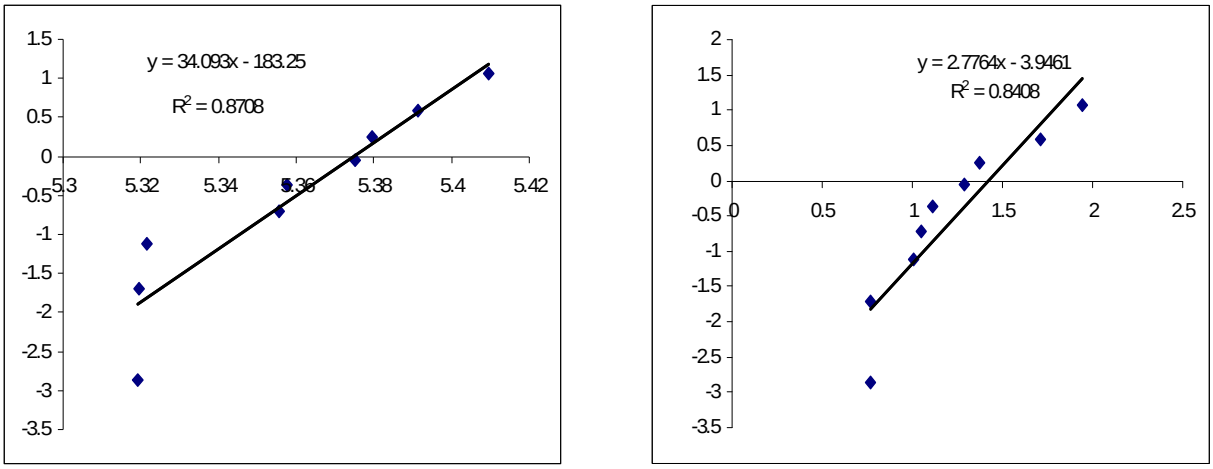

(a) (b)

Figure 4.52 Weibull plots for the (UTS) and elongation to failure, test piece thicknesses (0.75mm) cast with vibration (1.2g) after filling, fillability filling condition, pouring temperature 750C; (a) UTS (a) Elongation

A Weibull plot of all UTS is shown in Figure 4.53 and elongation to failure in Figure 4.54.

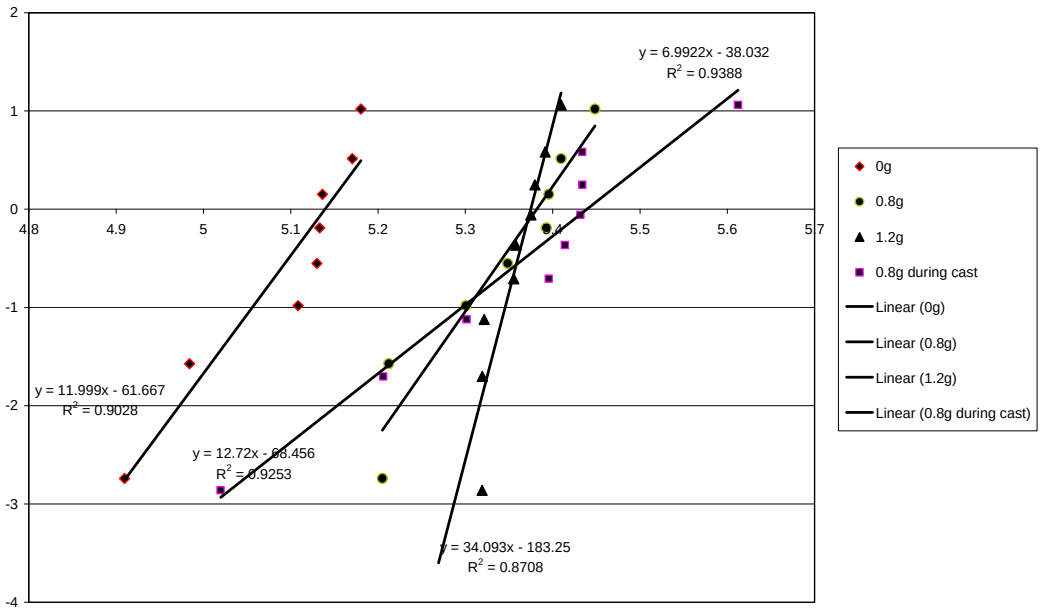

Figure 4.53 Weibull plots of UTS data for each method of casting

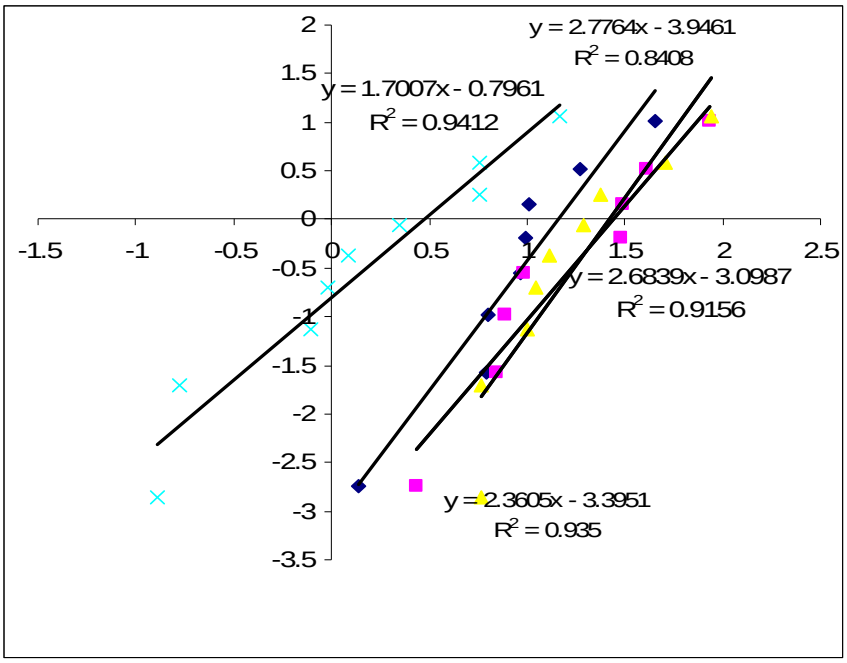

Figure 4.54 Weibull plots of elongation data for each method of casting

To evaluate the vibration influence on the quality of casting. A sample calculation was done to investigate the vibration effect on the Weibull parameter value σ in each method of casting, using the data which available in the Figures 4.54..

$$Fw = 1 - \exp(-(\frac{x}{\sigma})^{\lambda})$$

$$\ln\ln(\frac{1}{1-Fw}) = \lambda \ln x - \lambda \ln \sigma$$

From the base fit line to the data of UTS in each method of casting

$$\ln \sigma = \frac{61.667}{11.999}$$

$$\sigma = \exp(\frac{61.667}{11.999}) = 170MPa \text{ (Casting without vibration)}$$

$$\sigma = \exp(\frac{183.25}{34.093}) = 215.94MPa \text{ (Casting with vibration acceleration 1.2g)}$$

Assessment of the position parameter indicates that the position parameter of the castings made with acceleration from vibration of 1.2g was found to be 216MPa, compared with 170MPa in the casting without vibration. This indicates vibration has a positive input on performance of the castings.

Weibull best fit parameters were calculated using linear regression and the best fit parameters summarized in Table 4. 18 together with correlation coefficient.

Table 4.18 Weibull best fit parameters of the tensile strength distribution for each method of casting

Method of casting	λ	σ	R
Casting without vibration	12	170	0.9028
Casting with vibration (0.8) (after filling)	12.7	187	0.9253
Casting with vibration (1.2g) (after filling)	34	215	0.8708
Casting with vibration (0.8) (during filling)	7	225	0.9388

The results reveal the following;

(i) the Weibull modulus value for the casting with an acceleration of vibration of 1.2g after filling is 34, approximately three times greater than the Weibull modulus value for the casting made without vibration 12 (many shrinkage porosity as result from high cooling rate).

(ii) The Weibull modulus dropped from 12.7 for a casting with acceleration of vibration of 0.8g after filling to 7 for castings with an acceleration of vibration of 0.8g during filling.

(iii) The highest value of the Weibull modulus of the elongation to failure is 2.8. This was found in castings with an acceleration of vibration of 1.2g after filling. However,

the lowest value of 1.7 was found in castings made with an acceleration of vibration of 0.8g during filling.

Generally the weibull moudulus calculation revealed that the vibration reduced the scatter of mechanical properties in the casting, leading to improved reliability of castings.

4.10 Fractography

Green and Campbell showed that the distribution of the tensile results for cast aluminum is skewed with low properties, but there is a cut-off with high properties. They concluded that this is because of the entrained oxide films and associated defects [6].

4.10.1 Weakest casting

The SEM fractographs of the weakest specimen made without vibration (tensile stren135 N/mm^2 and elongation of 1.51%) are shown in Figure 4.55 (Appendix). From this figure, it can be seen that the fracture surface exhibits, localized ductile failure of the aluminum matrix and also contains bubbles and pores as casting defects. Using EDX analysis, we identified another defect as wrinkled oxide film; it was observed around the dendrite. Sometimes the draped oxide film peels off the dendrite, is shown in Figure 4.55 a, b and e, f.

Figure 4.55 shows the section containing two large bubbles which were found on the surface. The bubble with a diameter of about 150 ηm was found at the edge and underneath the top skin of the casting (see figure 4.55 b). One bubble, with an area about of 77500 μm^2 was found in the top half of the section and seems to be two bubbles joined together (see Figure 4.55 c). A high magnification view of each bubble in the section shows that the oxide film was draped around the dendrites on the inner surface of the bubbles (see Figure (4.55 a)).

Figure 4.56 (Appendix) shows fractographs of the weakest specimen which has been cast with the acceleration of vibration of 0.8g after filling, possessing tensile strength of 182 N/mm^2 and elongation 1.55%. Typically, ductile and discontinuity failures

were observed, together with smaller pores randomly distributed on the fracture surface (see figure (4.56d)).

Shrinkage pores of different sizes were found distributed in the section of the surface fracture. A large pore was in the middle with surface area about of 48500 μm^2 and the smaller one with area of 40,000 μm^2 was at the bottom of the field of view (see Figure (4.56 c and e)). EDX was used to identify the defect, as the oxide film was found on the fracture surface, as shown in a Figure 4.57 (Apeendix).

Fractographs of the weakest part cast with an acceleration of vibration 1.2g after the filling process are illusrated in Figure 4.58 (Appendix), with tensile strength 204,000 N/mm^2 and elongation (2.15%) Discontinuity failures of the aluminum matrix were found with cleavage of the silicon phase (see Figure (4.58 f)) and fine dimples were found in the fracture surface (see Figure (4.58 b and c)). No oxide films were found in the section of the fracture (see Figure 5.59 (Appendix)).

4.10.2Highest strength specimens.

Figure 4.60 (Appendix) shows the fractograph of the strongest specimen cast without vibration, with a tensile strength of 178 N/mm^2 and elongation 2.6%. Discontinuity failure and a number of dimples were observed on the fracture surface (see Figure (4.60b)).

Two big pores were found on the surface, one of area 16000 μm^2 was seen in the middle of the fracture surface (see Figure (4.60c)) and another of area 75400 μm^2 was found in the bottom half of its section. An oxide film was observed in the pores draped and peeling off the dendrite

SEM fractograph of the strongest specimen cast with the acceleration of vibration 0.8 after the filling, with a tensile strength 232 N/mm^2 and elongation 6.9% are

illustrated in Figure 4.61 (Appendix). The figure shows that the fracture surface is ductile and there is some discontinuity failure, and a number of dimples distributed randomly on the surface. One bubble, circular in shape, with a diameter of 160 μm was seen at the top of the section and a bubble trail at the bottom of the field of view. Oxide film was draped around the dendrites on the inner surfaces of the bubbles

Figure 4.62 (Appendix) shows the SEM fractography of the test piece with a high tensile strength 274 N/mm^2) and elongation 3.2%, which was cast with an acceleration of vibration of 1.2g after the filling process. Discontinuity failure was observed (see Figure (4.62d)). Only one bubble, elliptical in shape with area about of (45000 μm^2) was found underneath the top skin of the casting. The draped oxide film peeling off the dendrite, as a defect, was observed in the bubble (see Figure (4.62b)). Dimples were distributed randomly over the section.

Chapter 5

Fluidity theoretical and experimental

It is the objective of the work presented in this chapter to develop a mathematical model that enable calculation of the fluidity length of thin strips in investment casting which account for the effect of both mould surface roughness and vibration.

Surface roughness has been studied with the objective of calculation of the interfacial heat transfer coefficient (IHTC) during liquid contact and subsequent by the IHTC during separation of the solidifying metal from the mould (gap formation). There data are applied in a one dimensional model of solidification during filling of a channel. The effect of vibration is quantified and incorporated into the fluidity model, such that the velocity with and without vibration can be input.

5.1 Mis-run defects as a result of heat loss in a thin wall casting

Under the action of gravity liquids take the shape of their container. In the case of casting with fillability filling type conditions (when the temperature of the mould is more than the liquidus temperature) [1,6], the molten metal and mould should retain sufficient heat (due to its state, since no phase transformation before filling has occurred) and complete filling of the mould cavity can occur before solidification commences, so that the desired shape is obtained.

In the fowability filling type; during the filling process, the molten metal will continue to flow into the mould so long as it is in either a liquid or a semi-solid state. During this time molten metal loses heat energy to the mould walls when it passes through various parts of the mould such as the pouring basin, sprue and gating, until it reaches the mould cavity. This will cause a drop in the temperature of the liquid metal from the superheat temperature to below the liquidus temperature. After this point, a small amount of solidification begins; this causes a reduction in the velocity of the metal flow (due to increased viscosity) until it stops, when the temperature decreases to

somewhere above the solidus point. This may cause mis-run defects to occur in thin section castings causing the casting to be rejected [19].

5.2 Eliminating mis-run defects by improving the fluidity in the flowability filling type

Campbell [6] stated "With ceramic shell investment casting, it is not difficult to make the fluidity characteristic infinite in value, because we can raise the temperature of the mould to the melting point of the alloys. When this is done the melt continues to run until stopped by gravity, surface tension, or the mould wall". However, in practical casting conditions (with a flowability filling type of mould), the molten metal and the mould are very different in temperature.

From the literature available [e.g. 18, 42, 43, 115,] on fluidity in flowability filling type conditions (when the temperature of the mould is less than the liquidus temperature), it is clear that fluidity has a major effect on the filling of the mould. It can be improved by controlling factors relating to flow and heat transfer, including superheat, alloy composition and the resultant mode of solidification. However, fluidity improvement in thin wall investment casting is another matter; the surface tension is an additional factor which should be taken into account when calculating fluidity [5, 6, 19, 35, 115].

The technique to "increase" the metal head during casting to improve the fluidity in thin sections will be explored in the section dealing with the application of vibration during the pouring process or after the filling process.

5.3 Mathematical model of heat loss and fluidity of thin wall castings.

In recent years, it has been important to increase the efficiency of production by modelling of manufacturing processes. This has led many researchers to concentrate on mathematical techniques applied to process modeling [e.g 47,]. Analysis of fluid flow and heat transfer are frequently used in modelling to improve the quality and yield of castings by improving their fluidity characteristics [116]. To formulate expressions for filling, such as empirical formulas or charts, it is necessary to understand the fundamentals of the heat transfer and fluid flow mechanisms during the filling processes. This is because of the complex nature of the coupling between heat transfer and fluid flow during solidification. The present work, brings together the fluid flow, surface tension repulsion and heat transfer as a coupled thermal and mechanical problem, to analyze mathematically the rate of heat loss during casting (this procedure was used by Waleed, Al- Sammara, and Daws [117 and 118], they worked together as a team in military industry projects to improve the of duplex stainless steel melts in ceramic shell investment casting, using a centrifuge method, but this approach is enhanced here to evaluate fluidity during low frequency vibration conditions in thin wall investment casting). The following conditions have been assumed:

1- A one-dimensional model in x-direction (high thermal conductivity metal, thin section)

2- An isothermal boundary (assumed due to be the very short filling time)

3- Steady-state temperature distribution.

4- Isothermal boundary condition (constant wall mould temperature)

5.4 Derivation of model for fluidity

The model comprises a one-dimensional heat transfer model with phase change, under an established flow field in a thin ceramic channel under the influence of low frequency vibration throughout the casting cycle, as shown in Figure 5.1, below.

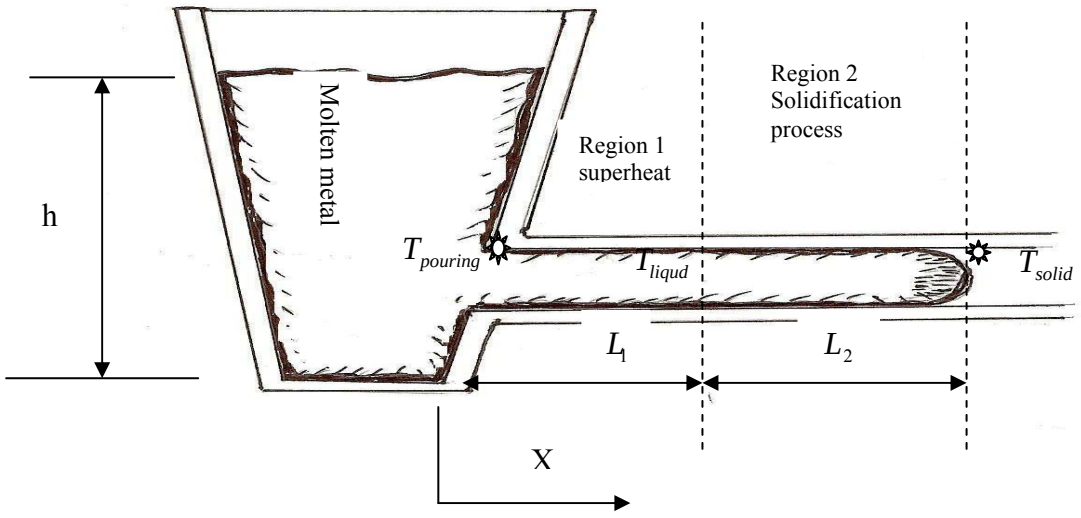

Figure 5.1 Mathematical geometry used to develop the analytical model

When the molten metal flows into the mould, it loses heat to the mould wall and begins to solidify at the liquidus temperature. When sufficient solid is formed, the remaining liquid will gradually cease to flow. Therefore, the total distance covered by the metal can be divided into two main regions of heat loss to the mould, as follows:

5.4.1 Heat Loss from Superheated liquid

Given the elemental control volume shown in Figure 5.2, the energy balance may be written as follows:

d

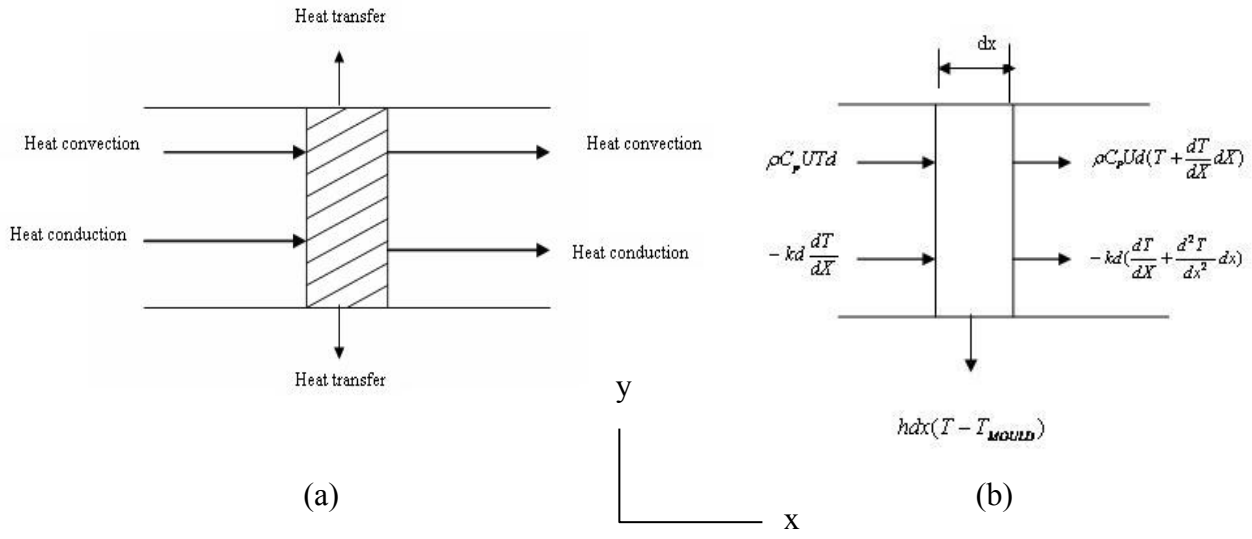

Figures 5.2 Elemental volume for energy analysis of superheated liquid

Heat energy convected in the left face + heat energy conducted in the left face = heat energy convected out of the right face + heat energy conducted out of the right face + heat transfer by convection out of the top and bottom faces of the liquid and conduction between the mould and the liquid surfaces.

Writing the energy balance to correspond to quantities shown in Figure (5.2),

$$-\rho C_P U d\frac{dT}{dx}dx + kd\frac{d^2T}{dx^2}dx = 2h_1 dx(T - T_{mould})$$

Where h_1, is the heat transfer coefficient in the superheat region, U_1 is the velocity of liquid metal, ρ is the density of the liquid, , k is the thermal conductivity of the liquid and T is the temperature of the molten metal, C_P is the specific heat, T_{mould} is mould temperature.

Dividing by $\rho C_P ddx$ gives

$$\alpha\frac{d^2T}{dx^2} - U\frac{dT}{dx} - \frac{2h_1}{\rho C_p d}(T - T_{mould}) = 0$$

When the heat loss reduces the superheat and the metal is still in a completely molten state (single phase), the following equation can be written:

$$U_1 \frac{dT}{dx} = \alpha \frac{d^2T}{dx^2} - \frac{2h_1}{\rho C_p d}(T - T_{mould})$$

$$\alpha \frac{d^2T}{dx^2} - U_1 \frac{dT}{dx} - \frac{2h_1}{\rho C_p d} T = \frac{-2h_1}{\rho C_p d} T_{mould} \quad \text{----------(5.1)}$$

The boundary conditions are proposed, from Figure (5.1),to be:

At X=0, T=T_p and at X=L_1, T=T_{liq} where T_p is the pouring temperature.

The general solution of the non-homogeneous differential equation (5.1) $T_{(x)}$ is the sum of a general solution, $T_{C.F(X)}$ for a homogeneous equation, and an arbitrary particular solution $T_{P.I(x)}$;

$$T_{(x)} = T_{C.F(x)} + T_{P.I(x)}$$

The homogeneous equation of (5.1) is:

$$\alpha \frac{d^2T}{dx^2} - U_1 \frac{dT}{dx} - \frac{2h_1}{\rho C_p d} T = 0$$

$$(\alpha D^2 - U_1 D - \frac{2h_1}{\rho C_p d})T = 0 \quad \text{----------(5.1.a)}$$

The roots of the equation are:

$$m_1 = \frac{U_1 + \sqrt{U_1^2 + \frac{8h_1\alpha}{\rho C_p d}}}{2\alpha}$$

$$m_2 = \frac{U_1 - \sqrt{U_1^2 + \frac{8h_1\alpha}{\rho C_p d}}}{2\alpha}$$

The solution of Equation (5.1.a) is:

$$T_{C.F(x)} = Ae^{m_1 x} + Be^{m_2 x}$$

The particular solution of the non-homogeneous equation (5.1) is: $T_{p.l(x)} = T_{mould}$

The general solution of Equation (5.1) is:

$$T_{C.F.(x)} = Ae^{m_1 x} + Be^{m_2 x} + T_{mould}$$ ----------(5.1.b)

Applying the proposed boundary conditions to Equation (5.1.b) to find the constants (A and B) gives;

Substituting the first boundary condition; $T_p - T_{mould} = A + B$

Substituting the second boundary condition, we find: $0 = Ae^{m_1 l_1} + Be^{m_2 l_1}$,due to the fact that m_1 is always positive and m_2 is always negative. Then: A=0 and $B \neq 0$, since m_1 is always positive and m_2 is always negative.

$B = T_p - T_{mould}$

$$\frac{T - T_{mould}}{T_P - T_{mould}} = \exp \frac{\left\{ U_1^{\,2} + \frac{8h_1\alpha}{\rho C_P d} x \right\}}{2\alpha}$$

And the liquid flows a distance L_1 before losing its superheat, where

$$L_1 = \frac{\ln\left\{ \frac{T_{Liq} - T_{mould}}{T_P - T_{mould}} \right\}}{\frac{U_1 - \sqrt{U_1^{\,2} + \frac{8h_1\alpha}{\rho C_p d}}}{2\alpha}}$$

5.4.2 Heat loss with solidification

In this region the metal starts to solidify and becomes a mixture of solid and liquid; the heat content is principally from latent heat, but partly from specific heat. This is illustrated in Figure (5.3):

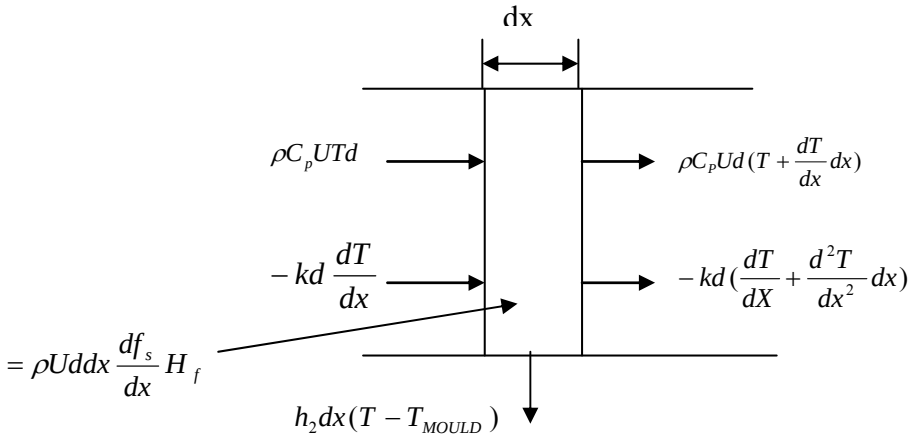

Figure 5.3 Elemental volume defined for energy analysis in the latent heat region

The latent heat $= m^{\cdot} H_f$

$$= \rho U_2 ddx \frac{df_s}{dx} H_f$$

where

$m^{\cdot}$ = mass flow rate

$m^{\cdot} = \rho uA$

f_s = solid fraction

H_f = latent heat of fusion (J/kg)

h_2 = heat transfer coefficient in a latent heat region

U_2 = velocity of metal in latent heat region

Writing the energy balance corresponding to the quantities shown in Figure (5.3), assuming unit depth in the Z direction, the following equation can be applied:

$$\alpha \frac{dT^2}{dx^2} - U_2 \frac{dT}{dx} - \frac{2h_2}{\rho C_p d}(T - T_{mould}) + U_2 \frac{H_f}{C_p} \frac{df_s}{dx} \frac{dT}{dT} = 0$$

$$\alpha \frac{dT^2}{dx^2} - (U_2 - \frac{UH_f}{C_P} \frac{df_s}{dT}) \frac{dT}{dx} - \frac{2h_2}{\rho C_P d} T = \frac{2h_2}{\rho C_P d} T_{mould} \quad \text{----------(5.2)}$$

The term $\frac{df_s}{dT}$ in Equation 5.2 makes the equation a non-linear differential equation, which has no exact solution. To solve Equation 5.2, the relationship between f_s and temperature is needed. Using the data for A356 alloys available from the literature [30], the relationship was plotted in Figure 5.4 as a solid fraction vs. alloy temperature

`It is clear that this is non-linear, but for the analysis it has been assumed that $\frac{df_s}{dT}$ is constant between the liquidus temperature (about 610ºC) and the coherency temperature (about 587ºC) and that the metal stops moving when the f_s reaches 0.5 (the coherency temperature) [17, 19].

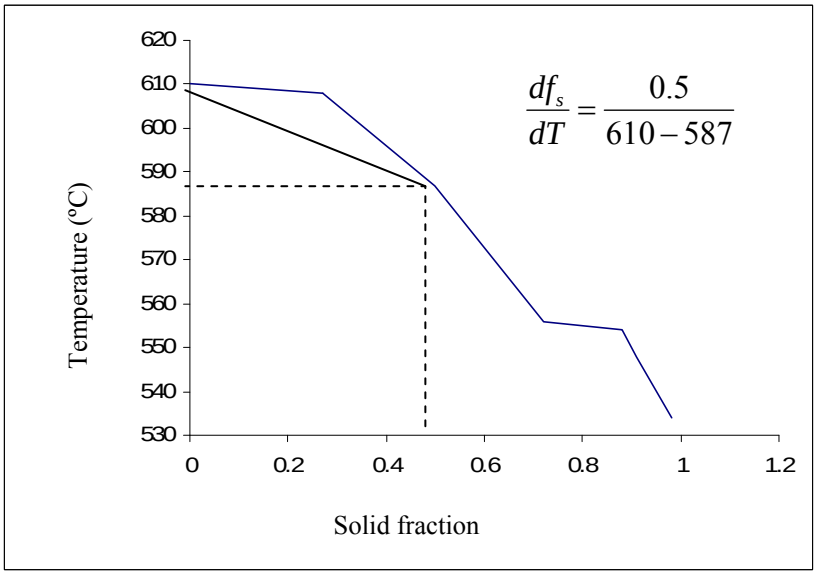

Figure 5.4 Temperature versus fraction solid in the AlSi7%alloy as reported in [30]

From Figure 5.4 we can estimate the value of $\frac{df_s}{dT}$ to be about ($0.0201\,K^{-1}$) and, when this is substituted into Equation 5.2, a linear differential equation can be obtained, which has an exact solution;

$$\alpha = \frac{d^2T}{dx^2} - (U_2 - \frac{UH_f}{C_p}(-0.0201))\frac{dT}{dx} - \frac{2h_2T}{\rho C_p d} = \frac{-2h_2T_{mould}}{\rho C_p d}$$

$$G = (U_2 - \frac{UH_f}{C_P}0{,}0201)$$

$$\alpha\frac{d^2T}{dx} - G\frac{dT}{dx} - \frac{2h_2T}{\rho C_p d} = \frac{-2h_2T_{mould}}{\rho C_p d} \quad \text{----------(5.3)}$$

To solve Equation 5.3, we used the procedure which was used to solve Equation 5.2 for the superheat region was used, of which the result was;

$$L_2 = \frac{\mathrm{Ln}\left(\frac{T_{sol} - T_{mould}}{T_{liq} - T_{mould}}\right)}{\frac{G - \sqrt{G^2 + \frac{8h_2\alpha}{\rho C p d}}}{2\alpha}}$$

The analytical solution obtained for L_2 assumes that the flow continues, at constant velocity, until 50% of the latent heat and the sensible heat of the liquid phase has been lost from the metal stream, i.e., $f_s = 0.5$. It is well known that fluid flow is arrested before $f_s = 1$, thus reducing the attribution of the heat of solidification to the total fluidity length. This is a fundamental difference between the flow mode of Fleming (skin freezing) and the present study (pasty freezing).

It is therefore necessary to account for the effect of f_s on L_f, in particular the effect on L_2. The calculated value of L_2 can be easily adjusted for the relative ratio of the heat lost during semi-solid flow by choosing the solid temperature T_{solid} with respect to the $f_{s(crit)}$, the critical fraction solid at which flow is arrested.

The fluidity of the metal is represented by the total distance covered by the molten metal in a thin channel: $L_{TOTAL} = L_1 + L_2$

5.5 The velocity effect in the fluidity.

Investigation

The result from the heat loss model indicated that the velocity of the molten metal in the channel was an important factor affecting fluidity. At this point, it is convenient to specify the velocity of the molten metal during the filling of the mould.

Previously, Campbell [1,2,14] stated that to produce a good casting, it was essential to fill the mould as far as possible without surface turbulence, by filling the mould at a certain velocity (less than a critical value of 0.5 m/s), to prevent defects resulting from the folding action of the free surface of the molten metal (bi-films).

In the present work, from the real-time X-ray image frames and microstructural analysis, it seems that the value of the velocity of $0.7\,ms^{-1}$ of the molten metal in thin wall investment castings has not quite this effect on the quality of the casting related to the bi-film defects, because no surface turbulence on the free surface of the liquid metal was observed in the experiment during casting. It has been observed that the metal front progressed under surface tension control; thereby, no folding action occurred on the surface of the liquid and thus no bi-films were incorporated into the bulk of the metal. This effect was predicted by Runyoro at. el. [110]

5.5.1 Modeling molten metal velocity

It is not necessary to consider frictional energy loss in this context [47]. As set out below a simple modification, including unsteady state continuity and the Bernoulli equation with additional terms, including the quantity of pressure generated due to surface tension [73], can be used to derive the velocity of the molten metal in a thin wall casting.

Pressure head = ρgh

Back pressure due to surface tension = $\frac{\gamma}{r}$ (neglecting the second radius of curvature and assumming a perfectly non-wetting system)

Effective pressure = $\rho gh - \frac{\gamma}{r}$

No flow can occur when $\rho gh < \frac{\gamma}{r}$, and thus velocity, $U = 0$

The metallostatic pressure required to cause metal to enter a channel of thickness r is:

$$\rho gh = \frac{\gamma}{r} \quad \text{----------(5.4)}$$

Assumptions:

A strip casting was measured in which only the γ component for one dimension was relevent, as only the channel thickness was considered as significant, (hence not $\frac{2\gamma}{\rho rg}$).

Adding the kinetic pressure head into Equation (5.4), to calculate the velocity U using the effective pressure head, it becomes:

$$\frac{1}{2}\rho U^2 = \rho gh - \frac{\gamma}{r}$$

$$U^2 = \frac{2}{\rho}(\rho gh - \frac{\gamma}{r})$$

$$2(gh - \frac{\gamma}{\rho r}) = U^2$$

$$U = \sqrt{2g(h - \frac{\gamma}{\rho rg})} \quad \text{----------(5.5)}$$

Consequently, the velocity in a thin wall casting under the influence of vibration at the positive phase (upward with respect to gravity) of the frequency cycle can be calculated by adding to Equation 5.5 the maximum acceleration generated due to vibration a (section 4.4.5). This then becomes:

$$U_{+p} = \sqrt{2(g+a)(h - \frac{\gamma}{\rho r(g+a)})} \text{ – – – – – – – – – (5.6)}$$

Therefore, the velocity of liquid metal can be quantified by 73% from the theoretical velocity U_f as illustrated in Figure 5.5. Hence the velocity under vibration condition is

$$U_v = 0.73U_f \text{ – – – – – – – – – – (5.7)}$$

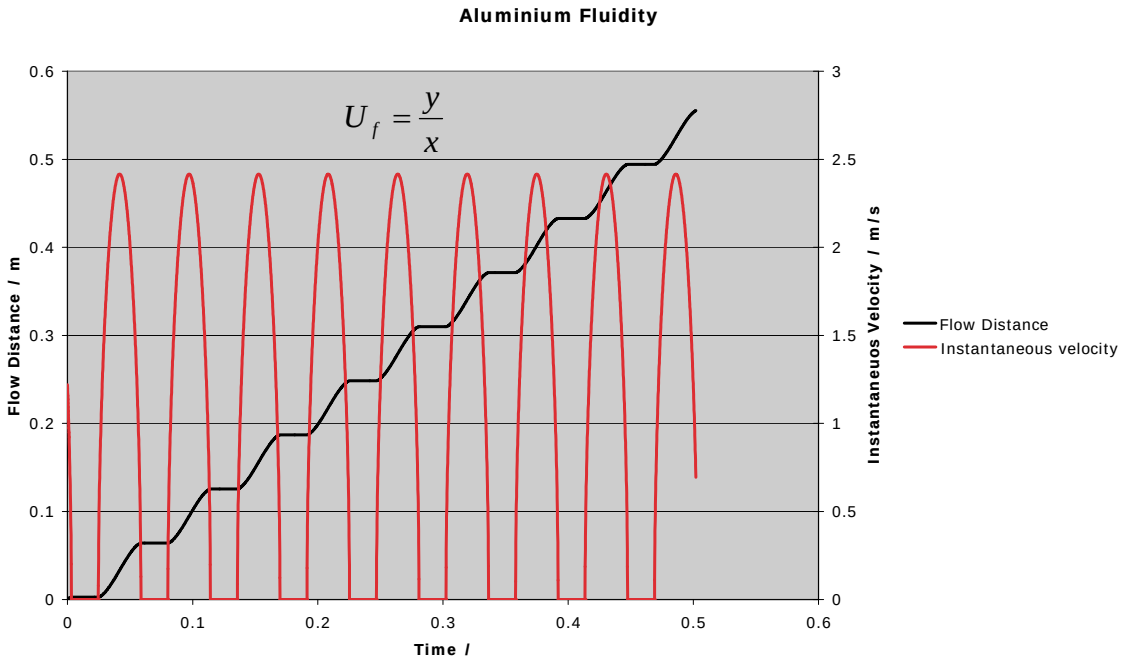

Figure 5.5 theoretical velocity of aluminum liquid metal under vibration

5.5.2 Velocity measurement in thin section without vibration conditions

The velocity of the liquid aluminum alloys in a thin section casting was measured in a real-time X-ray machine and modelled using the Flow-3D software package to compare with the velocity model in the present work.

The experimental result in the fillability filling type conditions, (with the mould temperature higher than the liquidus temperature), without vibration, indicated that the average velocity of the liquid metal front was between 0.68 m/s to 0.7m/s, compared with 1.02m/s calculated by Equation (5.5). This was measured near the junction of the runner and the test piece, with a channel thickness of 0.75mm and a metal head of 180mm. Generally, the average velocity measurement results for liquid metals running in a thin section reveal agreement with the value of the velocity estimated by using Equation (5.5) and they confirm the usefulness of the simple modification of the Bernoulli equation by adding a quantity which represents the back pressure due to surface tension in the thin section, estimated by ($\frac{\gamma}{r}$). The measured

velocity was always less than the theoretical velocity, which suggests that an error may result from ignoring the frictional force between the liquid metal and the mould surface when calculating the velocity, or the secondary radius of the curvature.

From experiments, it was observed that the molten metal was forced into the thin channel at a slightly high velocity by the momentum of flow before the metal reached the height required for the measurement of the velocity. This situation gave an incorrect velocity value through the thin channel, in particular, in the part of the junction between the sprue and the strip. For this reason, a simple modification to the mould design was done (increasing the filling time to 3 sec by reducing the exit area of the sprue in the runner system to about 7mm radius and channel thickness to 2mm (for clarity of the X-ray images (see Figure 3.13)). With this modification in design, the liquid metal reached the height required to make a velocity measurement and also eliminated the influence of the momentum flow on the velocity value).

The result indicated that the average velocity of the liquid metal near the junction between the test piece, 2mm thick, and the gate was found to be $0.75\,m/s^{-1}$, when the metal head was 80mm. This result showed good agreement with the velocity estimated by Equation (5.5) of $0.85\,m/s^{-1}$ and confirmed the modification to the Bernoulli equation.

The result of the experiment carried out in flowability filling type conditions with the temperature of the mould about 420°C, (lower than the liquidus temperature of 610ºC), using the mould design illustrated in Figure 3.11, and without vibration, is that the velocity of the liquid metal decreased with increasing distance of the meniscus from the channel entrance, until it reached 0.41m/s, when it stopped abruptly. Fleming [6, 17, 18] described this phenomenon during his explanation of pasty-type freezing in the solidification processes for Al-Si alloys. However, he

estimated the flow distance L from the simple equation L = U× t_f, which assumed that the liquid has an approximately constant velocity U, where t_f is a solidification time. It has been demonstrated previously (section 2.4.2) that the mode of solidification has an influence on the velocity of the metal in its semi-solid state during the solidification process.

The software package Flow-3D was employed to investigate the velocity of the liquid metal for the Al-7Si% alloys (the physical properties of the liquid Al-Si alloy were obtained from the Flow-3D database and are reported in Figure 3.16), without vibration in a thin channel of 0.7mm thickness, with a metal head 180mm in height. The velocity of the liquid metal front near the junction of the runner and the test piece was simulated in the Flow-3D calculation and was found to be 1.2 m/s^{-1} compared with $0.7\,m/s^{-1}$ as measured by the real-time X-ray image analysis program (fillability filling type). This difference in the velocity value was accounted for by the fact that the interface between the mould and the metal was assumed to be a no slip boundary condition in the Flow-3D software during simulation. This simulation is illustrated in Figure 5.6 (Appendix).

5.5.3 Flow velocity measurement under vibration condition

It is difficult to measure velocity of the liquid metal under vibration conditions using the X-ray machine, for the reason described in section 3.9.

The secondary dendrite arm spacing was measured to calculate the local solidification time along the strip cast under vibration conditions.

The microstructure at the tip of a $0.75mm$ thick strip was examined, as shown in Figure 5.7. The sample had been cast in the flowability filling type experiment under vibration conditions (0.8g), at a mould temperature of 420°C, and a pouring temperature of

750°C using the mould design illustrated in Figure 3.11. Measurements were made at the centerline of the polished section and Figure 5.8 shows typical microstructures, from which SDAS measurements were made.

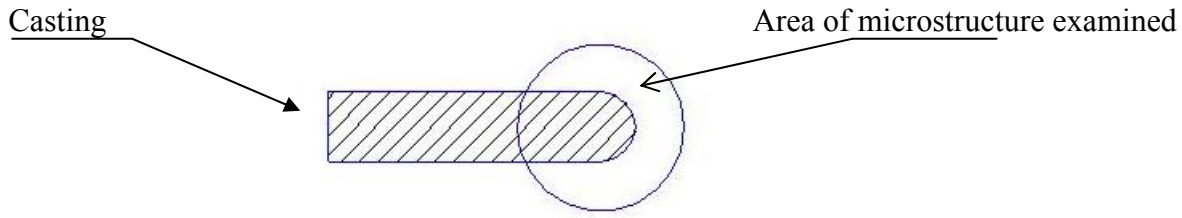

Figure 5.7 Scheme of the area of microstructure selected and examined

Using the regression relationship of SDAS as a function of the solidification time t_f ($\lambda_f = 10.7 t_f^{0.30}$) [114], the local solidification time t_f was calculated to be 1.2s, and fluidity, represented by the length of the casting obtained from the experiment, was measured to be about 120mm. Using the simple equation of fluidity length L= V* t_f [5], the velocity of the liquid metal was calculated to be $0.1\, ms^{-1}$, compared with $0.901\, ms^{-1}$ estimated by using Equation 5.7. Thus any clear definition of metal velocity was not possible. The reasons for this difference in the velocity value may come from an error in calculating the solidification time. The liquid metal flow could stop before the primary aluminum dendrites finished growing, or rapid solidification may increase the amount of the primary phase formed.

Actually, coarsening of the secondary dendrites arms proceeds only for the period from $L \rightarrow L + \alpha$, whereas the total solidification time in casting process also includes $L + \alpha \rightarrow \alpha + (\alpha + Si)$ and higher order eutectic solidification. So the solidification time

at which flow is arrested should be greater than the solidification time calculated using the Hamed correlation [114]. However, the flow arrest time of the 0.75mm thick strip casting without vibration was 0.23s, measured by using a digital video recording made with the real-time X-ray camera, and the fluidity of the casting which was obtained from experiment was 98mm. The average velocity in the channel without vibration conditions was $0.43\,ms^{-1}$. The result revealed disagreement with the velocity value about ($0.06\,ms^{-1}$), which was calculated by using the solidification time estimated using Hamed correlation, it's about (1.3 sec).

This indicates that the Hamed correlation $\lambda_f = 10.7 t_f^{\,0.30}$ is not likely to be particularly accurate in the case of the velocity measurement in thin wall investment castings. Nevertheless, when used in comparative ways, related to solidification time, it gives rather better results.

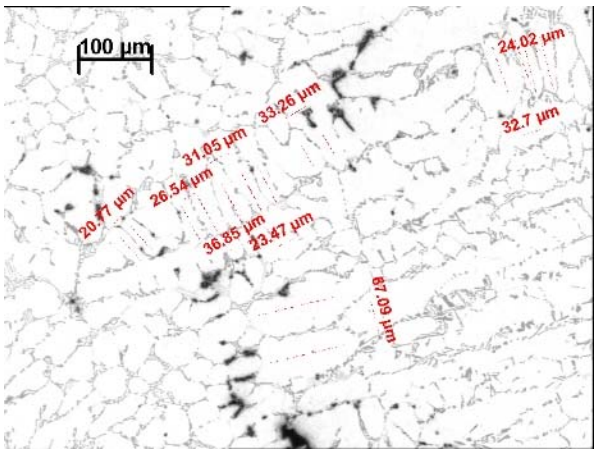

(1a)

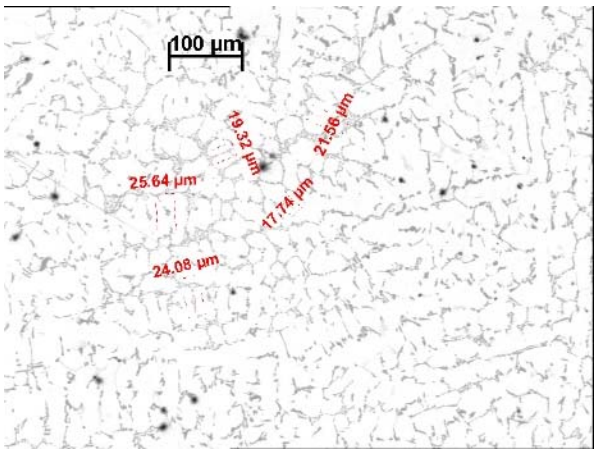

(1b)

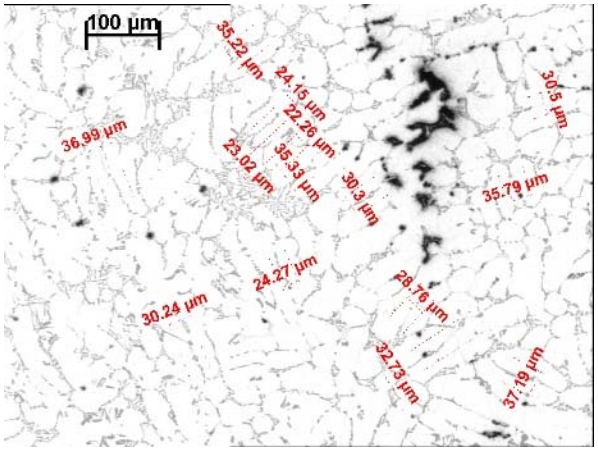

(2a)

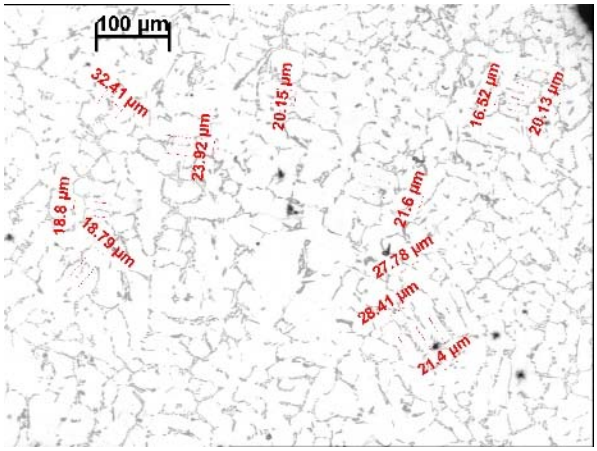

(2b)

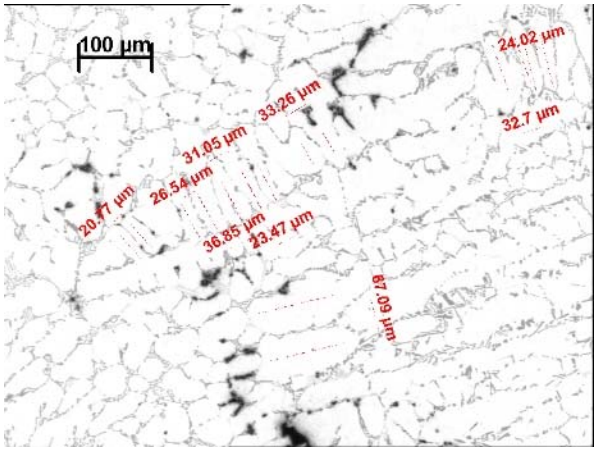

(3a)

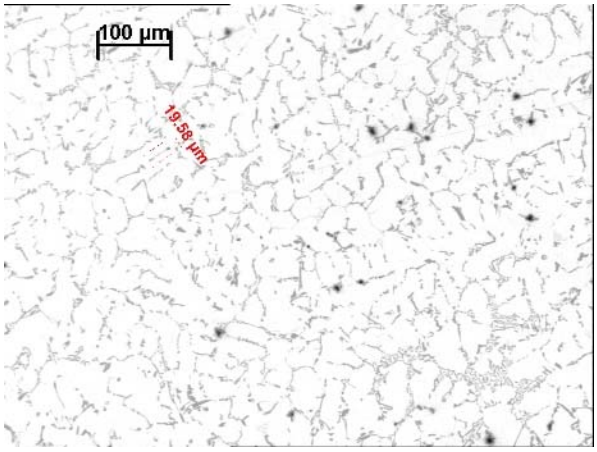

(3b)

Figure 5.8 Typical mid-thickness strip microstructures observed at the flow tips of (a) castings filled with vibration and (b) castings filled with 0.8g acceleration (pouring temperature, 750ºC; mould temperature 420ºC; metal head 170mm).

5.6 The heat transfer effect on fluidity

The use of simulation software in manufacturing processes has increased the efficiency of production. However, the result obtained from mathematical models depends on the accuracy of the data describing the thermophysical properties of the material involved in the modelling processes [116**].** (Also the equations describing the process, and the method of their solution).

To describe heat transfer in mathematical models, the heat transfer coefficient h is necessary, and is another factor affecting the fluidity value. At this point, it is convenient to specify the heat transfer coefficient between the molten metal and mould surface during the filling of the mould.

5.6.1 Calculation of a heat transfer coefficient

From the literature available [85,87,119], it emerges that the basic idea of heat transfer during the solidification processes in low melting point alloys in investment casting can be described in two stages. The first is an initial contact stage; liquid metal has penetrated (to a degree dependant upon the surface tension of the liquid metal and the surface microtopology of the mould) into the valleys of the rough surface of the mould upon which it rests. Immediately a thin skin of solid metal forms (it should be noted that the oxide film can be neglected in the calculation of the heat transfer coefficient [85]) at the contact areas between the liquid metal and the mould surface peaks upon which the liquid metal rests. It has been shown that the heat transfer coefficient can be estimated from measurements of the mould surface roughness, calculation of the contact area between the liquid metal and mould surface, and the residual non-contact area (a series of air pockets trapped in the valleys of the mould surface roughnesses). A heat transfer coefficient can then be calculated on the basis of the resistances to heat diffusion that are summed in parallel (See Figure (5.9)). The

formation of the air gap occurs next. Deformation, caused by the expansion and contraction of the thin skin of casting would result in an increase in the size of the gap or even complete separation between the casting and the mould. This situation causes a reduction in the contact area between the casting and the mould surfaces, and decreases the rate of heat transfer from the casting across the interface. In this case, (IHTC) can be assumed to be equal to the sum of the depths of the valleys in the surface profile for the ceramic mould and the casting surface. In this case, the heat transfer coefficient can be estimated by the size of the gap created due to the surface roughness of the two surfaces and the thermal conductivity of the gas in the gap (probably air). This is shown schematically in Figure (5.10).

From the description above it is clear that there are two different heat transfer coefficient values for a thin wall investment casting during the filling process; one for the superheat region (which would depend on the size of the contact area between the liquid metal and the peaks of the surface roughness of the mould), and another for the latent heat region (which would depend on the size of the gaps forming in the interface between the metal and the mould surface). Therefore, heat transfer coefficient estimates were obtained for a superheat and a latent heat region, separately.

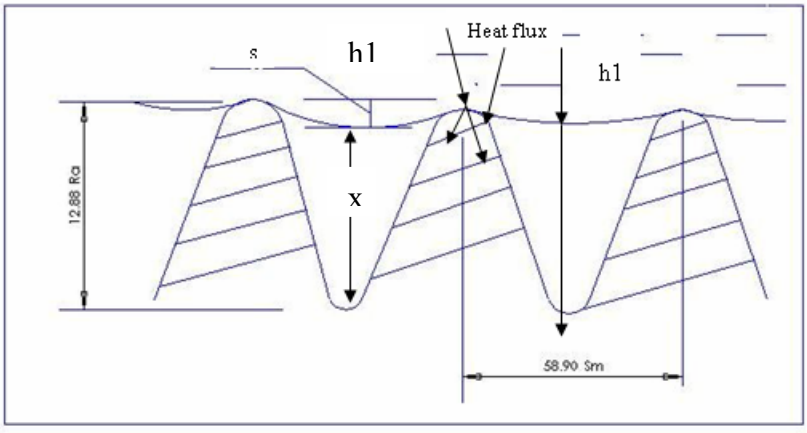

Figure 5.9 Metal-mould interface at the first stage and at the heat flux

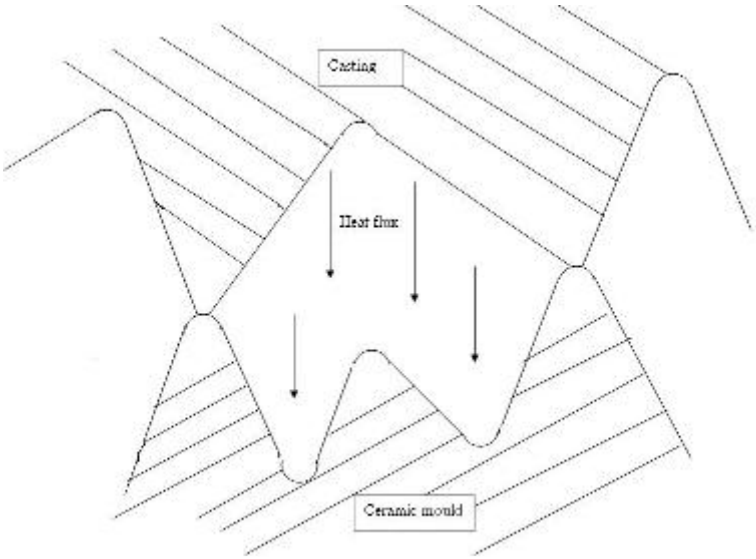

Figure 5.10 Metal-mould interface at the second stage (air gap forming)

The parameters of the surface roughness of the ceramic shell before casting, and the casting surface, were measured using Taylor Hobson surface profilometer device, and are summarized in Table 5.1. The table also includes the mean radius b of the asperity peaks of the rough mould surface, measured using the same instrument.

Table 5.1 Surface roughness data obtained from the ceramic mould and castings

Surface measured	$R_a(\mu m)$	$R_z(\mu m)$	$S_m(\mu m)$	b (μm)
Ceramic shell	2.2	12.8	58.9	5
Casting (flowability filling type)	4.07	21.9	303	
Casting (fillability filling type)	3.52	17.3	282	
Casting, vibration during filling (fillability filling type)	2.97	15.9	270	
Casting vibration after filling (fillability filling type)	2.75	15.0	170	
Casting vibration after filling (flowability filling type)	2.2	14	185	

R_a is the mean distance between the surface profile and the reference line, R_z is the mean distance between peak height and valley depths in the surface profile, S_m is the mean distance between profile peaks.

The sketch in Figure (5.11) shows the various surface parameters used during the calculation of the heat transfer coefficient between the ceramic shell and the casting.

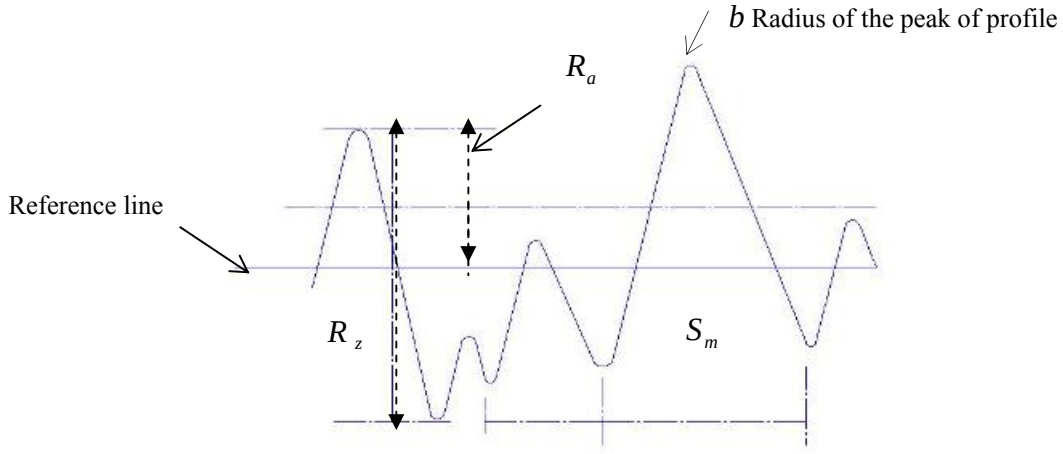

Figure 5.11 Schematic to show the definition of the surface roughness parameter.

5.6.1.1 Heat transfer coefficient calculation in superheat region

Under conditions of superheat, the liquid metals make a full contact with the radius of the peak on the profile surface during its propulsion forward into the channel. This enables the heat transfer coefficient between the mould and the casting to be estimated by subtracting the value for the penetration of the liquid metal into the surface roughness valleys, estimated by Timsit using [37] to be; $s = \frac{S_m{}^2 h}{8(\alpha^2 + bh)}$

(Where $\alpha = \sqrt{\frac{\gamma}{\rho g}}$; $b =$ radius of the asperity peaks in surface roughness profile; $h =$ pressure head), from the depths of the valleys in the surface profile of the ceramic mould, $x = (R_{z\,mould} - s)/2$, and the thermal conductivity of the air (k_{air}), which in this case gave a IHTC of $\approx 11800 Wm^{-2}K^{-1}$ and $\approx 13000 Wm^{-2}K^{-1}$ for casting with and without vibration respectively, (see Figure 5.9).

5.6.1.2 Heat transfer coefficient calculation in latent heat region

In conditions of semi-solid (latent heat release), an air gap is formed; its growth is related to deformation of the casting skin caused by the expansion and contraction during the process of solidification. This enables the heat transfer coefficient between the mould and the casting to be estimated by the size of the air gap (assumed to be equal to the sum of the depths of the valleys in the surface profile of the ceramic mould and the casting surface; ($z = \frac{\sqrt{R^2_{z(mould)} + R^2_{z(cast)}}}{2}$)) and the thermal conductivity of air (k_{air}). Using Griffiths' model ($h = \frac{k_{air}}{z}$) [85], this produced an IHTC of $\approx 6000 Wm^{-2}K^{-1}$ and $\approx 5000 Wm^{-2}K^{-1}$ for casting with and without vibration respectively.

The heat transfer coefficient between the casting and the wall of the mould as a function of the liquid metal surface temperature has been shown in Figure 5.12. It has been assumed that $\frac{dh}{dT}$ is linear relationship between the liquidus temperature and solidus temperatures.

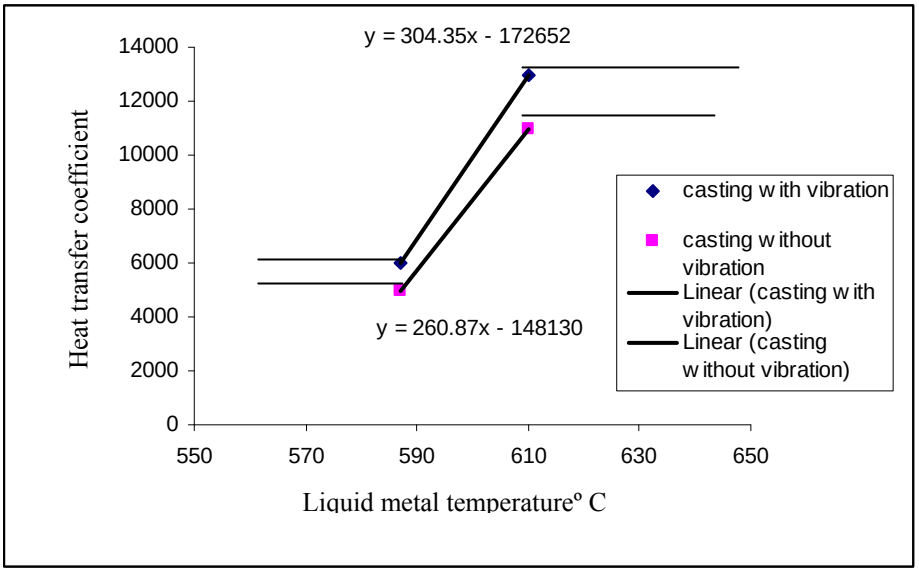

Figure 5.12 The variance of the calculated heat transfer coefficient with the temperature of the liquid metal

From Figure 5.12 the relationship between the heat transfer coefficient and the temperature of the molten metal was assumed to be linear;

$h_1 = 304.35T - 172652$ ----------(for casting with vibration)

$h_2 = 260.87T - 1481310$ ----------(for casting without vibration)

5.6.2 Analysis of the heat transfer coefficient calculation

From the calculation of the heat transfer coefficients made above, two points may be concluded. Firstly, the heat transfer coefficient is not a constant value in thin wall investment castings, but varies with time and temperature gradient. Stemmler [86] confirmed this, by estimating the heat transfer coefficient as a function of the temperature during simulation of Al7Si% alloy investment casting (see Figure (5.13)). Secondly, the value of the heat transfer coefficient which is obtained is not equated accurately in the superheat reign during the filling. There are two reason for this, which have not been taken into

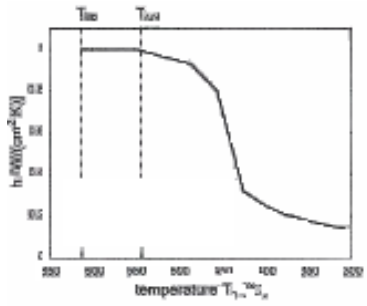

Figure 5.13 the effect of air gap formation between an AlSi7% casting and ceramic mould on the interfacial heat transfer coefficient value [86]

account during the heat transfer coefficient calculation in the superheat region; first, during the calculation it was assumed that the profile of the surface roughness for a ceramic mould was an ideal feature, as described in Figure 5.9, and the liquid contacts the ceramic surface only at the tip of every peak in the profile [35]. In fact, the nature of the surface profile reveals that it was not an ideal feature (see Figure 5.14), so it may be expected that the melt could touch the peak of the profile surface over a larger area than the area on the tip of the

peaks. Second, the solidification time (measured from the real-time X-Ray images) was about 0.24s, in the casting of the flowability filling type, (without vibration for a thickness of 0.75mm), but this was too short, if it is compared with the solidification time which was obtained from Fleming's model, which was about 0.6s. This indicates that the liquid metal lost heat very quickly in the superheat region; for this reason, therefore, the heat transfer coefficient should be higher than the value that was obtained from the estimate in the superheat region, which assumed heat was only lost in the strip itself, and not also the running system.

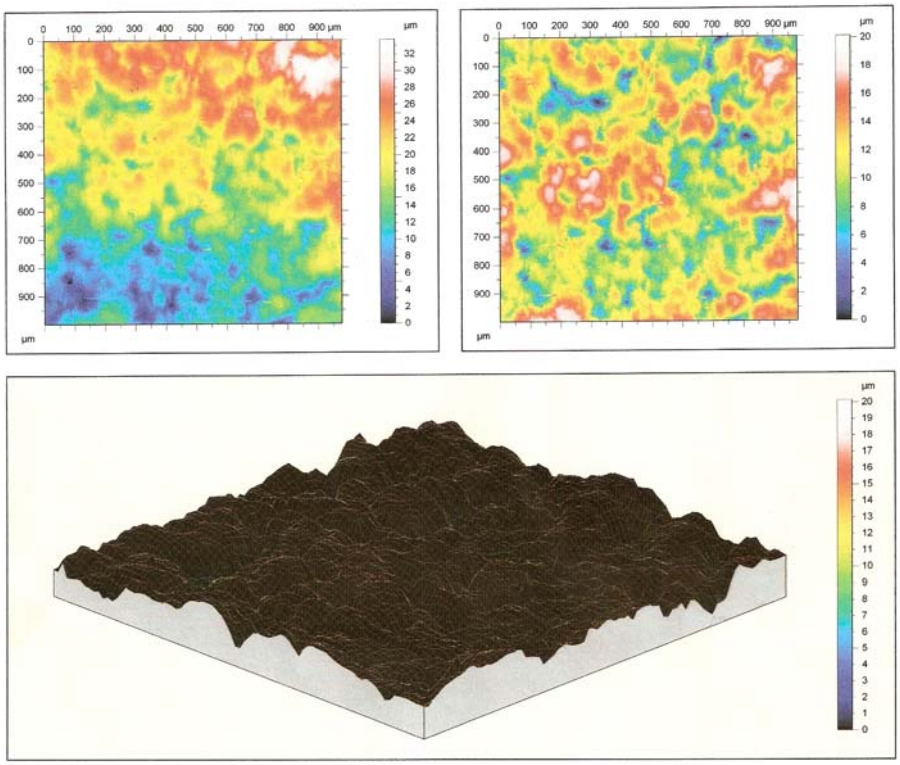

Figure 5.14 3D-surface roughness profile measured for ceramic mould

In addition, the solidification time for a casting with vibration under 0.8g conditions, was calculated from the secondary arm spacings (using the Hamed correlation [114]) and was found to be 1.2 s, compared with 1.3 s in the casting without vibration. This means that the liquid metal under vibration conditions loses heat faster than liquid metal does

without vibration. Kocatepe and Abu-Dheir [8 and 92], confirmed this observation and found that vibration during casting reduced the solidification time by 24%, compared with a casting without vibration, (see Figure 5.15).

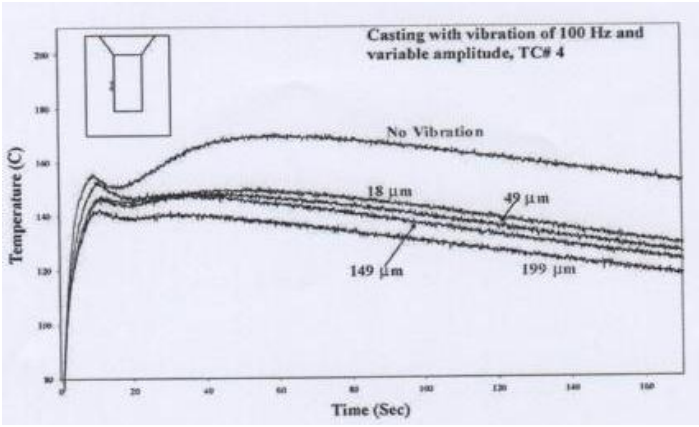

Figure 5. 15 Temperature-time profiles for casting poured under different case of vibration [8]

This indicated that the heat transfer coefficient when vibration is used was greater than without vibration. It is suggested that the reason for the increase in the value of the heat transfer coefficient can be attributed to the increase in the pressure related to the metal head, as a result of the acceleration due to the vibration in the bulk of the metal. This reduced the size of the air gap (ie, reduces its insulation) in the interface between the surface of the ceramic mould and the molten metals and increased the contact area, thereby increasing the heat transfer coefficient. This suggestion was supported by measuring the value of R_a on the surface profile of the casting without vibration, which was found to be $4.07\,\mu m$, compared with $2.97\,\mu m$ for casting with vibration. Fleming, cited by [2] and Pehlke [87] confirm this suggestion: he reported that any increase in the metal head of the liquid in the casting process was associated with an increase in the heat transfer coefficient as shown in Figure 2.30. The gain from the increased pressure in the bulk of the metal and increased heat transfer coefficient produced a casting with a good surface finish (see Table [5.1]). Alonso Rasgado [115] confirmed this by using vibration

in pressure die casting.

In the present work the heat transfer coefficient in the superheat region was calculated for a condition when the metal was in a liquid state with the contact area of the mould controlled by surface tension, density, metal pressure head and mould surface peak to peak distance in the profile. This gives the percentage of the total surface area in contact with molten metal. To find the true area of contact, an area with dimensions of $1mm \times 1mm$ from the surface roughness profile of the ceramic mould was chosen and many measurements made of the area where the melt would touch. Repeating this measurement procedure with many fields of the surface a roughness profile was developed and results are summarized in Table [5.2]. The measurement procedure is illustrated in Figure 5.16. The contact area that was obtained ranged between 2.5% and 5.5% of the total area chosen. The heat transfer coefficient in the superheat region was calculated by multiplying the heat transfer coefficient obtained from Sleicher's formula 5.7 [86] with the true area of contact.

The calculation of the heat transfer coefficient assumed that the heat of the melt is transferred from the bulk of the metal to the surface by convection and from the surface of the liquid metal to the surface of the mould by conduction.

Sleicher proposed the following relationship for calculating the heat transfer to liquid metals in tubes with a constant wall temperature:

$$N_{Nu} = 4.8 + 0.0156(N_{\mathrm{Re}})^{0.85}(N_{\mathrm{Pr}})^{0.93} \text{----------} 5.7$$

where all the properties are evaluated at the bulk temperature; the above equation is valid for Pe > 10^2

where N_{Nu} : Nusselt number (hd/k)

N_{Re} : Reynolds number ($\rho ud/\mu$)

N_{Pr} : Prandt number ($C_p \mu / k$

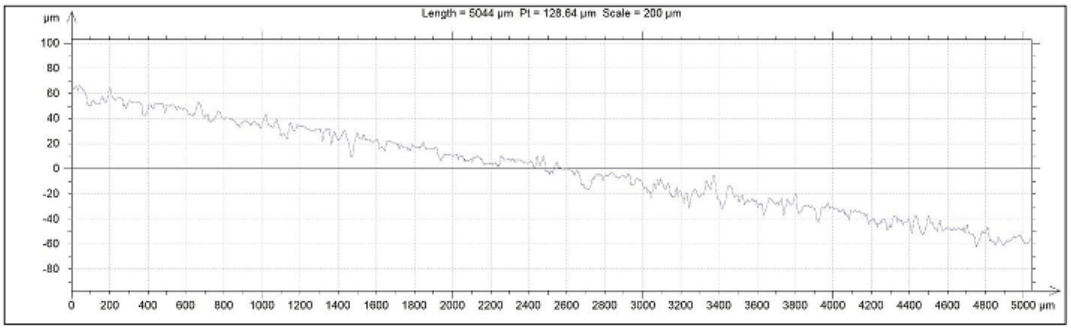

Stage (1)

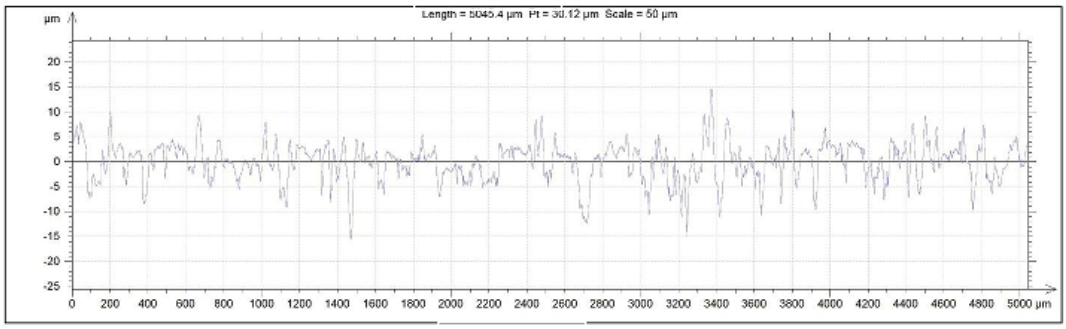

Stage (2)

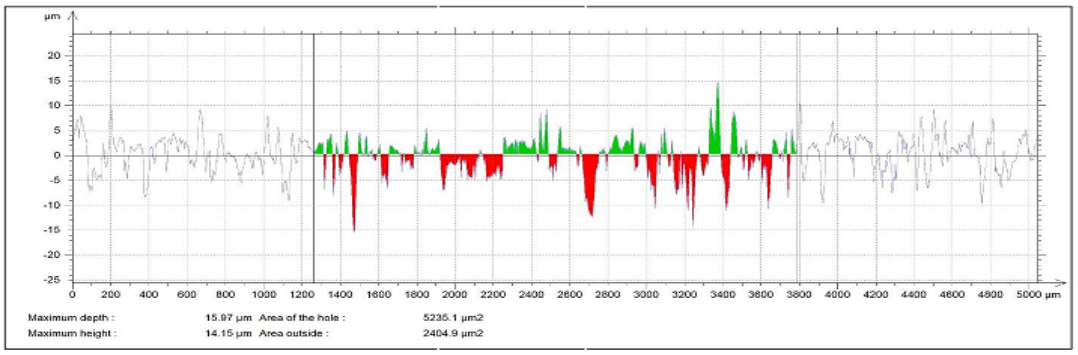

Stage (3)

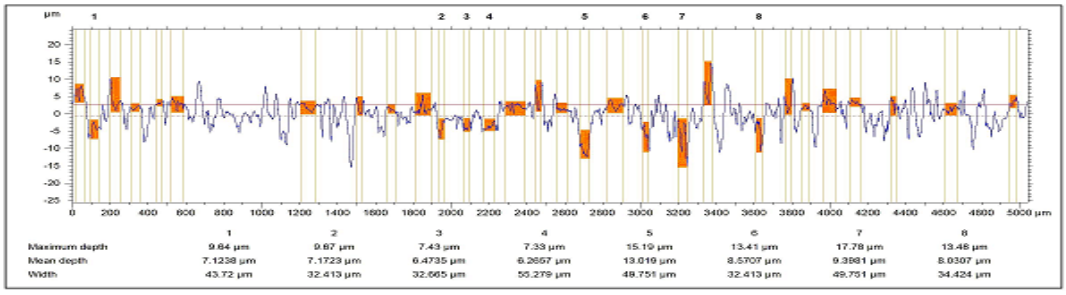

Stage (4)

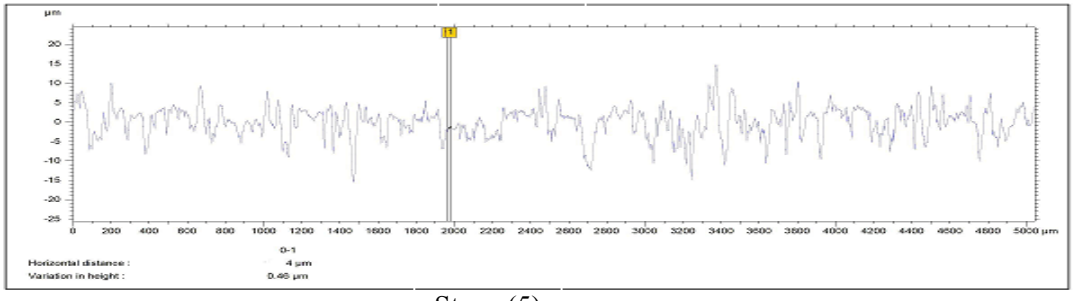

Stage (5)

Figure 5.16 shows the contact area in a ceramic mould which expected

The values of the thermophysical properties for the ceramic shell and the casting, as well as other data used in the heat loss model to calculate the fluidity of the A356 alloys in thin section in vibration conditions, are shown in Table 5.3

Table 5.3 Thermophysical properties of the A356 and the ceramic mould

Property	Value
Properties of the A356 alloy	
Thermal conductivity ($Wm^{-1}K^{-1}$)	88.6
Specific heat capacity ($Jkg^{-1}K^{-1}$)	917
Density (kgm^{-3})	2394
Coefficient of thermal expansion	24×10^{-6}
Latent heat (Jkg^{-1})	397,490
Liquidus temperature (K)	890
Solidus temperature (K)	850

The physical properties of the A356 alloys were assumed to be independent of temperature.

The heat transfer coefficient for A356 alloys with the properties given in Table 5.3, for flow in a channel 0.75mm thick, was found to be 14461 ($Wm^{-2}.K^{-1}$). This was comparable with $10000 Wm^{-2}K^{-1}$ for A356 alloys obtained by Stemmler in thick sections , in his simulation [38] see Figure 5.13. Vassilious et al.[14] using an inverse method, measured the heat transfer coefficient in a centrifugally cast investment casting, with complex geometry, and found a value of $28000 Wm^{-2}K^{-1}$.

5.7 Verification of the heat loss model

When all the parameters in the heat loss model (velocity of molten metal, interfacial heat transfer coefficient) were calculated, the model was tested and compared with the results of two series of experiments (with and without vibration), as well as with data from other researchers.

The comparison of the calculation of fluidity of the castings filled without vibration between the Flemings model and the heat loss model is shown in Table [5.4], using the same data in both formulas.

Table 5.4 The value of fluidity as computed by Fleming and in the heat loss model

Thickness of channel (mm)	Fleming formula (mm)	Heat loss model (mm)	casting conditions
0.75	**131**	**89**	**without vibration**
0.55	**87**	**56**	**without vibration**

From the table, it is clear there was a systematic difference between the two results whereby the heat loss model calculated fluidity lengths between 30 and 35% less than Flemings model. Fleming (i) did not take into account the effect of the thermal conductivity of the molten metal, but assumed that the temperature along the flow path in the mould was a constant, which plays an important role in the fluidity calculation related to the heat rate loss along the flow path; and (ii) did not take into consideration the effect of the solid fraction of the total volume (i.e., took a single phase case). So a high fluidity result was to be expected from Fleming's model.

The Flow-3D software package was applied to calculate the fluidity of the A356 alloy in a channel of 0.75mm thickness without vibration conditions, with a metal head of 170mm. The physical properties of the alloy were obtained from the database of the Flow-3D program, (illustrated in Figure 3.21). This was set up in the geometry modeller in Flow-3D. The heat transfer option was active during the calculation. The result revealed that the fluidity was about 300mm (See Figure 5.17). A wide difference between the result of the experiment and the Flow-3D result was observed. This may be due to the value of the heat transfer coefficient applied during the fluidity

calculation. Thus, this program needs modification to become suitable for fluidity calculation, and this is suggested as an avenue for further research.

The results of further calculations made using the heat loss model illustrate the response of fluidity length to pouring temperature, mould temperature, velocity and channel thickness (Figures 5.18, 5.19, 5.20 and 5.21) and indicate that the fluidity in the thin section is affected by many factors, such as pouring temperature, mould temperature, velocity of the molten metal, channel thickness and the heat transfer coefficient between the metal and mould; the major factor, however, is channel thickness. It is surprising that the heat loss model showed the latent heat of the alloy to be a decisive factor in estimating the value of the fluidity; the superheat is a secondary factor in determining the fluidity length.

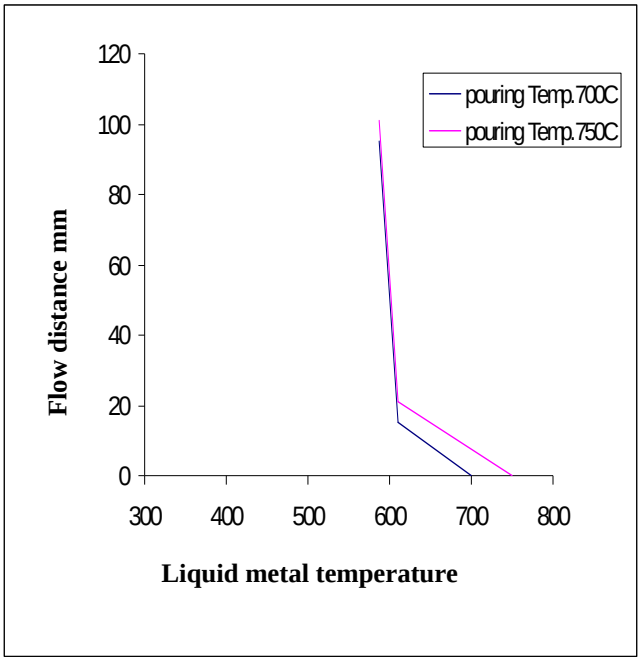

Figure 5.18 Theoretical calculation showing the pouring temperature effect on the fluidity; mould temperature is 450C, velocity of the liquid metal, 0.7m/s

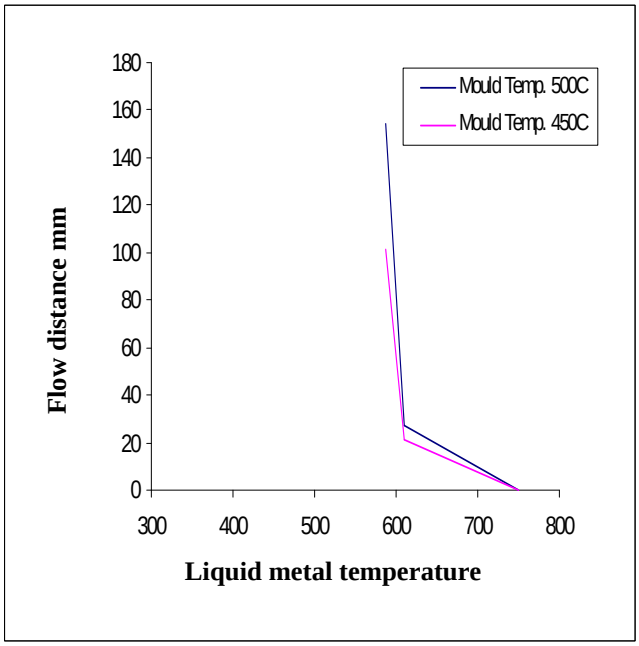

Figure 5.19 Theoretical calculation showing the mould temperature effect on the fluidity; pouring temperature is 750°C and velocity of the liquid metal is 0.7m/s

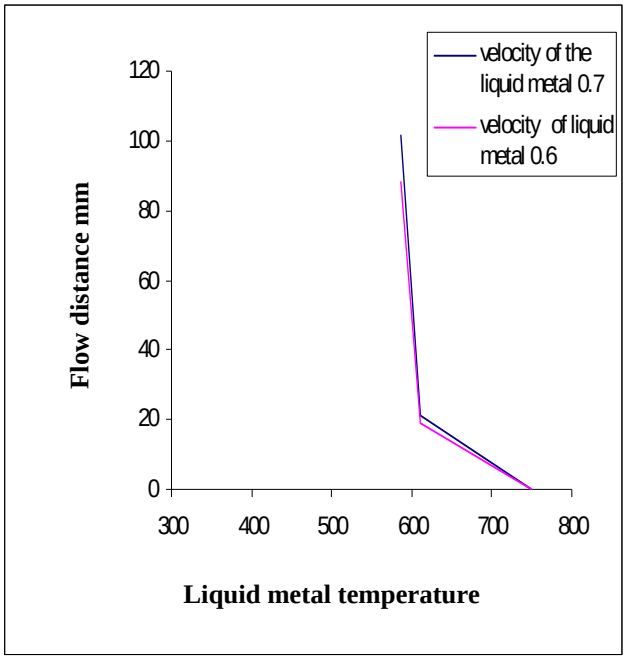

Figure 5.20 Theoretical calculation showing the velocity of the liquid metal effect on the fluidity; mould temperature is 450°C, pouring temperature is 750°C, channel thickness is 0.7mm

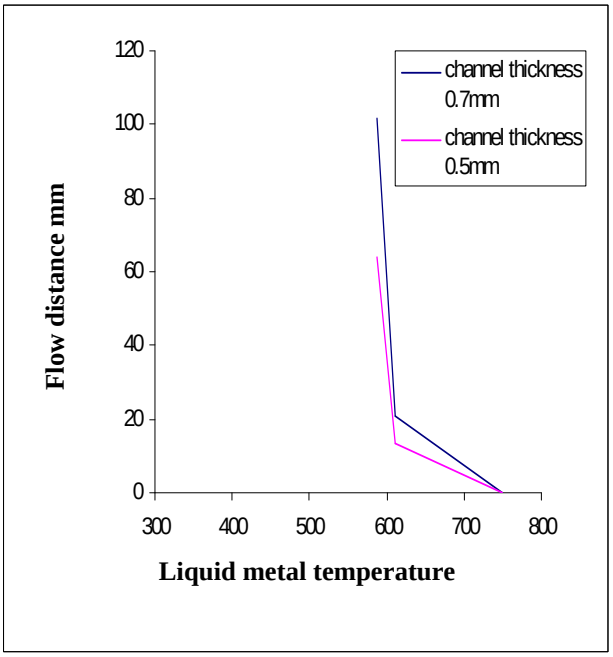

Figure 5.21 Theoretical calculation showing the thickness of the channel effect on the fluidity; mould temperature is 450°C, velocity of the liquid metal is 0.7m/s, pouring temperature is 750°C

5.8 investigations of the mechanical properties in each method of casting

The samples from each method of casting (cast without and with 0.8g acceleration of vibration during filling) were tensile tested to obtain their Ultimate Tensile Strength (UTS) and % Elongation values. The results are listed in Table 5.5. Scatter plots of the UTS and elongation as a function of the method of casting are shown in Figure 5.22 and Figure 5.23. According to the figures it can be seen that the average of the UTS and elongation of the specimens cast with vibration was about $230N/m^2$ and 3.70% respectively. This was more than the average of the UTS and elongation in the casting without vibration ($202N/m^2$ and 2.77% respectively). This indicated that vibration improves the mechanical properties of the casting. This finding confirmed the previous work of Campbell and Abu Dear [7-8].

In order to evaluate the quality of the casting which was obtained from each method of casting, a quality correlation ($Q = UTS + (150 \times \log(elongation))$) was used to estimate the quality for each method of casting. Table 5.6 shows the percentage variation in the quality of the thin wall investment castings, made with and without vibration. A 16% improvement was found in the case of casting with vibration.

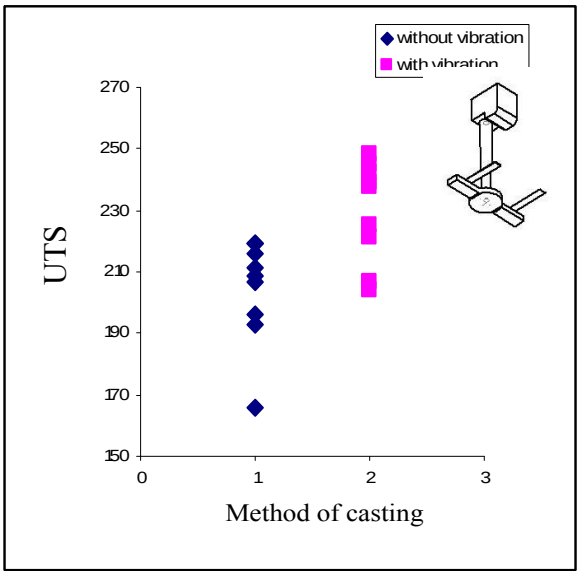

Figure 5.22 shows UTS as a function of the method of casting. Pouring temperature 750ºC, mould temperature 420ºC, metal head 170mm

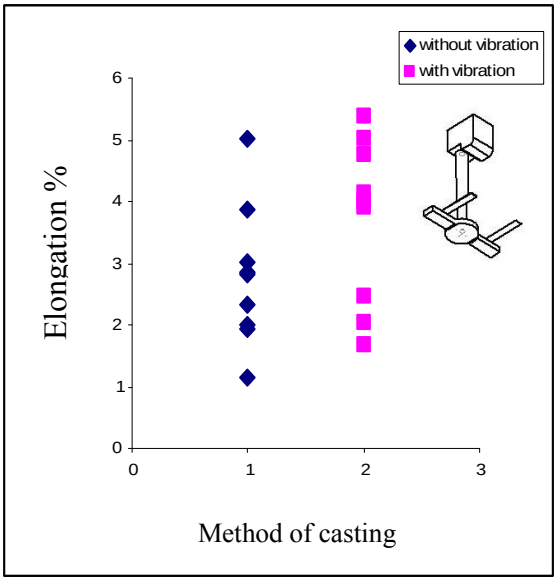

Figure 5.23 show elongation as a function of the method of casting. Pouring temperature 750ºC, mould temperature 420ºC, metal head 170mm

Table 5.6 shows the variation of the quality of the casting for casting with and without Vibration

Quality **Casting without vibration**	**Quality** **Casting with vibration**	**Average**	**Variation**
268.3	315.2	291.6	0.160

The effect of the vibration action on the quality can be quantified by assessing the reliability of a casting, using the Weibull modulus of the UTS and elongation.

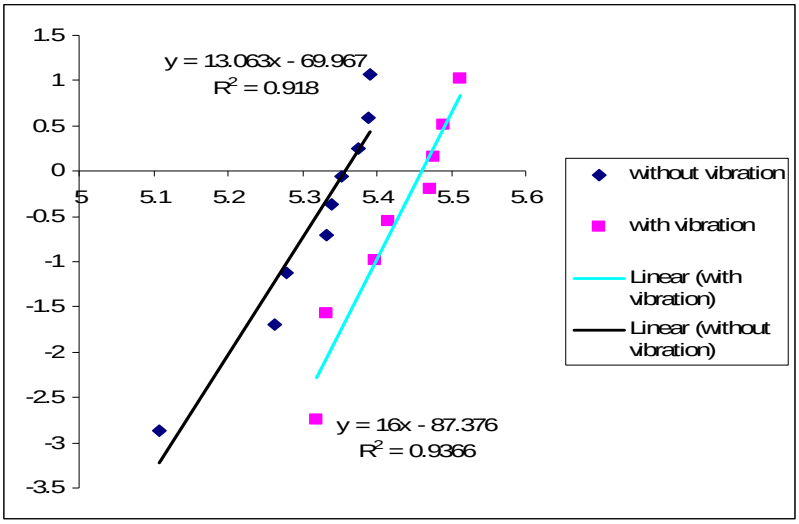

Figure 5.24 Weibull plot of UTS data for each method of casting

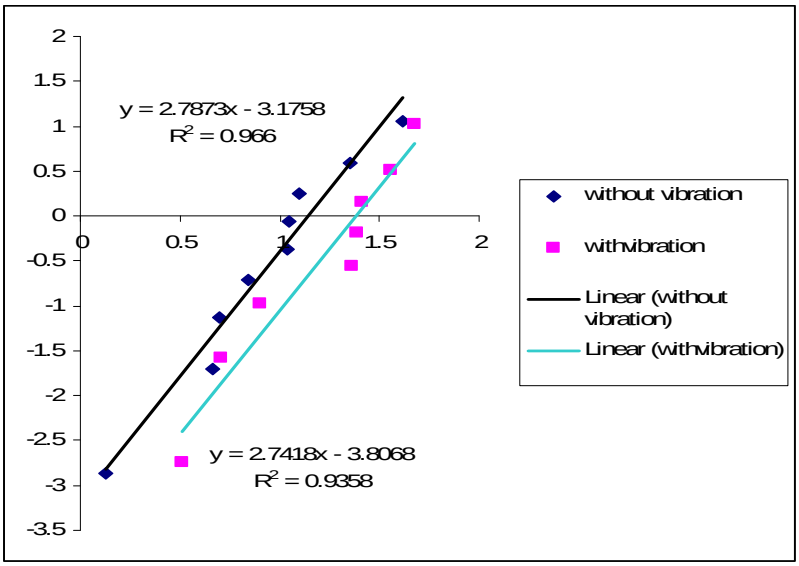

Figure 5.25 Weibull plot of elongation until failure; data for each test method casting

A Weibull plot of all the UTS test data is shown in Figure 5.24 and the results of elongation to failure in Figure 5.25. Weibull best fit parameters were calculated using linear regression.

The best fit parameters in Figures 5.24 and 5.25 are summarized in Table 5.7, together with the regression coefficient. According to this table, it is clear that the value of the UTS σ and Weibull modulus λ in the casting with vibration (about 235 and 16 respectively) was greater than the value which was obtained from the casting without vibration (about 211 and 13); by this it can be understood that vibration improved the quality of the casting.

Table 5.7 The best fit parameters of the Weibull plots for each method of casting

Casting method	Weibull modulus (λ)	position parameter (σ)	Regression coefficient (R)
Weibull plots of UTS			
Casting without vibration	13.063	211.9	0.918
Casting with vibration	16.000	232.332	0.936
Weibull plots of Elongation%			
Casting without vibration	2.787		0.966
Casting with vibration	2.747		0.935

A metallographic study was carried out to highlight the effect of vibration during filling on the microstructure of the castings in thin wall investment casting

One casting was randomly selected from each method of casting and was ground to remove 0.35mm of the thickness (50% of the section thickness). The polishing was completed using (Colloidal Sillca) powder to produce a mirror-like finish. The polished specimens were examined using an optical microscope. Figure 5.26 shows the microstructure of the casting made with 0.8g acceleration of vibration during filling, and Figure 5.27 shows the casting without vibration. The result revealed that in casting

with vibration, the size of the average dendrite cell was generally smaller (space length approx.23 μm). In contrast, in casting without vibration, the average size of the dendrite cell was substantially larger (typically 31 μm mm, with some dendrite cells well over 45 μm). It seems possible that this is the result of the increase in the cooling rate, due to the action of vibration, (described in section 5.7 earlier). Refined dendrite cells may be the reason for the improved elongation in the casting with vibration, Cáceres [140-141] found that there were refined dendrite cells and Si particle due to varying the solidification rate in Al7Si% alloys, which increased the ductility of the metal .

The shapes and sizes of the grain structure in the cast alloys play an important part in structure-sensitive properties.

The structure of the casting is sensitive to the cooling rate. A high cooling rate gives a fine grain size, while a slow cooling rate produces a coarse grain. This is due to the influence of the under-cooling on nucleation and growth processes[24].

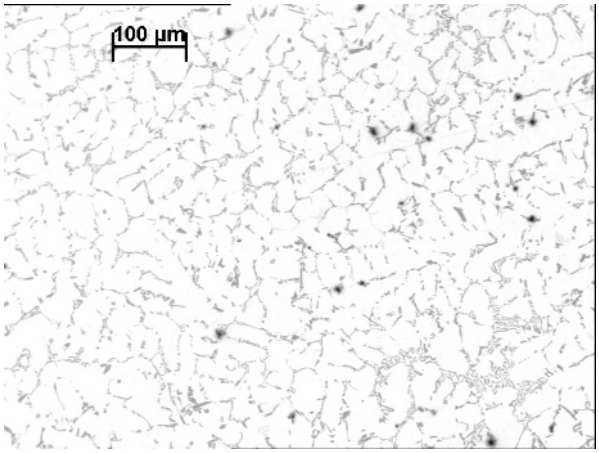

Figure 5.26 Typical mid thickness strip macrostructures observed at the flow tips in a castings filled with 0.8g acceleration,(pouring temperature is 750ºC, mould temperature is 420ºC, metal head 170mm)

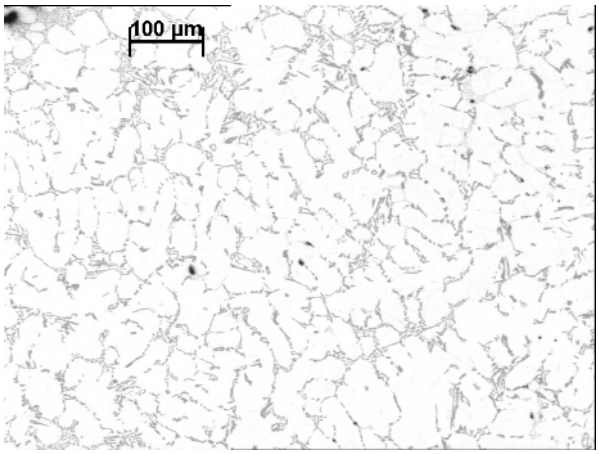

Figure 5.27 Typical mid thickness strip macrostructures observed at the flow tips in a casting filled without vibration, (pouring temperature is 750ºC, and mould temperature is 420 º C, metal head 170mm)

The grain size was measured on specimens from each method of casting. The grain size in castings with vibration, was about (0.1821mm), and was smaller than the grain size of castings without vibration, was about (0.2322mm) (see Figure 5.29 (Apendex)). This is the result of an increase in cooling rate due to the vibration action and also the fragmentation effect, providing extra growth sites. Grain refining is one of the reasons for the UTS improvement in the casting with vibration, According to the correlation of the yield stress as a function of the grain size ($\sigma_y = \sigma_1 + kd^{-\frac{1}{2}}$), we can estimate the increase in yield strength in the casting under vibration conditions.

Figure 5.30 shows the microstructure for each method of casting, using an image analysis system. The average size and the volume percent of the shinkage porosity and gas porosity measurement on a $10mm \times 15mm$ unit area ($1336\,\mu m^2$ and 1.1% respectively) in casting with vibration was smaller than that observed in casting without vibration, about (2832 and 2.9%). This suggested that, in addition, grain refinement plays an important part in improving mass feeding and reducing the resistance of interdendritic feeding during solidification Kim [142] The acceleration generated due to the vibration action increased mass feeding during solidification, resulting in the elimination or reduction in the size of shrinkage porosity. Dispersing the porosity improves mechanical properties.

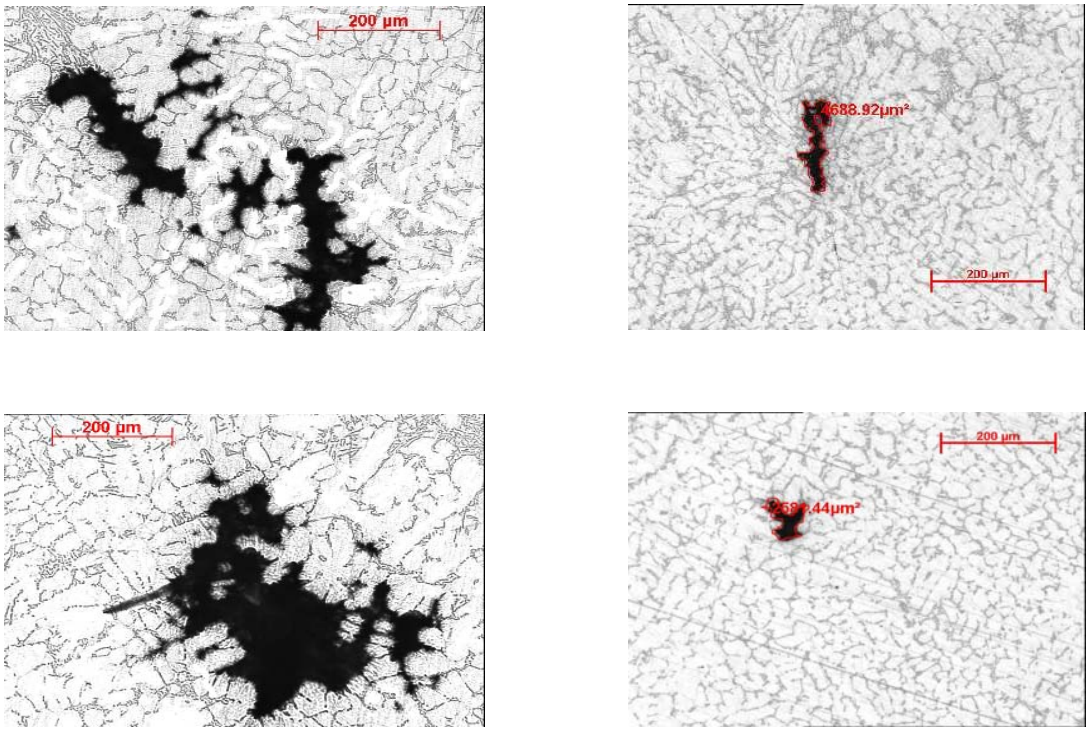

(a) **(b)**

Figure 5.30 porosity in a microstructures observed at (a) castings filled without vibration and (b) castings filled with 0.8g acceleration. Pouring temperature, 750ºC; mould temperature 420ºC; metal head 170mm.

5.9 Vibration enhanced fluidity

A series of experiments was conducted in fluidity filling type conditions to determine the effect of vibration on the fluidity characteristics of thin wall investment castings, with different pouring temperatures and with and without vibration.

Investigation of the results of the heat loss model with experimental data for different pouring temperatures (660°C, 700°C and 750°C), channel thickness (0.75mm) and mould temperature 420ºC was carried out. The fluidity was tested by pouring molten A356 alloy into a thin channel casting. The cross-sectional area along the thin channel was constant and the distance to which the molten metal flowed was measured. The test mould is illustrated in Figure 3.11. The mould was insulated by a ceramic fibre blanket to minimize variation in the mould temperature from casting to casting which

arose due to differences in the time taken to mount the mould on the vibrating table. Flow distance are listed in Table 5.8 and plotted in Figures 5.30, using fluidity as a function of the pouring temperature with and without vibration at 0.8g acceleration. The reason for choosing an acceleration of vibration of less than 1g was that it would eliminate any jetting flow phenomena during the filling process.

Figures 5.31 show that the fluidity increased in the casting with and without vibration with every increase in the pouring temperature; this result has been confirmed by many fluidity researchers [2, 16, 55, 63].

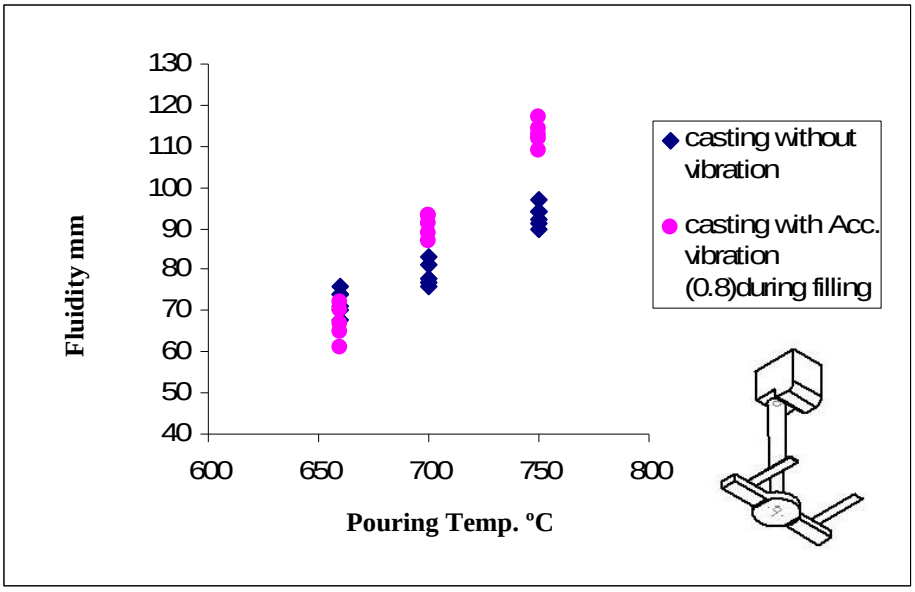

Figure 5.31 The fluidity of A356 alloy as a function of pouring temperature in the flowability filling type, according to the vibration techniques used during filling and gravity pouring

The two results (of the fluidity test and model calculation) with and without vibration were found to be comparable, as shown in Figures 5.32 and 5.33 with a channel thickness of 0.75mm. Generally, the results were in good agreement in the case without vibration, (see Figure 5.32), tends to confirm the heat loss model used in the present work. However, in the case of casting with vibration applied during filling the

experimental and theoretical results were different see Figure 5.33. It is suggested that this difference was due to the heat transfer coefficients estimated, surface tension [20,73,75,120], and the velocity of the metal in the latent heat region, which are variable parameters. These parameters are changes which occur when the temperature of the molten metal changes, but it was assumed that all parameters were of a constant value in calculating the fluidity.

The specific heat capacity, C_p, is another parameter that would affect the results of the heat loss model in calculating the fluidity, which was assumed to be a constant value in both the superheat and latent heat regions. However, the specific heat capacity changes with temperature and the state of the metal, whether liquid or solid. Therefore, it is surmised that the value of the specific heat equals the sum value of the $C_{P(liquid)}$ in the superheat region and the value of the $C_{P(solid)}$ in the latent heat, which can be estimated by the following formula:

$$C_{p(soild+liquid)} = f_s(T) \times C_{psol}(T) + (1 - f_s) C_{pliq}$$

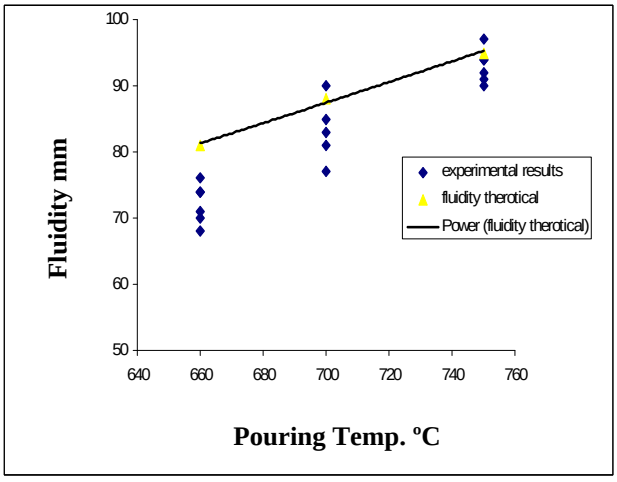

Figure 5.32 shows the relationship between the fluidity and the pouring temperature, casting without vibration, in a $0.75^{\pm 0.05}$ mm channel. A theoretical line is obtained from the heat loss model

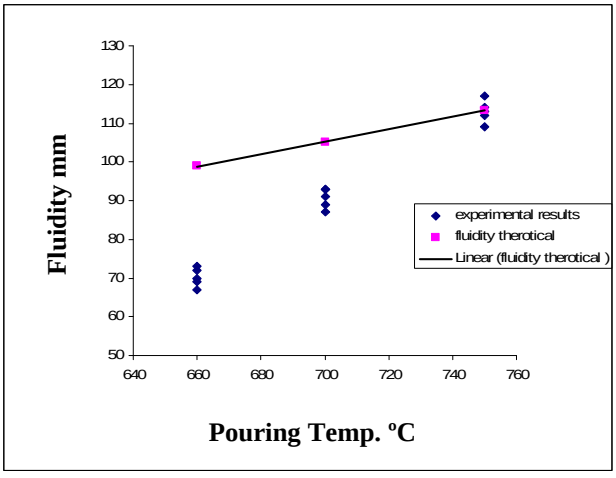

Figure 5.33 shows the relationship between the fluidity and the pouring temperature, casting with 0.8g acceleration of vibration during filling, in a $0.75^{\pm 0.05}$ mm channel. A theoretical line is obtained from the heat loss model

In the experiments for the fluidity measurement under vibration conditions, vibration was used in two ways for the purpose of comparison: (i) first, during the pouring process: (ii) second, after the filling process.

According to Table 5.8, the result shows that vibration had no effect on the fluidity when the vibration was applied after the filling process. This is because the heat loss from the molten metal to the mould walls starts when the melt flows through various parts of the mould components, the pouring basin, sprue and gating, before reaching the test piece. This situation caused a drop in superheat and ensured the metal solidified quickly in the thin section and then stopped. Consequently, vibration has no chance to affect the velocity of the molten metal in the fluidity test. Moreover, the solidification time in a thin section was momentary (0.23 s), measured by using a digital video recording real-time X-Ray camera and the stabilization time of the vibrating table used in these experiments was 2 seconds. This means that the liquid metal solidified before the vibration was applied. However, the results showed an improvement in the fluidity when vibration was used during the pouring processes (see Figure (5.31)), because there was sufficient time for the metal to remain in a liquid or semi-solid state. This gave more chance for the vibration action to increase the velocity of the liquid metal during the pouring process, thereby improving the fluidity.

In practice the vibration was observed to have an inverse action on improving the fluidity, in cases when the filling process in thin wall investment casting was carried out at low pouring temperatures (660ºC (see Figure (5.31)). It may be the case that the vibration motion increases the capacity for crystallization in the liquid metal as the casting temperature declines (nucleation phenomenon) [44]. This situation led to a

reduction in the solidification time, (about 0.16s) if compared with the solidification time in castings without vibration, (about 0.23s) (using Equation 4 to estimate the velocity of the liquid metal in vibration conditions and obtaining the fluidity from the experiment. With this, the value of the solidification time could be estimated by using the simple equation of velocity, which was found to be 0.16 s). In this regard, it will be necessary to modify the present criteria (mathematical models of fluidity with a low pouring temperature under vibration conditions) (see Figure5.33). This suggestion is endorsed by Boris [106].

In addition, the increase in the heat transfer coefficient between the molten metal and the mould, as a result of the vibration pressure, is likely to have led to an increase in the heat loss during casting [35]. This caused a reduction in the solidification time and thereby affected the fluidity value. However, in the case of casting under vibration with a high pouring temperature, the duration of the liquid stage was greater than the duration of the liquid stage when the casting was done at a low pouring temperature. Thus, the improvement in the velocity of the liquid metal in the liquid stage, and the reduction in the viscosity in the semisolid stage as a result of the contact break-up between the particles of the melt [106] during vibration, exceeds the influence of the increased heat transfer coefficient on the fluidity in thin wall casting. For this, the results are in agreement, and this also confirms the heat loss model used in the present work (see Figure 5.32).

From the results described above it can be concluded that it is better in the flowability filling type to apply the vibration in the investment casting method at a high pouring temperature to improve fluidity and increase the production rate of castings free of mis-run defects. In the fillability filling type regime, however, it is more convenient to apply vibration after the filling process.

Chapter 6

Discussion

6.1 Filling of thin channels without vibration

In this study, the experimental results showed that the filling capability, as assessed by the metal head needed to fill a given section thickness in a thin wall investment casting, required two types of filling (Figure 4.1). The first type of filling, the Flowability filling type, is confined between the pouring temperature and the mould temperature when the mould temperature is less then the liquidus temperature and controlled by the heat contents of the metal-mould system. The filling capacity in this region is familiar, with the fluidity controlled by the known effects of flow velocity and heat transfer [6,18,42,52,115]. Therefore any increase in the filling capacity should be associated solely with the increased heat content in the system (Figure 4.2). Theoretical analysis related to the heat loss during filling takes into account the solidification process, which was described in detail in Chapter 5.

The second type of filling, the Fillability filling type, occurs when the metal and the mould temperatures are greater than the liquidus temperature. In these conditions, the heat content in the system is sufficient to keep the metal in a liquid state and eliminate the influence of solidification on the filling. In this case, no improvement in the filling capabibilty would be expected from an increase in the heat content of the system arising from increased pouring temperature (Figure 4.3). This is confirmed by experimental results, which showed about a 3% decrease in the metal head required to fill a given section thickness when the pouring temperature was raised from 660ºC to 750ºC. This increase in the filling capacity was in regard to the thermophysical properties. In evaluating the thermophysical properties, such as density ρ and surface tension γ, they change as a function of the temperature. A simple calculation can be

made, using the density (ρ) and surface tension (γ) with respect to temperature correlations for the alloy ($\rho = \rho_O + (T - T_O)(\frac{d\rho}{dT})$) and ($\gamma = \gamma_o + (T - T_O)(\frac{d\gamma}{dT})$), respectively. From these correlations it is clear that the value of the density and the surface tension will change by 0.9% and 3% respectively, for A356 alloys, when the temperature changes from 670ºC to 750ºC. Substituting these values into the equation $h = \frac{\gamma}{\rho r g}$ to estimate the critical metal head height required to fill, strip of thickness 0.55mm it was found h 166mm. The calculation gives a close result for the metal head height of 160mm, which is obtained from the experiment. So, it can be concluded that the foundry parameters, such as the pouring temperature and the runner system, has no impact on the filling capability in thin wall castings in fillability filling type conditions. Therefore, in such conditions the filling capability is most likely to be controlled by the mechanical balance of surface tension and hydrostatic pressures. This concept was originally proposed by Fleming [15].

Regarding Figure 4.4, if the filling capability is improved, and assuming that the liquid metal does not wet the mould, it must be the case that the pressure force acting on the molten metal front overcomes the resistance to filling due to surface tension. This happens when the internal pressure at the interface is $\rho g h$, exceeding the resistance (back pressure) due to surface tension $\frac{\gamma}{r}$; if the internal pressure is insufficient to force the melt into the narrow section, surface tension will tend to stop the flow of the melt and cause a mis-run defect (this is a common defect in castings with thin section). Campbell quantified this problem in thin wall investment casting by the equation below [5, 6,].

$$\text{External pressure - Internal pressure} > \frac{\gamma}{r} \quad \text{---------(6.1)}$$

In conditions where the metal head does not wet the mould, i.e. the contact angle θ =180º, the pressure due to surface tension is 2 γ / r for the situation of a circular-section tube of radius r (two radii at right angles) (see Figure 4.5), while γ / r is the pressure in the case of filling a narrow plate of thickness 2r. In cases where the metal wets the mould, γ / r becomes negative, so the surface tension in fact assists the metal to enter the mould (the capillary phenomenon) [6].

Three forces act on the interface between the internal pressure and external pressure which is presented in a liquid metal: atmospheric pressure (Pa), hydrostatic pressure (Ph) and the back pressure (Pm) within the mould cavity.

The total internal pressure is hydrostatic pressure, due to the depth of the melt head (ρgh) and the atmospheric pressure (Pa). The external pressure is the sum of the atmospheric pressure (Pa) and the back pressure, due to residual gas present in the mould cavity (Pm) [67].

In order to fill a thin plate, the balanced forces at the interface between internal pressure and external pressure must be equal [6,43].

$$P_a + \rho gh = \frac{\gamma}{r} + P_m + P_a \qquad \text{----------(6.2)}$$

It is clear that the atmospheric pressure acts equally on both sides of the liquid front, cancelling any effect. In the present work, the effect of the back pressure (gases within the mould which cannot escape rapidly enough through the pores of the mould) on the head driving the filling of the mould, was eliminated by using a vent added to the runner system. Then it becomes possible to ignore Pm from the right-hand side of Equation (6.2) and Equation (6.1) is simplified to

$$\rho gh = \frac{\gamma}{r} \quad \text{----------(6.3)}$$

.

$$h = \frac{\gamma}{\rho gr} \quad \text{----------(6.4)}$$

Equation (6.4) may be used to calculate the metal head required to cause the molten metal to enter and fill the thin section in the filling process. This is tested against the experimental data, assuming that the values of the surface tension and the density of the liquid metal are 1N/m and $2400\,Kg/m^3$ [18] (See Figure 6.1). The results show good agreement, assuming that the effects of the metal flow (momentum) are regulated to be negligible. It is interesting to note that in the experiments the measurement of the pressure head always exceeded that of the theoretical pressure head. This suggests that the selected value of the surface tension may be in error.

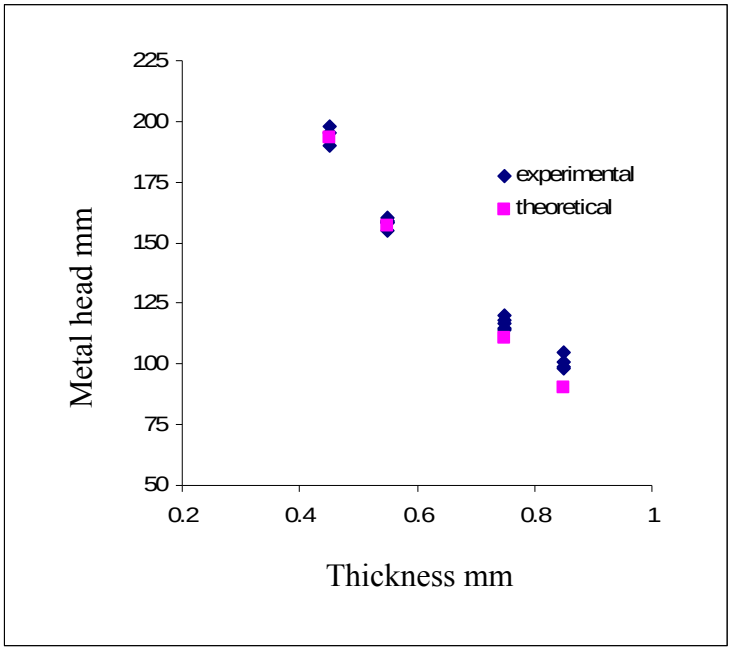

Figure 6.1shows the theoretical metal head compared with that in the experiment for metal head

6.1.1 Surface tension effect on filling capability

From Figure 4.4, it can be seen that the test piece at a certain thickness was filled with molten metal until it reached the point at which surface tension arrested the liquid metal. This indicates that the metal head is inversely proportional to the wall thickness and is controlled by the surface tension of the liquid metal. At this point, it is clear that the surface tension is an effective parameter during the filling process in thin wall investment casting. Therefore, surface tension can be calculated using Equation 6.3 and fitting it to the data of Figure 4.4; it gives $\gamma = 1.02 Nm^{-1}$. The value which is obtained for surface tension is in general agreement with the published data on A356 alloys [68,71]. See Figure 6.2.

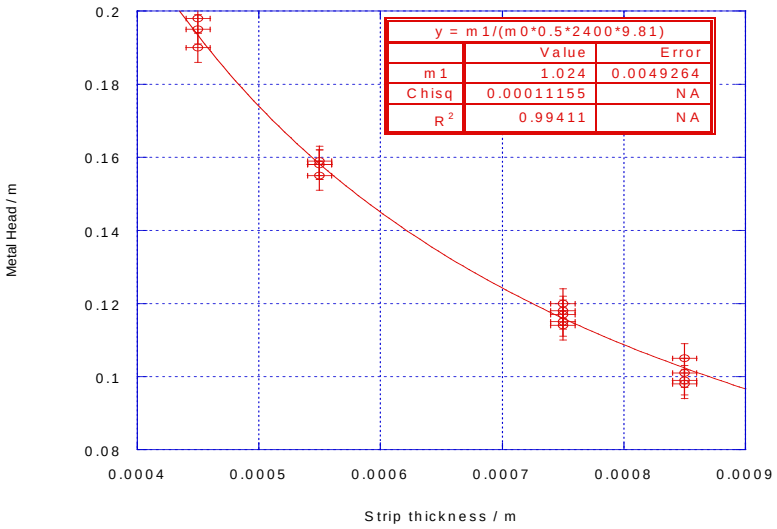

Figure 6.2 Surface tension estimation by fitting Equation 6.3 to the experimental data

Investigation of published data [68] indicates that a low surface tension value for liquid aluminum is associated with adsorption of monolayer of oxygen (see Figure 2.19). Hence, in the present work we expect that the flow of liquid Al will have a thin monolayer of oxygen during filling, without vibration (a clean surface).

6.1.2 Effect of velocity on the filling

In the casting experiments the metal flow during filling is controlled and governed by the force of gravity. To obtain the velocity of the metal at the exit of a sprue of height h, we have $(v^2 = 2gh)$. In the case of thin wall investment casting, when the liquid metal begins to flow into the thin section, the pressure generated from surface tension with respect to the thickness of the channel leads to a decrease in the velocity of the metal. To estimate the velocity of the liquid metal, the surface tension pressure repulsion must be taken into account. Therefore, the velocity equation becomes

$$(v^2 = 2g(h - \frac{\gamma}{\rho rg})\text{---------}(6.5)$$

Equation 6.5 indicates that the surface tension reduces the velocity of the liquid metal; therefore, surface tension would be expected to increase the critical velocity at which surface turbulent fluid flow arises Runyoro [44].

Results of the real-time X-ray studies shown in Figure 4.8 showed the measured liquid metal velocity at different points along the flow path of the metal to be between $0.65\,ms^{-1}$ and $0.7\,ms^{-1}$, compared with $1.01\,ms^{-1}$ (metal head 170mm, strip thickness 0.7mm), obtained from Equation 6.5. This error may come from neglecting the effect of the friction drag parameter on the liquid metal flow or from not taking into account the discharge coefficient (the ratio between the exist area of the sprue and the cross section area of the strips) in the calculation.

6.1.3 Flow pattern in thin wall casting

In general, fluid flow within investment casting is unsteady and non-uniform. The Flow-3D software package can be used, by applying continuity and Navier-Stokes equations during simulation, to simulate the flow pattern.

In a test piece oriented in vertical direction (see Fig.4.13 (1-26)) the liquid metal transfers from the gate in the runner system to the upriser and is then arrested by the

force of surface tension. Because the metallostatic pressure is insufficient to overcome the resistance caused by surface tension, the liquid metal continues to progress into the upriser. During it's progress, the internal pressure starts to build in the bulk of the liquid until it reaches a critical head At this point, the metallostatic pressure overcomes the resistance of surface tension at the junction area between the test pieces and the bottom of the upriser. The meniscus of the liquid front bursts, to trigger the liquid metal flow into the test piece at a high velocity of about 0.8 m/s and it continues to flow until stopped by the wall of the mould, then starts again in a vertical direction until it reaches a point which has insufficient metallostatic pressure, such as is shown in (Fig.4.6 (10-22)).

A horizontal test piece (see Fig.4.14 (1-32)) shows that the liquid metal transferred from the gate in the runner system to the upriser and was arrested in the thin section under the action of surface tension. Internal pressure is built during the progress of the liquid metal into the upriser until it reaches a critical head; the liquid metal flows into the test piece after the internal pressure has become sufficient to overcome the surface tension. From the above description, it is clear that in the flow pattern for both horizontal and vertical strips there is a delay for the metal entry into the strip whilst the metallostatic pressure head increases (the X-ray image supports this). This delay come from the back pressure due to surface tension, and this is shown in the models, suggesting that they are of some use in the fillability regime.

A simulated flow pattern revealed that there was agreement with the flow pattern which was obtained from the experiment and that the meniscus of the liquid front in the thin section moves under the control of surface tension. No surface turbulence was observed during simulation (see Fig. 5.14 (1-32)). This was similarly observed in the Figure.4.7 frame (1-16) from the real-time X-Ray video.

6.2 Casting with vibration

The technique to increase the internal pressure in casting, so as to overcome the surface tension in thin sections will be explored with the application of vibration after the filling process. This concept assumes that the vibration generates additional acceleration to improve the filling capability in the positive phase of the vibration frequency cycle and pressure from this is added to the internal pressure to force the melt to enter the thin section. However, during the negative acceleration phase of the cycle, it might be expected that any positive effect would be reversed, resulting in no net effect. However, the reverse action seems not to occur. This is further discussed below.

In the practice of thin wall investment casting in the fillability filling regime, the practical results reported in Figure 4.15 showed that vibration had a significant effect on the ability of the metal (especially if it is a metal with a high surface tension and low density) to flow within thin sections, increasing the filling capability by approximately 90% compared with casting without vibration. This suggests that, in thin wall investment casting, vibration is a suitable technique either for increasing the yield of castings free from mis-run defects or able to facilitate the casting of thinner or more extensive wall sections.

From Figures 4.16 a and b, it is clear that the filling capability in thin wall investment casting under vibration conditions was governed by the acceleration generated from the vibration, and that the effect depended only on the applied acceleration, neither frequency nor amplitude having a dominant effect. Any increase in acceleration led to a reduction in the critical metal head needed to fill the section. It was also observed that, if the casting was vibrated with 1g acceleration, the critical metal head was approximately half that produced by casting without vibration. This suggests that the accelerations due to gravity and vibration may be summed in the positive phase of the cycle.

In addition to the improvement of the filling capability in thin wall investment casting because of the vibration effect, the ceramic mould design also played an important role in improving the reliability of the production rate. When the mould was made with a small critical metal head, it makes the runner system in consequence easy to build, lighter and more capable of reducing the amount of metal lost.

To account for the effect of the applied vibration, a simple balance has been made between metallostatic pressure and surface tension force by adding a pressure component due to maximum acceleration (a). A simple calculation was carried out to evaluate the size of the metal head with vibration (see Figure 6.3).

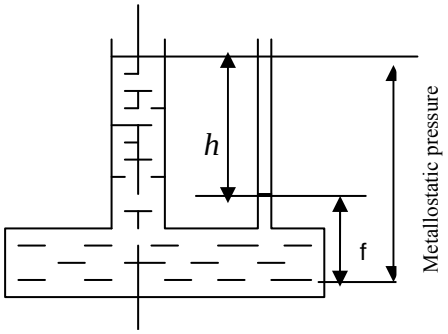

Figure 6.3 Simple geometry to measure the metal head h and metallostatic pressure

In conditions where the whole casting is vibrated with low frequency and in a vertical direction, the pressure experienced at any depth within the liquid depends on both the vibration and the height of the liquid column. So the internal pressure in molten metal becomes

$$P_{\text{int}} = P_a + \rho g h + P_{vibr}$$

$$P_{vibr} = \rho s h$$

where (s) is the maximum acceleration due to vibration, thus:

$$P_{\text{int}} = P_a + \rho h(g + s)$$

Substituting the internal pressure generated due to vibration conditions into the balance force in Equation 6.2 in a thin section:

$$P_a + \rho h(g + s) = \frac{\gamma}{r} + P_m + P_a$$

(P_a) is cancelled from each side of the equation and (P_m) is ignored on the right-hand side of the equation on the basis of no internal gas back pressure, so

$$\rho h(g+s) = \frac{\gamma}{r}$$

$$h = \frac{2\gamma}{\rho r(g+s)} \qquad \text{----------} \quad (6.6)$$

This assumes that the second radius of curvature (r_2) in the thin section is much greater than the meniscus curvature, as defined by the half plate thickness, and therefore r_2 can be disregarded in the calculation.

The maximum acceleration is obtained for the second derivative of the sinusoidal vibration equation

$$s_{\max} = 4a(\pi f)^2$$

Substituting for ($s_{\max}$) in Equation (6.6)

$$h = \frac{\gamma}{\rho r(g + 4a\pi^2 f^2)} \qquad \text{----------(6.7)}$$

Equation (6.7) can be used to estimate the filling capability related to the critical metal head required to force the molten metal to fill a section of given thickness under the action of vibration and fillability filling type conditions, and tested against the experimental data, assuming the values of the surface tension and the density of the liquid metal to be 1.02 N/m and 2400 Kg/m^3. The results show agreement when the acceleration is less than 1g: however, there is less agreement when the acceleration of the vibration is 1g or more. The experimental measurement of the pressure head is always less than the theoretical pressure head (see Figure 6.4 and 6.5).

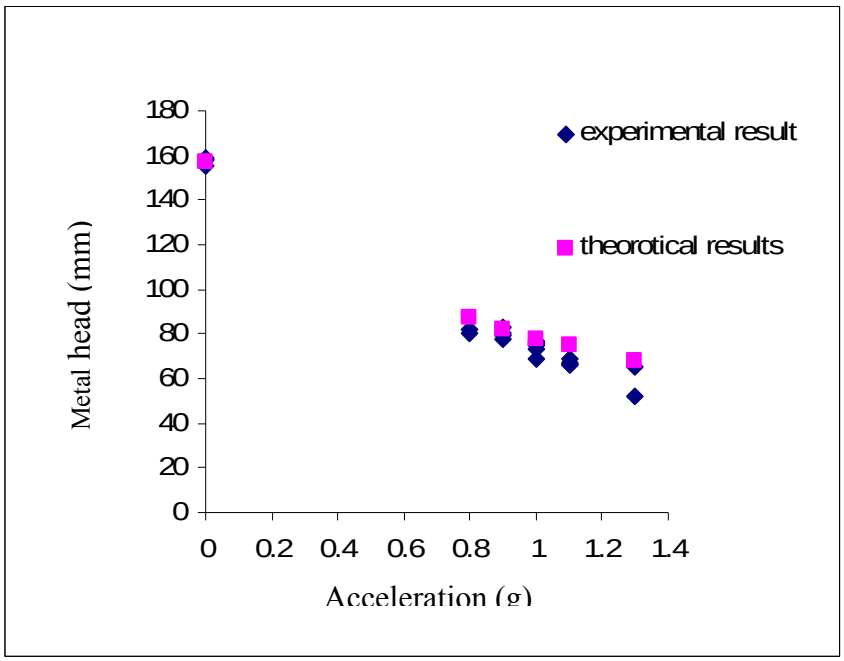

Figure 6.4 Comparison between the experimental results and the theoretical results of the metal head required to fill strips of thickness 0.75mm

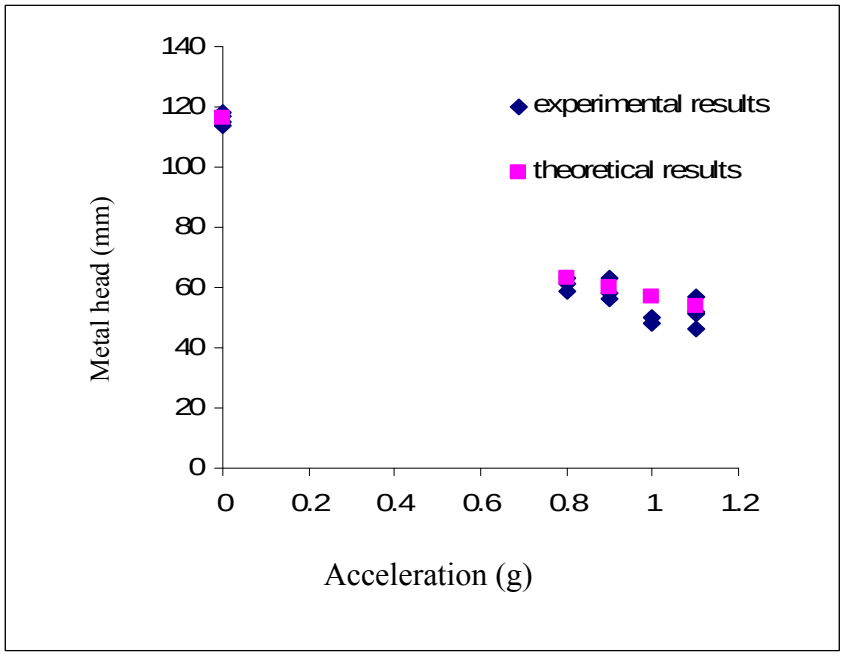

Figure 6.5 Comparison between experimental results and theoretical results for a metal head, strip thicknesses 0.55mm

The additional of vibration acted in conjunction with the force of gravity through the additional acceleration generated from the vibration mould. This led to an increase in the internal pressure of the liquid metal, facilitating the flow. It can be seen that the best fit line calculated using equation 6.6 is plotted as Figure 6.4 and 6.5 passes through the data point where $4\pi^2 f^2 a = 0$ (no vibration), but the calculation of the metal head needed to fill both 0.55mm and 0.75mm strips is greater than that measured experimentally. One source of the difference between the theoretical and experimental data may be the surface tension coefficient used in the calculation. The value of 1.024 N/m^{-1} was derived previously from the experimental data when filling the strips of different thickness without vibration. It has been suggested previously by Campbell that the surface tension coefficient of a moving or flowing liquid aluminum alloy is different from that of stationary liquid, due to the differing degrees of surface oxidation [6]. In order to investigate this possible effect, Equation 6.6 was fitted to the vibrated mould experimental data for 0.55mm and 0.75mm strips. Figures 6.6 and 6.7 show the best fit lines obtained by adjusting γ. For both strip thicknesses a value of γ of $0.92\,N/m^{-1}$ was obtained. However, closer inspection of the best fit lines showed that in both data sets the best-fit values appear to be an under-estimation of the surface tension for acceleration of less than 1g, and, conversely, an over-estimation for acceleration more than 1g. Separating the results for a<1g and a>1g, surface tension values of $0.92\,Nm^{-1}$ and $0.82\,Nm^{-1}$ respectively are obtained (see Figures 6.8 (a and b)). The difference may be due to a change in the liquid front advance. This result is discussed in section 5. So we expect that the flow of liquid aluminum will have a thick monolayer of oxygen (a dirty surface) during filling with vibration (see Figure 2.19)

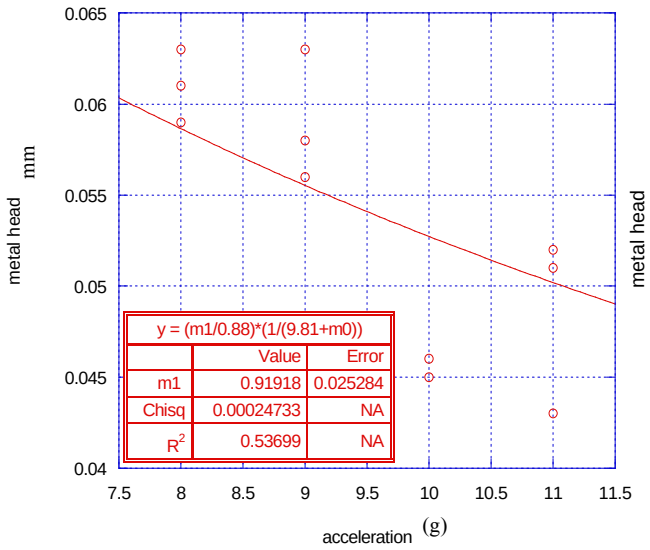

Figure 6.7 $\gamma = r\rho h(a+g)$ Strips of thickness (0.5mm)

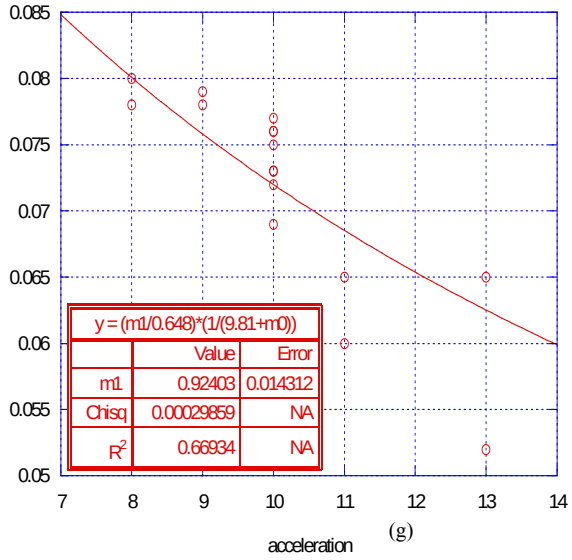

Figure 6.8 $\gamma = r\rho h(a+g)$ Strips of thickness (0.7mm)

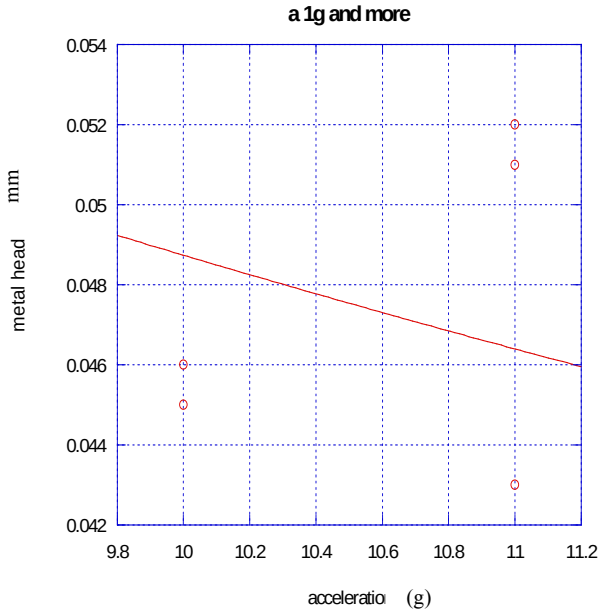

(a)
$\gamma = r\rho h(a+g)$

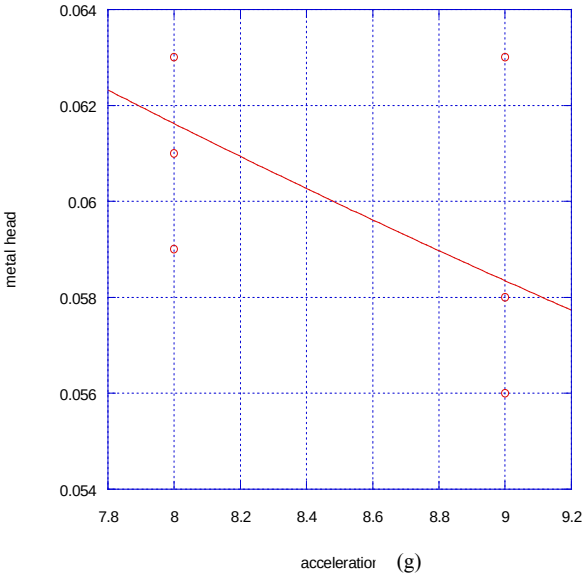

(b)
$\gamma = r\rho h(a+g)$

Figure 6.8 Surface tension calculation, strips of thickness 0.75mm: (a) with vibration condition more than 1g; (b) with vibration conditions less than 1g

6.2.1 Effect of velocity on the filling capability in thin wall casting with vibration

In the case of casting without the action of mechanical vibration, the fluid flow moves under the force of gravity, as discussed in section (5.3.2). Vibration applied after the filling process in the fillability filling type condition caused additional acceleration to be expressed in two directions: one perpendicular to the flow direction, which adds to the potential energy related to gravitation; and the other along the flow direction, which adds to the kinetic energy related to the velocity. This indicates that the inherent variation in the acceleration due to vibration affected the liquid metal flow, through the variation of the driving force, in particular by internal pressure. This variation is reflected in the filling capability related to the metal head (see Figure 4.11). To obtain the velocity, U of the advancing front in a thin section with metal pressure head h, we have:

$$U = \sqrt{2(g - 2\pi^2 f^2 a \sin 2\pi ft)(h - \frac{\gamma}{\rho r(g - 2\pi^2 f^2 a \sin 2\pi ft)})} \,. \qquad \text{----------(6.8)}$$

Equation 6.7 was applied to calculate the velocity of the liquid metal in the positive phase of the frequency cycle and the resulting flow lengths obtained by step-wise integration. Results are shown in Figure 6.10 (calculation does not taken in to account, when square root is - ve). For flow and fluidity modelling it was assumed that the liquid filled a channel under the action of vibration at a constant velocity is quantified by 73% from velocity obtained from equation 6.8.

In addition to the surface tension effect, quantified by Equation 6.8, it is clear that the acceleration related to frequency and amplitude is another parameter which plays an important part in controlling the velocity of the liquid metal. Any increase in vibration frequency is associated with an increase in the flow velocity and length, thus leading to an improvement in the filling capability (see Figure 6.9.).

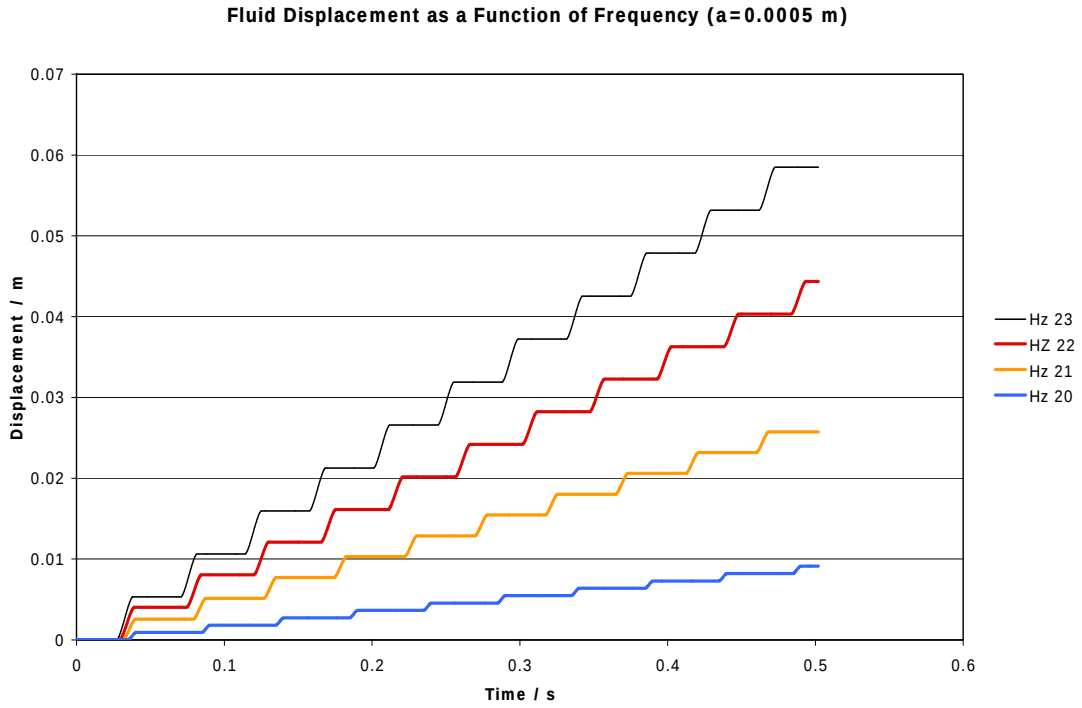

Figure 6.9 shows the effect of acceleration on the filling capability using velocity model (Equation 6.7) in a different frequency cycle

Figure 6.9, indicates that the threshold acceleration defined as required to force liquid metal into the thin channel at a certain metal head, can be estimated by applying Equation 6.7.

Mathematically speaking, Equation (6.7) indicates that, if the value of the square root is negative, the molten metals will not flow, since the back pressure exceeds the combined pressure arising from metallostatic and acceleration sources. In the mercury experiments the metal head required for the mercury to enter the strips with thicknesses of 0.06mm under zero vibration was 75mm; however, under 0.9g acceleration due to vibration, the head was reduced to 40mm.

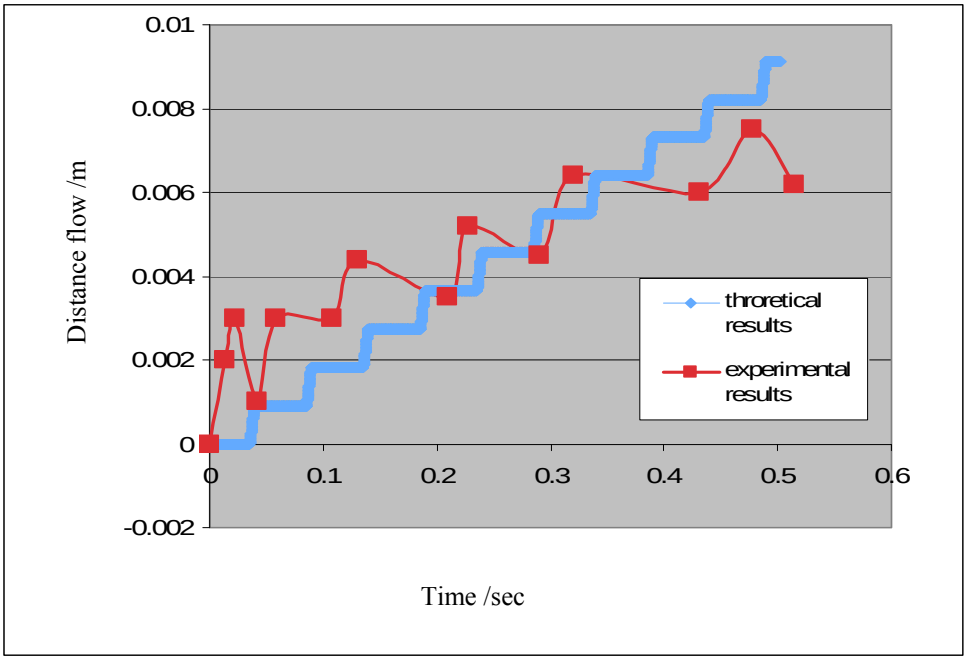

Figure 6.10 Comparison between the experimental results and theoretical results of flow velocity of mercury in a strip of thickness 0.060mm, frequency 20 Hz, amplitude 0.5mm

According to Figure 6.10, the flow distance of the mercury in the positive frequency cycle, as obtained from the high speed camera, was compared with the distance calculated using Equation 6.7. An agreement was observed between the experimental and theoretical results. Errors between observed and derived data may come from any of the following: i) neglecting the influence of the friction drag parameter on the liquid metal flow during calculation: ii) the variation of the back pressure due to surface tension, as a result of minor variation of channel thickness along the strip; iii) unstable movement of the vibrating table during filling; iv) assuming that the reverse movement of the meniscus front of the liquid during the negative phase of the vibration cycle is zero.

6.2.2 Mode of liquid advance during the application of vibration

From the literature available [96, 98 and 103], it is possible that the vibration energy affects the equilibrium hydrodynamic system on the free surface of the fluid and leads to resonance excitation oscillation. This harmonic motion is known as "Faraday excitation" [127].

There are two reasons for the appearance of the Faraday excitation and droplet ejection phenomena on the free surface of a liquid:

(i) Resonance effects, when the frequency of resonant vibration exceeds the natural frequency of the liquid. Campbell calculated the frequency of a resonant standing wave which leads to metal ejection, by using the relation of the velocity of surface wave:

$$f^2 = \frac{\pi\gamma}{4\rho}\left(\frac{2n+1}{D}\right)^2$$

where n = harmonic number and D = diameter of ingot, m

According to Figure 2.32, the frequency of resonant in amplitude 0.5mm was found to be 100 Hz compared with 13-25 Hz frequency which is used in the present work.

[ii] Casting size effects: when the casting thickness corresponds to a quarter of the wavelength, then a standing wave is possible (see Figure 2.31).

$$h = n\lambda / 4$$

where $h =$ ingot height, m and λ = wavelength, m

$$c = \lambda f$$

where c is the velocity of sound in the liquid, $1.3 \times 10^3 ms^{-1}$ for low melting- point metals [93] $f = nc / 4h$

In the order of casting for strips with height 100mm, the critical transitional frequency f was found to be (12000 Hz); however the maximum frequency used in the present work was (15-25 Hz).

It is clear from the above consideration that the vibration with low frequency in the thin wall investment casting which applies in the present work does not lead to Faraday excitation. The Faraday excitation and droplet ejection phenomena play no part in the flow pattern and filling process in the present case. This limitation, referring to the energy resulting from the frequency of vibration which is applied in thin wall casting, is insufficient for the Faraday excitation phenomenon to occur, and most sizes of castings in thin wall vibration investment casting are smaller than the wavelength of the frequency of vibration. This means that no standing wave can be generated in the casting and, when it cannot, the droplet ejection phenomenon cannot occur. Therefore we expect no Faraday excitation to have occurred in thin wall investment casting with strips of about 0.75mm thickness when a low frequency cycle is applied which results in an acceleration of between 0 and 2g.

Considering the mode of liquid advance under the action of vibration, Figures (4.23 a-b) reveal that the peak acceleration arising from vibration is an important parameter, with prominent effect on the front morphology. In cases where the acceleration of vibration was less than 1g, the liquid metal front advanced as a coherent liquid. However, jetting at the free surface occurred when the acceleration of vibration was more than 1g.

Previously, Evans and his co-workers [127] observed microjetting phenomena during the gravity casting of Al-7Si-0.4Mg alloy. They found that microjetting occurred in sections with thickness below 6mm, the effect becoming more pronounced as section thickness reduced, although they did not investigate sections thinner than 3mm. Campbell [6] noted that microjetting "does not seem to occur in all narrow channels and the precise conditions for its occurrence are not yet known. The gaseous environment surrounding the flow may be critical to the behavior of the oxide film and its failure mechanism".

It seems possible that jetting is the result of the maximum upward velocity generated by the

application of the vibration.

The following analysis is of an elementary nature but it gives some indication of the parameters involved and their relative importance. It is not intended at this stage to be a rigorous mathematical analysis of the effect of vibration on the fillability filling type.

The parabolic motion of a particle on the liquid surface can be calculated from the equation $S = ut + \frac{1}{2}gt^2$ in which u, the initial velocity V_{max}, is the maximum upward velocity imposed by the vibration, such that $S = V_{max}t + \frac{1}{2}gt^2$ where $V_{max} = 2\pi af\cos(2f\pi t)$ and at $t = 0$ $V_{max} = 2\pi af$. Hence the distance traveled can be calculated from formula $S = V_{max}t + \frac{1}{2}gt^2$. Thus when the "particle" trajectory is calculated relative to the imposed motion of the mould ($M = a\sin 2f\pi t$) it is possible to determine that when the acceleration due to vibration exceeds 1g the liquid can eject droplets. This is shown in Figure 6.11b.

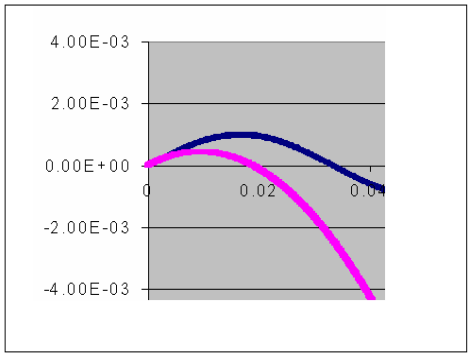

(a) Particle ejecting in (0.8g) vibration conditions

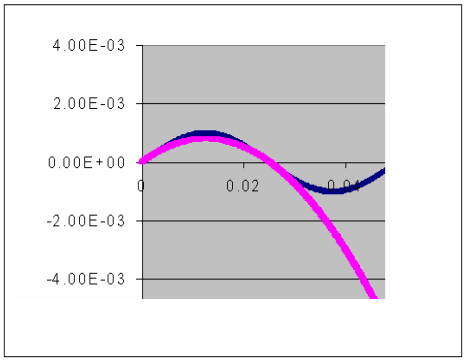

(c) Particle ejecting in (1g) vibration conditions

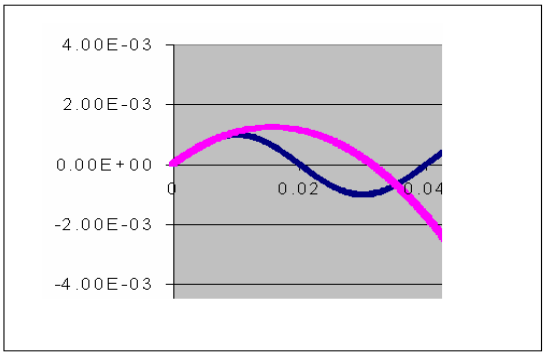

(b) Particle ejecting in (1.2g) vibration conditions

Figure 6.11. imposed mould motion and calculation face body motion under vibration condition of (a) 0.8g (b) 1g (c) 1.2g.

From Figures 6.11 (a, b and c) we can observe that the parabolic curve for particle distance is under the wave motion curve ($m = a\sin(2f\pi t)$) if Acc. < 1g and it is tangential with the curve motion if Acc. = 1g. However, it exceeds the wave motion curve when Acc. > 1g (upward motion of the liquid). So we expect that the jetting on the surface in thin wall investment casting under vibration conditions occurs only when the acceleration exceeds 1g and the 1g acceleration indicates the threshold for the jetting flow filling area. This correlation with experimental observation (see Figure 4.23).

From the standpoint of casting integrity and quality, jetting during the filling process is undesirable. It can be eliminated by reducing the vibration energy related to the amplitude and frequency during casting. Hence, it is useful to examine this problem and establish the energy conditions of the threshold for its occurrence [7]. Figure 4.24 indicates that for the range of conditions studied experimentally the acceleration defining the parameters of amplitude and frequency have no independent influence on the manner of the liquid's advance. Instead it is only the resulting acceleration that determines the free surface form/ morphology.

6.2.3 Liquid jet length

In the present work, the jet length was assessed by the greatest observed length of the wave in advance of the nominal free surface position after filling; this is illustrated by Figure 6.12 .

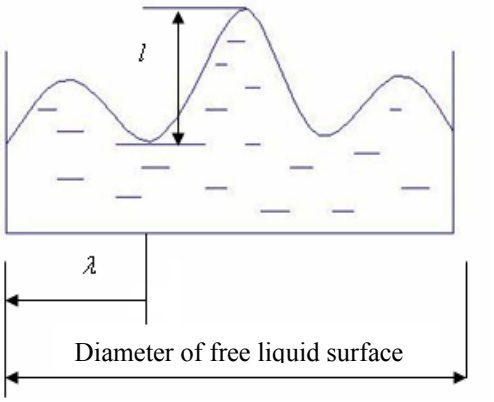

Figure 6. 12 Simple geometry identifying length of jet

In the case of casting without vibration, when the filling process depends on gravity alone, the gravity waves in the hydrodynamic system of the liquid metal on the free surface are damped due to energy dissipation. This is the result of the liquid metal viscosity μ, but occurs only slowly [96 and 103].

However, in cases when the acceleration vibration is due to more than 1g being used after the filling process, the vibration energy arising from of the positive phase of the frequency cycles is transferred to the bulk of the liquid metal, leading to an increase in the instantaneous velocity of the object on the free surface of the liquid. The velocity of the object of the liquid acts as a vector, increasing the force acting to deform the liquid free surface. The deformation can be qualified by the height of the wave which obtained on the free surface after vibration is applied. From the approach summarized in Figure 6.11, jet length can be calculated by measuring the distance between the peak point of the parabolic curve and the peak point of the motion curve at the positive phase in the frequency cycle. This was found to be 2mm when the vibration of acceleration was 1.3g. This was comparable but not identical to 5mm, the jet length which was obtained from the experiments (see Figure 4.25 and Figure 4.30). This error occurred because the experiments were made in different conditions, for example, a different metal head and ignoring the effect of back pressure due to surface tension in thin casting. However, the result from Figure 6.11 is useful for specifying the front of the morphological transition for the liquid, but is not suitable for calculating the jet length.

In addition to the acceleration effect, the metal head is another factor which influences the length of jetting. As the metal metallostatic pressure in the side riser increases, it is found that the length of the metal “jet” entering the strip increases (see Figure 4.26 and Figure 4.30).

6.2.4 Propagation flow in thin wall investment casting with vibration in fillability filling type

Two mechanisms of the liquid advance in thin wall castings were deduced from the experimental results:

(i) Discontinuously propagating flow in vibration conditions

(ii) Continuously propagating flow without vibration.

The differences in these mechanisms due to modification the surface tension at the advancing liquid front.

Anson and Gruzleski measured the dependence of the surface tension of A356 alloy on the degree of oxidation of the liquid alloy surface, observing a decrease in surface tension of 20% from 1.02 to 0.84 N/m [67]. Campbell [129] proposed a contrary effect, whereby the oxide front on the liquid alloy surface increases the surface tension (or effective surface tension) due to the mechanical strength of the film formed. TEM direct observation of the strength of oxide films σ_y on A356 alloy has been measured by Storaska [130] as approximately 15GPa, but he observed very small drops with defects, failing at σ_y << 15GPa. What should be considered, however, is the influence of the contribution of the solid oxide on the back pressure effect. Assuming the surface of the advancing front to be perfectly non-wetting, with a contact angle of 180º and neglecting the secondary major radius of curvature of the advancing front, the stress acting upon the surface film can be calculated as that of a thin-walled cylinder.

Capillary back pressure in a thin channel ($\rho gh = \frac{\gamma}{r}$) equals (5000 Pa) at a metal head of approximately (200mm). The hoop stress calculation can be applied to determine the pressure required to rupture the film (see Figure 6.13).

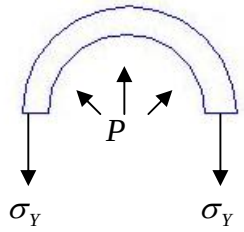

Figure 6. 13 Simple geometry to identify tensile stress σ_y

The tensile stress σ_y in a thin cylinder can be evaluated by the formula:

$$\sigma_y = \frac{pr}{t} \quad \text{--------[37].}$$

where $r = 2 \times 10^{-4} m$,

Assuming that σ_y the tensile strength of the Al_2O_3, is that reported by Storaska of 15GPa (this value with no defects) and the film on the advancing surface is neither young nor old, with a thickness t at 0.01 μm, then the pressure p to rupture the film becomes $7.5 \times 10^6 Pa$. This is effectively additive with the surface tension but was unobserved in the experimental result, this is because the amorphous oxide film which rapidly forms on the free surface of the liquid metal has many defects, such as liquid cracks and porosity [21-23 and 131-132] in a situation when the time taken to form it is insufficient to develop the amorphous film to a stage where it becomes a monolayer film. This weak structure fails when the internal pressure of the liquid bulk is enough to overcome the surface tension beneath the amorphous film. This indicates that the back pressure due to oxide film no longer acts during the filling process in thin wall investment castings.

Campbell [6] has suggested a mechanism which could be an observed reduction in the "effective" surface tension of a moving liquid metal meniscus in a continuously propagating flow. He has described how the surface oxide covering the liquid metal can be considered a series of chain links, some of which are strong, but others of which are weak. The Campbell concept is illustrated in Figure 6.14, and this concept can also be used to explain the mechanism of filling by a discontinuous propagation flow (vibration conditions) in thin channel castings with no wetting, the metal flow being arrested by capillary back pressure under the action of surface tension. It seems that when the metals transfer from the negative to the positive phase in the frequency cycle, the imperfect oxide film ruptures under the increased effective pressure due to the accelerated vibration. This creates a split region on the surface of the metal front. At the same time, the acceleration increases the kinetic energy relative to the velocity. This velocity is affected as a vector pushes aside the splitting film to keep the metal feeding into the thin channel and this causes the flow to advance. When the mould reaches the peak point in the positive phase of the frequency cycle, the movement of the meniscus of the metal front is checked (see Figure 6.15). Immediately an oxide film forms on the surface of the meniscuses of the metal front and this gives the right conditions for the monolayer of oxide to become thicker. This process contributes to a reduction in the surface tension value [67, 68, 71, 74, and 76] and thereby reduces the resistance of the back pressure due to surface tension.

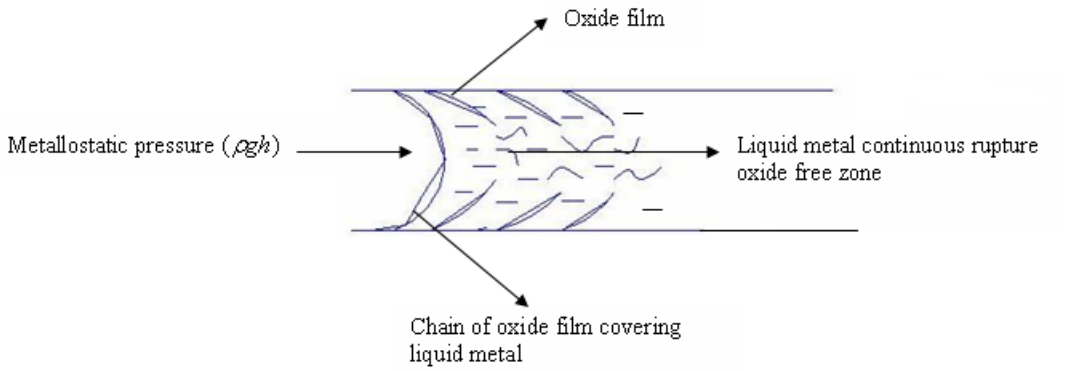

Figure (6.14) Simple geometry showing continuous propagation flow in thin section

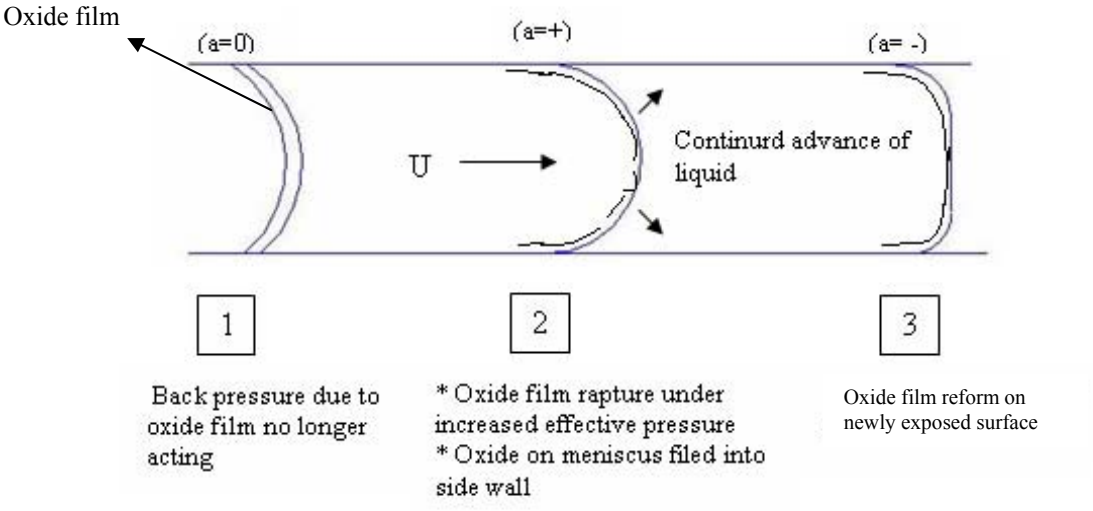

Figure 6.15) Simple geometry showing the discontinuous propagation flows under vibration conditions

The contact angle between the molten metals and the mould surface is another factor which influences the degree of back pressure ($\gamma \cos\theta$). The contact angle of advancing and receding flows in thin channel are generally known to differ, the contact angle normally being reduced on receding flows [133-138] (See Figure 6.16). Thus the effective back pressure fluctuates with both the degree of oxidation of the metal surface that affects surface tension and the direction of liquid flow that affects the contact angle. This in turns alters the radius of curvature of the meniscus. Elsherbini and Jacobi [139] measured the receding contact angle $\theta_{\min}$ and found it to be about 150º when the advancing contact angle $\theta_{\max}$ is 180º (These measurements were done in non- wetting conditions between a substrate and liquid).

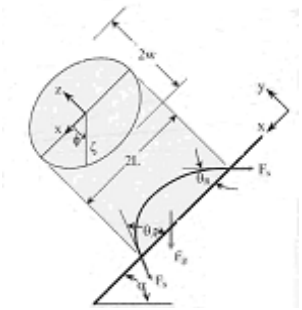

Figure 6.16 Illustration of the maximum ($\theta_{\max}$) and minimum contact angles ($\theta_{\min}$) for drops sliding on inclined surface [139]

In addition, the nature of the propagation flow under vibration affects the magnitude of the contact angle. This change in the contact angle influences the radius of the meniscus of the metal front. See Figure 6.17. To account for the effect of the radius of the meniscus on the value of back pressure $\frac{\gamma \cos\theta_{\min}}{r}$ under vibration conditions:

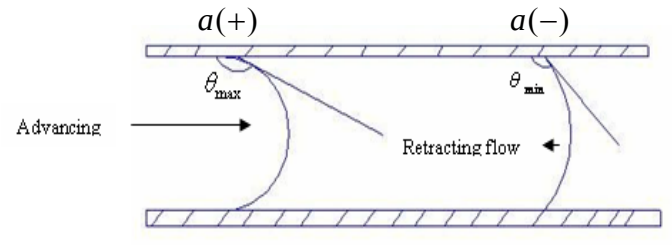

Figure 6.17 simple geometry identifying advance angle and receding angles under vibration conditions

A simple calculation was carried out to evaluate the radius of the meniscus liquid front in a case of the receding angle $\theta_{\min}$; see Figure 6.18

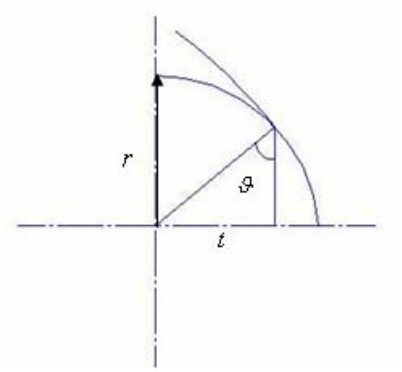

Figure 6.18 simple geometry identifying the radius of meniscus front

$$\sin\vartheta = \frac{t}{r}$$

Where t = half strip thickness, r = radius of meniscus

$$\vartheta = \theta_{\min} - 90$$

$$\sin 60 = \frac{\sqrt{3}}{2}$$

$$r = \frac{2t}{\sqrt{3}}$$

In the situation when the meniscus of the metal front is arrested (positive phase of the frequency cycle), the radius r of (0.45mm), receding angle θ_{min} of 150º, back pressure due to surface tension was found to be (1578Pa). This was comparable with (2342Pa), the back pressure which was obtained from radius r of (0.35mm), advance angle θ_{max} 180º, when the liquid metal moves from the negative to the positive phase of the frequency cycle.

Reductions of surface tension force due to a change of the contact angle and the radius of meniscus seem to be the reason why the reverse action of the vibration (the liquid metal returning to the previous point) does not occur at this stage.

The simulation of the flow pattern which was obtained from the Flow-3D software package (see Figure 4.31 and 4.32) under vibration conditions revealed disagreement with the observed flow of liquid mercury (see Figure 4.29) in a point of the propagation flow. No discontinuous flow was observed in the modelled flow pattern and no jetting was found on the free surface of the liquid advance during simulation. This disagreement in results was described in section 4.4.6.

6.2.5 Effect of vibration time on the filling capability

The minimum vibration time which was used in the experiments was 10sec. This limitation arose due to the stabilization time of the vibrating table; this is about 3s. Figure 4.18 and Figure 4.21b show that the vibration time had no great effect on the filling capability even when it reached 40sec. This is because the filling capability related to the metal head is markedly dependent on the acceleration due to vibration, as described previously in section (6.2), using Equation 6.7 to calculate a filling time of the Al liquid metal needed to fill a section of 0.75mm thickness, until it reaches the critical metal head of 86mm estimated by using Equation 6.4 This was found to be (0.31 sec),

compared with the 10sec and 40 sec operation time which were used in the experimental work (see Figure 6.19).

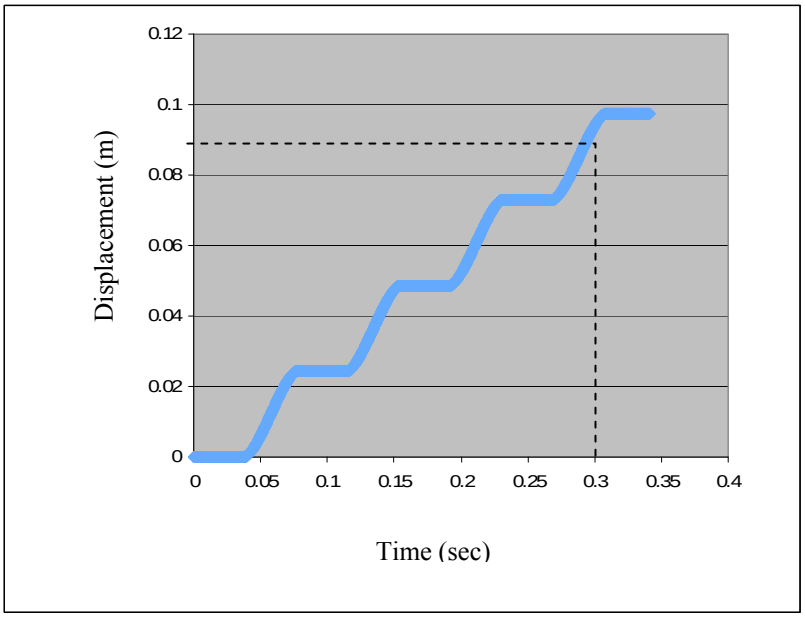

Figure 6.19 shows the time required to fill a section 0.75 mm thick, with a metal head of 120mm

This indicates that when the operation time exceeded 0.35s (depend on channel lengths), the vibration plays no part in the effect on the filling capability related to metal head when the vibration was applied after filling. However the percentage of variation in the relative filling area with respect to time increases when the acceleration of vibration exceeds 1g (See Figure 4.19 and Figure 4.21a). It is suggested that a longer time should be allowed for jetting to occur more often; this gives opportunities for the jets to join together and encourages an increase in the related filling area (see Figure 4.20).

From practical observation when the vibration was more than 1g, marks that appeared as lines on the surface of the casting were observed and are illustrated in Figure 4.23. This mark is believed to occur as a result of the ‘confluence’ between meniscuses of joining metal fronts.

The width of the marks was around 0.1mm to 0.25mm, depending on the thickness of the strip. The mechanism of the joined action of jetting is illustrated in Figure (6.20).

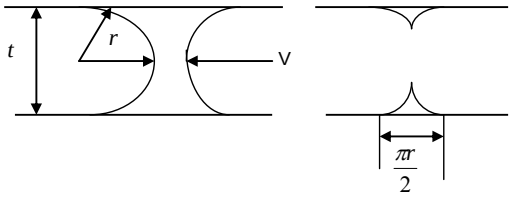

Figure 6.20 Simple geometry for jetting joint action

The modes of propagation suggest that the surface of the advancing liquid metal streams that collide are free from oxide. This is so because the oxide is ruptured and folded onto the surface of casting (see Figure (6.21)).

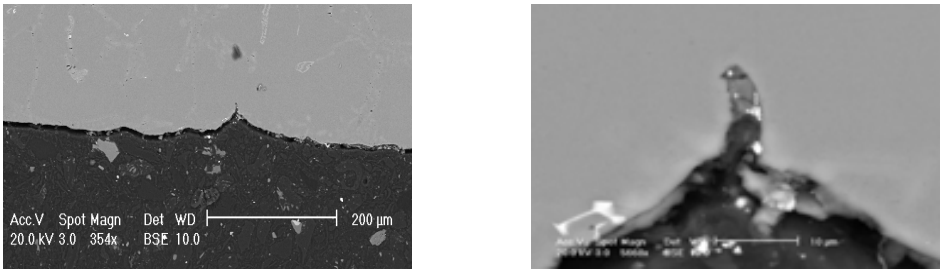

Figure 6.21 shows the microstructure for the joint area between two jets

6.3 Surface turbulence and surface film entrainment

Surface turbulence is a flow phenomenon generated at the free surface of the fluid flow. The Reynold number (a dimensionless number, inertial with the viscous force in the bulk of the liquid) is often used to assess the possibility of turbulence in the bulk of the liquid, but it is not useful for assessing the instability on the free surface of the liquid advance during the filling process in the casting [5].

In casting, we consider the stability of the free surface to prevent the entrainment of the surface film as the result of the folding action on the free surface from entering the bulk of the liquid metal and then damaging the casting [6]. The Weber number (a dimensionless number, inertial with the surface tension pressure, which can be evaluated by the correlation ($We = v^2 \rho r / \gamma$) is generally used for the liquid flow in the casting [5]. The Weber number characterizes the relative free surface stability of a fluid flow. When $We = 1$ the free surface becomes unstable and surface turbulence can arise.

In the present work the Weber number was found to be 0.013 when the velocity due to acceleration was $0.12\, ms^{-1}$ ($U_{\max} = 2\pi fa$). This indicates that the velocity is what the parameter has to consider when assessing the possibility of surface folding and entrainment. However, the geometry of the filling system is another factor which helps to generate surface turbulence on the free surface for the advance of the metal. The Weber number in thin wall casting is very small in value and depends on the thickness of the section [14]. This indicates that the surface tension is a control parameter effect on the stability of the free surface in the fluid flow. Therefore we expect that not much folding action on the free surface and entrainment can occur when the liquid metal flows in a thin section with dimensions less than 0.75mm. Such a view can be seen in Figure 4.6 and 4.7. So it is believed that most of the surface film entrainment is a defect such as oxide film or collapsed and deflated bubbles in thin wall investment castings with and without vibration, were generated in a feature of the runner system, such as a basin or sprue. These defects are discussed below.

6.3.1 Bubble entrainment

Bubbles, formed as a result of the folding of the free surface, are entrained in the bulk of the liquid metal; they mix and move with the stream of the melt, some of them being

trapped inside the casting and others escaping out of the cavity of the mould through the vent (see Figure 4.6 (1-18)). Moving bubbles leave a trail behind them, which they lift into the casting as the double-sided oxide film as observed in Figures 4.61 and 4.62.

6.3.2 Oxide film entrainment

Oxide entrainment is known to lead to nucleation of other casting defects, such as gas pores, intermetallic phases and shrinkage pores, the oxide acting to heterogeneously nucleate these defects [5]. In the present work, in all groups of the castings, the oxide films were often found to be associated with bubbles and shrinkage pores (see Figures 4.55, 4.57, 4.61 and 4.62) covering the dendrite surface.

6.4 Effect of the filling process on the distribution of casting defects

In the present work, metallographic examination was used to assess the size and quantity of casting defects formed within each type of casting. The distribution of defect sizes in each method of casting is illustrated by Figure 4.36. For castings without vibration, the data in Figure 4.36 and Table4.15 show the large number of casting defects, about 20, and the small peak defect size, about (1000-2000 μm^{-2}). However, in the case of casting with acceleration 0.8g of the vibration after filling, the curve shows a small number of casting defects, about 15, and a small peak defect size, about (1000-2000 μm^{-2}). Table 4.15 shows that the number of defects reduces from 97 to 53, when the acceleration of vibration increases from 0 to 1.2g respectively.

Cumulative probability distributions of defect size were plotted for each method of casting and there are illustrated in Figure 6.22. The data in this figure show that the maximum defect size was reduced when the acceleration of vibration increased. This indicates that distribution of casting defect sizes is affected by mould vibration. Thereby it is necessary to qualify the filling sequence in each method of casting.

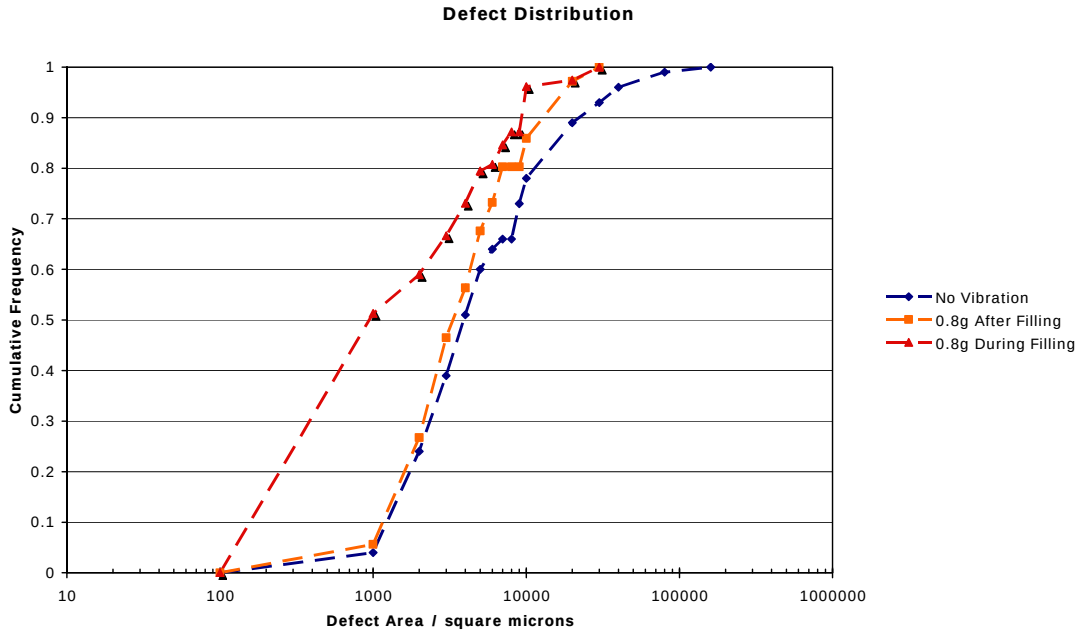

Figure 6.22 Cumulative probability distributions of defect size in each method of casting

6.4.1 Effect of the Liquid metal flow and vibration on bifilm distribution

In the present work, the surface film entrainments were formed in the basin, due to pouring of the charge from the crucible into the basin and within the running system. In the case of casting without vibration, the entrained oxides moved within the metal stream sections appeared to hold back the flow and delay entry of the liquid metal into the section; this situation caused the surface film entrainment to be arrested at the entrance of the thin section or to float to the surface of the upraiser, in the case of bubbles (see Figure 3.4.6 (1-9)). During this period, the main liquid metal continued to flow into the upriser and build a metal head greater than the critical metal head. Liquid metals would again start to flow into the thin section under the control of surface tension, while the oxide that are smaller than the width of the section enter it as part of the stream, but no surface folding action was observed during this stage (see Figure 4.6, 4.7, 4.13 and 4.14 in both the vertical and the horizontal tests.

When the vibration is applied after filling, vibration pressurized the liquid metal into the

thin section, as described above. During the arresting phase, the entrained surface films precipitated in the gate of the runner system under the action of gravity, such as oxide film or floated to the surface such as porosity. As the metal then starts to flow discontinuously into the thin section, most of the small bubbles moves from the bulk of the liquid to the interfacial surface between the mould and the liquid metal, due to the momentum force which is generated from vibration, thereby causing the small bubbles to adhere to the wall surface. Bubbles creep on the surface in the direction, as a result of the vibration movement, until it reaches the free surface of the liquid front and bursts (see Figure 4.34 and 4.35). However, oxide film was observed close to the edges surface of the strips in the vibrated castings. It may be that the old and young oxide film [5] moves to the surface of the casting as a result of the nature of the flow propagation (discontinuous flow) under vibration conditions. (see Figure 6.23).

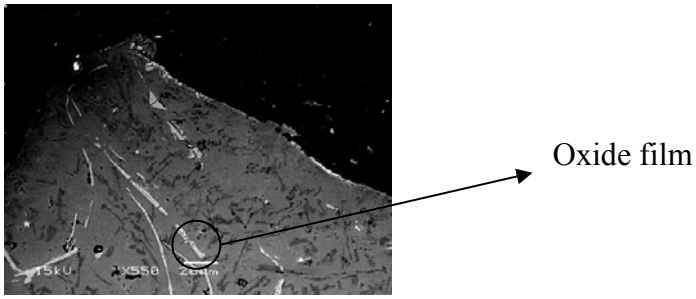

Figure 6.23 SEM micrographs show the oxide film extruded to the edge of the test piece 0.55mm thick casting with 2g acceleration of vibration, in the fillability filling type

When vibration was applied during the filling process, practically, in the part of the basin and sprue the surface film entrainment is caused by the folding action on the free surface of the liquid front as a result of the turbulence motion generated on the surface by vibration influencing the equilibrium hydrodynamic system; but this energy in the present work is not enough to create droplet ejection phenomena. The entrained surface film moved with the metal stream as the liquid flowed in the basin, sprue and gate in the runner system, and into

the thin sections without delay. However, only entrained surface oxide films smaller in size than the channel thickness can pass. After the liquid metal entered the thin section and started to flow within it, the free surface of the liquid front became stable, because the fluid flow was controlled by the surface tension at this stage. So it's expected no folding on the free surface to generate surface film entrainment. In addition, the motion of the vibration started to move the entrainment defects, such as gas bubbles to the free surface, where they burst. This indicates that more surface film entrainment can occur in casting using vibration during filling than in casting using vibration after filling.

6.5 Effect of vibration on the quality casting.

The quality of the casting related to mechanical properties is influenced by the number and size of the defects [3-4]. In this study, the quality of each method of casting was assessed by the density of the defects within the thin strips.

According to Figures 4.43 to 4.46, it can be seen that the average of the UTS and elongation of the specimens in the case of vibration with accelerations 0.8g and 1.2g were $214N/m^2$, $212N/m^2$ and 3.5%, and 3.7% respectively. This was more than the average of the UTS and elongation ($170N/m^2$ and 2.5% respectively) in the castings made without vibration.

In order to evaluate the quality of the casting which was obtained from each method of casting, a quality correlation ($Q = UTS + (150 \times \log(elongation))$ was used to estimate the quality for each method of casting. Calculation results are listed in a Table 6.1

Table 6.1 the quality of each method of casting vs number of defects`

Method of casting	Quality index, Q	Number of defects per 100 mm^2
Casting without vibration	230	97
Casting with vibration after filling (0.8g)	295	61
Casting with vibration during filling (0.8g)	229	71
Casting with vibration after filling (1.2g)	295	51

From Table 6.1 its clear that quality improved with vibration. This indicates that the castings can be ranked in order from best to worst as follows: casting with acceleration of vibration of 1.2g, casting with acceleration of vibration of 0.8g after filling, casting without vibration and casting with acceleration of vibration of 0.8g during filling. The reason for this improvement in the quality is regard to the effect of acceleration as a vector is to break down into smaller sizes the defects such as pores, associated with oxide film or bubbles (see Figure 6.20 and 6.22). Some of these small pores escape to the free surface of the liquid by floating and bursting, and others are removed by the driving force generated due to acceleration from the bulk of the liquid to the interfacial surface between the metal and the mould. The nature of the propagation flow of the liquid metal during vibration assists these pores to creep to the surface of the mould until they reach the free surface of the liquid, where they burst. A diagram of this is shown in Figure 4.34.

In the present work, the vibration continued to act even when the metal started to solidify; this situation increased the mass feeding during solidification and hence, reduced the number and the size of the shrinkage pores as evidenced by the reduced number of defects per unit area (Table 6.1).

6.6 Effect of the vibration on the casting reliability

As a result of the instability in the free surface of the liquid metal oxide entering the bulk of the metal and then being randomly distributed under the effect of bulk turbulence, eventually, oxide films are frozen inside the casting and become the sources of the cracks or hot tears which damage the casting [17,18,19]. The number and distribution of the entrained defects are strong determinants of the scatter of the mechanical properties of castings. The Weibull distribution is a good statistical method to describe the distribution of the mechanical properties of castings and the Weibull modulus of tensile strength has been used before to quantify reliability as a function of filling [69,70, 71]. The Weibull modulus indicates the scatter of the mechanical properties of castings. The lower the value of the Weibull modulus the greater the scatter of the mechanical properties and this reflects unreliable casting performance

From Table 4,14 is clear that the majority of failures occur close to the average value of UTS with a low elongation for each method of casting. There is also a tail in the high elongation with a number of sets of casting. These results reflect the Weibull plot (see Figures 4.49 to 4.52)

The Weibull analysis of the tensile strength data of the samples subjected to vibration indicates that there is a clear advantage for the thin wall investment casting to have an acceleration of vibration of 1.2g after filling, since the reliability, as quantified by the Weibull Modulus is trebled. However, there is only a small improvement to the reliability of the casting with an acceleration of vibration of 0.8g after the filling process. The best fit parameters in Figure 4.53 and quality Q with respect to number of defects N are summarized in Table 6.2, together with the correlation coefficient R.

Table 6.2 The best fit parameters of the Weibull plots and quality index, number of defects and R^2 for Weibull best fit data.

Method of casting	Q	λ	σ	N	R
Casting without vibration	230	12	170	97	0.9028
Casting with vibration (0.8) (after filling)	295	12.7	187	61	0.9253
Casting with vibration (1.2g) (after filling)	295	34	215	51	0.8708
Casting with vibration (0.8) (during filling)	229	7	225	71	0.9388

Table 6.2 shows that the quality of the casting with vibration after filling in a fillability filling type test are more reliable than casting without vibration, in proportion to the number of the oxides, gas pores, bubbles and shrinkage pores in the castings.

In the case of casting without vibration, the Weibull modulus was 12. When applying 0.8g acceleration of vibration after filling, the Weibull modulus became 12.7. This indicates that the small improvement in reliability is governed by the driving force of the flow of the liquid metal, generated from the vibration application. This force seems to reduce the number and size of the defects, such as gas pores and shrinkage pores, in the casting. This is reflected in the distribution of these defects, thereby reducing the scatter in strength. Surprisingly, in casting with an acceleration of vibration 1.2g, the modulus is trebled from 12 to 32. This improvement in reliability is highly significant and is believed to come from the increase of the force of the acceleration due to vibration, which breaks and removes most of the small gas pores and shrinkage pores in the casting and frees them to come to the surface and burst. However, the reliability was reduced when vibration with 0.8g acceleration is used during filling. This may be, when the metal flow in the casting feature (basin, sprue and gate) is turbulence flow resulting from vibration and is generated on the

free surface of the liquid, this increases the folding action on the surface, thereby increasing the surface film entrainment in the bulk of the liquid. Moreover, there is no delay between filling of the side risers and strips, nor accumulated surface film in the gate of the runner system. This assists much of the surface film entrainment to pass into the thin section when the liquid metal flows inside the thin section.

The result of the Weibull analysis of the elongation reveals no great improvement in reliability between the castings made without and with vibration (1.2gand 0.8g) after filling. Low reliability was found with casting with vibration of 0.8g acceleration during filling (see Figure4.54). This indicates that vibration during the casting phase increases the distribution of the elongation properties. This is perhaps caused by the small number and size of the gas pores and shrinkage pores with a specimen cast with 1.2g vibration after filling. However, vibrations decrease the distribution of elongation in the casting when vibration is applied during filling. This could be caused by a large number of defects such as pores in the casting.

6.7 process map for thin wall casting with and without vibration

Based on the acceleration of the low frequency cycle of the vibration after filling, the flow pattern in the thin section modeled using Flow-3D program, experimental observation of mercury filling transparent mould and experimental measurements of filling capability of the thin wall investment castings in the fillability filling regime, an operation map can be constructed (Figure 6.24). The aim of this operation map is to provide a summary of the phenomena and mechanisms controlling filling and integrity or a chart to use as a guide to the engineering casting to achieve a good quality casting with a thickness of 0.75mm, free of misrun defects. The map is divided into three parts, each part being identified by a different acceleration applied after filling. The map focuses on the importance of the acceleration of vibration in thin wall investment casting. The green and white areas enclosed by lines ABDC and CDFE respectively are identified as the propagation flow of

the metal front represented by the jetting and non-jetting flows. The blue Line (1) defines the critical metal head required to fill the thin section, which decreases with increased acceleration of the vibration after filling, and the brown line (2) represents the reliability of the mechanical properties identified by the Weibull modulus for the casting without and with acceleration of vibration 0.8g and 1.2g after filling. The pink Line (3) defines the number of defects measured in area ($100\,mm^2$). If casting is carried out without vibration with insufficient metal head, it reduces filling capability and misrun defects occur in the casting. However, if the metal head is sufficient to overcome the surface tension resistance in a thin section (unreliable runner system design), the casting is not of good quality and is unreliable. If the thin wall casting is carried out with a vibration of less than 1g acceleration, it results in improved filling capability related to the metal head, a design which is easy for the runner system, produces no misrun defects and achieves a good quality, reliable casting. There is no effect of the operation time on the filling capability and no jetting, owing to the cohering metal advance. If the casting is carried out with vibration greater than 1g acceleration, there is greater improvement in the filling capability, good quality and reliability of the casting and the jetting metal advance and no effect of the vibration time on the filling capability

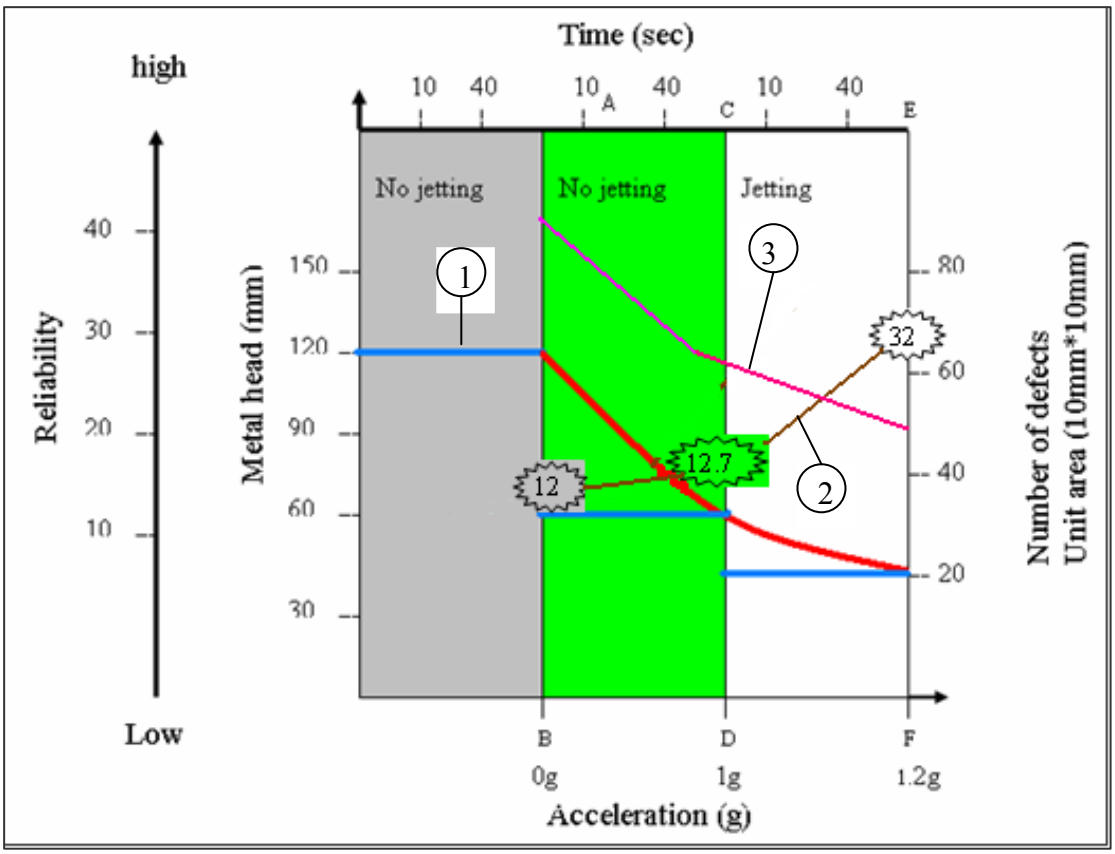

Figure 6.24 Operation map for the thin wall investment casting with thickness 0.75mm under vibration condition (0g, 1g, 1.2g) after filling, fillability filling type. A356 alloys, pouring temperature 750ºC

Chapter 7
Conclusions

The general following conclusion can be drawn from the present work:

(I) the thin wall casting with and without vibration in the fillability condition

Filling thin sections with a thickness of less than 0.75mm is possible if sufficient head pressure is applied. Vibration is a suitable technique for generating the additional pressure and preventing misrun defects in thin section castings.

The metal head required to fill a thin section is depends on the applied acceleration from vibration, but not the individual vibration acceleration parameter amplitude and frequency separately. Generally, the acceleration due to vibration leads to a reduction in the critical metal head; in castings vibrated at 1g acceleration it is approximately half that of castings made without vibration.

The calculation of molten A356 alloy in air depends on the filling conditions. Without vibration a best fit value of $\gamma = 1.02 Nm^{-1}$ was obtained whereas with vibration a value of $\gamma = 0.92 Nm^{-1}$ was found.

During the liquid metal advance, two front morphologies are observed namely coherent liquid front when the acceleration is less than 1g and jetting at the free surface when the acceleration is greater than 1g.

Jetting flow occurs in thin wall investment casting when the acceleration of the vibration is equal to or greater than 1g and the length of jetting is controlled by the acceleration

Two features of the flow propagation were observed during casting

(a)- Continuous metal advance occurs when casting without vibration.
(b)-Discontinuous metal advance when casting with vibration.

The time of the vibration operation has no effects on filling capability related to metal head.

Under acceleration s of less than 1g the metal head height h required to fill a section thickness $2r$ using an imposed sinusoidal vibration cycle of amplitude a and frequency f can be calculated using the formula ($h = \frac{2\gamma}{\rho r(g + 4a\pi^2 f^2)}$) where γ is the surface tension coefficient and ρ the liquid alloy density.

Entrained surface oxide films in the thin wall investment castings appear gas pores associated with oxide films and shrinkage porosity. All were responsible for failure of tensile specimens and scatter of the mechanical properties. The Weibull modulus of the UTS of batches of specimens cast with and without vibration showed that for all accelerations <1g the material was inherently unreliable with a Weibull modulus of tensile strength in the range 12 to 12.7. Samples cast with an acceleration of 1.2g shown significantly improved reliability with a Weibull modulus of UTS of 38

(ii) Thin wall investment casting with and without vibration under fluidity control

The ability of the liquid metal to flow in the thin section is controlled by the heat content in the system; increasing the heat content of the system leads to an increase in the fluidity in thin wall investment castings.

A heat loss based mathematical model of fluidity was developed and showed that the latent heat of the alloy was the principal is a decisive determinant of the fluidity, and the superheat of the liquid the secondary influence.

Application of vibration during filling of thin wall investment has no effect on fluidity at pouring temperature less than 700C. At apouring temperature 750C and applied vibration of 0.8g resulted increase in fluidity of 17%

Solidification time in a thin wall investment castings under vibration conditions is shorter than solidification time in casting without vibration, by 9%

The UTS of a casting with vibration is bigger than the UTS of a casting without vibration. This was suggested to be due to a reduction in the size and the number of the shrinkage porosity in the casting as a result of the increase mass feeding during solidification

A good surface finishing was obtained from the casting with vibration. This was suggested to be due to an increase in the internal pressure in the bulk of the liquid as a result of vibration.

Chapter 8
Future work

450 test pieces and 140 series of casting experiments were done to investigate the influence of vibration on filling a thin section using A356 alloy, with low density and low melting point. Hence, it is recommended that future work should investigate effect of vibration on the filling of high melting point and density alloys such as nickel superalloys..

In the present work, the effect of vibration in a vertical direction on the ability of the metal to fill and flow in the thin section was investigated. Three dimensional analyses should be conducted that reflect the filling conditions more realistically should be developed.

The three-dimensional vibration motion should be examined to see how it affects the number and size of the bubbles etc. in the entrainment surfaces film and how these entrained bubbles and pores move into the bulk of the liquid metal to achieve a high quality of casting and a high Weibull modulus.

REFERENCES

1- J. Campbell; “Castings”, Oxford, Butterworth-Heinemonn Ltd 1991

2- Surathkal, P.O.Sriniviasnagar, Mangalore. "Science and Engineering of Aluminum Casting Practice", National Institute of Technology Karnataka 22 September 2006.

3- N. Green and J. Campbell," Statistical Distributions of Fracture Strength of Casting Al7%Si-Mg alloy", Material Science and Engineering, 1993, A 173, p 261-266

4- N. Green and J. Campbell," Influence of Oxide Film Filling Defect on the Strength of Al- 7%Si-Mg alloys Casting", Trans. AFS, 1994, 102, p. 341-347.

5-J.Campbell; "Thin Wall Casting", Material Science and technology, march, 1988, Vol. 4, p194-204

6- J. Campbell, “Casting” 2nd Edition, UK, 2003.

7- J. Campbell," Grain refinement of solidification metals vibration: review", Conference paper, the metals society, University of Warwick, Coventry, 15-17September 1980.

8-Numan Abu-Dhrie, Marwan Khraisheh, Kozo Saito, Alan Male, Silicon morphology modification in the eutectic Al-Si alloy using mechanical mould vibration" materials Science and engineering A393(2005) 109-117.

9- Kadir Kocatep, "Effect of low frequency vibration on porosity of LM25 and LM6 alloys", Materials and design 28 (2007), p.1767-1775.

10- Kocatepe K. and Burudett C. F., j. Mater. Sci., Vol. 35, 200, pp. 3327-3335

11- Campbell, D.Z.Li, "Filling System for Investment Casting Ni-base Turbine Blade", Journal of Material Processing Technology, 148(2004), pp.310-316.

12- Danielb: Tool and Manufacturing Engineering Handboock, Dallas-1979, USA, Pp 20-1, 21-6, 20-9, 20-20.

13-J. Campbell," Casting practice the 10 rules", Butterworth Heinemann, oxford, UK, 2004

14- Vassilious, D. I. Pantelis, G. C. Vosniakos," Investigation of centrifugal casting condition influence on part quality", the 3rd international conference on manufacturing engineering (ICMEN), 1-3 October 2008, Chalkidiki, Greece

15- Flemings, F. R. Mallard, E. F. Niiyama and H. F. Taylar," fluidity of aluminium", Trans. AFS, 1962, 70, 1029-1039

16- Beely, " foundry technology", Butterworth and Co (publishers) Ltd London: 88 kingway, 1972 p. 21-38.

17- Flemings," Solidification Process", McGraw- Hill, 1974 p. 219-229.

18- J. Campbell," Review of Fluidity Concepts in Casting", Cast Metals, Vol. o.4, pp. 227-237.

19- Internet [http://www.picotech.com/suface- tension].

20- Takamichi Iida,"The Physical Properties of Liquid Metals", Clarendon Press, Oxford, 1988.

21- Klaas s. Agema, Derek j. Fray, "Preliminary investigation on the deformation behaviour of an oxide scale on molten aluminum", department of materials science and metallurgy, university of Cambridge.

22- S. Impey, D. J. Stephenson and J. R. Nicholls," The influence of surface preparation and pretreatments on the oxidation of liquid aluminum and aluminum magnesium alloys", Inst. of material, 29-31 march 1963, p. 323-337

23- M. Divandari, J. Campbell:" A new technique for the study of aluminum oxide films", J. aluminum Trans. Vol.2, No.2, 2000.

24- William D. Callister, Jr., "Materials science and engineering an introduction", copyright © 2003 John and Sons. Inc.

25- ASM Handbook, Vol. 15, Casting, Section introduction and Historical Development, December 1999.

26- Young, James. F., and Shone, Roberts," Material and processes", New York, 1985, pp. 906-908-930.

27- ASME; Metal Handbook, vol.3: Casting and Forming, USA 1976, pp.237-240.
28- ASM Handbook, Vol 15, Section: Modeling and Casting Processes.

29- ASM Handbook, Vol 15, Casting, Section: Patterns.

30- Snowden, J., I, and Sikkenga, L.A. ," Investment Casting", A Growth Industry. Michigan 49441, USA Rep-1988, pp 13-17.

31- Dardi, l. E, "Metallurgy advancement in investment casting technology", Conference Paper, ASM, Metals Park, OH, USA, 1986, P. 25-39

32- John m. Svoboda, "Nickel and Nickel base alloys." Steel Foundary, Society of America, ASME; Metal Handbook, vol.3 casting

33- Mishael F. Ashby," Engineering Materials 1", 2005 P.311-322

34- J. Campbell, and I. D Olliff; “Static and Dynamic Criteria for Filling of the thin section”, AFS Metals Research Journal, Vol. 7,pp. 5561(1971).

35- Flemings, F. R. Mallard, E. F. Niiyama and H. F. Taylar," fluidity of aluminium", Trans. AFS, 1962, 70, 1029-1039.

36- kondic," A new Test for Fluidity", British Foundry, Dec. 1959. p. 75-83

37- Murthy, S. Seshan and Kishore, "CG Iron-Processing Variable, Casting Characteristic and Mechanical Properties," Advanced Casting Technology, Conference Kalamazoo, Michigen USA, (12-14) November, 1986

38- Ragone, D. V., Adams, C. M. and Taylor, Trans. Am. Foundym. Soc., 64, 640 (1956).

39- Horacek and J. Cilecek " On the problem of fluidity and filtering in investment casting ", Seven Word Conference on Investment Casting, Munich, 1988

40- D. V. Neff: "Molten Metal Pumping, Degassing, and Filtration Technology to produce high quality Aluminium Casting", Advance Casting Technology, Conference, Michigan, USA, (12-14) Nov. 1986.

41- Green N. R. (2007) university of Birmingham, UK. Personal communication.

42- Merton C. Flemings," Fluidity of Metal-Techniques for Producing Altar- thin section Casting," British Foundry, Jul. 1964 p. 312-323.

43- Lun Sin and D. Dule; "Influence of Process Parameters on Fluidity of Investment Casting", A Zg10 magnesium alloy. Materials Science and Engineering, Volume 386, 2004, pp.34-42.

44-Runyoro J., Boutorabi S, M. A. and Campbell. "Critical gate velocity for film-forming casting alloys," A Basis for Process Specification, AFS Transactions, Vol. 100, 1992, P225-234.

45- Tiryakioglu M., Askeland D. R., Ramsay C. W. (1993). TAFS.101, P. 685-691.

46- J. T. Cross and A. S. Usmani, "The analysis of mould filling in the casting using the finite element method, "Journal of Material Process Technology, Vol. 38,(1993), p.291-302.

47- Hwang W. E. and Stoehr R. A., "Modeling of Fluid Flow". ASM Handbook, Vol.15, 1988. p 867-876.

48- W. S.Hwang and R. A.Stoehr, "Fluid flow modeling for computer-Aided design of casting". Journal of metals, vol. 35, no. 10, Oct. 1983, p. 22-29.

49- Flow-3D Manual, Flow Science Inc.

50- Hammad, Y. Mohammed," Fluid Mechanics", Al Maaref Establishment, Al-Escandria, Egypt, 1967.

51- White F. M., "Fluid Mechanics", Third edition, McGraw-Hill Inc, 1994

52- Hlinka, J. W., V. Paschkis, V.Puhr, F.S,"how much super heat is lost in runner", Modern Castings, V40, N4, Oct. 1961, P.119-126

53- Kim, P. V. Desai and J. G. Hartley, "Moving Free Surface Heat Transfer Analysis by Continuously Deformation Finite Elements", Numerical Heat Transfer, Vol. 10, p.147-163, 1986.

54- H.S- Cahndraseckairiah and S.Sechan, "Effect of foundary variables on casting fluidity of investments casting Ni-base alloys", AFS Transection, p855-859.

55- kondic ,V.," Fundamental Characteristic of Casting Fluidity", J. Institute of Metals, Vol. 75, No. part 8, Apr. 1949, P. 665-678.

56- Olliff, I. D., Lumby, R. J., Kondic, V," Effect of casting condition and melting atmosphere on fluidity of air-and vacuum-melted alloys", J. foundry trade, Vol.119, Oct. 7, 1965, p. 469-478.

57- Inaba, H," The fluidity of alloys in high temperature (part 1 and part 2) testing apparatus of fluidity in high temperature", Shika Rikogaku Zasshi, Vol.22, No.57, Jun, 1981.

58- lang, G, Aluminum, Vol.48, No.10, Oct. 1972. Abstract- Compendex.

59- Rivsa, R.A.A., BilonI, "Fluidity of AL-Cu alloys with superheat", Zeitschrift fur metallkunde, Vol. 71, No.4, April. 1980, 264-268.

60- Flemings, M.C., Conrad, H.F., Taylor, H.F, " Aluminum alloys fluidity test", Modren Castings, Vol.36, No.2, Aug., 1959, p.86-97.

61- Brezina M. and V. Kondic, "Flow phenomena in investment casting", British Foundrymen, Vol.66, No.12, Des. 1973, p.337-348.

62- Evans, E.R., "Fluidity of molten cast Iron", J. British Cast Iron Research Association, Vol.4, No.2, Oct, 1951, p.86-138.

63- Adefuye PhD thesis, (Fluidity of Aluminium-Silicon) Casting Alloys 1997.

64- Portevin and P. Bastien," Castability of Ternary alloys", J. Institute of metals Londen, Vol.54, 1934, p.45-58.

65- T. P. Hoar and Atterton , " Penetration of molten metal into compacted sand", J. Iron Steel Inst., 166 No.1, 1950, p.1-16.

66- M. Sahoo, L. V. Whiting," foundry characteristic of sand cast Zn-Al alloys", Trans AFS, 1984 Vlo.92, 1984, p. 861-870.

67- Anson and Gruzleski;" The Surface Tension of Molten Aluminum and Al-Si-Mg Alloy under Vacuum and Hydrogen Atmospheres", Metal. And Mate Transaction, Vol. 30, pp1999-1027.

68- Goumir and Joud: Acta. Metall. ,Vol.30, pp1397.

69- [http://www.answers.com/topic/heat-transfer-coefficient].

70- T. Iida and R. I. L. Guthrie, "The physical properties of liquid metals", Oxford university Press, Cambridge, UK. 1988.

71- B. J. Keene;" Review of data for the surface tension of pure metals", Int. Mater. Rev. , 1993, vol.38, pp157-92.

72- Metallurgical and Material Transactions Vol. 36B, April, 2005.

73- Steven J. Roach and Hani Henein," A New Method to Dynamically Measure the Surface Tension Viscosity, and Density of Melts," Metallurgical and Materials Transaction, Vol. 36B, October 2005, p. 667-675.

74- Goicoechea and Garcia:" Surface tension of binary and ternary aluminum alloys of the system Al-Si-Mg and Al-Zn-Mg" J. of Mater. Sci. 27 1992, pp 5247-5252.

75- Zushu l. Kenneth C. and Kusuhiro Mukai, "Measurement of the Density and Surface Tension of Ni-based Superalloys in the Liquid and Mushy states", Metallurgy and Material Transaction, Vol. 36B, April 2005, p247-253.

76- Joonho Lee and Kasuki Morita, " Effect of Carbon and Sulpur on the Surface Tension of Molten Iron", Steel Research 73 (2002) No. 9 p367-372.

77- Lee, J. Morita, K. ISIJ intern. 42 (20002) No.6, P.588-94.

78- Jimbo, T., Shora, A., Cramb, A.W; Trans. ISS (1994) P.48-55

79- Divkar, M. Hajra, J.P; Jakkobsson,A.; Seetharman,S.; Metal. Mete. Trans. 31B 2000, P.267-76

80- S. Jones, M.R. Jolly, K. Lewis,'' Development of "Rule of Mixtures" Techniques or Predicting Ceramic Shell Properties for Investment Casting.

81- [http://www.picotech.com/ wxperimentsheat-transfer-coefficient].

82-[http://www.QATS.com/thermalfundamentals/understanding-heat-transfer-coefficient].

83- Robert S., Brodkey and Harry C. Hershey," transport phenomena", Mc. Graw-Hill, 1989, p. 514.

84- Timsit," the True Area of Contact between A Liquid and A Rough Solid: Elementary Considerations," Paper presented at the Second International Conference on Metrology and properties of Engineering Surface , Leicester Polytechnic, Leicester, Gt, Britain, April 14-16 1982.

85- W. D. Griffiths," A Model of the Interfacial Heat-Transfer Coefficient during Unidirectional Solidification of an Aluminum Alloy", Mechanical and Materials Transaction, Vol. 31B, April, 2000, p. 285-295.

86- Stemmler, G. Laschet, L. Hass, M. Schallmo and F. Hediger," Simulation of Investment Casting: Coupling of Contact and Heat Transfer Calculation between Casting and Mold during Solidification", Modeling of Casting, Welding and Advance Solidification Process.

87- K. Ho and R.D. Pehlke, "Transient method for determination of metal-mould interfacial heat transfer", Paper read at 87th ASF Casting Congress, Rosemont, Illinois, April 10-15, 1983

88- K. Ho and R.D. Pehlke," Mechanism of heat transfer at metal-mould interface", AFS Trans., 1984, vol. 92, pp. 587-98.

89- R.D. Pehlke: Proc," Modelling of Casting", Welding and Advanced Solidification Processes VII, M. Cross and J. Campbell, eds. TMS, Warren- dale, PA, 1995, pp. 373-80.

90- K. Narayan Prabhu," Heat transfer in sand casting", Surathkal, P.O. Srinivasnagar, Mangalore. "Science and Engineering of Aluminum Casting Practice" National Institute of Technology Karnataka 22 September 2006.

91- Nishida and Matsubara;" Effect of Pressure on Heat at the metal Mould casting interface", British Foundryman 69 (1976) 274-278.

92- Deshpande and M. M. Makhlouf, "The Effect Mechanical Mold Vibration on the Casting Characteristics of Aluminum –Copper alloys", LMPC 2007 P.310-326.

93- J. Campbell," effect of vibration during solidification; review", journal the Metals Society and America society, for the metals, International metals reviews, 1981, No.2.

94- Levinson. D. W, A. H. and Rostoker; "Influence of vibration on fluidity and filling during investment casting on Aluminium", AFS Transaction, Vol.63, pp. 686, (1955).

95- Wachter, W. J; Written Discussion on “Influence of Vibration on Fluidity and Filling Investment Casting on Aluminium", AFS Transaction, Vol.63, pp.686, (1955).

96- Dmitri V. Lyubimov, Tatianna P. Lyubimov, "Vibration Influence on Fluid Interfaces", R. Mecanique333 (2004), p467-472

97- Farady, Philos. Trans. R. Soc. London 121 (1831) 299

98- Cabeza, V. Gibiat, C. Negreira "Observation of height localized structures in Faraday experiment with height dissipative fluids" Physica A 327 (2003), p34-38.

99- Roynal E, Kumar S. "Faraday Instability with a polymers Solution" European Physical Journal B9, 175-178 1999.

101- Lyubimov, M. V. Khenner, and M. M. Shotz," Stability of fluid interface under tangential vibration", j. fluid dynamic, vol.33,No.3, 1998.

102- mitri V. Lyubimov, Anatoly A. Cherepanov, Tatiana P. Lyubimov, and Bernard Roux," interface orienting by vibration", C.R. Acad. Sci. Paris, t. 325, p.391-396, 1997

103- G. K. Forster, A. D. D. Craik, "Second-harmonic resonance with Faraday Excitation", Wave Motion 26 (1997) 361-377.

104- G. H. Wolf, "Dynamic stabilization of the interchange instability of a liquid-gas Interface", Phys. Rev. Lett 24 (1970) 444-446.

105- A. H. Cottrell," the mechanical properties of matter", Wiley p.409, 1964.

106- Boris Ouriev, " Rheology and Rheometry of aluminium alloys: influence of shear and vibration on aluminium flow properties", solid state phenomena, Vlo.116-117 (2006) p.558-564.

107- John Campbell; Properties of Cast Metals, 66th World Foundry Congress, 6-9 September 2004, Istanbul, Turkey.

108- R.M. Pillai, K.S. Biju Kumar," A simple inexpensive technique for enhancing density and mechanical properties of Al-Si alloys", journal of materials process technology 146(2004) 338-348.

109-Alonso Rasgado, K. Davey :" Vibration and casting surface finish." Journal of Materials processing Technology, 153-154 2004, p. 875-880.

110- Runyorod, Boutorobi S.M.A and Campbell: Trans AFS 1992 Vol.100 PP. 335-234

111- Cox, M. Wickins, J. P. Kuang, R. A. Harding, and Campbell," Effect of the Top and Bottom Filling on Reliability of Investment Casting in Al, Fe, and Ni based alloys", Material Science and Technology November 2000. Vol.16.

112- - Waloddi Weibull, Stockholm," statistical distribution function of wide applicability", journal of applied mechanic, 1951, p.293-297

113- Khalili, and k. Kromp, "Statistical Properties of Weibull Estimation", Journal of Material Science, 26 (1991), P. 6741-6452.

114- Hamed and R. Elliott, "The dependence of secondary dendrite arm spacing on Solidification condition Al-7Si-0.5Mg alloys", Cast Metal, Vol. 6, No.1, 1903, p.36-41

115- Chandraschariah, "Effect of Foundry Variables on Fluidity of Investment-cast Nickel base Superalloys", AFS Transaction pp 94-124.

116- Griffiths and s. Jones, "laser Flash Diffusive Measurement", IRC in Materials for High Performance Application, University of Birmingham.

117- Al-Sammara and Dows, "Fluidity of steel in investment casting", Conference Paper, Baghdad University, 1996

118- Waleed, Al-Sammara, and Daws," Production of turbine blade using centrifuge investment casting method", Conference paper, Al- Anbir University, 1997.

119- Hallam and W. D. Griffiths, "A Model of the Heat-Transfer Coefficient for the Aluminum Gravity Die-Casting Process." Mechanical and Materials Transaction,Vol. 35B, April, 2004, p.1-14.

120- Mills and R. F. Brooks," Measurement of Thermophysical Properties in high Temperature Melts", Material Science and Engineering A178 (1998) p.77-81.

121- Halvaee a. and Campbell j, "Critical mould entry velocity for aluminum bronze casting", AFS Transactions, Vlo.105, 1997, p.18-46.

122- Griffiths, "Mould Filling-Modern Practice", Science and Engineering of Aluminum Casting Practice, National Institute of Technology Karnataka 22 September 2006.

123- S. Jones, M.R. Jolly, K. Lewis; "Development of “Rule of Mixtures” Techniques for Predicting Ceramic Shell Properties for Investment Casting

124- Sirrell, B. Holliday, M. Campbell, J.; Journal, Modelling of casting, welding and advance solidification process, Vol.5, p. 915-933

125- J.Campbell; "Casting Defect in Vacuum-Investment-Cast Ni-base Turbine Blade", Trans. Metall. 2003.

126-Lennart Backerud, Guocai Chai, Jarmo Tamminen; " Solidification characteristic of aluminum alloys", Foundry Alloys. Vol. 2, Copyright © 1990.

127- Crail and J. G. M. Armitage," Faraday excitation Hysteresis and Wave Instability in a narrow rectangular wave tank", Fluid dynamic Research Volume 15 March, 1995, p. 129-143.

128- Evan, "The Filling of Plaster Block Investment Mould by Aluminium 6.5%

Silicon Magnesium alloy",PHD Thesis, University of Birmingham, March 1997.
129- Personal conversation.

130- Storaska, j. m. Howe, "In-transmission electron microscopy investigation of Surface-oxide, stress-relief mechanisms during melting of sub-micrometer Al-Si alloy particles", material science and engineering A356 (2004) 183-190.

131- Silva, and D. E. J. Talbot," Oxidation of Liquid Aluminum – Magnesium alloys", Light metals, 1989, p. 1035-1040.

132- Sleppy," Oxidation of Molten high-purity Aluminum in Dry Oxygen", Journal of the Electrochemical Society, December 1961, Vol. 108. No. 12, p.1097-1102

133- Finn Knut Hansen, "The measurement of surface energy of polymer by means of contact angles of liquid solid surface", department of chemistry, university of Oslo.

134- Yulli, and D. Shikhmurzaev," Dynamic Contact Angles and Flow in Vicinity of Moving Contact Line", Journal Fluid Mechanics and Transport Phenomena, Vol., 42, No. 3 March 1996.

135- Hansen, R. S. and M. Miotto,"Relaxation Phonomena and Contact Angle Hysteresis", J. Amer. chem.. Soc., 79, (1957). P.1765.

136- Johnson, R. E., R. H. Dettre and D. A. Brandreth," Dynamic Contact Angles and Contact Angles Hysteresis", J. Colloid Interf. Sci., 62,205 (1977).

137-Boris Krasovitski and Abraham Marmur, " Drop down the hill: theoretical study of limiting contact angle and the hysteresis range on a tilted plate", Langmuir, 2005, Vol. 21, p. 3881-3885.

138- E. Pierce, F.J. Carmona, A. Amirfazli, "Understanding of sliding and contact angle results in tilted plate experiments", Colloids and surfaces A: physicochem. Eng. Aspects 323 (2008) 73-82.

139- A.I. EISherbini, A.M. Jacobi, "Retention forces and contact angle for critical liquid drops on non-horizontal surface", Journal of Colloid and interface Science 299, 2006, p.841-489

140- British standard, "BSEN 10002: Part 1", 2000

Table 3.1 Chemical composition specification for A356 alloy

Si	Fe	Cu	Mn	Mg	Zn	Ti
6.7-7.5	0.25	0.20	0.10	0.25-0.45	0.10	0.20

Table 3.2 Running system dimension

Pouring basin depth (mm)	40
Sprue inlet radius (mm)	12
Sprue inlet diameter (mm)	9
Sprue length (mm)	90
Runner cross section area (m^2)	60×10^{-3}

Table 3.3 Recorded dimensions of wax test samples with thickness 0.75mm

No. test piece	Measurement thickness (mm)	Average thickness (mm)	Maximum variation (mm)	Variation (%)	
1	0.73 0.74 0.75	0.74	0.02	2.7	Accept
2	0.76 0.74 0.74	0.74	0.02	2.7	Accept
3	0.75 0.73 0.75	0.746	0.02	2.8	Accept
4	0.74 0.73 0.75	0.74	0.02	2.7	Accept
5	0.76 0.75 0.74	0.75	0.02	2.6	Accept
6	0.74 0.73 0.75	0.74	0.02	2.6	Accept
7	0.76 0.75 0.74	0.75	0.02	2.6	Accept
8	0.74 0.73 0.75	0.74	0.02	2.6	Accept
9	0.74 0.74 0.76	0.746	0.02	2.8	Accept
-------	--------	-------	-------	-------	--------
-------	--------	-------	-------	-------	--------
-------	--------	-------	-------	-------	--------
-------	--------	-------	-------	-------	--------
200	0.72 0.74 0.76	0.74	0.04	5	Accept

Table 3.4 Recorded dimensions of wax test samples with thickness 0.55mm

No. test piece	Variation thickness (mm)	Average thickness (mm)	Maximum variation (mm)	Variation (%)	
1	0.53 0.54 0.56	0.543	0.03	5.5	Accept
2	0.53 0.56 0.55	0.546	0.03	5.4	Accept
3	0.53 0.56 0.55	0.546	0.03	5.4	Accept
4	0.56 0.55 0.53	0.543	0.03	5.5	Accept
5	0.53 0.54 0.56	0.543	0.03	5.5	Accept
6	0.53 0.54 0.56	0.543	0.03	5.4	Accept
7	0.56 0.53 0.56	0.55	0.03	5.4	Accept
8	0.55 0.54 0.55	0.546	0.01	1	Accept
9	0.55 0.55 0.54	0.546	0.01	1	Accept
--------	--------	--------	---------		------
--------	--------	---------	---------	-------	---------
----------	----------	---------	---------	--------	---------
-------	---------	-------	-------	--------	--------
150	0.53 0.54 0.55	0.54	0.02	3	Accept

Table 3.5 Composition of the secondary slurry

SECONDARY				
Filler (200mesh fused silica)	Polymer (Adbond BV)	Wetting Agent (Victawet 12)	Antifoam (Burst RSD 10)	Deionised Water
7.70 *kg*	456g	1.8g	28.5g	1216g

Table 3.6 Composition of the primary slurry

PRIMARY				
Filler(200mesh Zircosil) (200mesh fused silica)	Polymer (Adbond ADII)	Wetting Agent (Victawet 12)	Antifoam (Burst RSD 10)	Deionised Water
Zircon *kg* 20 660g Silica	35g	1.8g	2.9g	74g

Table 3.7 Experimental conditions used to investigate filling capability in thin sections under vibration condition, fillibility filling type

Frequency (Hz)	Amplitude (mm)	Acceleration (g)	Number of tests piece			
			0.45 thickness	0.55 thickness	0.75 thickness	1.00 thickness
13.68	2.15	0.81	4	10	10	10
14.71	2.11	0.9	0	10	10	5
15.31	2.14	1.01	0	20	15	0
16.18	2.09	1.1	0	20	15	0
17.17	2.04	1.21	0	20	15	0
17.98	2.01	1.31	5	20	15	3

Table 3.8 Experimental conditions used to investigate metal advance in a vibration casting in a fillibility filling condition.

Frequency (Hz)	Amplitude (mm)	Number of test pieces	
		Thickness 0.55 mm	thickness 0.75mm
22.2	1.01	3	3
19.5	1.32	3	3
17	1.71	3	3
15.3	2.1	3	3
14.71	2.11	3	3
15.98	1.78	3	3
18.03	1.38	3	3
15.6	2.14	3	3
17.73	1.73	3	3
20.03	1.38	3	3

Table 3.9 Experimental conditions used to investigate jet length on the free surface of the liquid metal in casting with vibration

Frequency (Hz)	Amplitude (mm)	Metallostatic pressure	No. of strip thickness 0.55mm
15.37	2.14	100	3
16.18	2.09	100	5
17.17	2.04	100	4
17.97	2.03	100	3

Table 3.10 Experimental conditions used to study the effect of vibration time on metal head and relative filling area.

Time (sec)	10	20	40	60	No. of stripe thickness (0.55)
Frequency (Hz)	14.71	14.71	14.71	14.71	12
Amplitude (mm)	2.11	2.11	2.11	2.11	
Time (sec)	10	20	40	60	12
Frequency (Hz)	17.17	17.17	17.17	17.17	
Amplitude (mm)	2.04	2.04	2.04	2.04	

Table 3.11 Details of the fluidity experiments of casting under vibration condition with thickness 0.75mm.

Frequency (Hz)	Amplitude (mm)	Pouring Temperature ˚C	Mould Temperature ˚C	No. of Test pieces of thickness 0.75mm	Casting conditions
13.68	2.15	700C	400C	4	Vibration after filling
13.68	2.15	665C	400C	6	Vibration during pouring
13.68	2.15	700C	400C	6	Vibration during pouring
13.68	2.15	750C	400C	6	Vibration during pouring

Table 4.1 Summary of the experimental results to confirm the fillability filling type region and flowability filling type region by the critical metal head in the strip with thicknesses 0.75mm and 0.55mm, metallostatic pressure 200 mm, pouring temperature 750ºC.

Stripe No.	Metal head for thicknesses (mm)			Mould temperature C
	0.45 mm	0.55 mm	0.75 mm	
1	>200	175	120	400
2		148	127	
3		165	130	
4		171	130	
5		181		
1	>200	160	130	550
2		165	135	
3		167	125	
4		158	132	
5		169	128	
1	>200	155	110	660
2		158	115	
3		160	117	
4		159	120	
5		140	114	
6		158	108	
7		154	118	
1	>200	150	95	700
2		155	114	
3		160	105	
4		148	118	
5		153	110	

Table 4.2 Summary of the experimental results to determine the effect of the pouring temperature on the metal head in different thicknesses in flowability filling type at a constant mould temperature of (400˚C)

Pouring temperature ˚C	Metal head (strip thicknesses 0.45mm)	Metal head (strip thicknesses 0.55mm)	Metal head (strip thicknesses 075 mm)
660	>200	198	155
	>200	>200	158
	>200	>200	165
		>200	147
700	>200	198	135
	>200	195	140
	>200	192	145
		191	138
750	>200	175	118
	>200	170	110
	>200	168	127
		172	120
		165	125
		171	128

Table 4.3 Results of experiments for the pouring temperature effect on the metal head in thin section (0.45mm, 0.55mm, 0.75mm), fillability filling type, mould temperature 660˚C ≈ 700˚C.

Pouring temperatureºC	Metal head (strip thickness 0.45mm)	Metal head (strip thickness 0.55mm)	Metal head (strip thickness 0.75mm)
668	197	165	115
	195	160	110
	>200	155	108
	>200	152	116
	>200	154	118
	>200	150	105
	>200		114
700	195	160	115
	>200	150	110
	>200	165	105
	>200	155	100
	>200	152	114
750		151	
	197	155	110
	192	160	115
	198	151	105
	190	154	112
	>200	101	98
			105
780	198	155	109
	192	154	117
	191	160	98
	>200	150	105
	>200	152	98

Table 4.4 Results of experiments for different strip thicknesses effect on filling capability in the fillability filling type, mould temperature 660˚C to 700˚C, pouring temperature 750˚C, metallostatic pressure 200 mm.

Metal head (strip thickness 0.45mm)	Metal head (strip thickness 0.55mm)	Metal head (strip thickness 0.75mm)	Metal head (strip thickness 0.85mm)
195	155	114	99
190	158	117	101
198	158	120	105
>200	159	115	98
>200	160	110	
	158	115	

Table 4.5 Results of experiments to determine flow velocity in fillability filling type casting, pouring temperature750˚C, mould temperature 660˚C-700˚C.

No. point	X-distance (mm)	Y-distance (mm)	Time (sec)	Velocity (ms^{-1})
1	137.5	58.7	0	0
2	113.3	58.9	0.034	0.71
3	77.1	59.12	0.086	0.695
4	47.2	59.61	0.131	0.66.
5	24.1	58.6	0.165	0.67

Table 4.6 Results of the experiment to determine the velocity in fillability filling type casting, pouring temperature750ºC, mould temperature 660ºC-700ºC, using X-ray machine

No. point	X-distance (mm)	Y-distance (mm)	Time (sec)	Velocity (ms^{-1})
1	115.5	111	0	0
2	90	110.6	0.034	0.75
3	56.9	110.5	0.079	0.735
4	31.4	110.3	0.113	0.75
5	4	111.8	0.149	0.748

Table 4.7 Results of experiments to determine metal velocity in flowability filling type casting, pouring temperature750˚C, mould temperature 400˚C.

No. point	X-distance (mm)	Y-distance (mm)	Time (sec)	Velocity (ms^{-1})
1		50.06	0	0
2	117.9	49.7	0.034	0.62
3	95.6	48.9	0.084	0.44
4	74	48.3	0.132	0.42
5	50	49.1	0.18	0.41

Table 4.8 Experimental results of the effect of acceleration due to vibration on the metal head with strips of thicknesses $0.55^{\pm 0.05}\,mm$ and $0.75^{\pm 0.05}\,mm$. Pouring temperature750˚C $\pm$ 5 ºC. Mould temperature 620˚C to 660˚C, vibration time 10s.

Aceeleration (g)	0.0	0.8	0.9	1.0	1.1	1.3
Strip thicknesses (0.55mm)	157	78	79	76	65	52
	159	80	78	75	60	65
	159	80	78	77	65	52
	158	83	75	76	66	54
	152			73		
Strip thicknesses (0.75mm)	117	59	56	46	43	
	120	63	63	52	51	
	120	61	58	52	52	
	117	55	60	54	47	
Strip thicknesses (0.45mm)	>100	>100	>100			
	>100	>100	>100			
			>100			

Table 4.9 Experimental results of the effect of vibration time on the metal head and filling relative area with a strip ($0.55^{\pm 0.05}\,mm$) thick, Pouring temperature. $750C \pm 5$ ºC, Mould temperature ≈ 620 ºC to 660 ºC, acceleration of vibration varying between 0.8g to 1.3g

		Acc. (g)	Relative filling area (mm^2)	Metal head (mm)	Acc. (g)	Relative Area (mm^2)	Metal head (mm)
Time (sec)	10	0.8	67	82	0.9	70	79
			70	80		95	78
			61	79		87	83
	20		65	87		105	75
			69	82		78	80
			73	90		92	72
	40		60	74		76	75
			61	82		99	81
			69	78		80	78
		Acc. (g)	Relative filling area (mm^2)	Metal head (mm)	Acc. (g)	Relative Area (mm^2)	Metal head (mm)
Time (sec)	10	1.1	300	69	1.3	300	52
			260	62		360	48
			240	73		290	65
	20		380	65		400	60
			365	73		430	50
			345	63		461	48
	40		400	66		460	58
			420	70		474	48
			395	62		425	50

Table 4.10 Dependence of the relative filling area as a function of vibration time and acceleration in strip thickness 0.55mm, pouring temperature 750ºC, and mould temperature 660-750 º C

Acceleration (0.8g)								
Vibration time (sec)	Relative filling area (mm)	metal head (mm)	Average relative filling area (mm)	Average metal head (mm)	Range relative area (mm)	Range metal head (mm)	Range area %	Range metal head %
10	67	82	66	80.3	5.7	7.7	8%	9%
	70	80						
	61	79						
20	65	87	69	86				
	69	82						
	73	90						
40	60	78	63.3	78.3				
	61	81						
	69	76						
Acceleration (0.9g)								
time (sec)	relative area (mm)	metal head (mm)	Average relative area (mm)	Average metal head (mm)	Range relative area (mm)	Range metal head (mm)	Range relative area %	Range metal head %
10	70	79	84	80	7.7	4.4	8.7%	5.6%
	95	78						
	87	83						
20	105	75	91	75.6				
	78	80						
	92	72						
40	76	75	85	78				
	99	81						
	80	78						
Acceleration (1.1g)								
time (sec)	relative area (mm)	metal head (mm)	Average relative area (mm)	Average metal head (mm)	Range relative area (mm)	Range metal head (mm)	Range relative area %	Range metal head %
10	178	69	166.6	68	44.4	2	23%	2.9%
	165	62						
	157	73						
20	205	65	192	67				
	191	73						
	177	63						
40	195	66	211	66				
	215	70						
	223	62						
Acceleration (1.3g)								
time (sec)	relative area (mm)	metal head (mm)	Average relative area (mm)	Average metal head (mm)	Range relative area (mm)	Range metal head (mm)	Range relative area %	Range metal head %
10	258	52	267.6	55	53.4	4.7	18%	8.9%
	267	48						
	278	65						
20	280	60	283.3	52.6				
	293	50						
	277	48						
40	310	53	314	50.3				
	295	48						
	339	50						

Table 4.11 Experimental results to determine the effect of the vibration parameter (frequency and amplitude) on the flow of liquid metals in strip with thickness of ($0.55^{\pm 0.05}\,mm$) and using A356 alloys, Pouring temperature $750C \pm 5$ ºC, Mould Temperature ≈ 620 ºC to 660 ºC.

Frequency (Hz)	Amplitude (mm)	Acceleration (g)	Jetting	Metal head (mm)
14.71	2.11	0.92	Non	80
15.98	1.78			74
18.03	1.38			83
24.03	0.77			81
22.2	1.01	1.0	Yes	70
19.5	1.31			73
17.04	1.71			76
15.39	2.1			75
16.18	2.09	1.1	Yes	67
17.73	1.73			65
20.03	1.38			70
21.9	1.14			63

Table4.12 Experimental results from experiments to determine the effect of the metal head on the length of jetting at a constant acceleration of vibration (1g), with a strip thickness of $0.55^{\pm 0.05}\,mm$, Pouring temperature $750C \pm 5$ ºC, Mould temperature ≈ 620 ºC to 660ºC.

Metal head (mm)	Acceleration (g)	Jet length (mm)
45	1	3
		2.5
		2.8
51	1	4.7
		5.2
		5
55	1	6.5
		7
		7.1
60	1	7.2
		7
		7.3
64	1	8.1
		8.3
		8

Table 4.13 Experimental results to determine the effect of the acceleration of vibration on the length of jetting at constant metal head (45mm), with a strip thickness of ($0.55^{\pm 0.05}\,mm$) and using aluminum alloys, Pouring Temperature $750C \pm 5$ ºC, Mould Temperature ≈ 620 ºCto 660ºC.

Frequency (Hz)	Amplitude (mm)	Acceleration (g)	Length of jetting (mm)
15.37	2.14	1	3
			2.5
			2.7
16.18	2.09	1.1	5
			4.1
			3.9
17.17	2.04	1.2	5
			5.2
			4.8

Table 4.14 summary result of the experiment to determine the velocity of mercury in each frequency cycle, using high speed camera.

No. point	X-distance (mm)	Y-distance (mm)	Time (sec)	Velocity (ms^{-1})
1	0		0	0
2	0.002	1	0.014	0.132
3	0.003	2	0.022	
4	0.001	1	0.042	0.125
5	0.003	2	0.058	
6	0.003	1	0.108	0.092
7	0.0044	3	0.123	
8	0.0035	2	0.21	0.127
9	0.0052	2.5	0.228	
10	0.0045	2	0.29	0.06
11	0.0064	4	0.32	
12	0.006	2	0.431	0.051
13	0.0075	4.5	0.468	
	0.0062	3	0.515	

Table 4.15 number of defect in each interval of 1000 μm^2 increase in defect size

size of defects (μm^2)	Number of defects			
	Casting without vibration	Casting with vibration after filling (0.8g)	Casting without vibration during filling (0.8g)	Casting with vibration after filling (1.2)
0-1000	4	4	40	11
1000-2000	20	15	6	10
2000-3000	15	14	6	6
3000-4000	12	7	5	5
4000-5000	9	8	5	7
5000-6000	4	4	1	5
6000-7000	2	5	3	3
7000-8000	0	0	2	2
8000-9000	7	0	0	2
9000-10000	5	4	7	
10000-20000	11	8	1	
20000-30000	4	2	2	
30000-40000	3			
40000-80000	3			
80000-160000	1			
Total number of defects in the unit area of 10mm × 15mm for each method of casting				
	100	71	78	51

Table 4.l6 hardness measurement for each method of casting

	No. test piece	Hardness value for each (3mm) distance from the edge of the width of the specimen to a nother				Average hardness	Variation of hardness
casting without vibration	1	80.4	79.5	80.5	81.2	80.4	1.7
	2	82.2	80.6	81.3.	79.2	80.82	3
	3	81.1	77.2	77.4	78.8	78.62	3.9
	4	80.8	80.6	83.5	79.8	81.42	3.7
	5	77.7	78.1	80.1	77.1	78.25	3
	6	83.4	79.9	80.3	81.1	81.17	3.5
Casting Acc. Vibration (0.8g)	1	91.9	92.1	88.0	92	91	4.1
	2	91.8	91.9	90.5	90.2	91.9	1,7
	3	92.1	91.8	91.6	91.2	91.6	0.9
	4	90.9	91.3	91.6	91.8	91.4	0.9
Casting Acc. Vibration (1.2g)	1	87.2	92.1	90	88.5	89.45	3.6
	2	89.8	90.1	88.2	87.9	89	2.7
	3	90.6	90.8	88.7	87.6	89.42	3.2
	4	91.2	89.1	90.3	88.9	89.87	2.3

Table 4.17 UTS and elongation of the specimens for each method of casting: without vibration, with vibration 0.8g and 1.2g acceleration after filling and vibration 0.8g acceleration during filling. Pouring temperature 750ºC, mould temperature 660ºC-700ºC.

Casting without vibration		Casting with acceleration of vibration (0.8g) ,after filling	
Elongation %	U.T.S	Elongation %	U.T.S
5.21	165.4	2.32	200.47
2.22	146.066	6.9	232.41
3.56	170.09	2.67	220.41
2.21	169.01	1.55	182.176
1.15	135.58	2.43	210.82
2.69	177.77	4.4	219.294
2.63	169.55	4.44	183.529
2.74	176.02	5.0	223.529
1.14	188.02	2.44	184.4
1.82	192.02	3.23	213.8
misrun		Failed during test	
Failed during test		Failed during test	
Casting with acceleration of vibration (1.2g), after filling		Casting with acceleration of vibration (0.8g), during filling	
Elongation %	U.T.S	Elongation %	U.T.S
6.79	219.529	0.46	182.34
3.04	204.262	0.41	151.36
2.85	211.76	2.13	224.53
3.25	210.58	0.9	229.07
2.16	212.25	2.13	220.44
2.15	204.235	1.09	229.01
3.64	216	3.2	273.77
3.95	215	0.9	200.6
5.52	223.52	1.14	228.57
2.73	204		
Failed during test		Failed during test	
Failed during test		Failed during test	

Table 5.2 Radius of the peak in a surface roughness profile of the ceramic mould, distance between two peak around (50 to 60 μm).

measurements (1mm)	True area of contact estimation (μm)	measurements (1mm)	True area of contact estimation (μm)	measurements (1mm)	True area of contact estimation (μm)
1	2	2	3	3	2
	2		4		2
	3		2		2
	3		2		3
	2		4		3
	4		3		4
	2		3		2
	4		2		3
	3		5		2
measurements (1mm)	True area of contact estimation (μm)	measurements (1mm)	True area of contact estimation (μm)	measurements (1mm)	True area of contact estimation (μm)
4	4	5	3	6	4
	2		3		4
	2		3		2
	2		4		3
	4		5		3
	3		3		4
	3		2		5
	4		2		2
	3		2		2
	2		3		2
No. measurements (1mm)	True area of contact estimation (μm)	No. measurements (1mm)	True area of contact estimation (μm)	No. measurements (1mm)	True area of contact estimation (μm)
7	3	8	5	9	5
	3		3		5
	3		3		3
	2		2		3
	2		2		2
	4		2		4
	2		4		2
	4		3		4
	4		3		3
	2		2		2

Table 5.5 UTS and elongation measured in 0.75 mm thick strip cast with and without vibration of 0.8g acceleration during filling. Pouring temperature 750ºC, mould temperature 420ºC

Casting without vibration		Casting with acceleration of vibration (0.8g) , during filling	
Elongation %	U.T.S	Elongation %	U.T.S
1.14	165.5	1.67	204
1.94	193	2.02	207
2.01	196	2.46	221
2.32	207	3.9	225
2.82	208.5	4.01	238
2.86	211	4.12	239
3.01	216	4.75	242
3.86	219	5.37	248
5.02	219.2	Failed during test	
mis-run		Failed during test	

Table 5.8 Results of the fluidity experiment

Pouring temperature ºC	Fluidity Casting without vibration, mm	Fluidity Casting with vibrating 0.8g, mm	Vibration condition
660	71	70	During filling
	70	67	
	68	65	
	74	72	
	74	61	
	76		
700	83	91	During filling
	90	89	
	77	93	
	81	87	
	85	93	
750	91	117	During filling
	94	114	
	90	109	
	92	112	
	94	113	
	97	107	
750		90	After filling
		92	
		94	
		88	

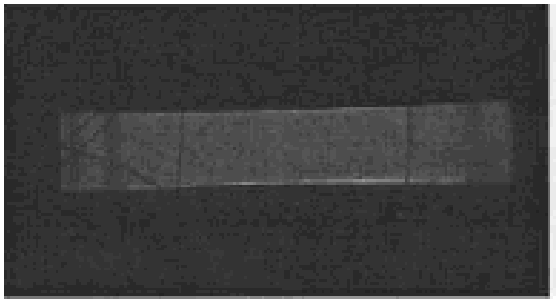

(1) Time:

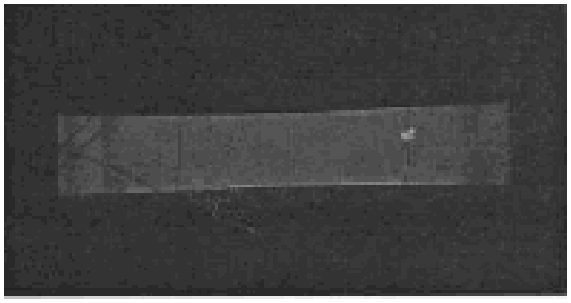

(2) Time: 0.000

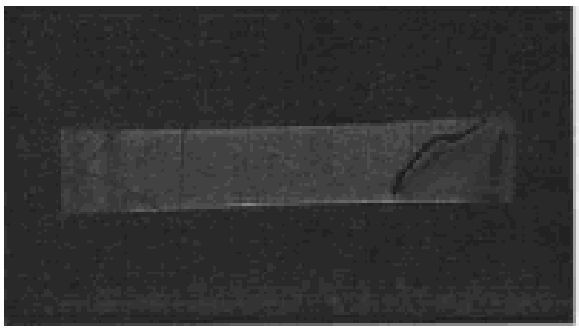

(3) Time: 0.034

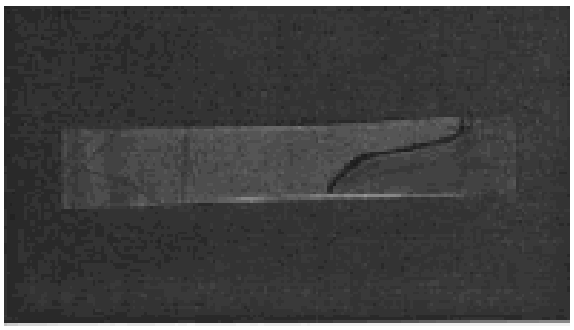

(4) Time: 0.086

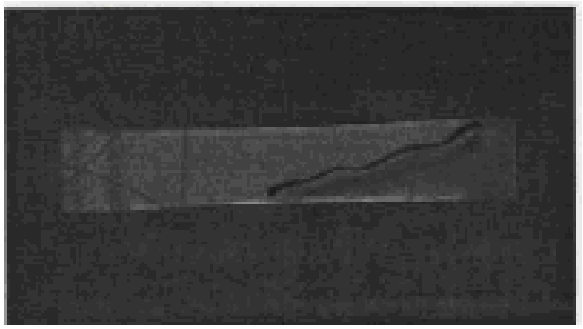

(5) Time: 0.131

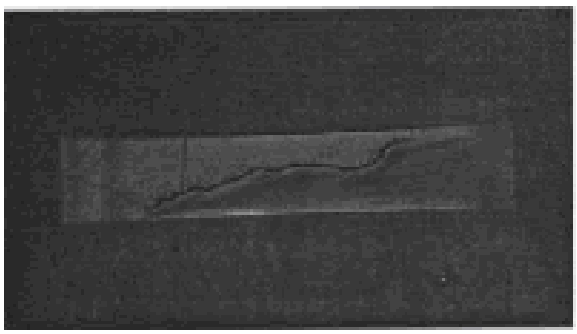

(6) Time: 0.165

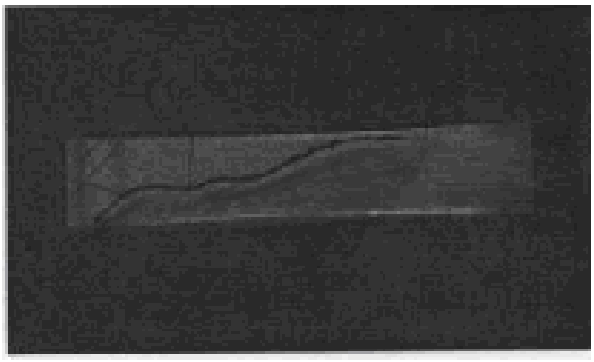

(7) Time: 0.178

Figure 4.7 Frames from real-time X-ray video, strip thickness of 0.75 mm, cast without vibration, A356 alloys, using fillability filling type, mould temperature 660˚C to7 00˚C, pouring temperature 750˚C.

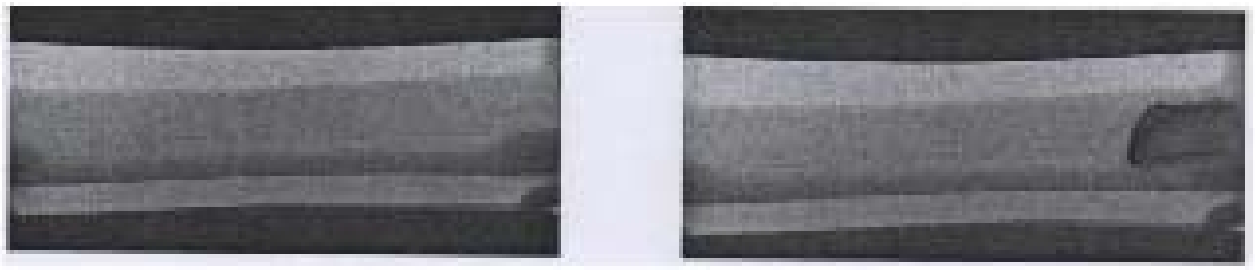

(1) Time: 0.00

(2) Time: 0.034s

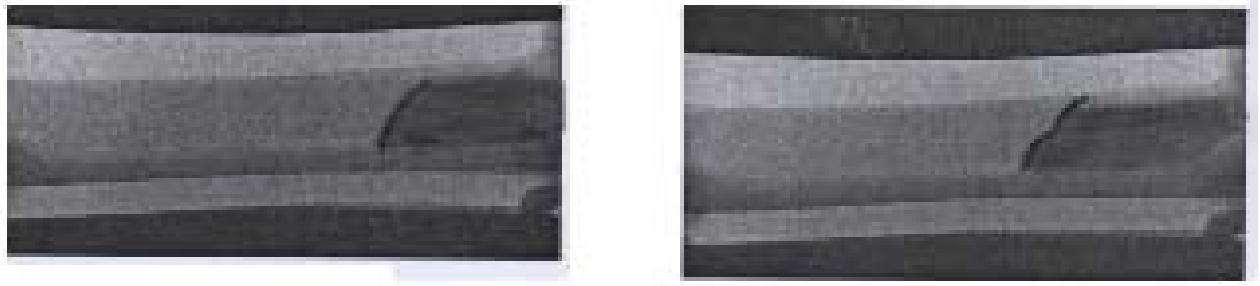

(3) Time: 0.0.084s

(4) Time: 0.132s

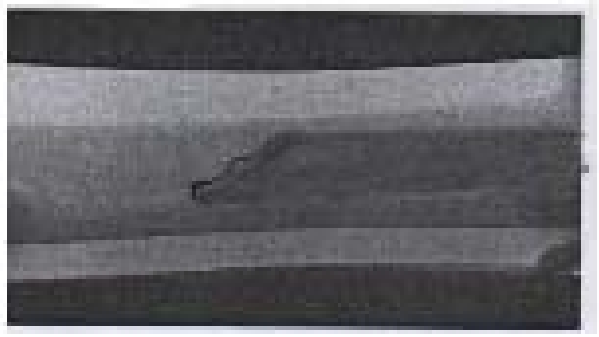

(5) Time: 0.180s

Figure 4.12 Images from (1-5). Metal velocity measurement in flowability filling type, real time X-Ray, test piece thicknesses 0.75mm, mould Temperature 400˚C, pouring Temperature 750˚C

(1) time:

(2) time:

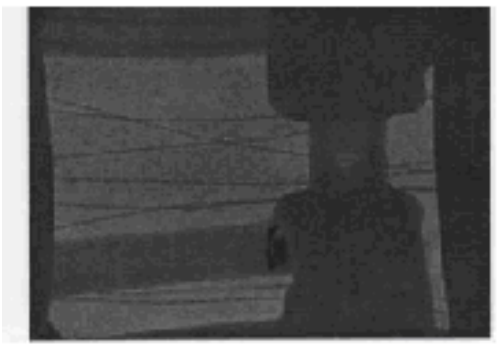

(3) time: 0.00

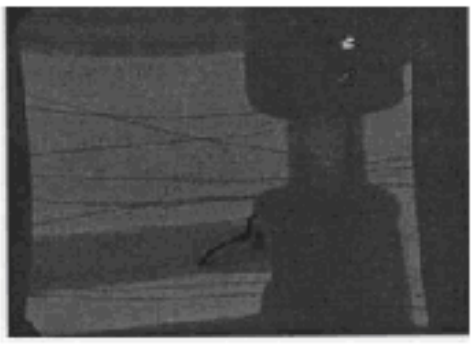

(4) time:0.034

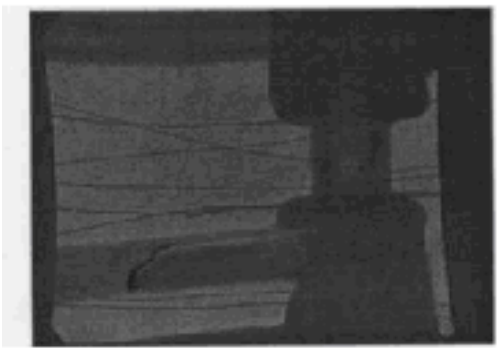

(5) time:0.79

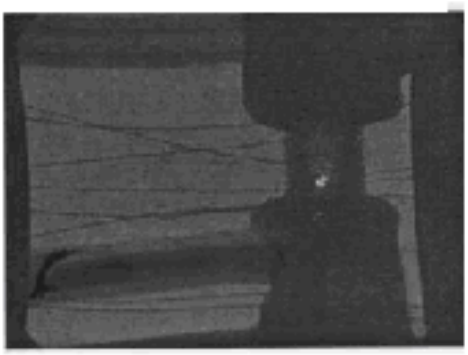

(6) time:0.113

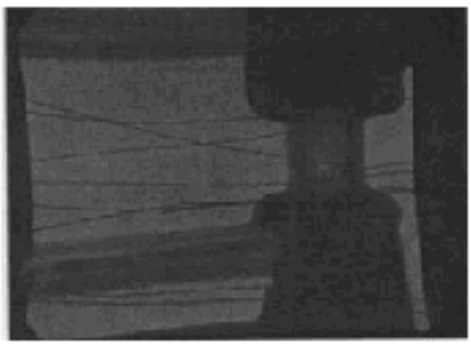

(7) time: 0.149

Figure 4.9 Frames from real-time X-ray video, strip with thickness 2mm, set in horizontals direction, casting without vibration, A356 alloys, using fillability filling type, mould temperature 660ºC to 700ºC, pouring temperature 750ºC.

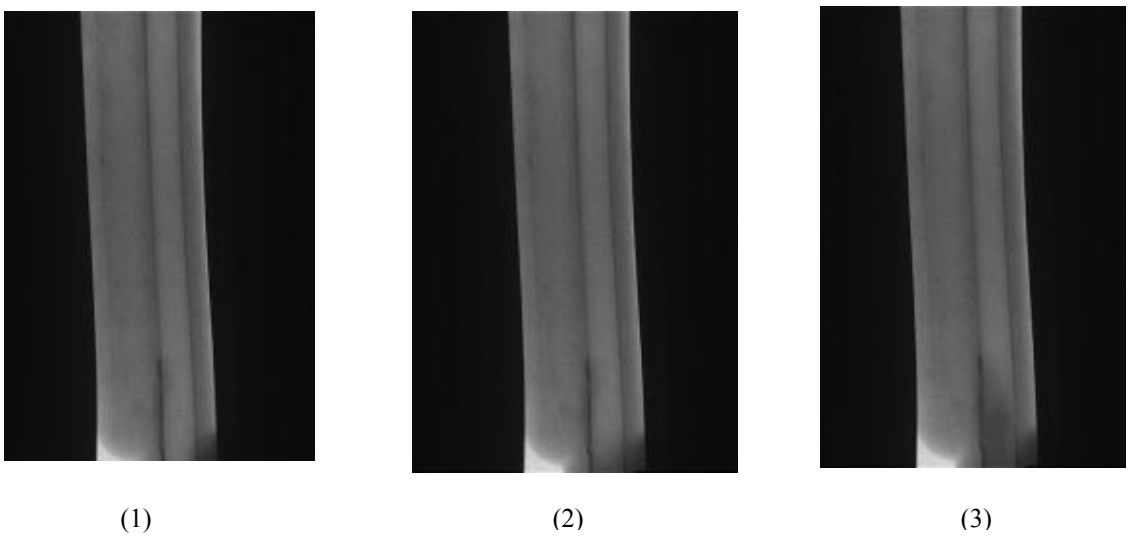

(1) (2) (3)

(4) (5) (6)

(7) (8) (9)

Figure 4.6 Frames from real-time X-ray video, showing the strip with thickness 0.75 mm, set in vertical direction, cast without vibration, A356 alloys, using fillability filling type, mould temperature 660˚C-700˚C, pouring temperature 750˚C.

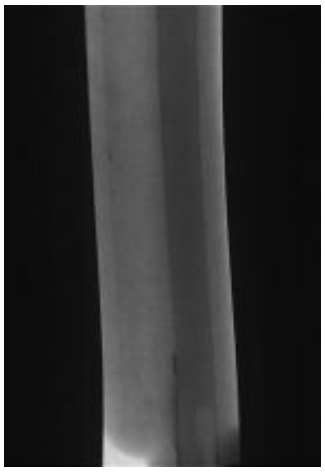

(10)

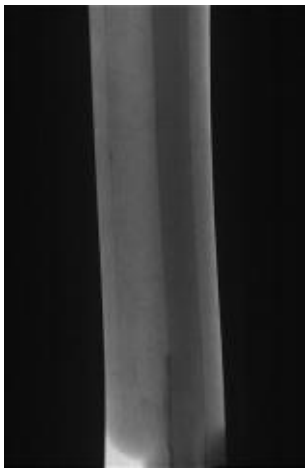

(11)

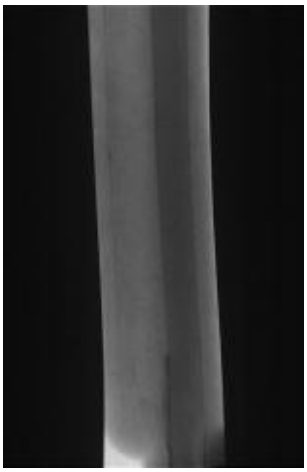

(12)

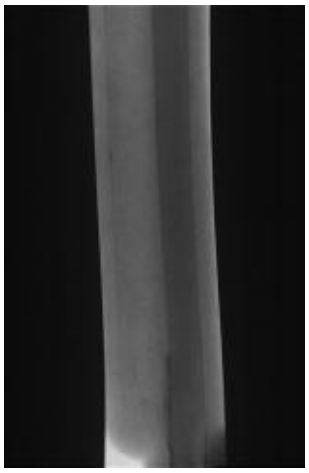

(13)

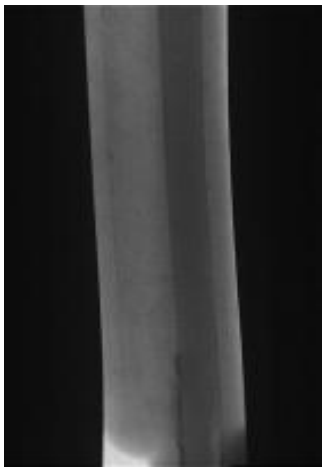

(11)

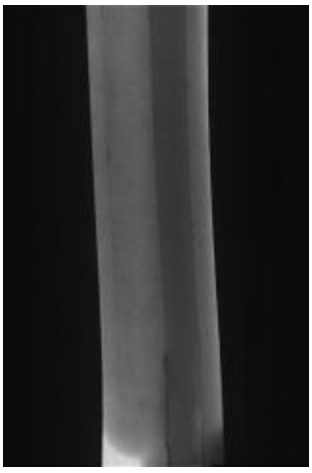

(12)

(11)

(13)

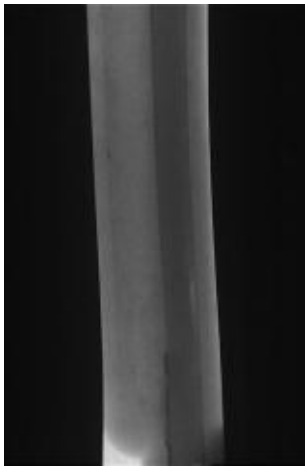

(14)

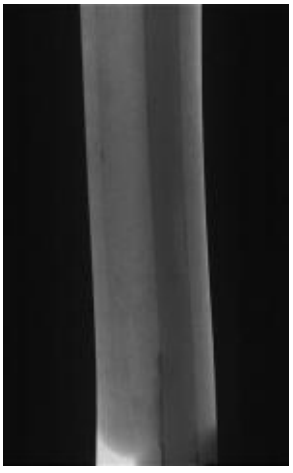

(15)

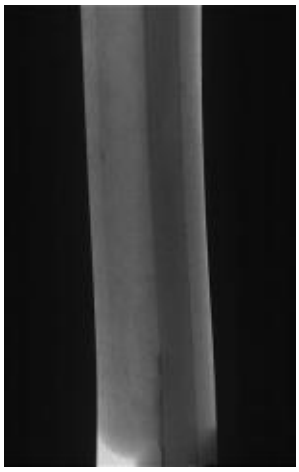

(16)

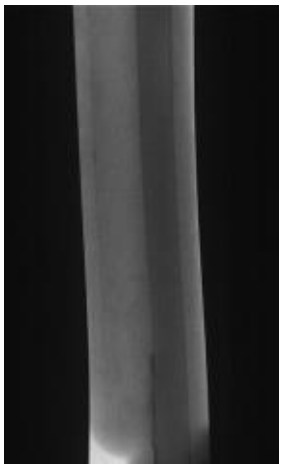

(17)

(18)

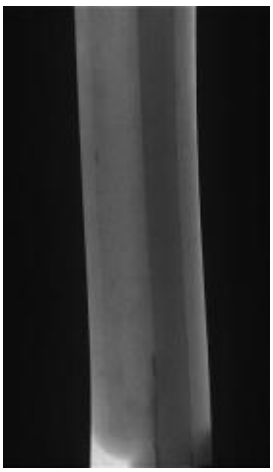

(19)

(20)

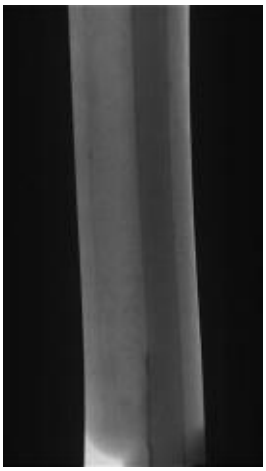

(21)

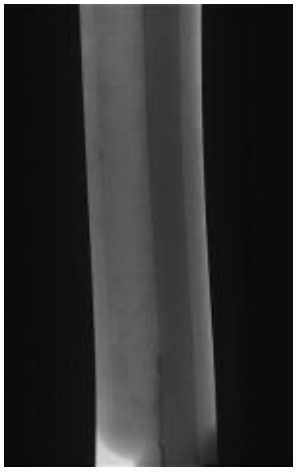

(22)

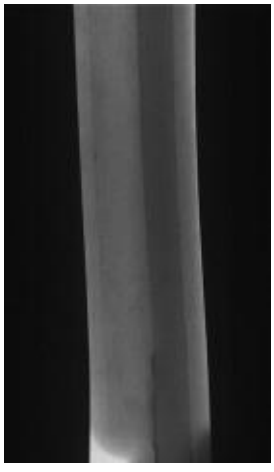

(23)

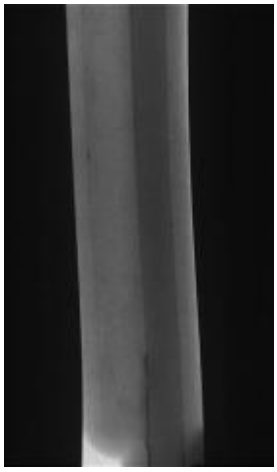

(24)

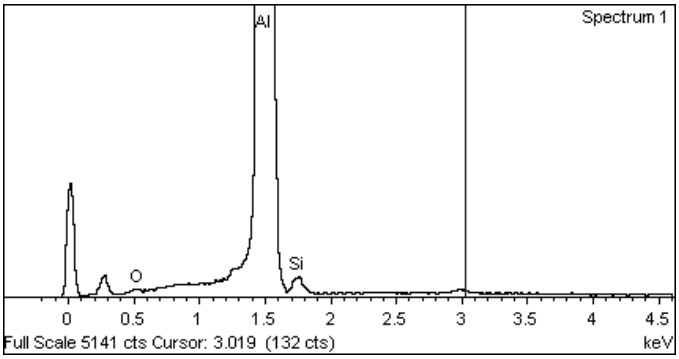

(a)

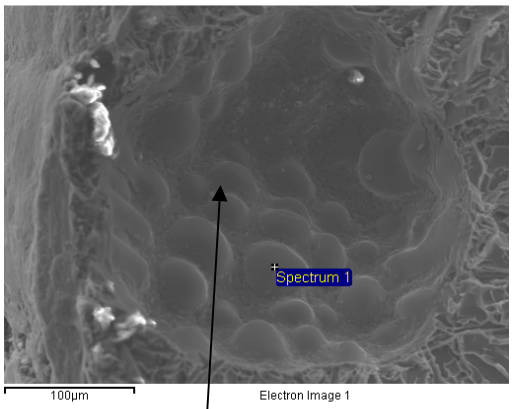

(b)

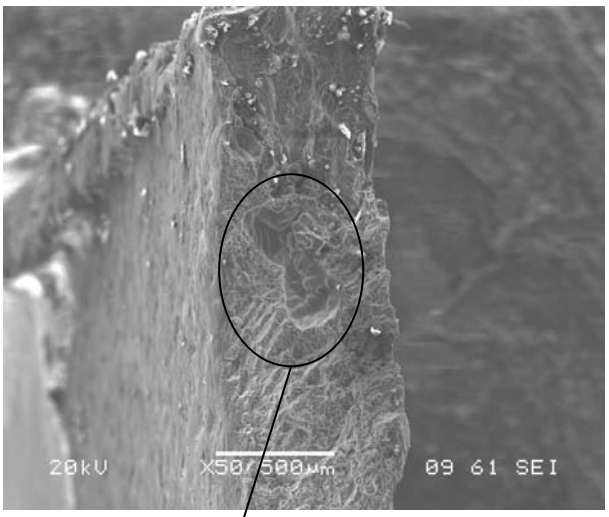

(c)

(d)

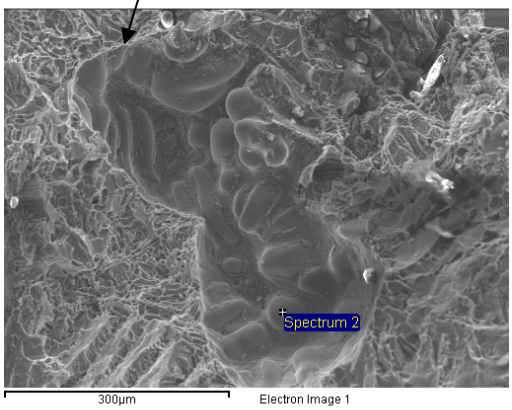

(e)

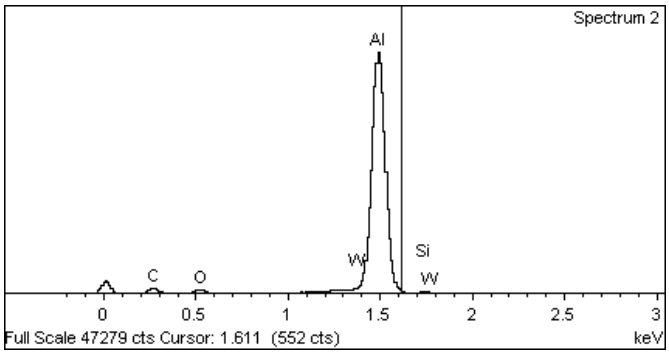

(f)

Figure 4.55 EDX and SEM secondary electron micrographs of fracture surface of the casting without vibration, low tensile strength, containing two large bubble, showing film draped over dendrites and dimples.

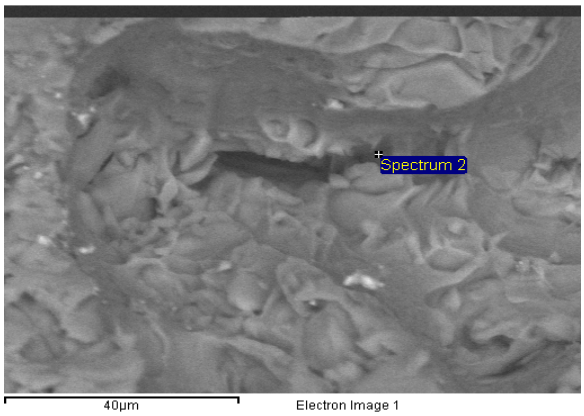

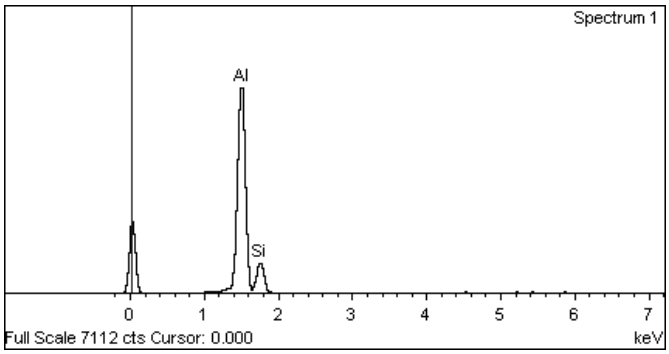

(a)

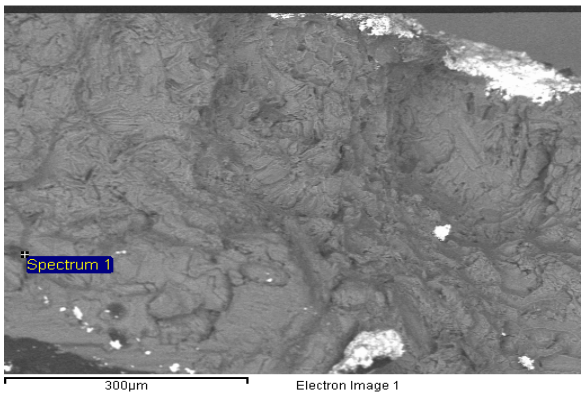

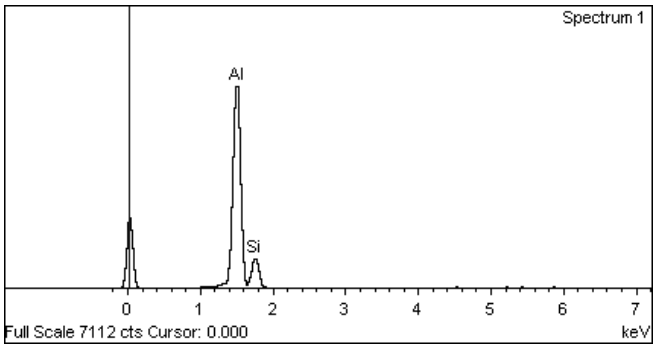

(b)

Figure 4.59 EDX, casting with vibration 1.2g after filling, low tensile strength, fillabillity filling type.

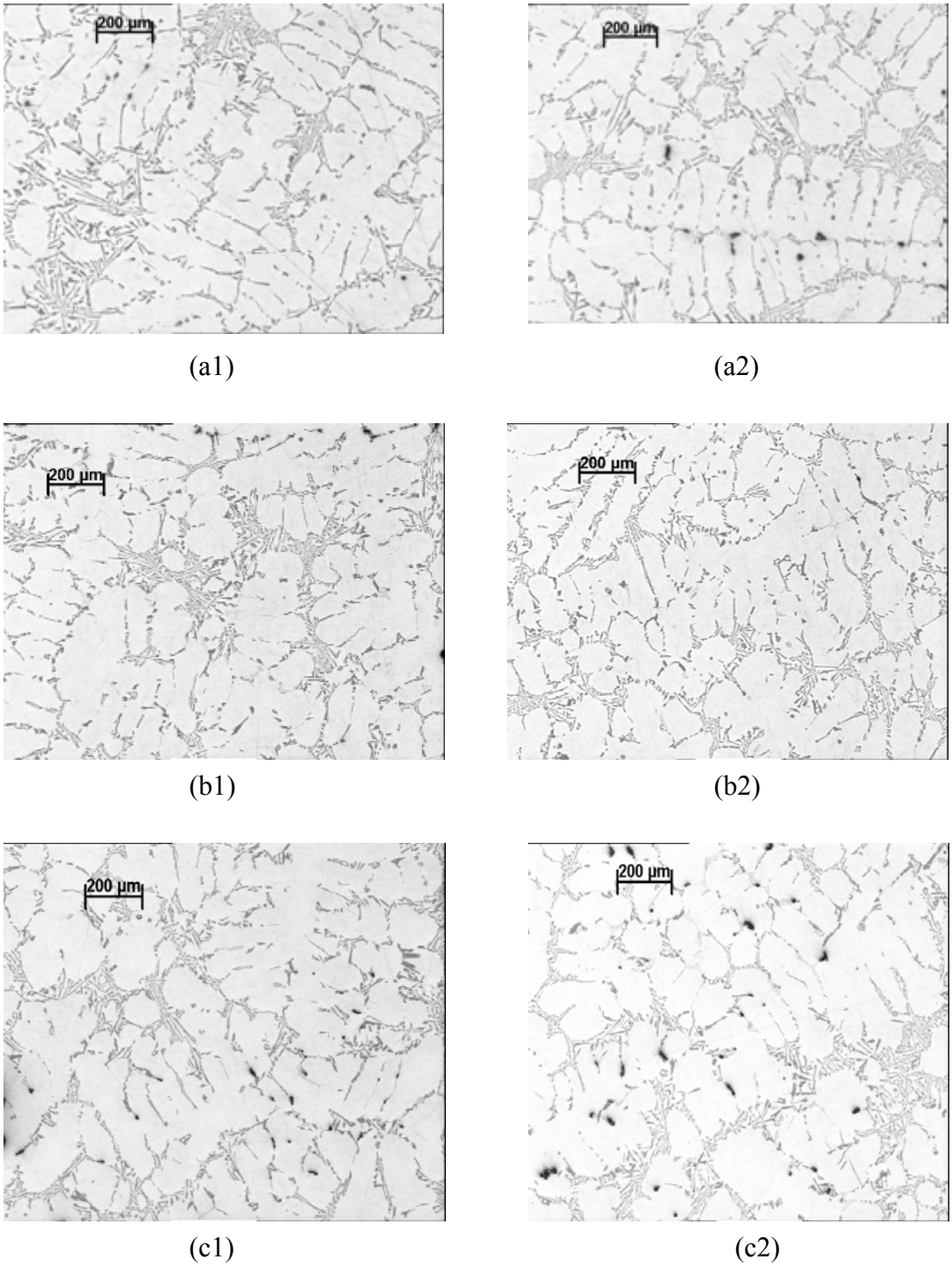

Figure 4.37 Optical micrographs of each method of casting; (a) casting without vibration (b) casting with 0.8g acceleration of vibration after filling (c) casting with 0.8g acceleration of vibration during filling, showing the as-cast microstructure

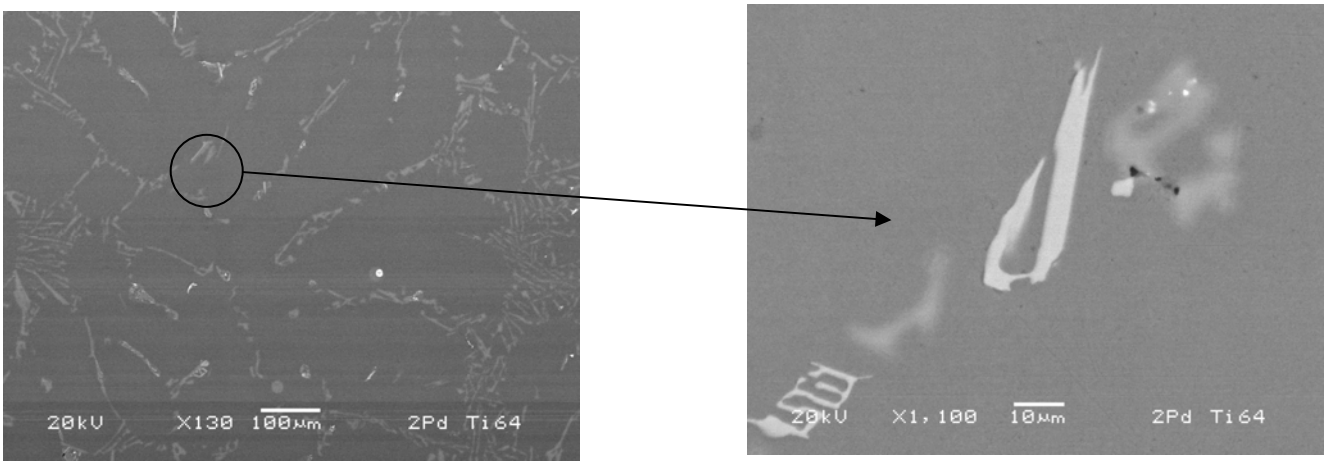

(a1) casting without vibration

(b1) casting without vibration

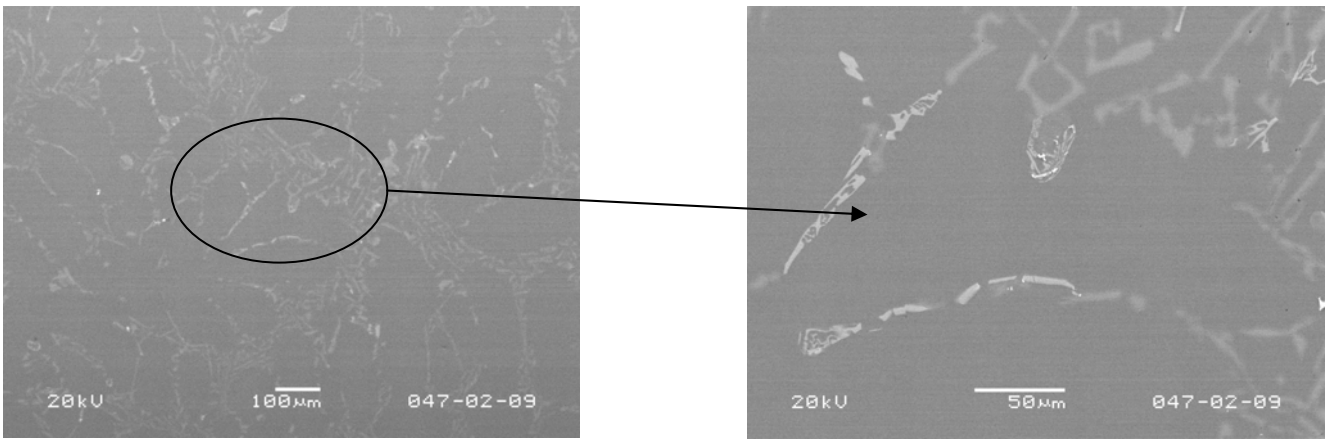

(a2) casting with vibration after filling

(b2) casting with vibration after filling

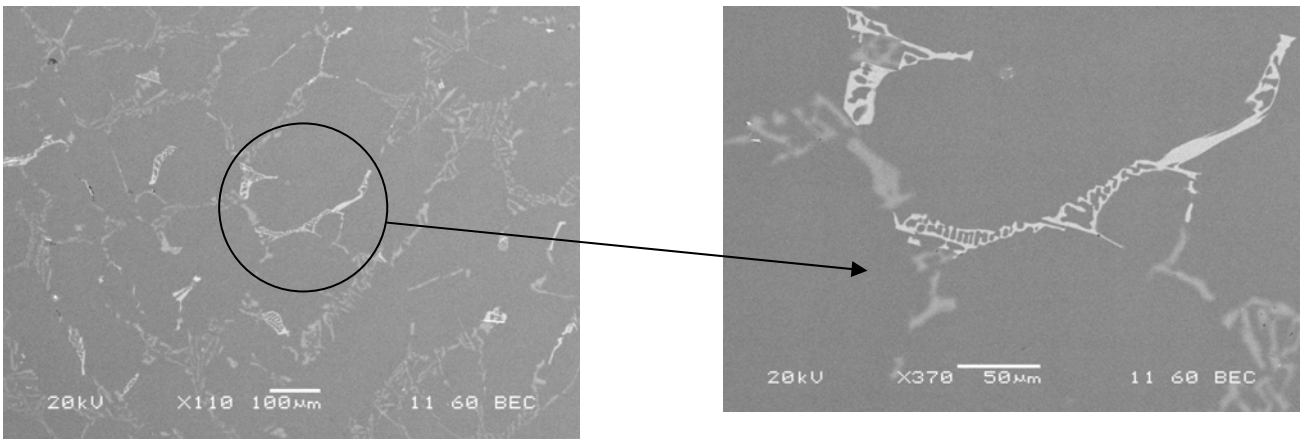

(a3) casting with vibration during filling

(b3) casting with vibration during filling

Figure 4.38 (a) SEM micrographs of the frame chose randomly from each method of casting. (b) the circle area in the lift-hand side were highly magnified and are illustrated on the corresponding right –hand side.

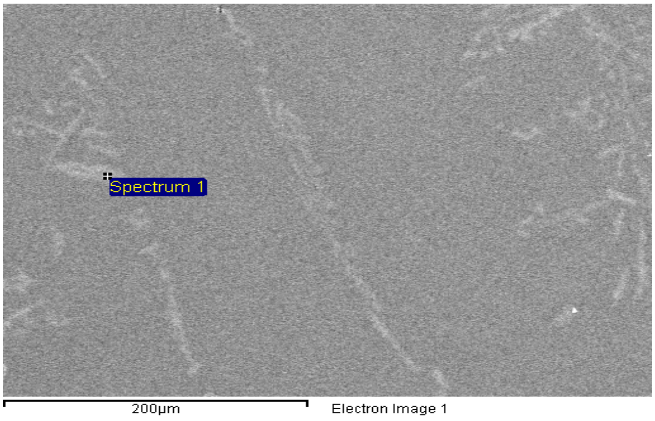

(a1)

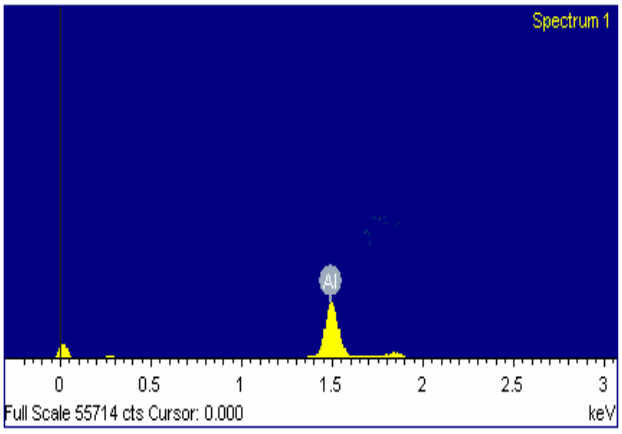

(b1)

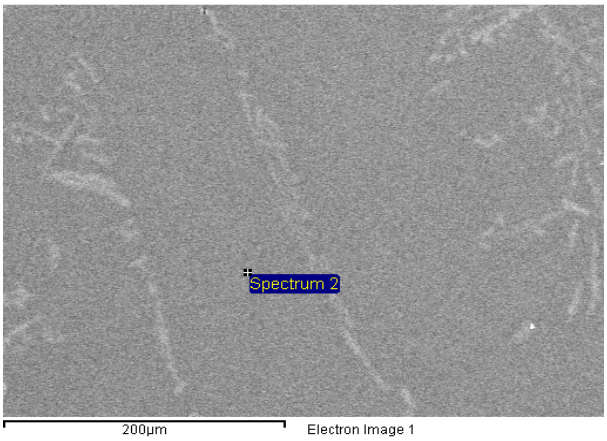

(a2)

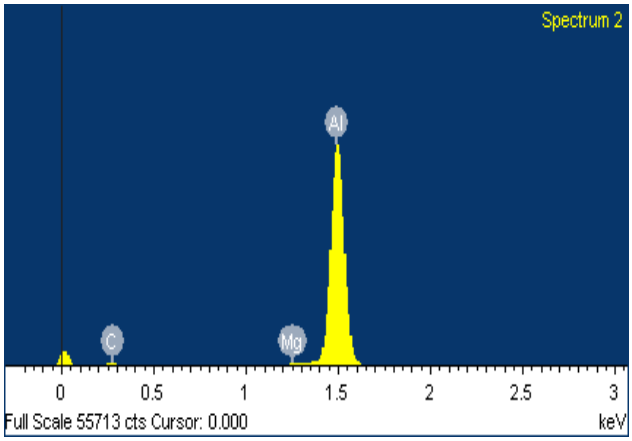

(b2)

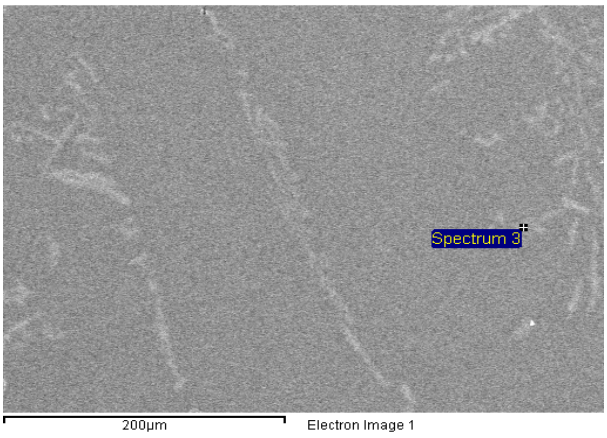

(a3)

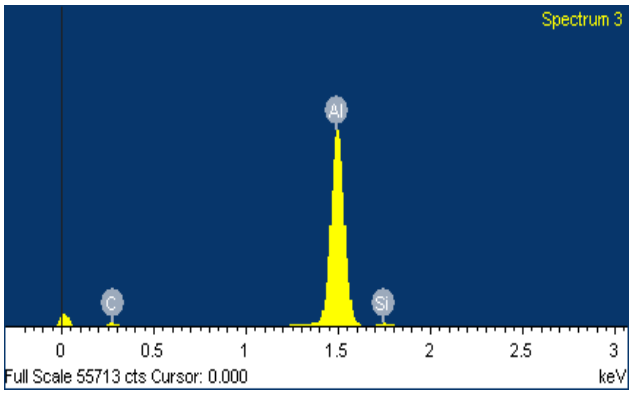

(b3)

Figure 4.39 (a) SEM micrographs of the casting without vibration, fillability filling type, showing the phases of casting, (b) the EDX spectrum of each phase

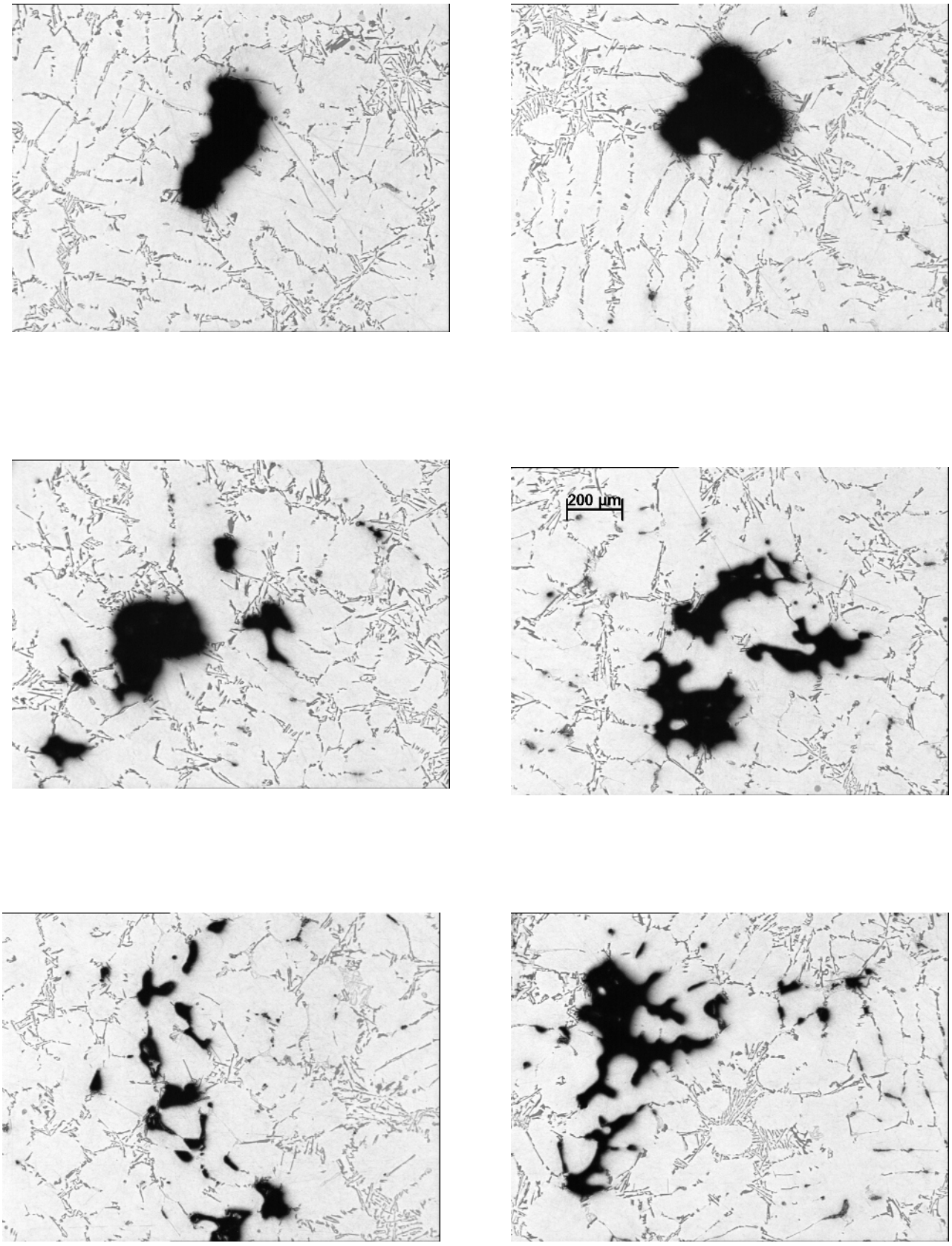

Figure 4.33 Polished surface of an area 10mm × 10 mm from the casting without vibration, showing the microstructure and the defects as collapsed bubble, gas pores and shrinkage pores

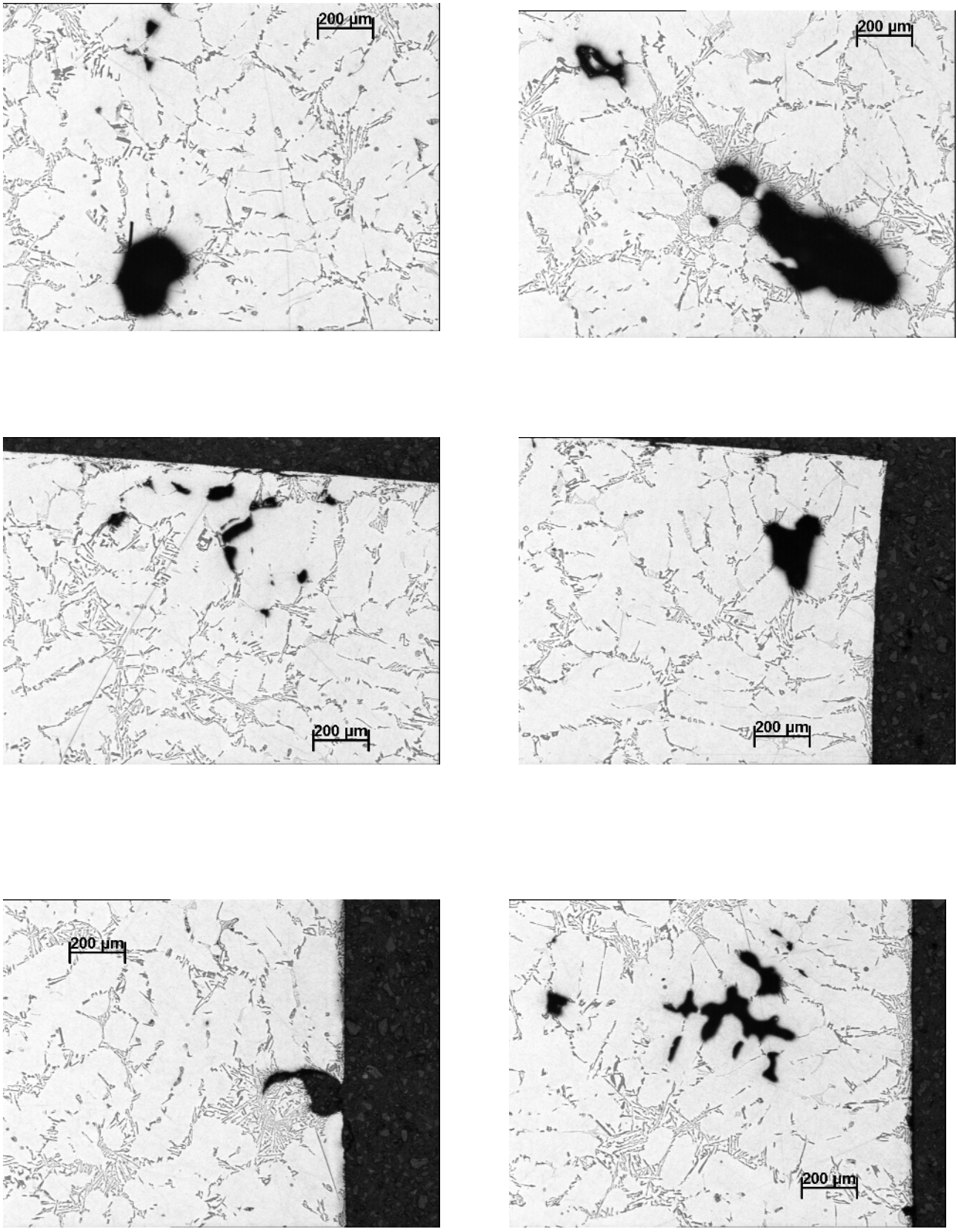

Figure 4.34 Polished surface of an area 10mm × 10 mm from the casting with 0.8g acceleration of vibration after filling process, showing the microstructure and the defects as collapsed bubble, gas pores and shrinkage pores.

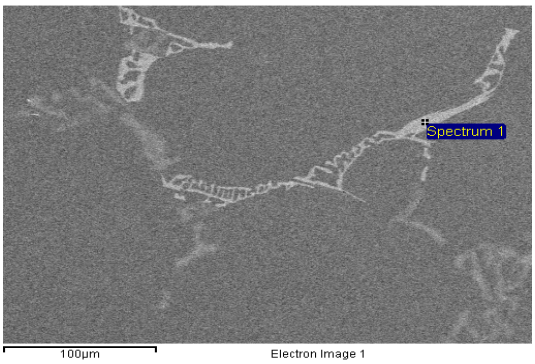

(a1)

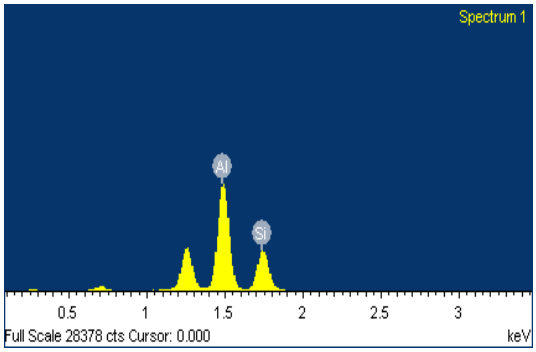

(b1)

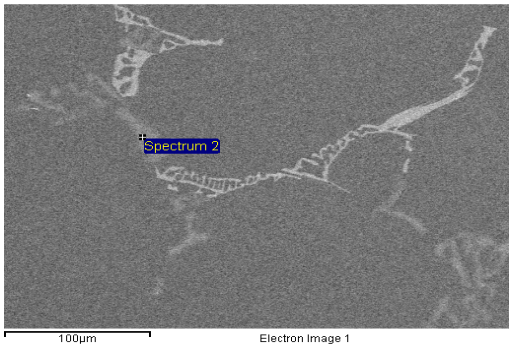

(a2)

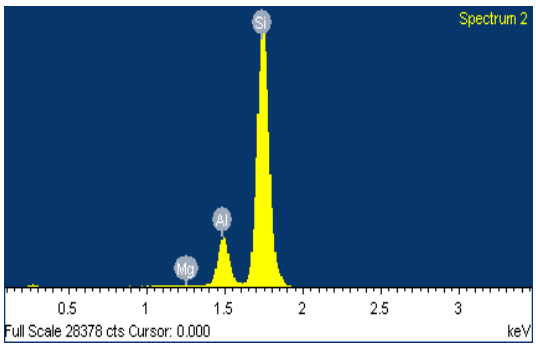

(b2)

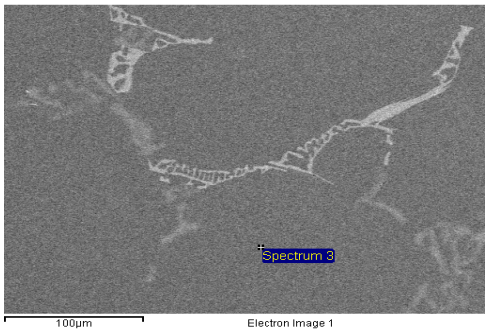

(a3)

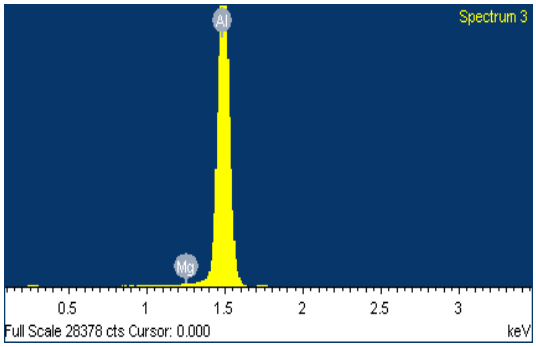

(b3)

Figure 4.42 (a) SEM micrographs of the casting with 0.8g acceleration of vibration during filling process, flillability filling type, showing the phases of casting, (b) EDX spectrum for each phase

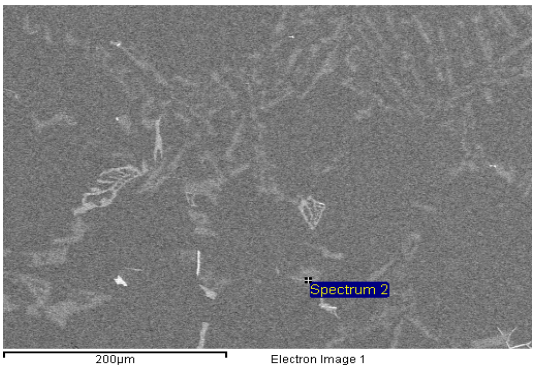

(a1)

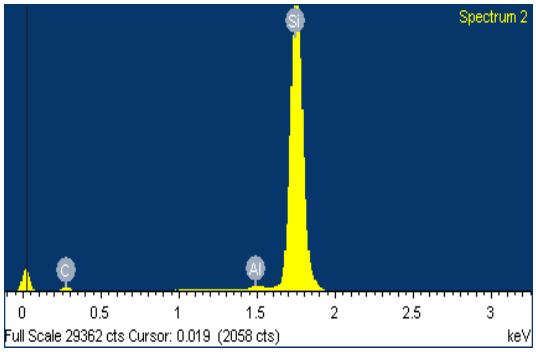

(b1)

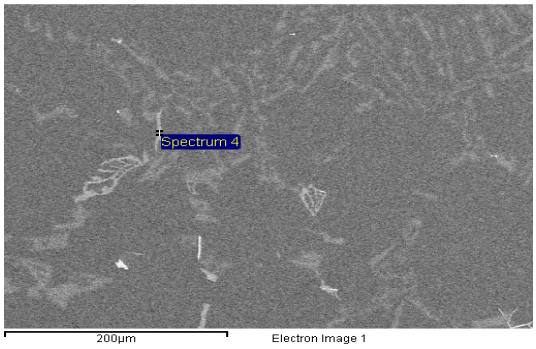

(a2)

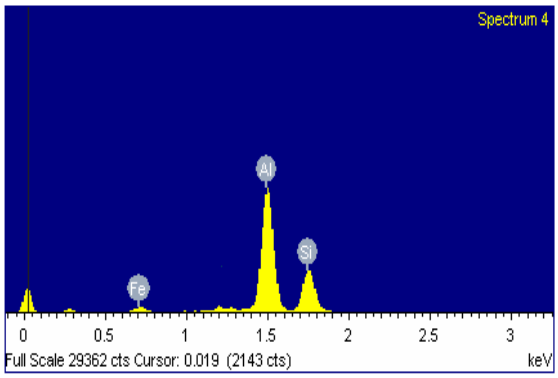

(b2)

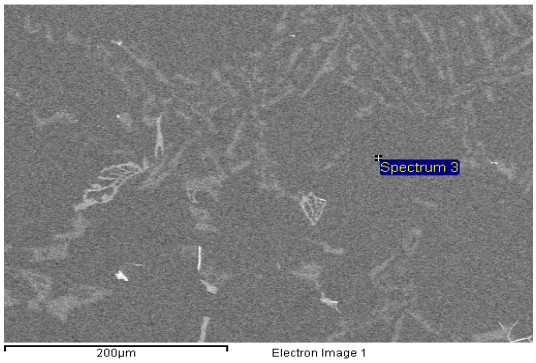

(a3)

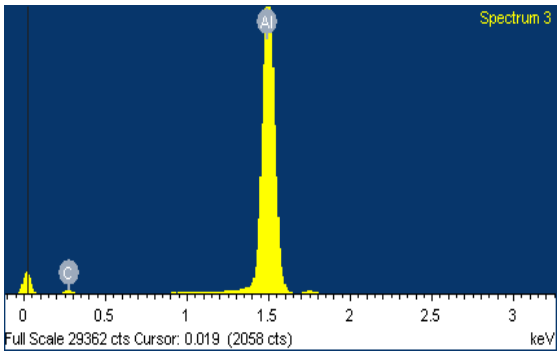

(a3)

Figure 4.40(a) ESM micrographs of the casting with 0.8g acceleration of vibration after filling process, fillability filling type, showing the phases of casting, (b) the EDS spectrum for each phase

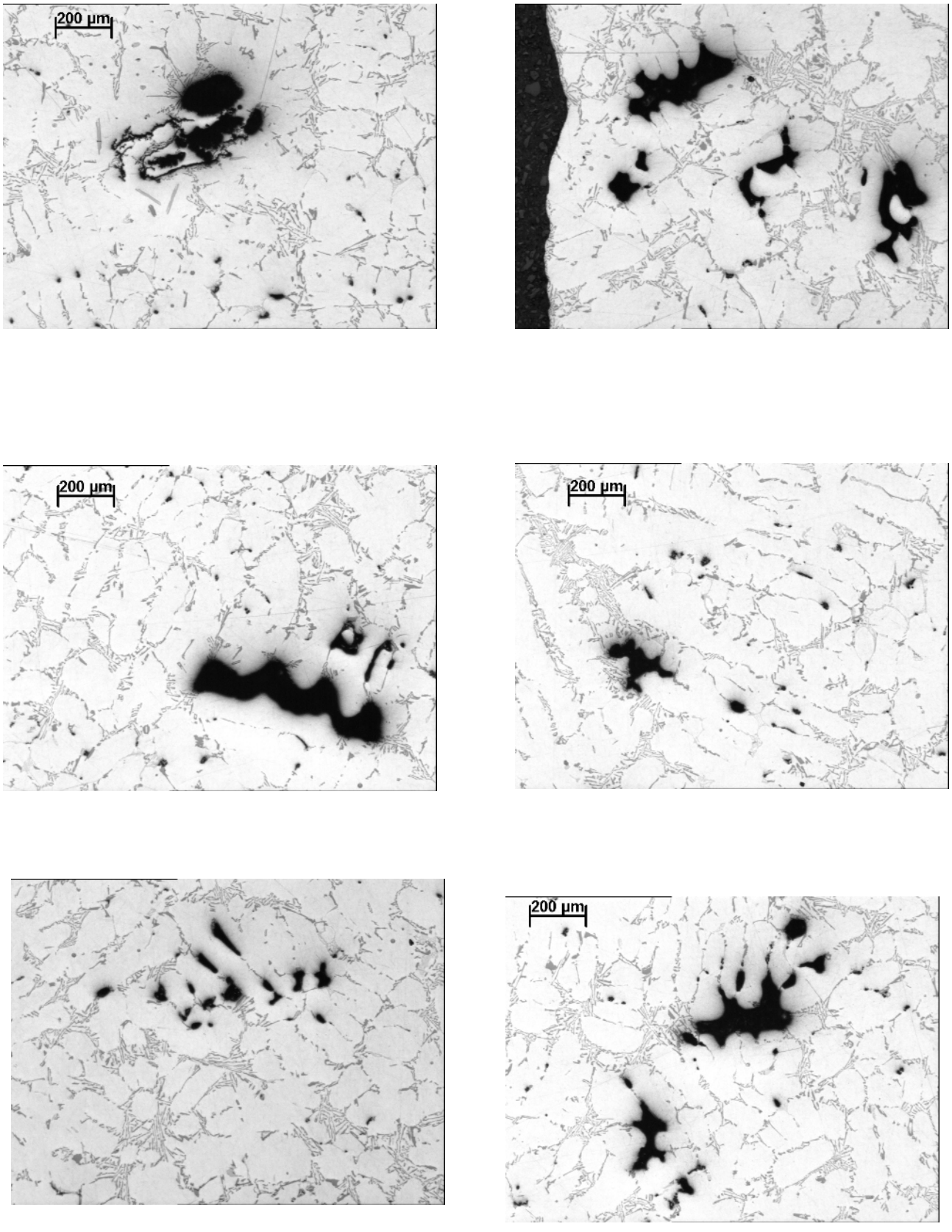

Figure 4.35 polished surface of an area 10mm × 10 mm from the casting with 0.8g acceleration of vibration during filling process, showing the microstructure and the defects as collapsed bubble, gas pores and shrinkage pores

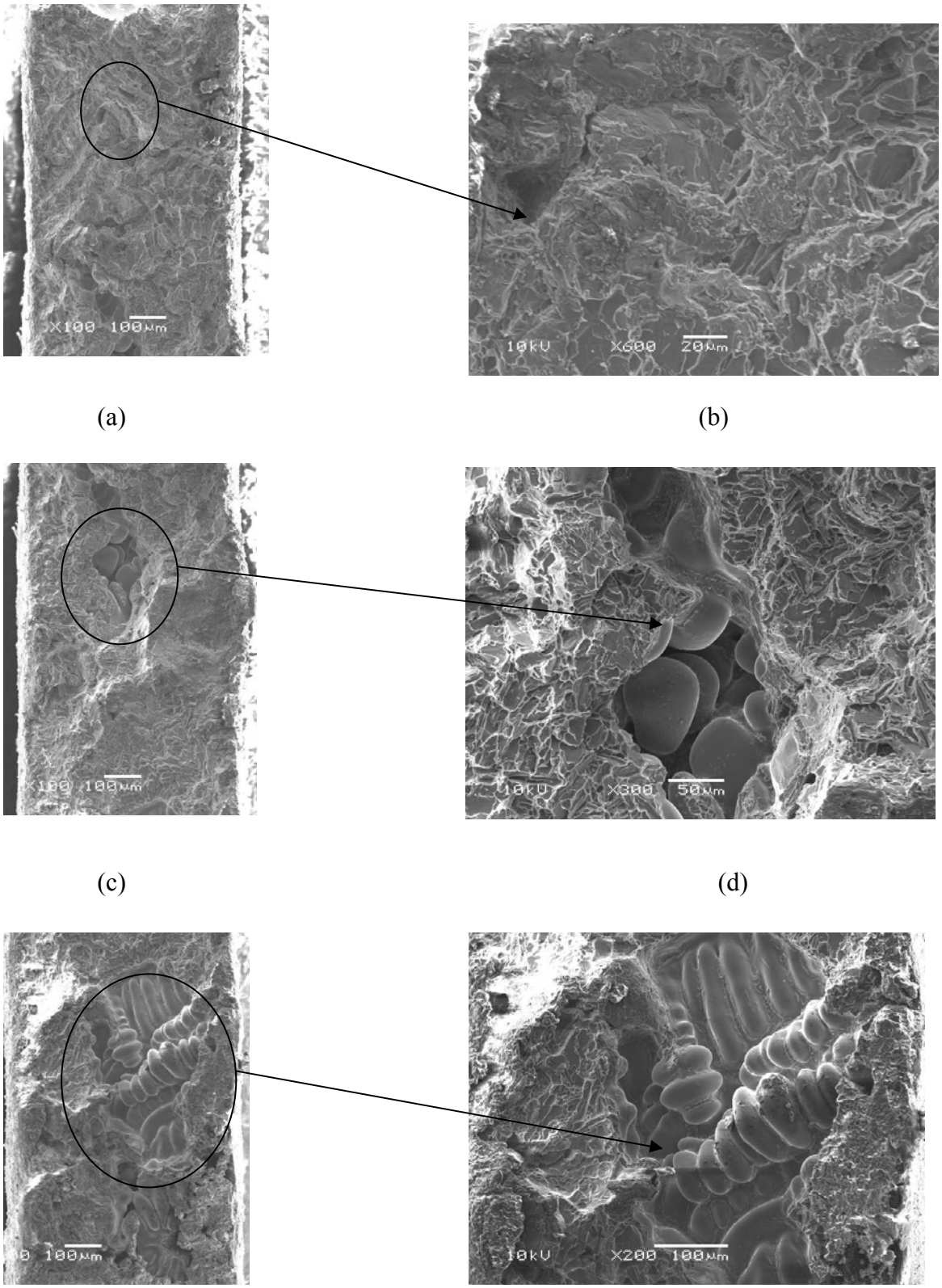

Figure 4.60 SEM secondary electron micrographs of fracture surface of the casting without vibration, high tensile strength, containing shrinkage porosity in the middle of the casting, showing film draped over dendrites and dimples.

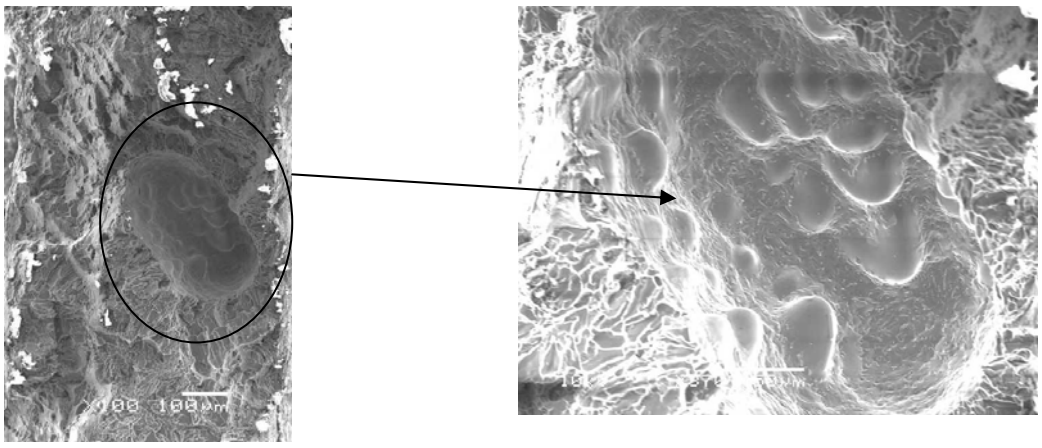

(a) (b)

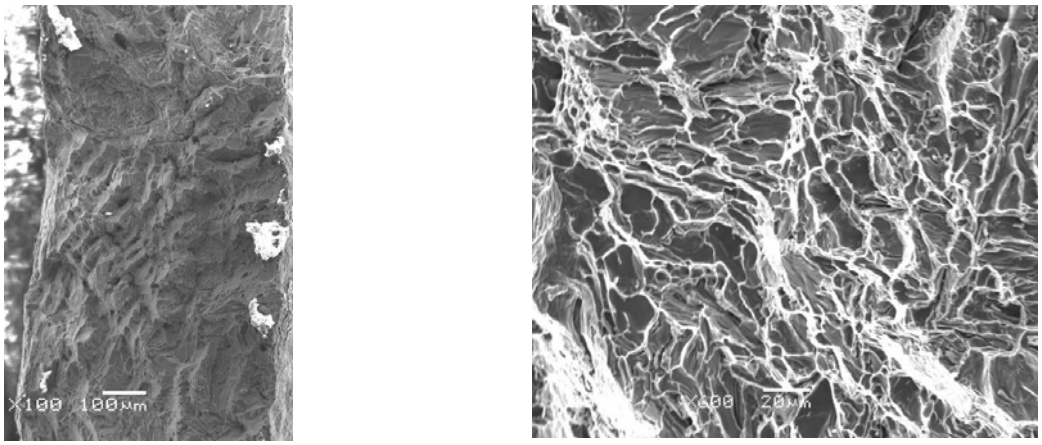

(c) (d)

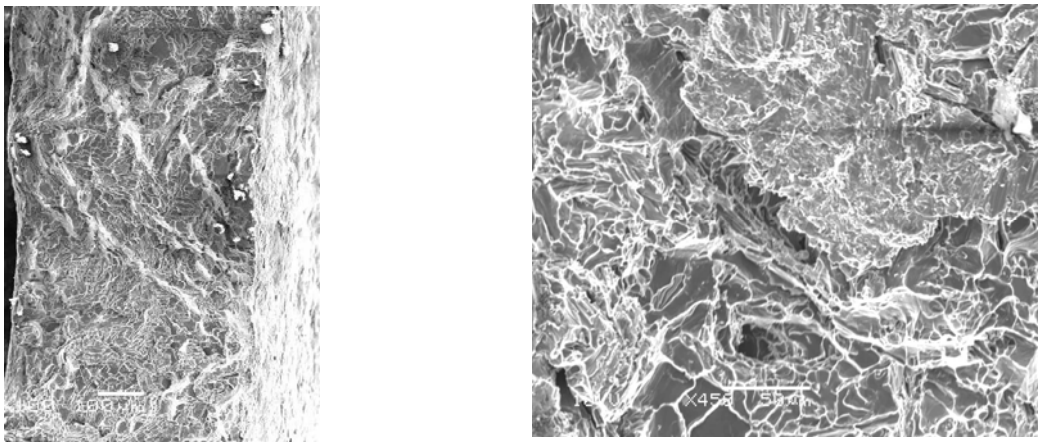

(e) (f)

Figure 4.62 SEM secondary electron micrographs of fracture surface of the casting with 1.2g acceleration of vibration after filling, high tensile strength, containing gas porosity on the edge of the casting, showing film covering the dendrites

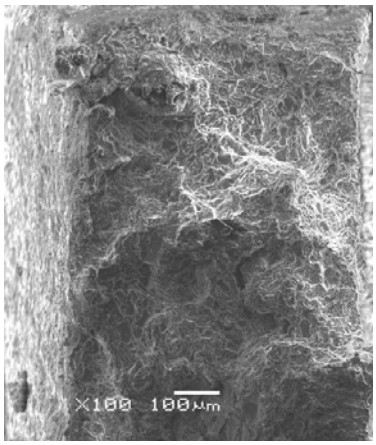

(a)

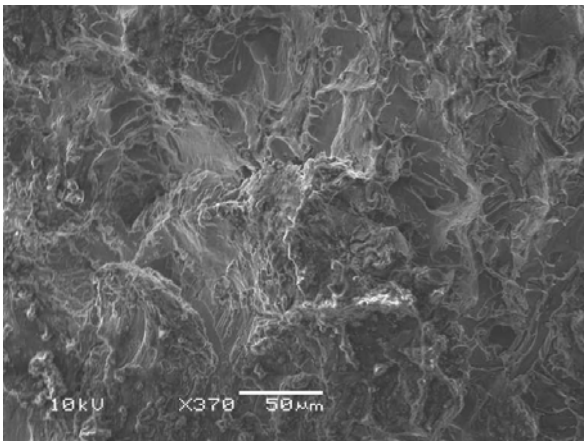

(b)

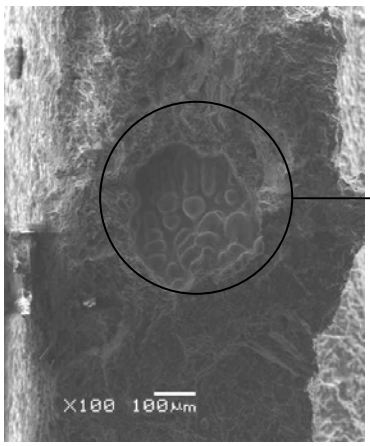

(c)

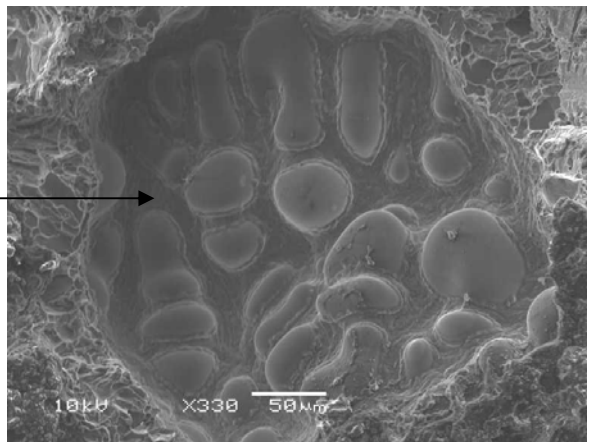

(b)

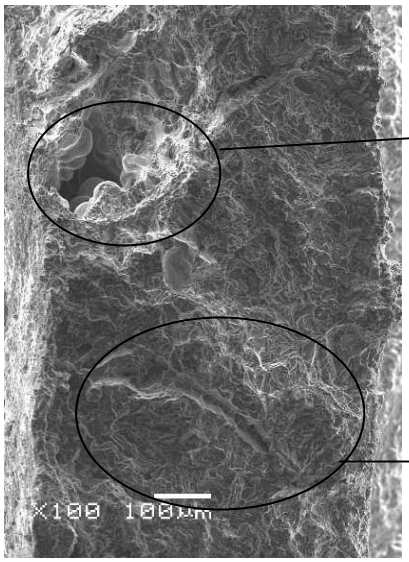

(e)

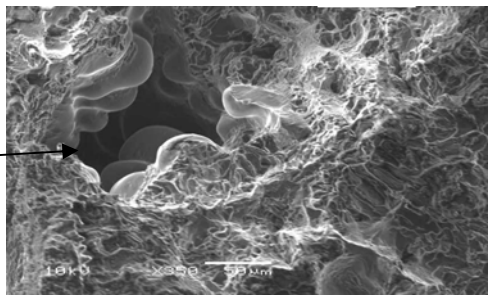

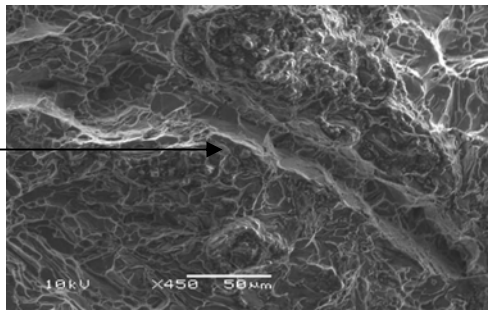

Figure 4.61 SEM secondary electron micrographs of fracture surface of the casting with 0.8g acceleration of vibration after filling, high tensile strength, containing gas porosity and shrinkage porosity the large one on the middle of the casting, showing film covering the dendrites and dimples

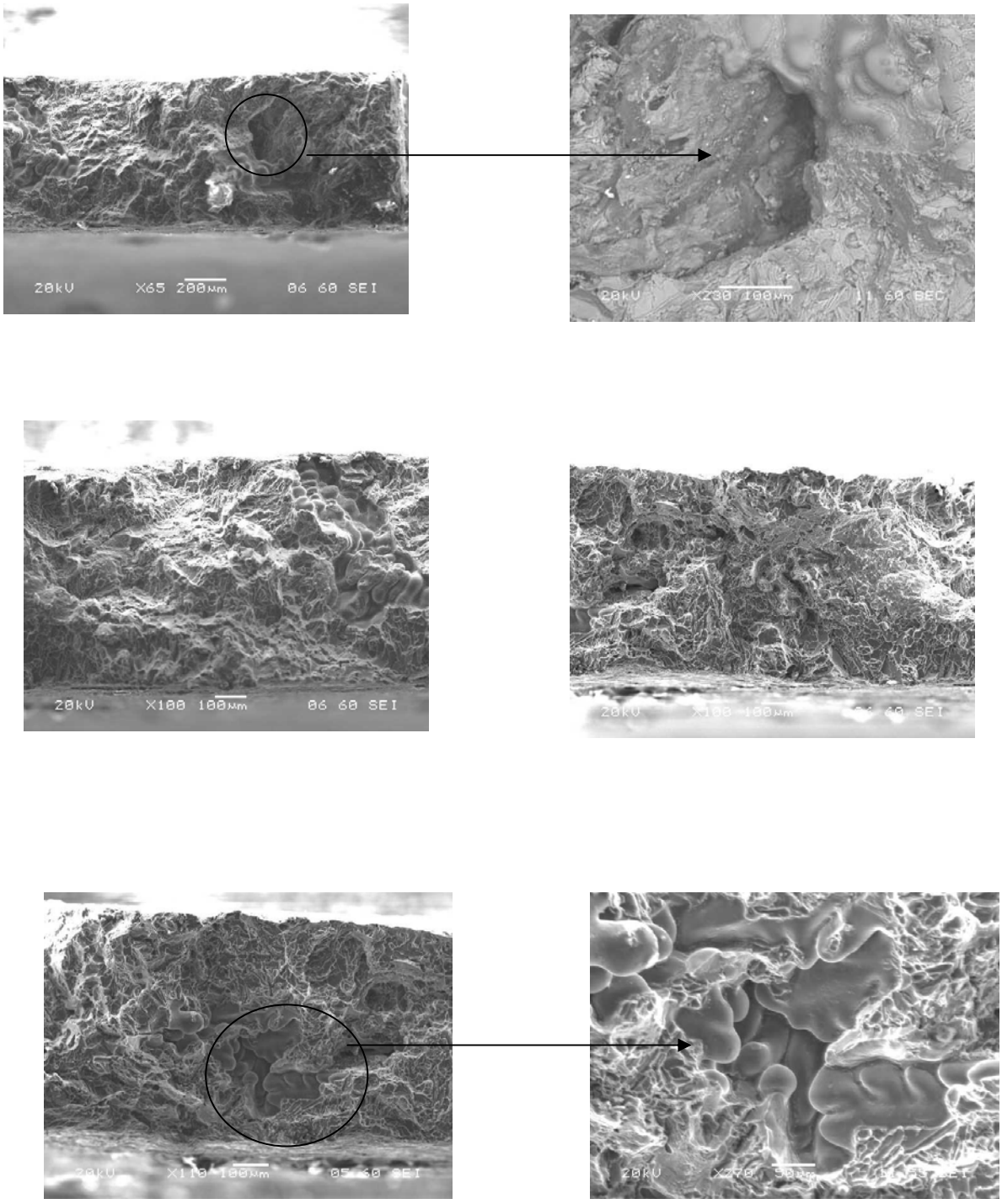

Figure 4.56 ESM secondary electron micrographs of fracture surface of the casting with 0.8g acceleration of vibration after filling, low tensile strength, containing gas porosity and shrinkage porosity the large one on the middle of the casting, showing film covering the dendrites and dimples

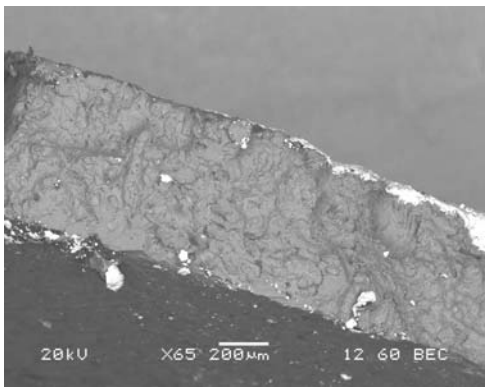

(a)

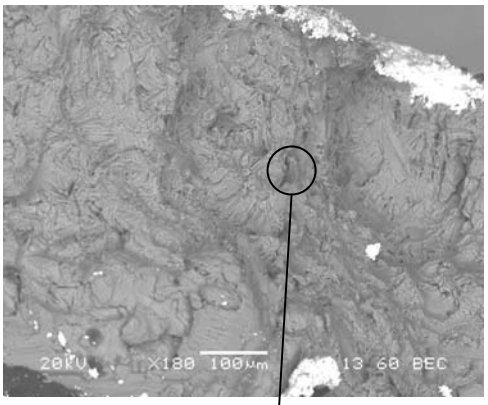

(b)

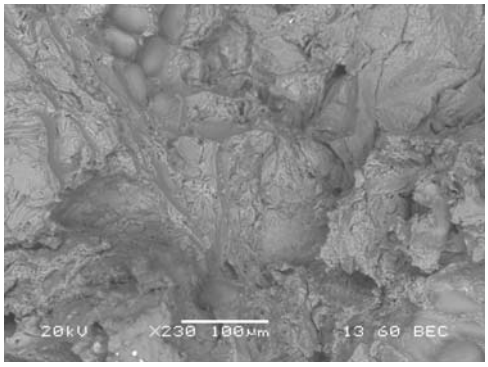

(c)

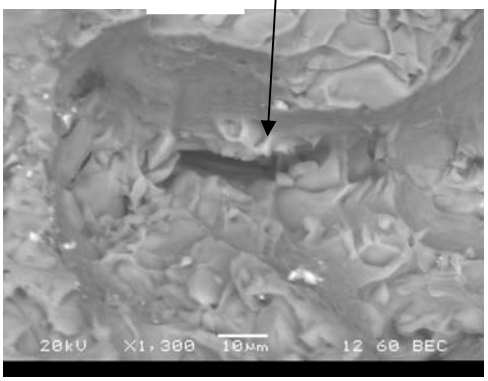

(d)

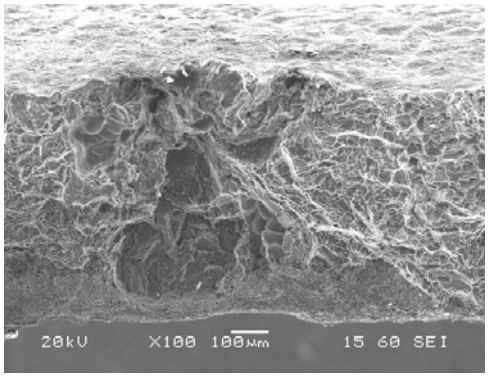

(e)

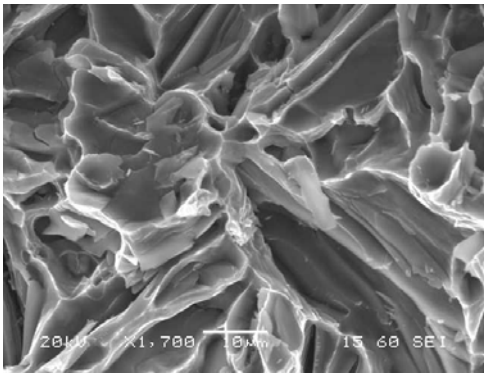

(f)

Figure 4.58 SEM secondary electron micrographs of fracture surface of the casting with 1.2g acceleration of vibration after filling, low tensile strength, showing dimples and discontinuities fracture surface

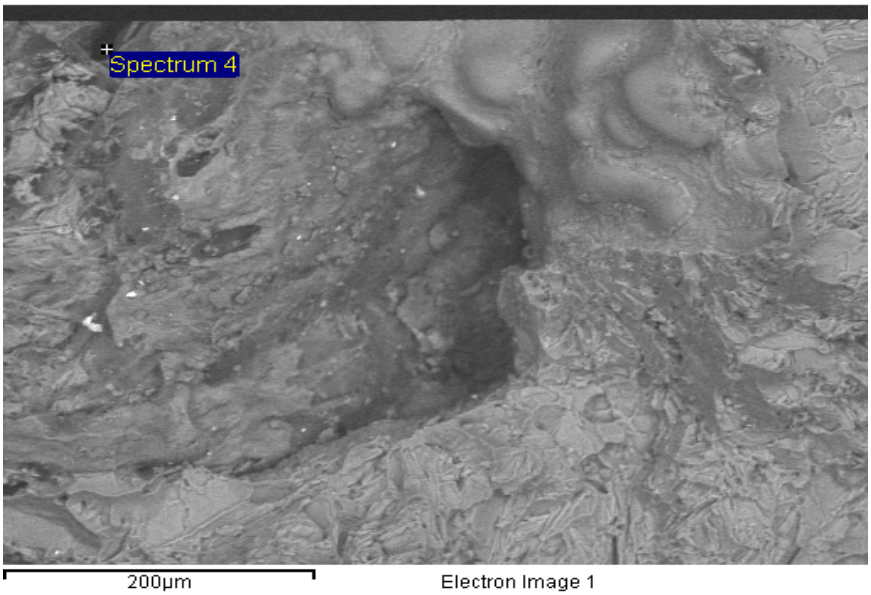

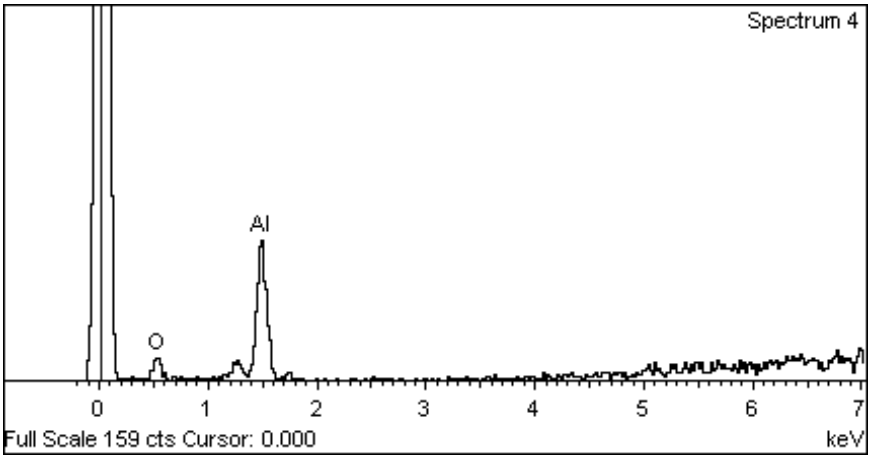

Figure 4.57 EDX, casting with vibration 0.8g after filling, low tensile strength, fillabillity filling type.

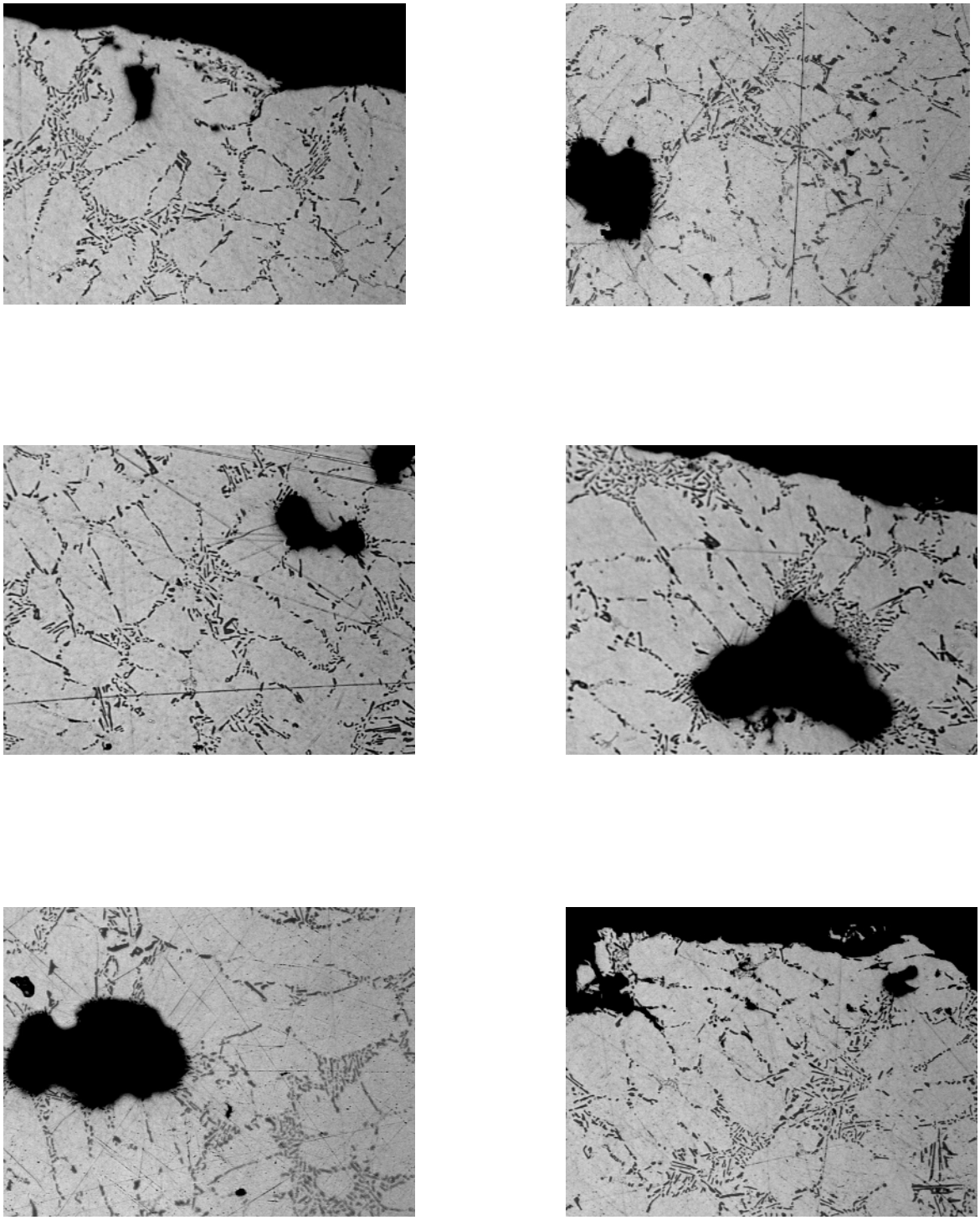

Figure 4.41 Polished surface of an area 10mm × 10 mm from the casting with 1.2g acceleration of vibration after filling process, showing the microstructure and the defects as collapsed bubble, gas pores and shrinkage pores.

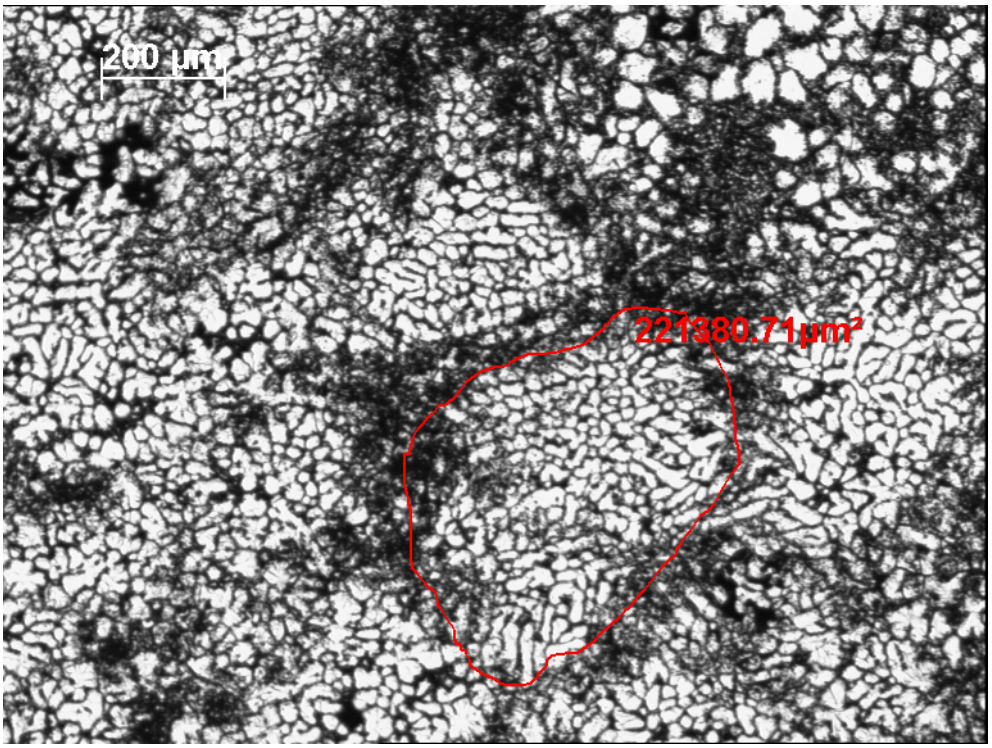

(a)

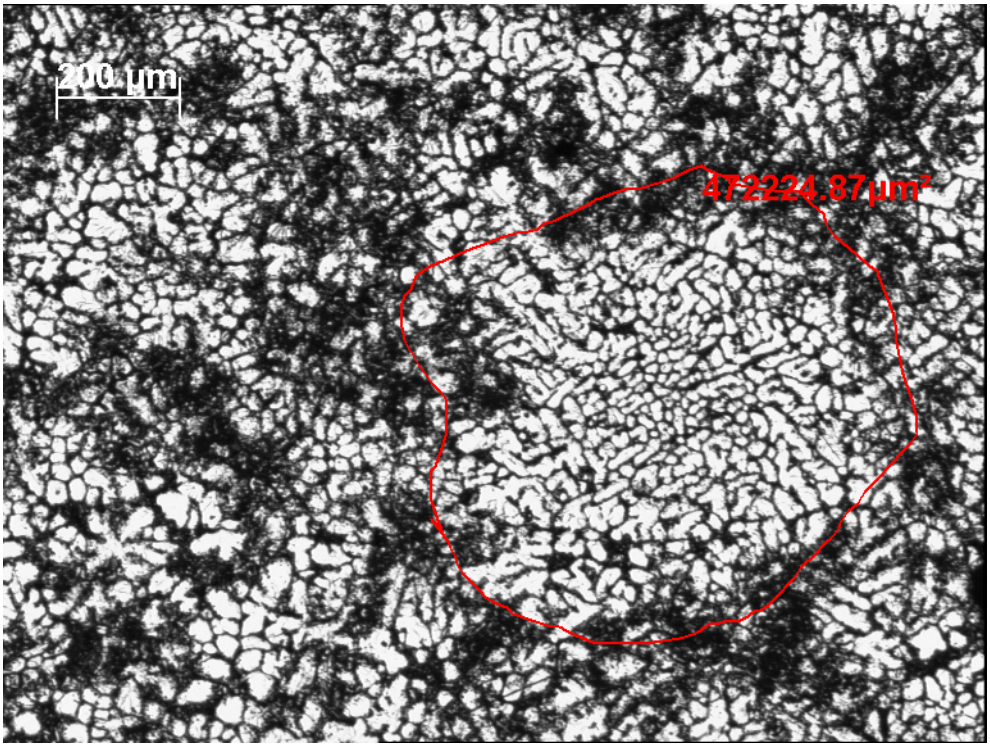

(b)

Figure 5.30 typical mid-thickness strip microstructure (a) casting filled with 0.8g acceleration (b) casting filled without vibration (pouring temperature 750ºC; mould temperature 420ºC; metal head 170mm)

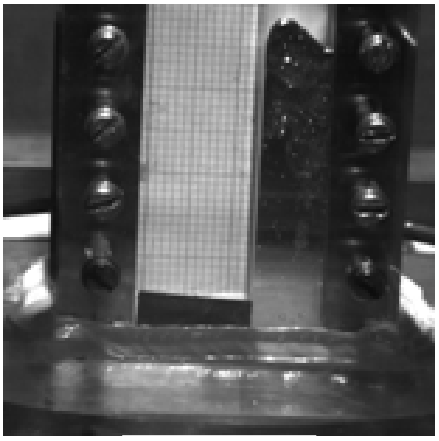

Time = 0s

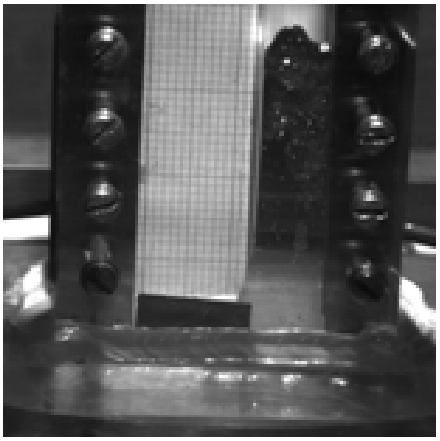

Time = 0.022s

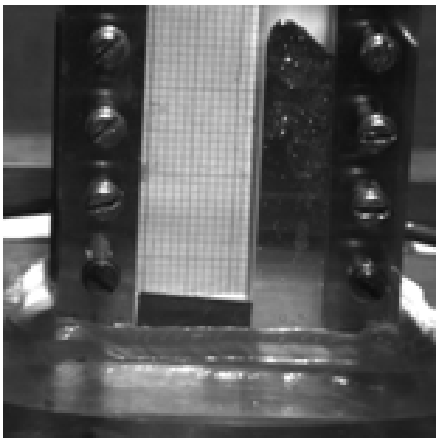

Time = 0.045s

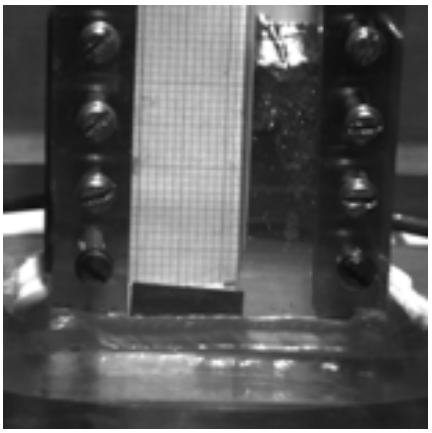

Time = 0.1086s

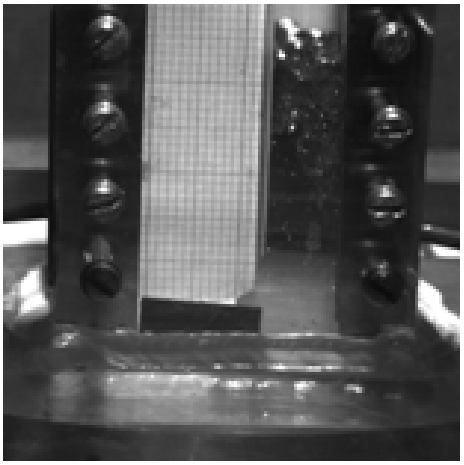

Time = 0.16s

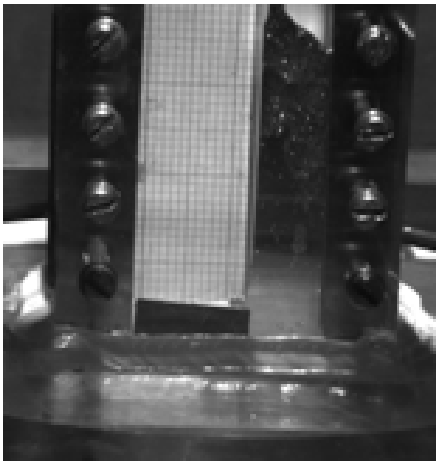

Time = 0.21s

Figure 4.29 Frames of a speed camera show the mould filling sequence with mercury. The Plexiglas mould vibrated with 0.9g acceleration

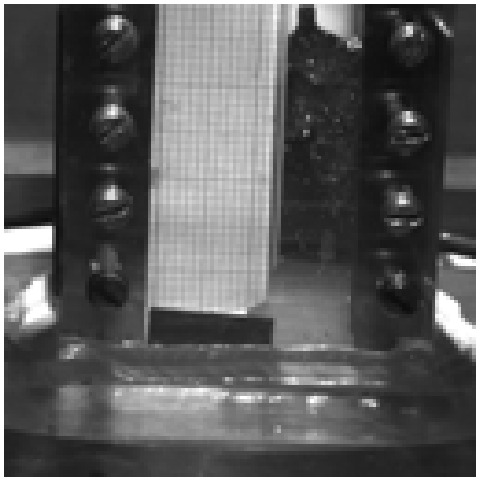

Time = 0.228s

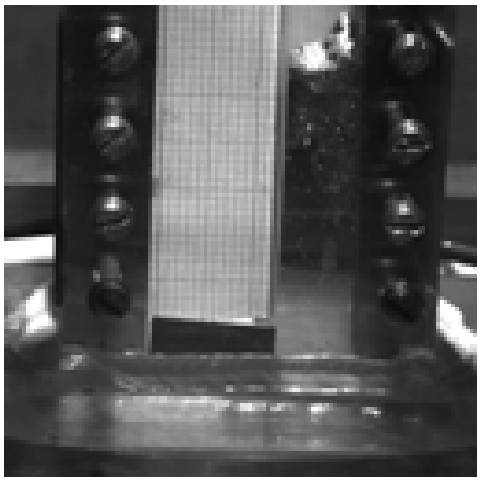

Time = 0.290s

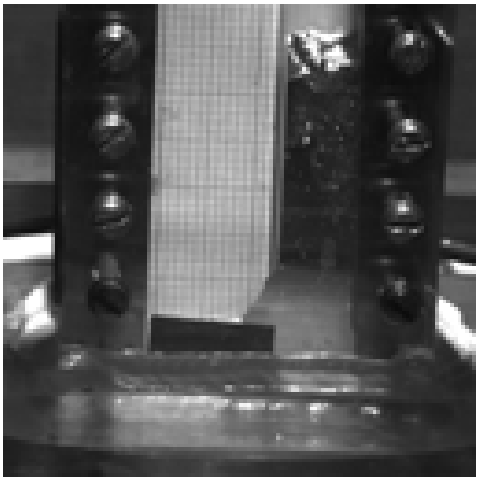

Time = 0.320s

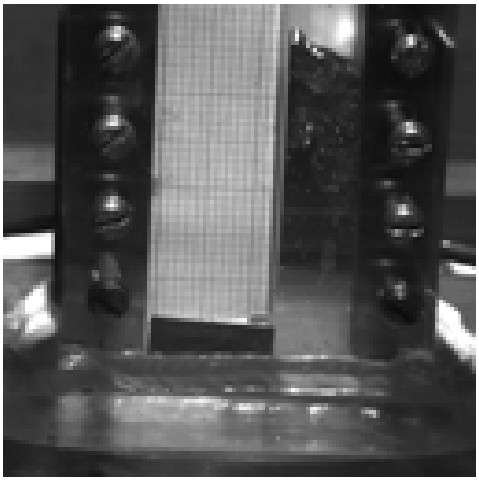

Time = 0.431s

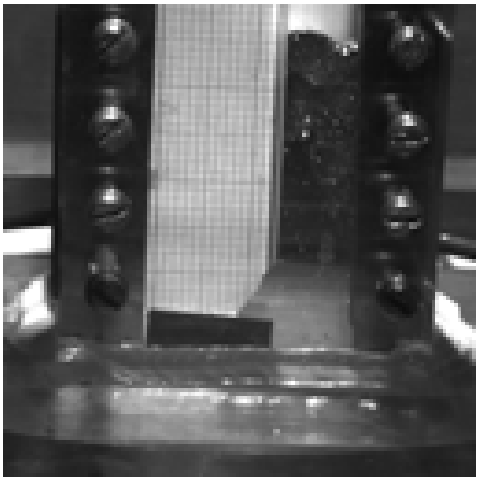

Time = 0.478s

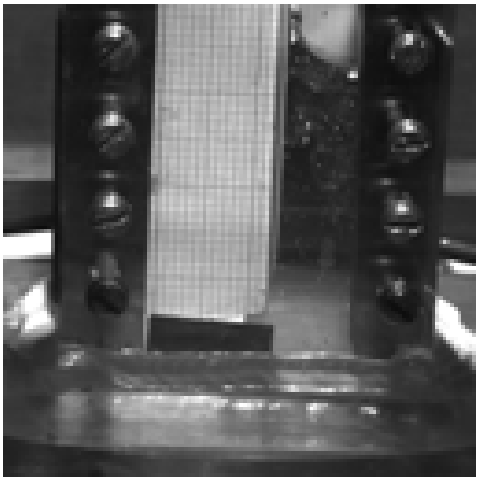

Time = 0.540s

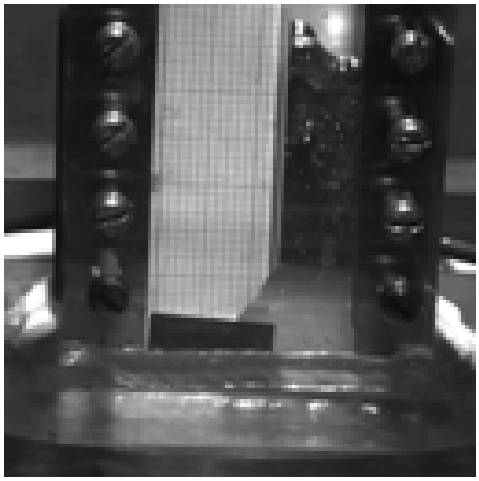

Time = 0.566s

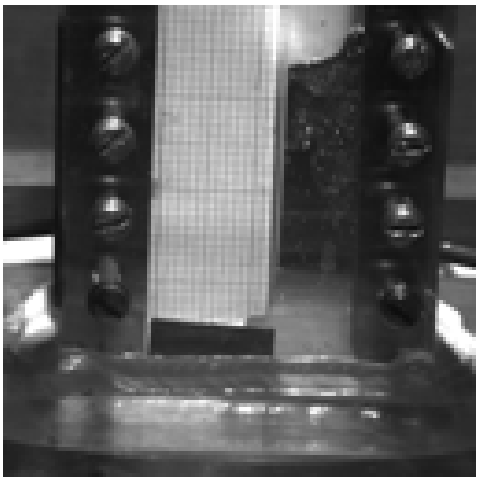

Time = 0.602s

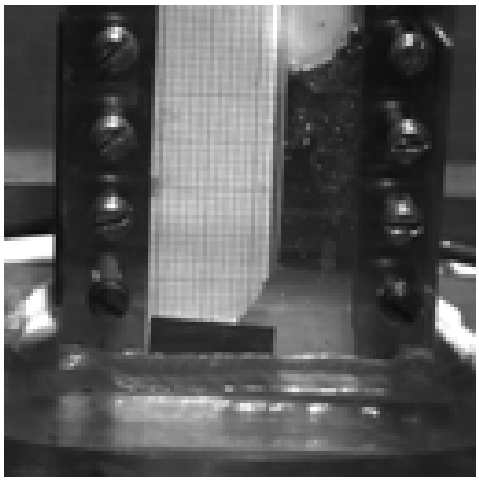

Time = 0.642s

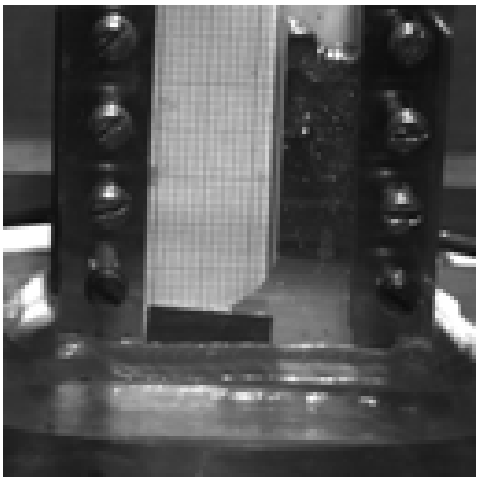

Time = 0.652s

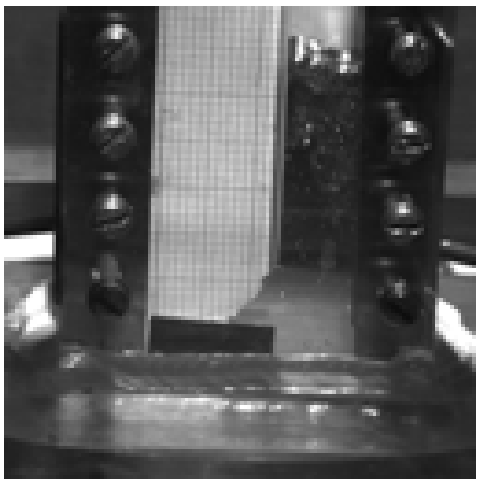

Time = 0.662s

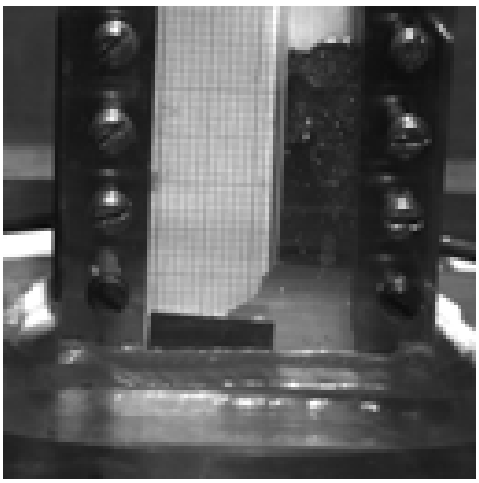

Time = 0.7s

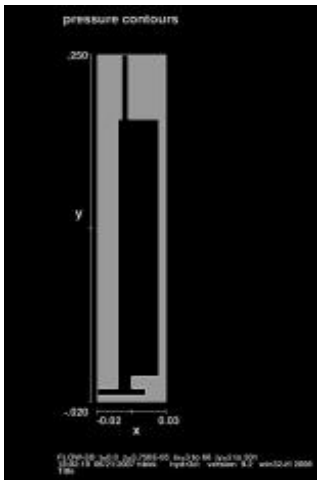

(1) Time: 0.00

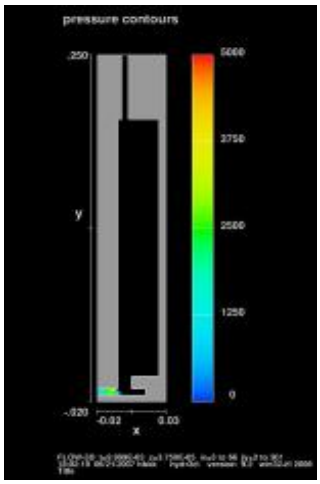

(2) Time: 0.009

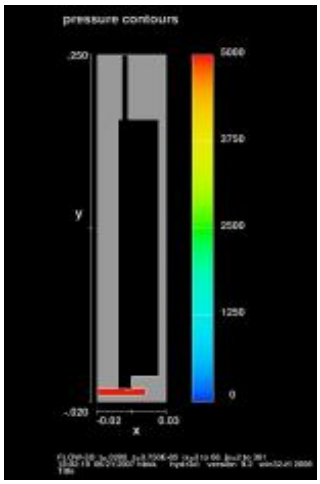

(3) Time: 0.01

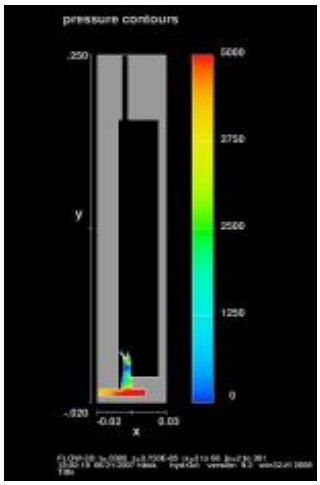

(4) Time: 0.03

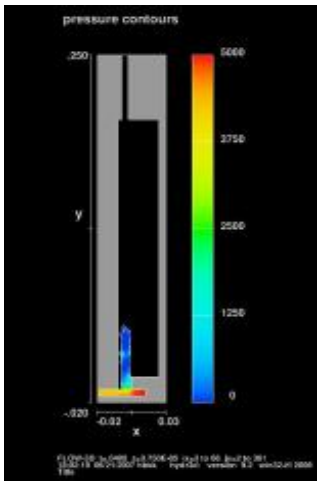

(5) Time: 0.04

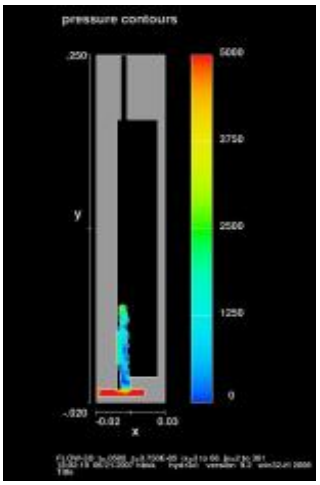

(6) Time:

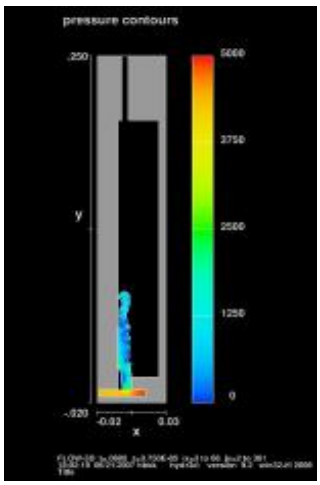

(7) Time: 0.06

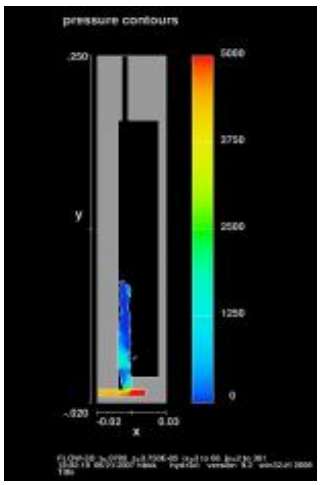

(8) Time: 0.07

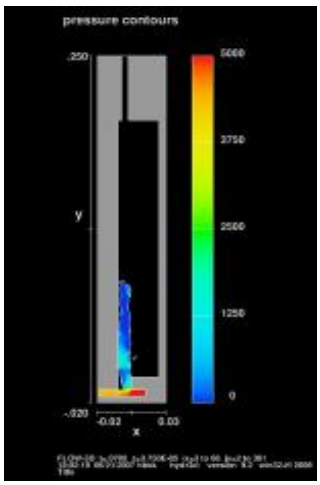

(9) Time: 0.08

15mm

Figure 4.13Flow-3D model of the liquid metal flow into a strip with thickness 0.75mm, without vibration, and an applied pressure of 4500 P_a at the inlet, equivalent to a 200 mm metal head.

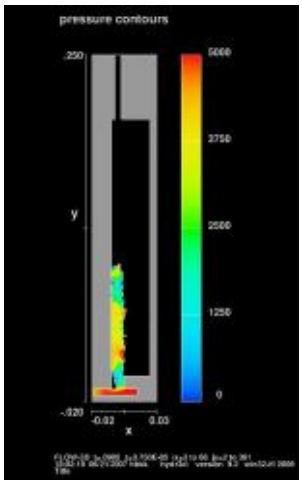

(11) Time: 0.09

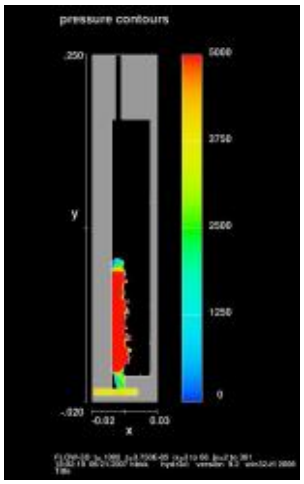

(12) Time: 0.1

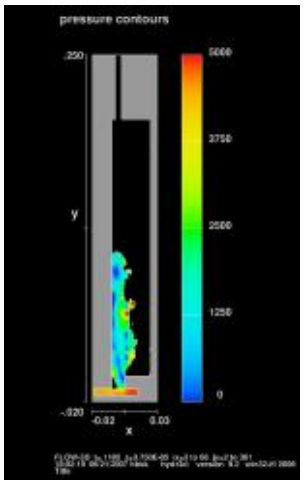

(13) Time: 0.11

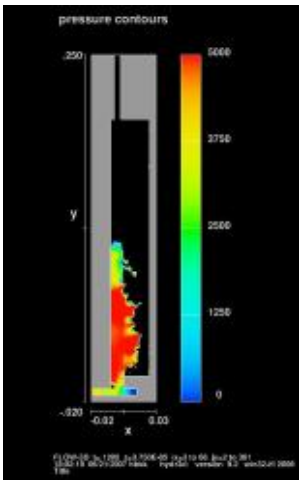

(14) Time: 0.12

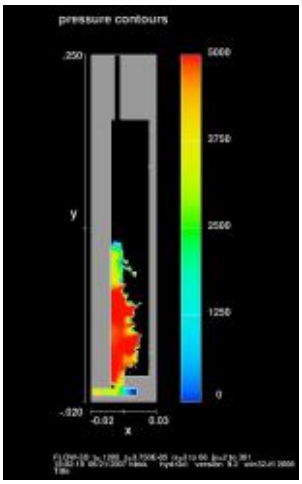

(14) Time: 0.13

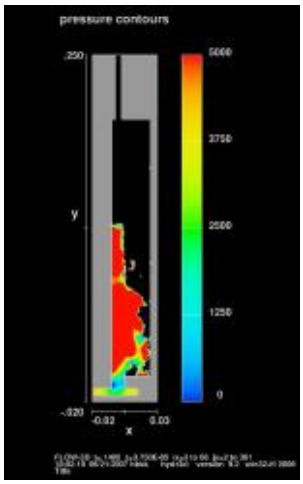

(15) Time: 0.13

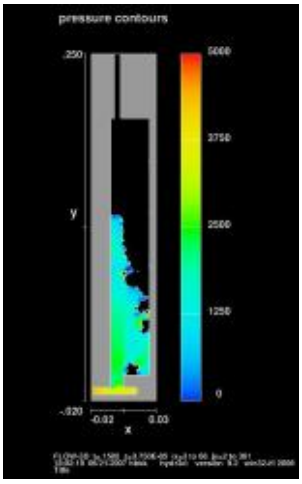

(17) Time: 0.15

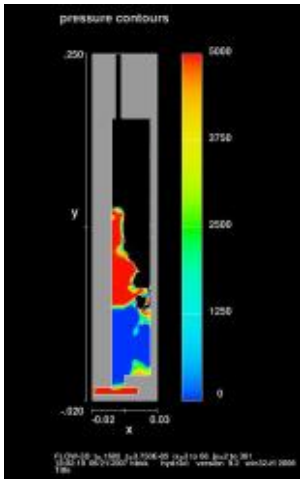

(18) Time: 0.16

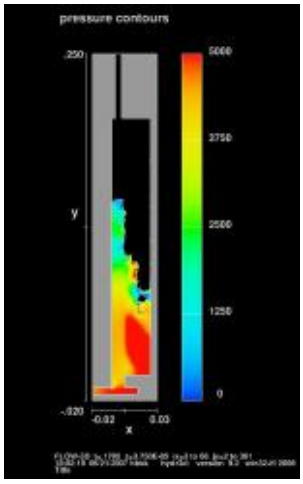

(19) Time: 0.17

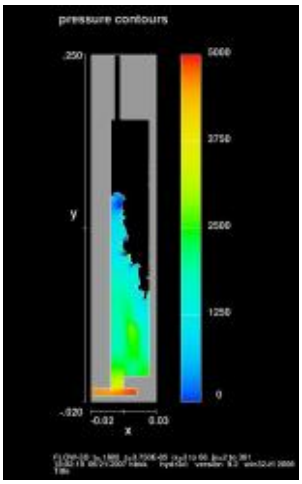

(20) Time: 0.18

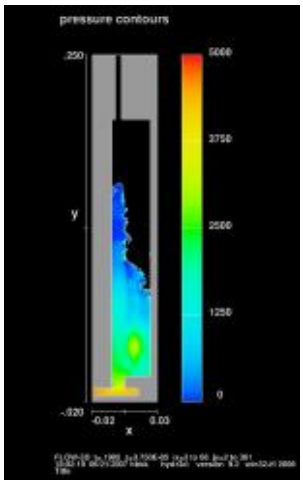

(21) Time: 0.19

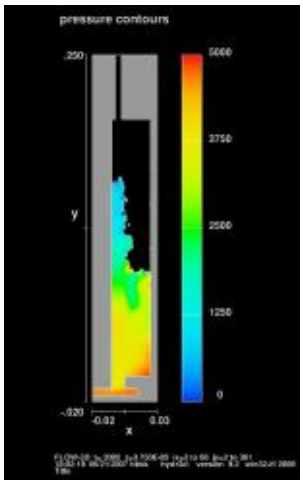

(22) Time: 0.2

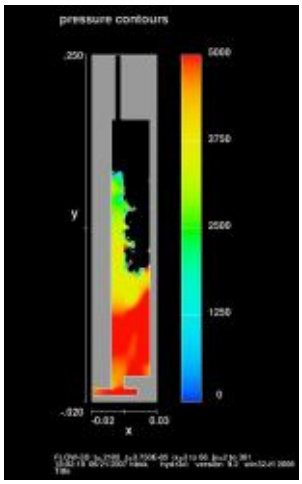

(23) Time: 0.21

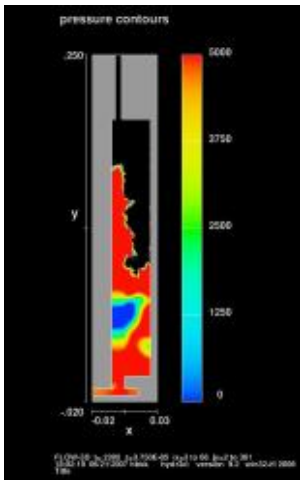

(24) Time: 0.22

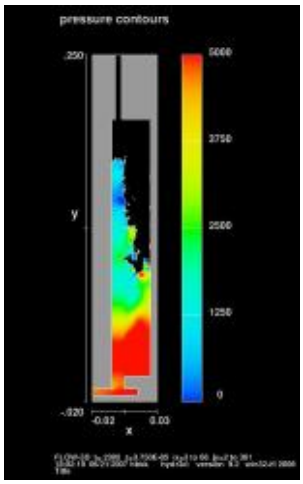

(25) Time: 0.23

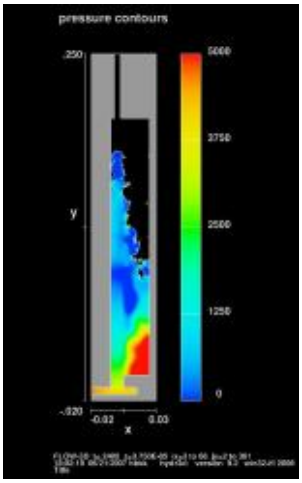

(26) Time: 0.24

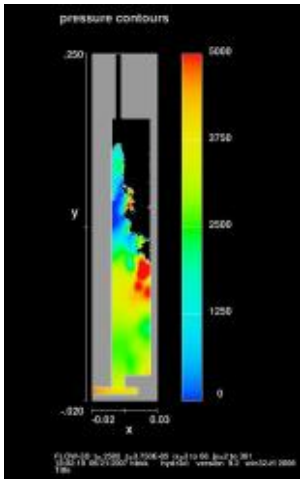

(27) Time: 0.25

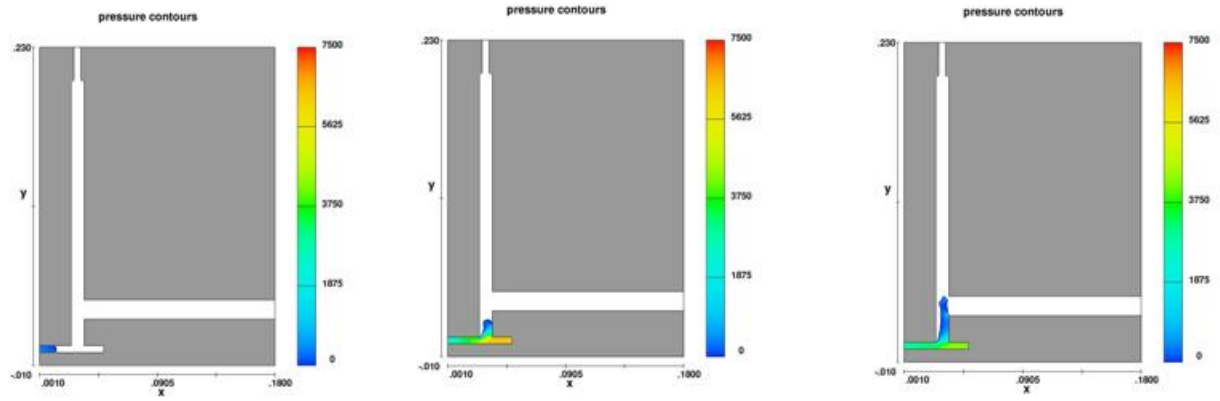

(1) Time: 0.009 (2) Time: 0.04 (3) Time: 0.05

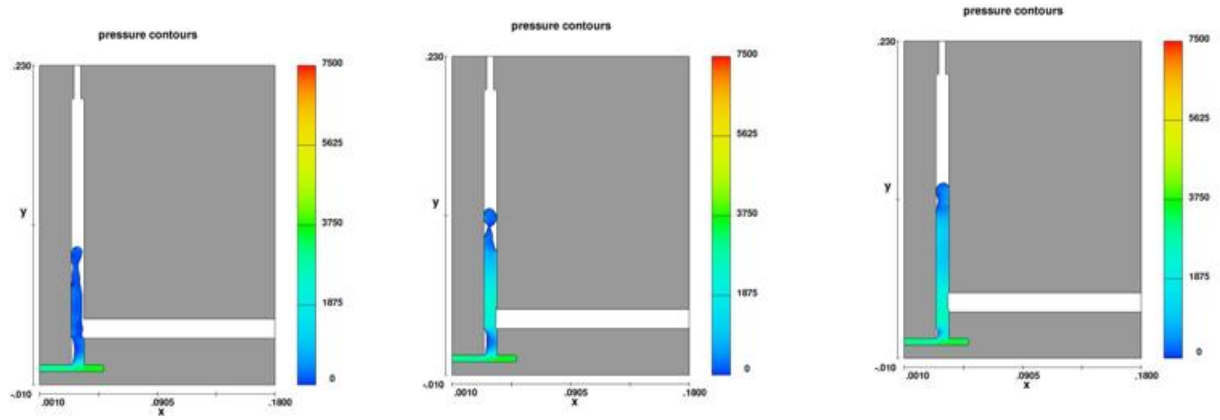

(4) Time: 0.08 (5) Time: 0.1 (6) Time: 0.14

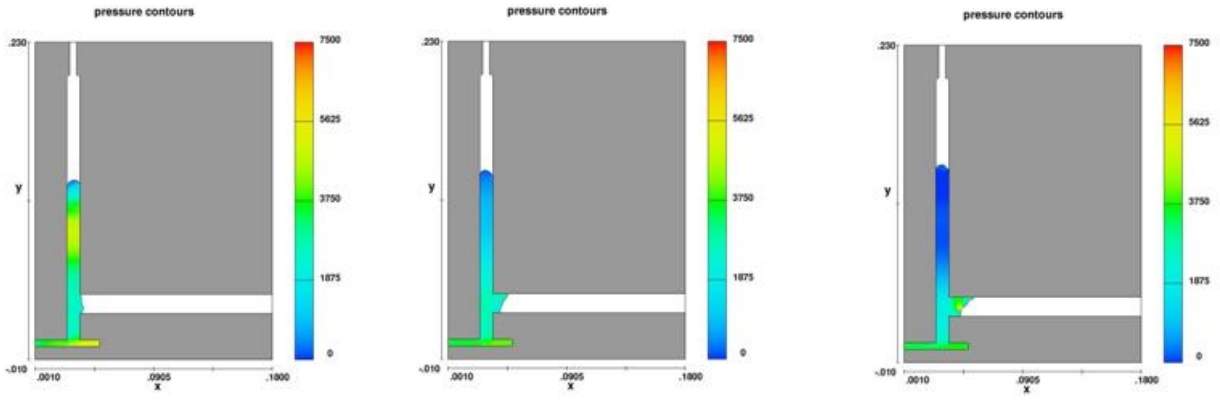

(7) Time: 0.15 (8) Time: 0.16 (9) Time: 0.17

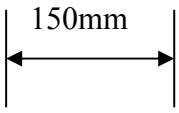

Figure 4.14 Frames of the Flow-3D modeling of the liquid metal flow into strip with thickness 0.75mm, without vibration, and an applied pressure of 4500 P_a at the inlet, equivalent to a 200 mm metal head.

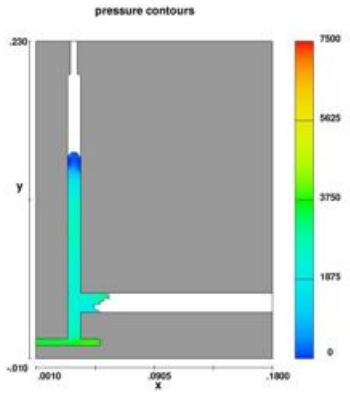

(10) Time: 0.18

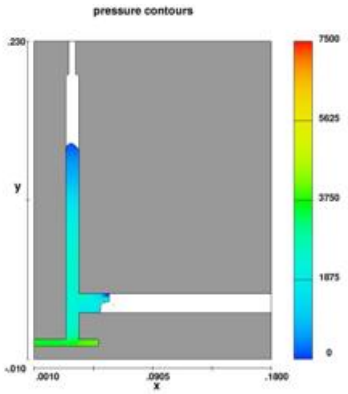

(11) Time: 0.19

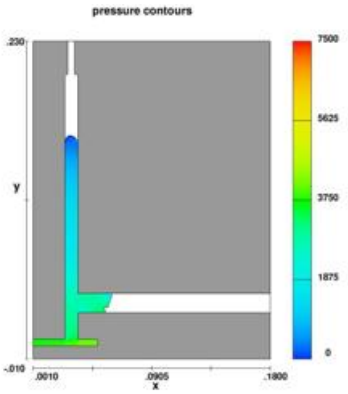

(12) Time: 0.20

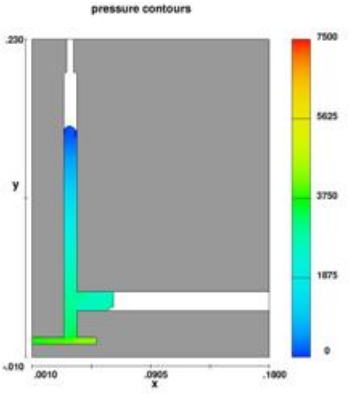

(13) Time: 0.22

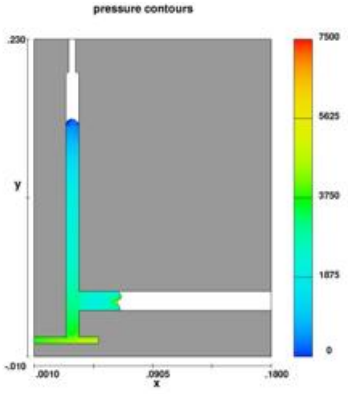

(14) Time: 0.23

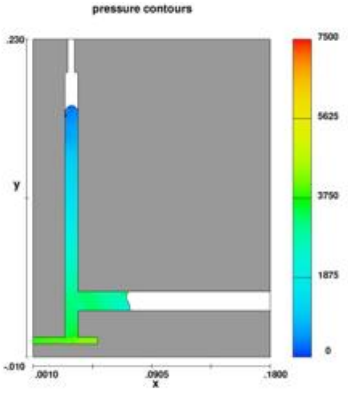

(15) Time: 0.24

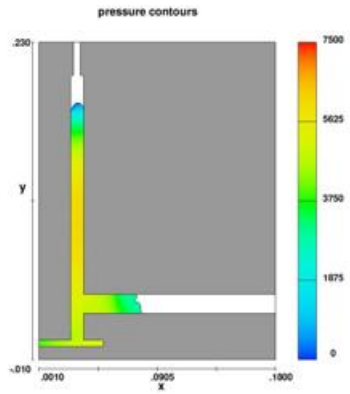

(16) Time: 0.25

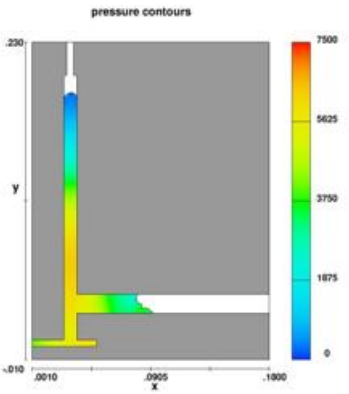

(17) Time: 0.26

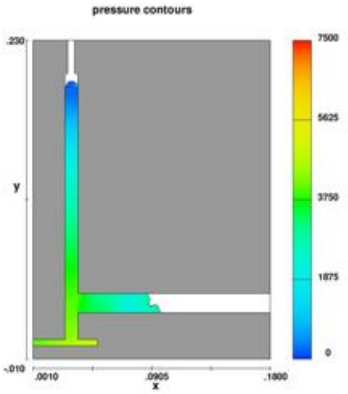

(18) Time: 0.27

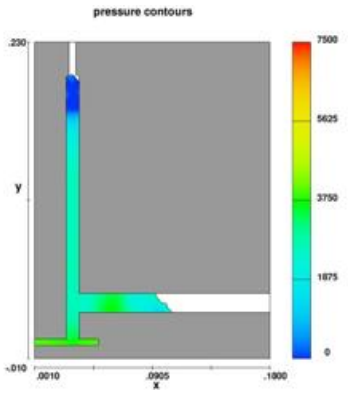

(19) Time: 0.28

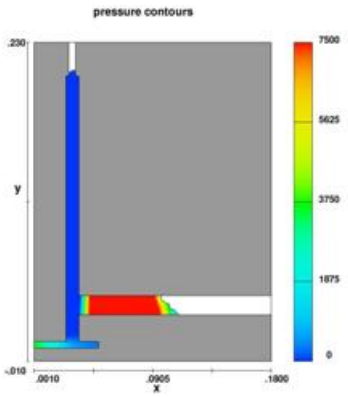

(20) Time: 0.30

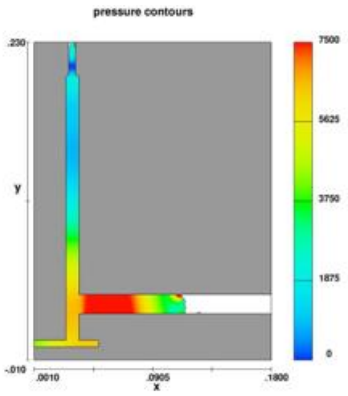

(21) Time: 0.32

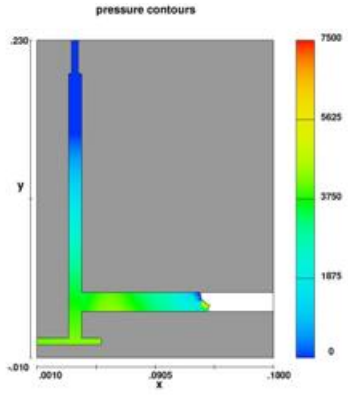

(22) Time: 0.35

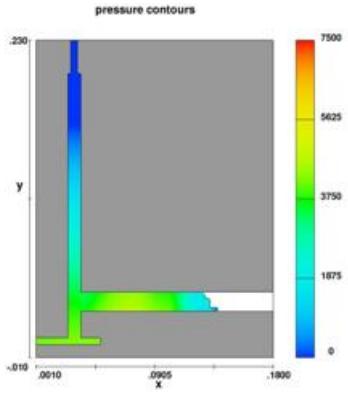

(23) Time: 0.37

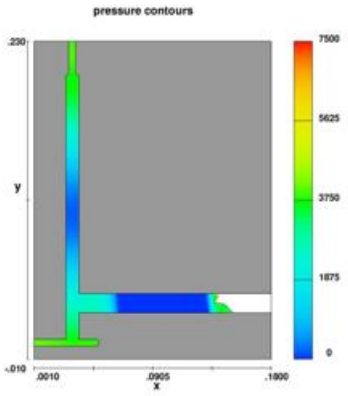

(24) Time: 0.40

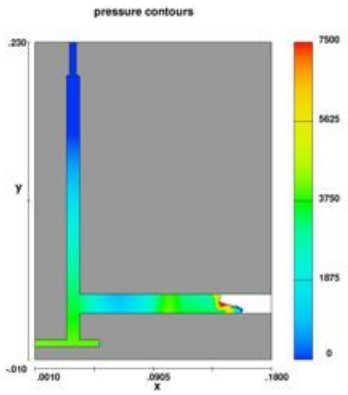

(25) Time: 0.41

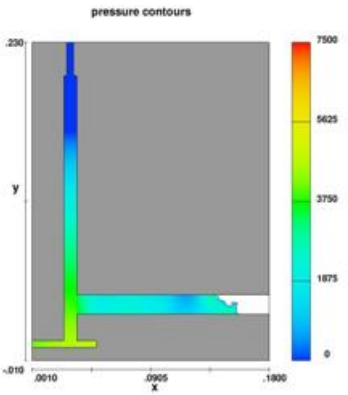

(26) Time: 0.42

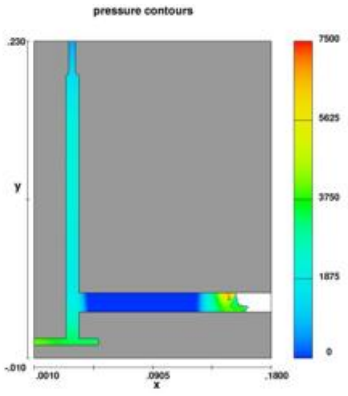

(27) Time: 0.44

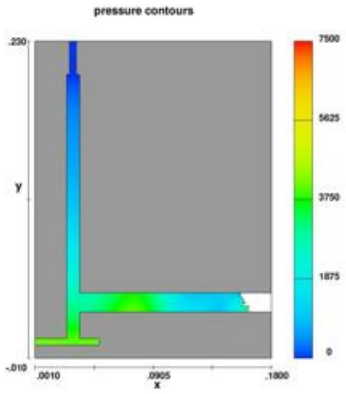

(28) Time: 0.46

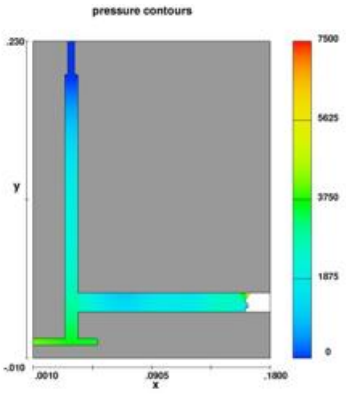

(29) Time: 0.47

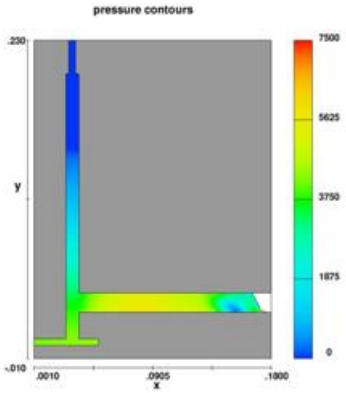

(30) Time: 0.48

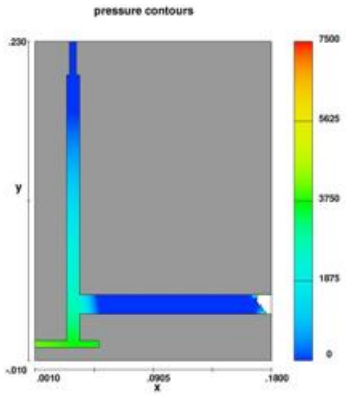

(31) Time: 0.49

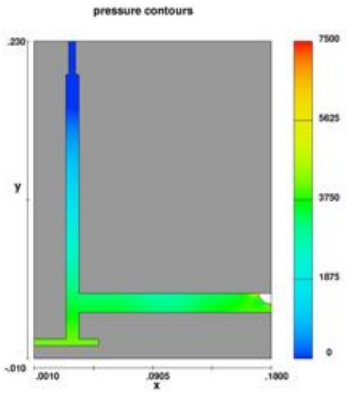

(32) Time: 0.50

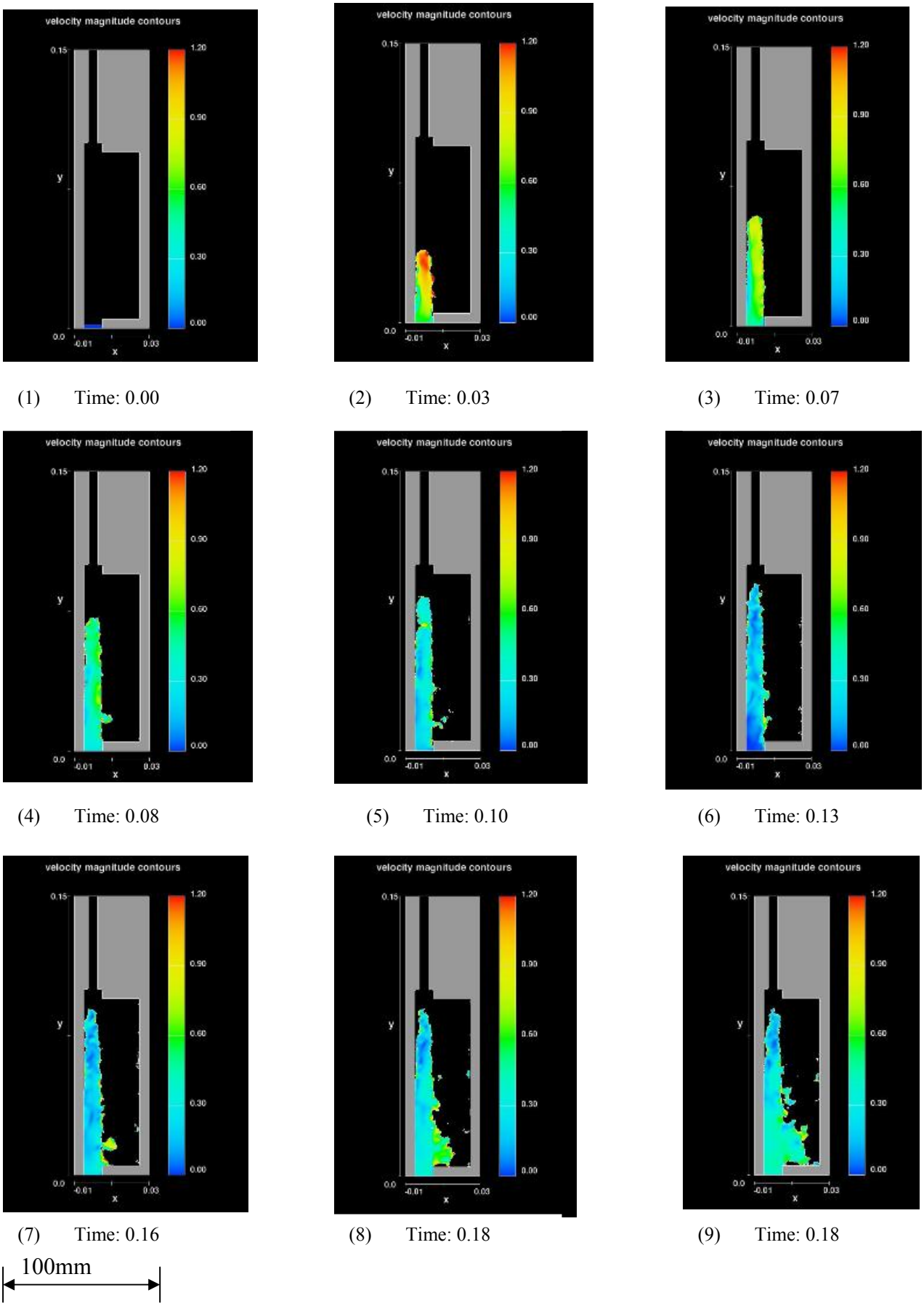

Figure 4.31 Frames of the Flow-3D modeling of the liquid metal flow into strip with thickness 0.55mm, sets vertical direction, metal height 100mmnin, vibration condition, pressure was estimated by gravitation and acceleration of vibration and applied as a boundary condition.

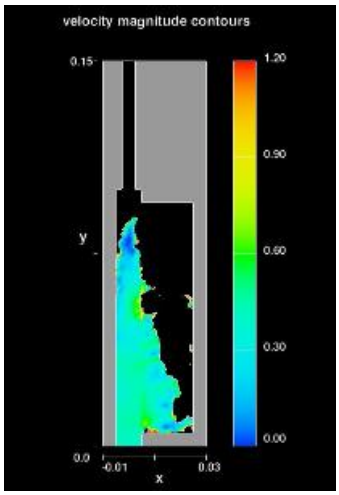

(10) Time: 0.19

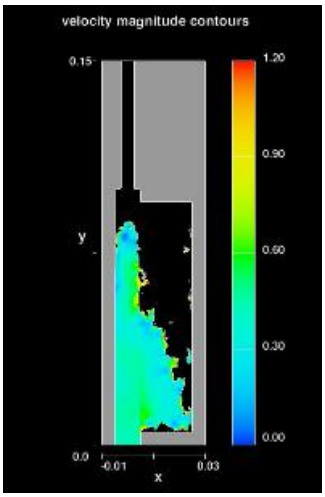

(11) Time: 0.20

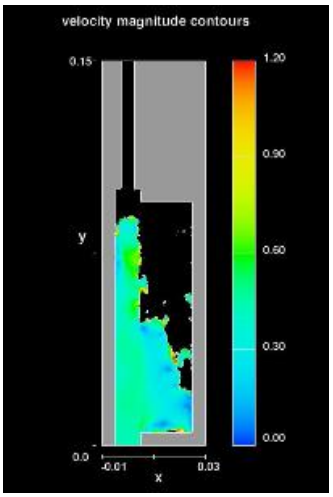

(12) Time: 0.23

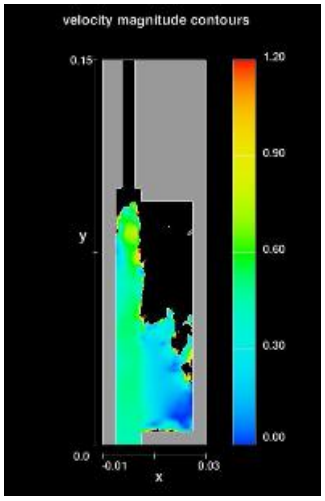

(13) Time: 0.24

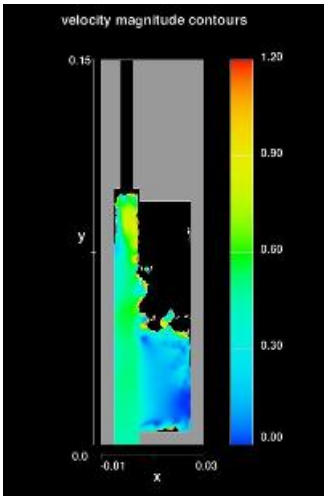

(14) Time: 0.25

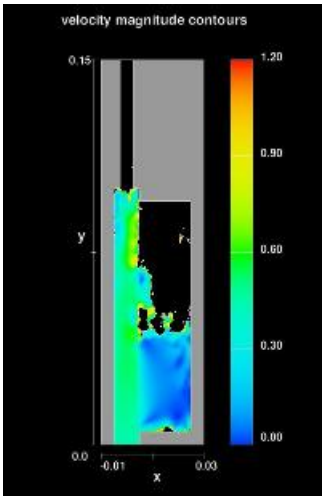

(15) Time: 0.26

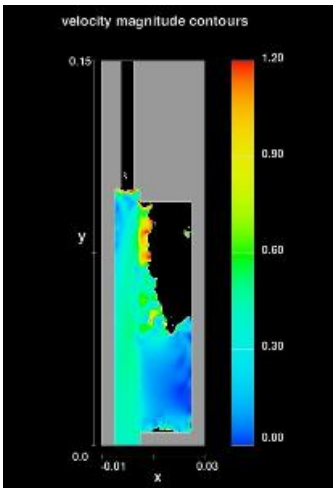

(16) Time: 0.27

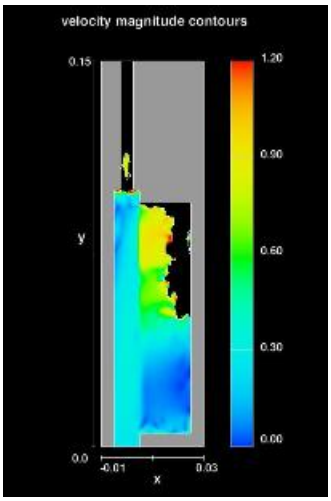

(17) Time: 0.28

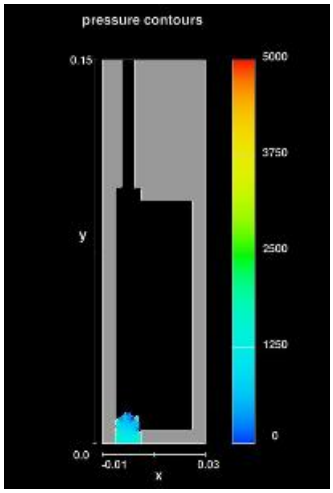

(1) Time: 0.01

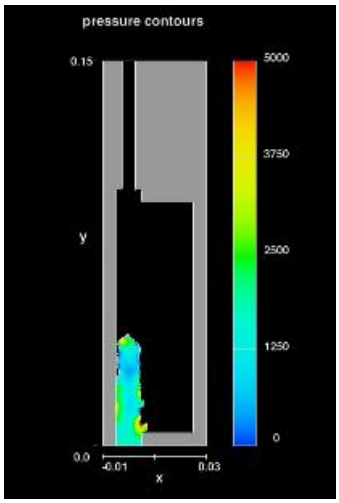

(2) Time: 0.03

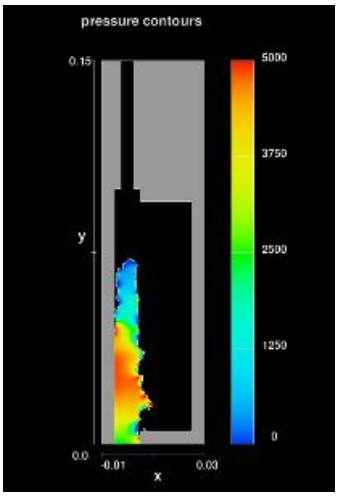

(3) Time: 0.07

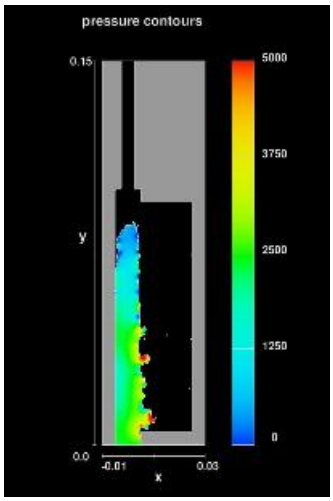

(4) Time: 0.08

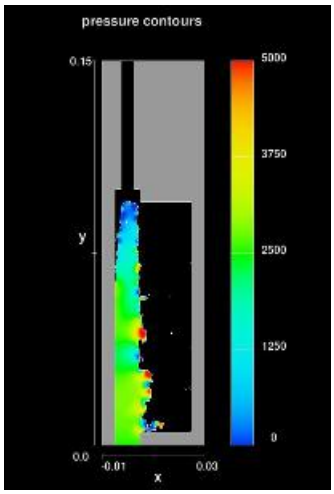

(5) Time: 0.09

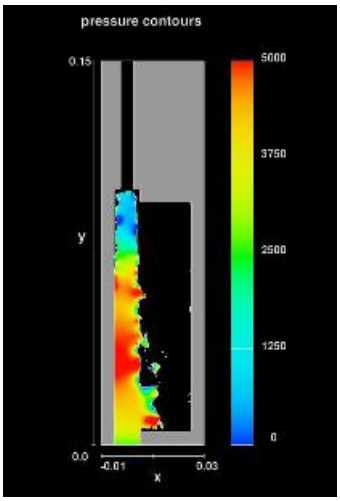

(6) Time: 0.12

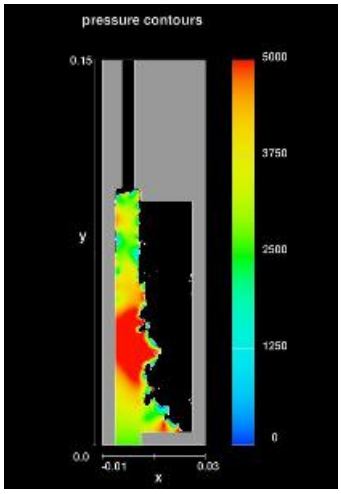

(7) Time: 0.14

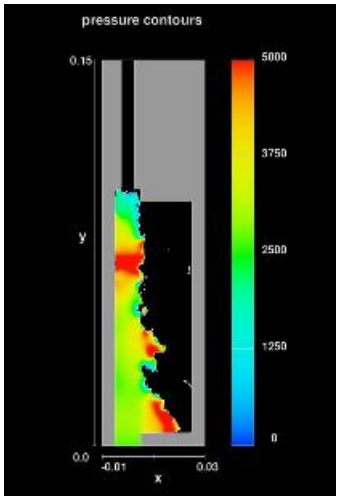

(8) Time: 0.16

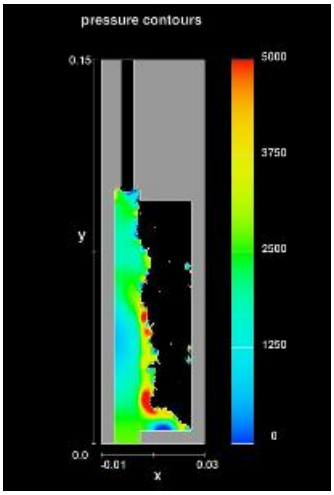

(9) Time: 0.18

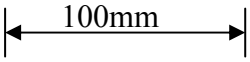

Figure 4.31 Frames of the Flow-3D modell the liquid metal flow into a strip with thickness 0.55mm, sets vertical direction in filling runner system with height 100mmnin vibration condition, the vibration pressure is applied as a boundary condition in the next second of simulation.

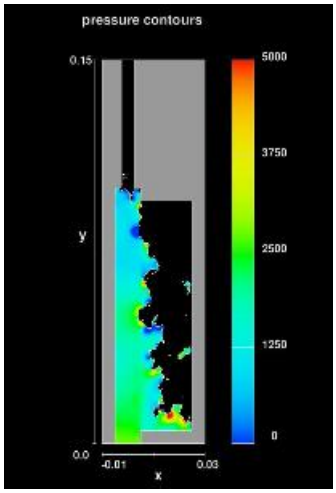

(10) Time: 0.20

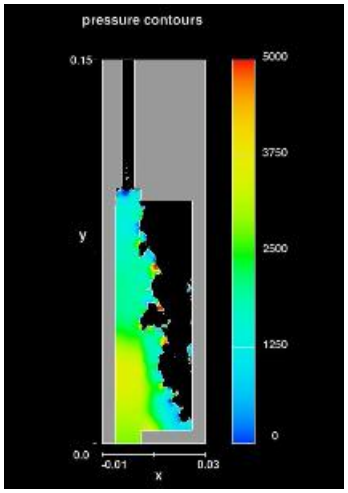

(11) Time: 0.21

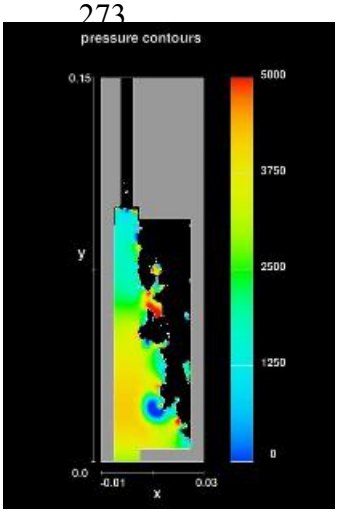

(12) Time: 0.22

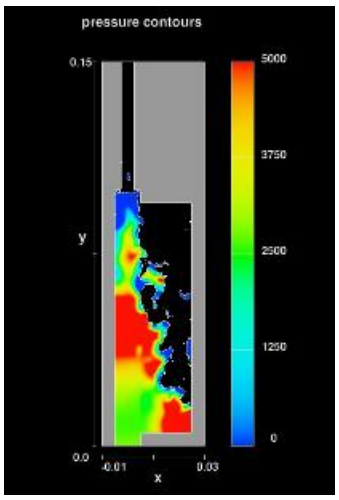

(13) Time: 0.24

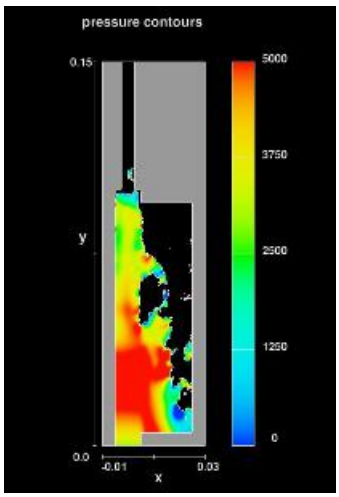

(14) Time: 0.25

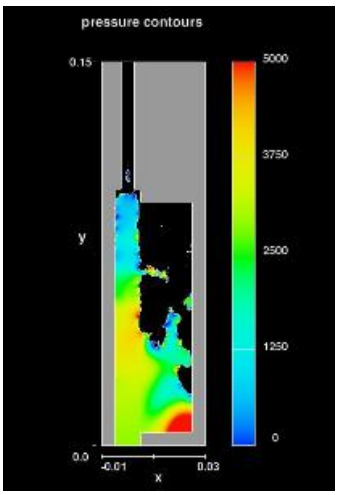

(15) Time: 0.26

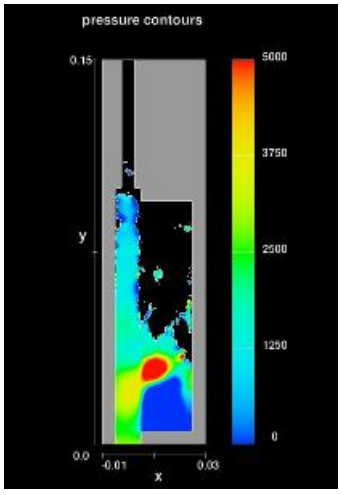

(16) Time: 0.28

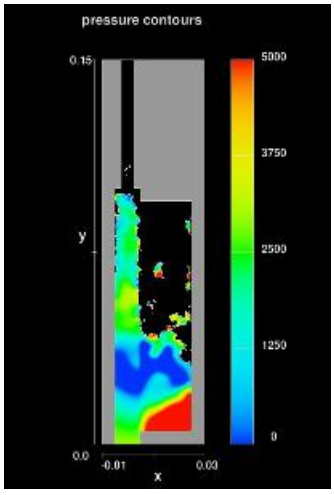

(17) Time: 0.30

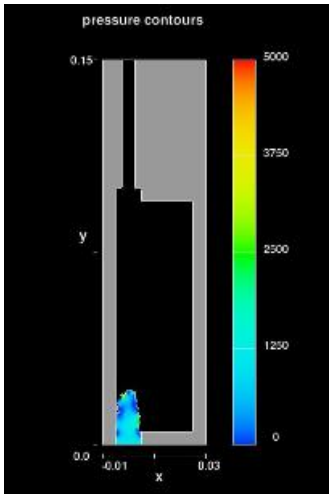

(1)

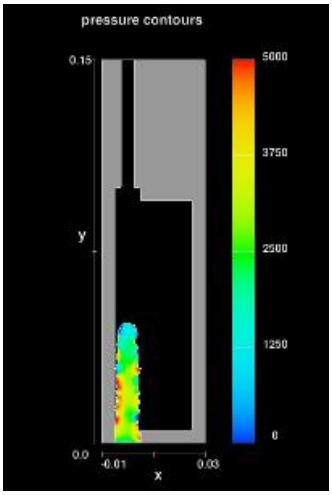

(2)

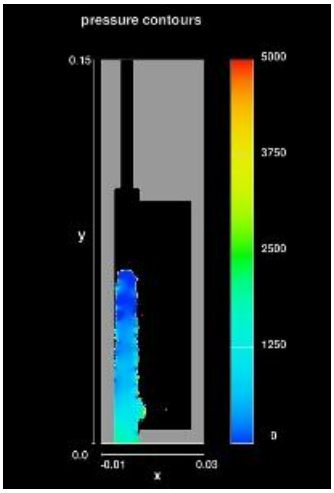

(3)

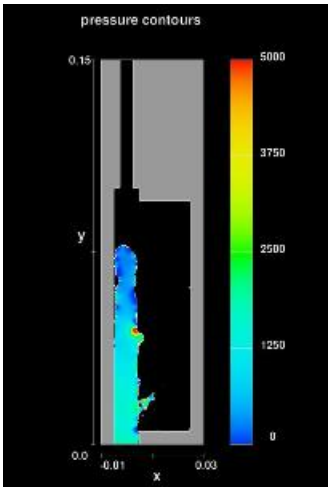

(4)

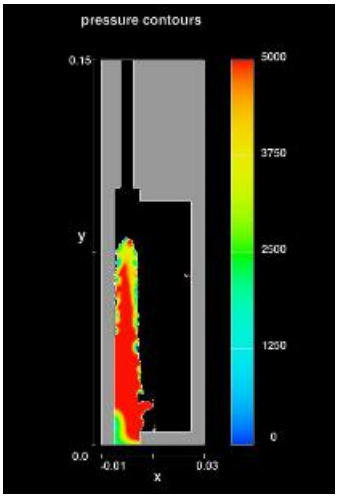

(5) Time: 0.1

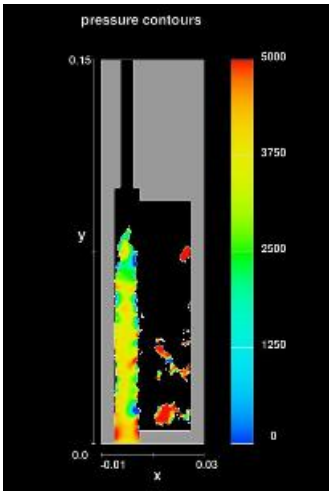

(6) Time: 0.12

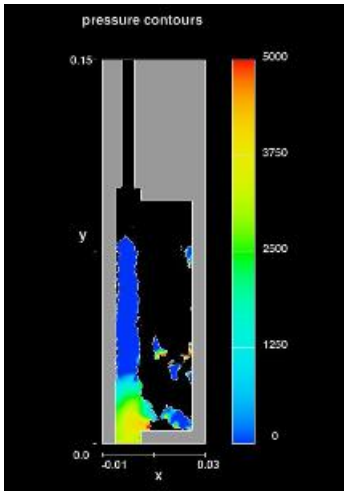

(7) Time: 0.13

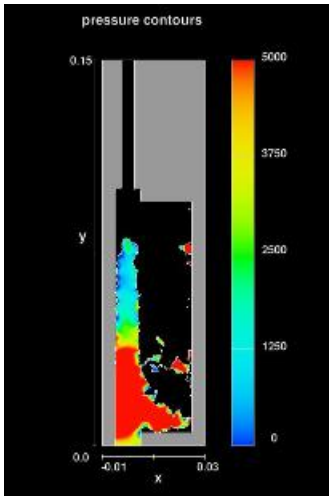

(8) Time: 0.15

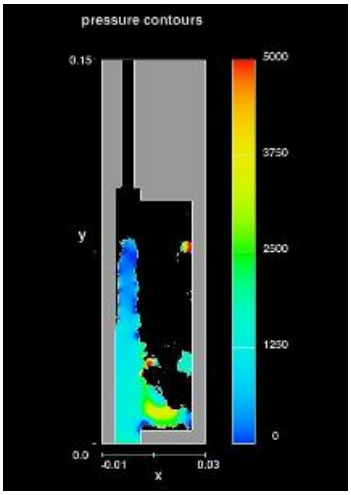

(9) Time: 0.16

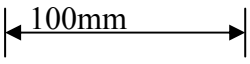

Figure 4.32 Frames of the Flow-3D model the liquid metal flow into a strip with thickness 0.55mm, sets vertical direction, metal height 100mm, vibration condition, the vibration pressure depend on time is applied as a boundary condition in the next second of simulation.

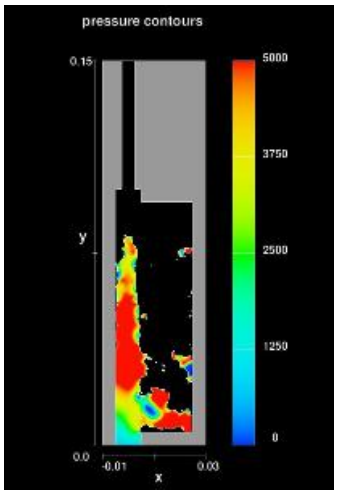

(10) Time: 0.17

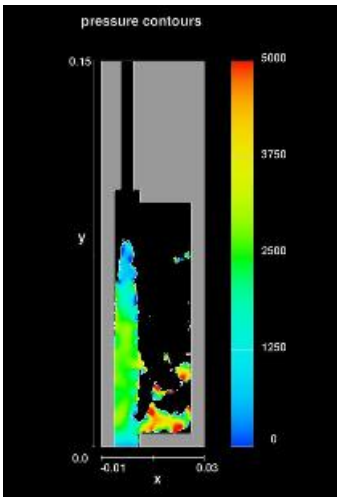

(11) Time: 0.18

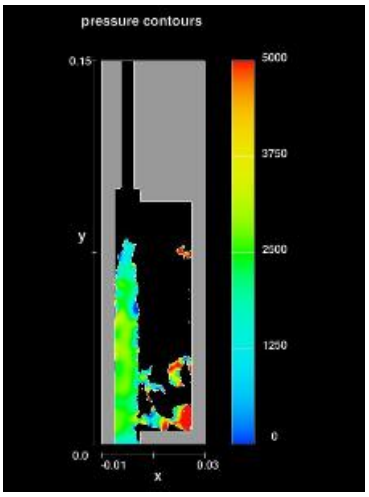

(12) Time: 0.19

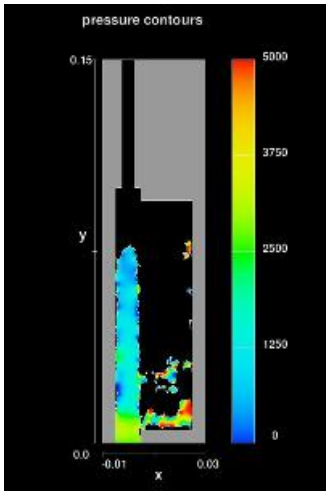

(13) Time: 0.20

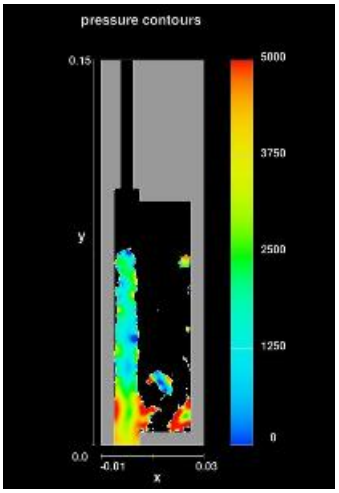

(14) Time: 0.21

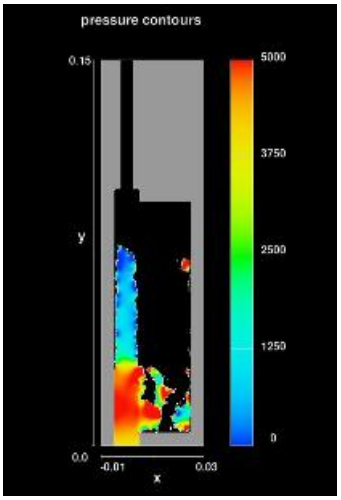

(15) Time: 0.22

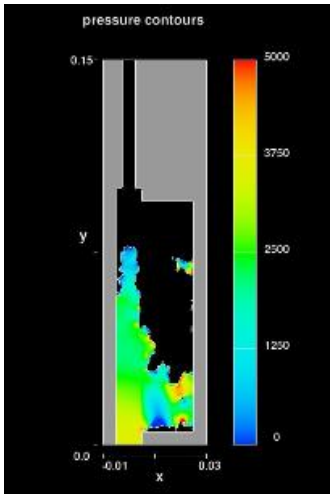

(16) Time: 0.23

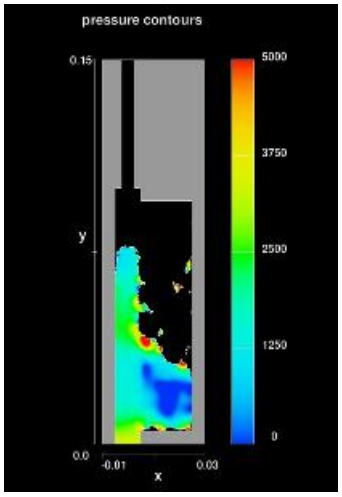

(17) Time: 0.26

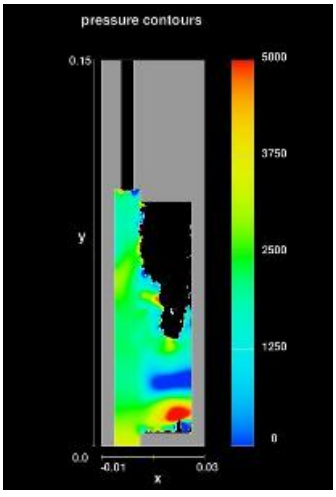

(18) Time: 0.33

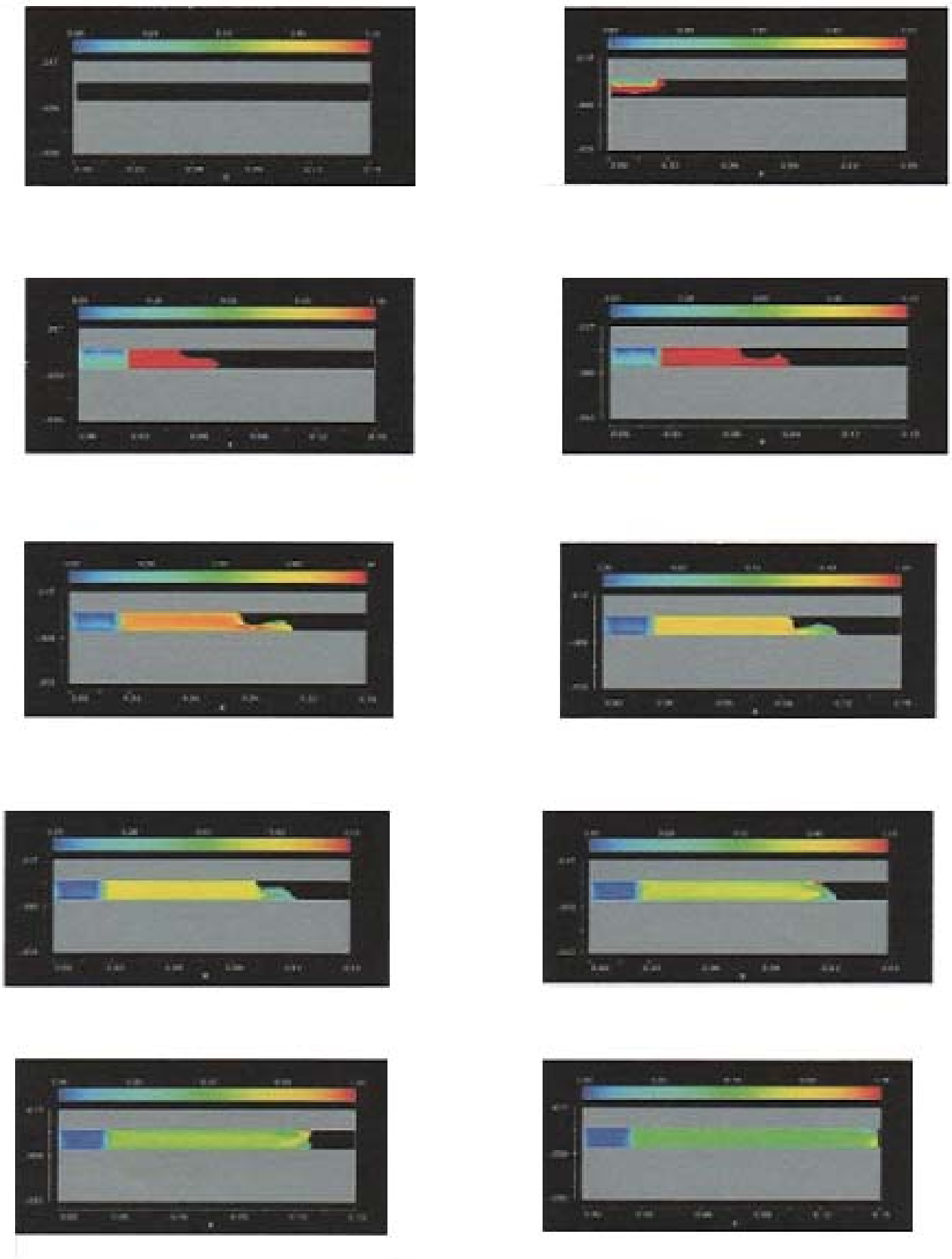

Figure 5.6 Flow-3D model of the liquid metal velocity into strip with thickness 0.75mm, without vibration.

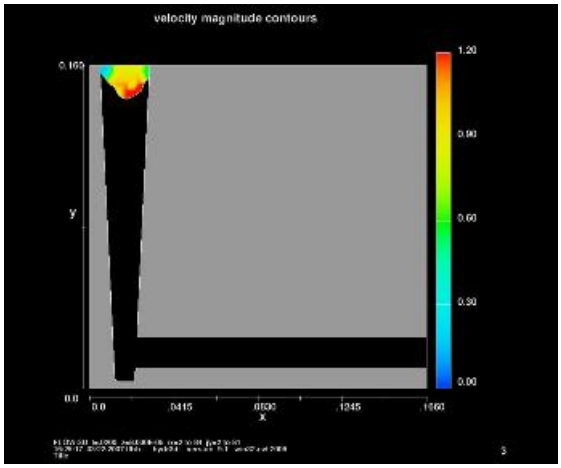

(1)

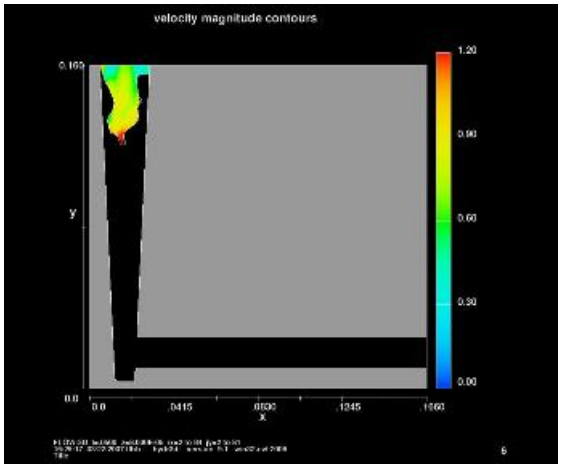

(2)

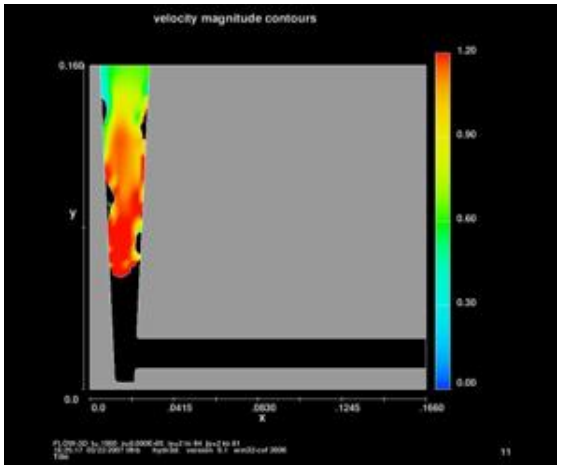

(3)

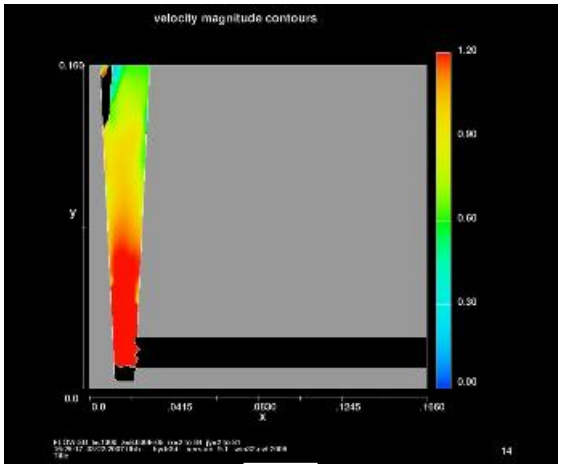

(4)

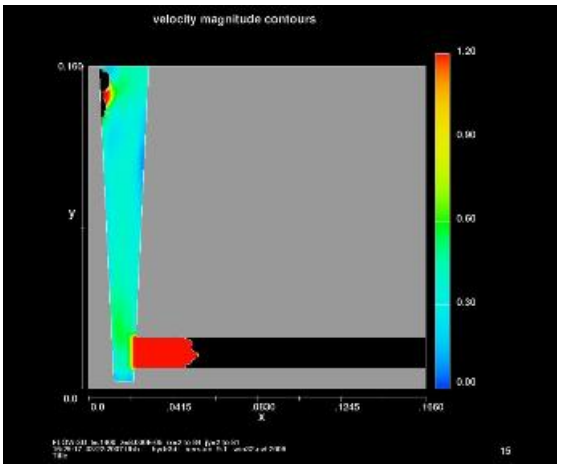

(5)

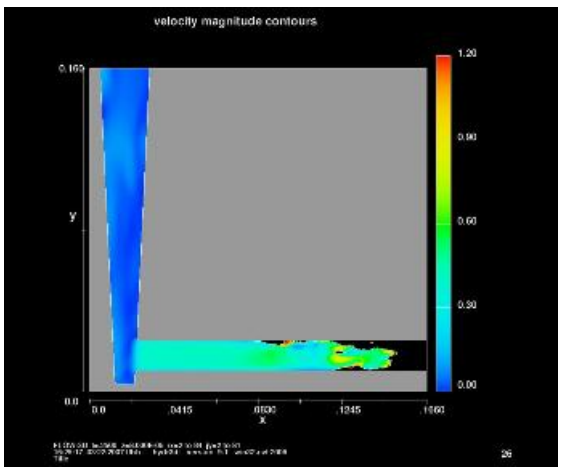

(6)

Figure 5.17 Flow-3D model of the fluidity in thin section of 0.75mm, without vibration.